In vitro models of bone-forming tumours: from target to treatment

Franceschini, N.

IN VITRO MODELS OF BONE-FORMING TUMOURS

From target to treatment

Natasja Franceschini

Publication of this thesis was financially supported by the Department of Pathology, Leiden University Medical Center and Chipsoft

In vitro models of bone-forming tumours:
From target to treatment

Proefschrift

ter verkrijging van
de graad van doctor aan de Universiteit Leiden,
op gezag van rector magnificus prof.dr.ir. H. Bijl,
volgens besluit van het college voor promoties
te verdedigen op woensdag 9 november 2022
klokke 10.00 uur

door

Natasja Franceschini
geboren te ‘s-Gravenhage
in 1993

Promotor
Prof. dr. J.V.M.G. Bovée

Co-promotor
Dr. A.M. Cleton-Jansen

Leden promotiecommissie
Prof. dr. I. Meulenbelt
Prof. dr. J.J. Molenaar (Prinses Maxima Centrum)
Prof. dr. M.A. Tryfonidou (Universiteit Utrecht)
Dr. A.B. Mohseny

Contents

Chapter 1

General introduction

Bone-forming tumours of the skeleton: clinical presentation, histology and molecular pathology

Bone-forming tumours of the skeleton comprise a group of tumours of mesenchymal origin. These tumours are characterized by bone deposition and include osteoma, osteoid osteoma, osteoblastoma and osteosarcoma. The current knowledge of the clinical presentation, histology and molecular pathology of these tumours is reviewed in detail in **chapter 2**. In general, the group of bone tumours can be divided into two groups based on the molecular pathology (1). There are tumours with a simple or a complex karyotype. Simple karyotype tumours are driven by specific gene mutations or translocations. In contrast, complex karyotype tumours typically do not harbor specific genetic alterations, but instead show many chromosomal alterations, copy number alterations and aneuploidy. Based on these criteria, osteoma, osteoid osteoma and osteoblastoma are tumours with a simple karyotype, whereas osteosarcoma is an example of a tumour with a complex karyotype.

Osteoid osteoma and osteoblastoma are bone forming tumours with an indistinguishable histology (2, 3). In both entities, trabeculae with woven bone are present, which are lined by active osteoblasts (4, 5). Both tumours are not malignant, but osteoblastomas can be locally aggressive. The distinction between osteoid osteoma and osteoblastoma is mostly based on size, where osteoid osteoma is smaller than 2 cm and osteoblastoma is larger (2). Osteoid osteoma and osteoblastoma are tumours with a simple karyotype, with frequent translocations in *FOS* (87%) and to a lesser extent *FOSB* (2%) (6). The translocation of *FOS* leads to a truncation of the FOS protein. This rearrangement has previously been discovered in epithelioid hemangioma (7, 8), and more recently also in cementoblastoma (9). The identification of *FOS* rearrangements in osteoid osteoma and osteoblastoma has led to the discovery of a novel diagnostic tool, where FOS immunohistochemical expression can be detected and osteoid osteoma and osteoblastoma can be more easily distinguished from other bone-forming lesions (10, 11). FOS and FOS B can form a heterodimer with JUN proteins to form the AP-1 transcription factor, regulating proliferation and differentiation (12, 13). The exact role of FOS or FOS B in the pathogenesis of osteoid osteoma or osteoblastoma is not completely understood.

Osteosarcoma is a malignant tumour of the bone, and typically diagnosed in children and adolescents (2). Histologically, it is characterized by osteoid production. Different histological subtypes are recognized, including the most common high-grade conventional osteosarcoma and low-grade osteosarcoma such as parosteal osteosarcoma (2). Tumours usually arise in the long bones. Osteosarcoma is a tumour with a complex karyotype: it is characterized by massive chromosomal abnormalities, copy number alterations and aneuploidy. Chromoanagenesis, including chromothripsis where chromosomes shatter into fragments and are randomly stitched together, is relatively frequent compared to other cancer types (14, 15). Given the molecular complexity of osteosarcoma, recurrent alterations are not often

identified. Among the most commonly altered genes are *TP53* and *RB1*, and genes involved in cell cycle regulation and genome stability, such as *MDM2*, *CDK4*, and *ATRX* (15-19).

Therapeutic strategies for bone-forming tumours: current strategies and advancements

Osteoid osteoma and osteoblastoma

Patients with osteoid osteoma typically present with nocturnal pain, which can be relieved by salicylates or NSAIDs (20). Some tumours spontaneously regress within 6 years (21). Removal of the tumour is necessary when symptoms of pain persist. Where removal of the tumour in the past has mostly involved open excision, in recent years techniques have become less invasive, for example using image-guided techniques such as radiofrequency ablation (22). For osteoblastoma, patients also present with pain, although NSAIDS usually do not relief pain (23). Instead, osteoblastoma requires surgical removal (24).

Osteosarcoma

The current standard therapeutic strategy for high-grade conventional osteosarcoma is a combination of surgery and (neo)adjuvant chemotherapy. Currently used chemotherapeutic agents include doxorubicin, cisplatin, methotrexate and ifosfamide (25). Although the introduction of chemotherapy in the 1970s has greatly improved the outcome for osteosarcoma patients, the last five decades have not shown improvements in overall survival (26, 27). Since high-grade conventional osteosarcoma is mainly diagnosed in children and young adolescents, with an incidence of almost 15 per 100,000 in the United States, the burden of highly toxic chemotherapy for this vulnerable patient group is high (28). This emphasizes the need for novel therapeutic strategies, in particular for patients with metastasis or resistance to chemotherapy. In recent years an exponential increase in publications of osteosarcoma could be observed, in particular *in vitro* studies (29). A large part of these studies explore traditional Chinese medicine as novel therapeutic options, but also drugs targeting recurrent genetic alterations have been described. An overview of currently ongoing clinical trials where novel therapeutic targets are being tested in osteosarcoma is shown in **Table 1**.

Table 1. Overview of currently ongoing registered clinical trials for novel therapeutic options in osteosarcoma patients.

Category	Target	Drug	Clinical Trial Number	Clinical Trial Phase
Therapies targeting cell cycle / genome maintenance	CDK4/CDK6	Palbociclib	NCT03526250 NCT03709680	2 1
		Abemaciclib	NCT02389244 NCT02644460	2 1
	PARP	Talazoparib	NCT04901702	2
		Olaparib	NCT03233204	1
Therapies targeting receptor tyrosine kinases	RTK	Lenvatinib	NCT04154189 NCT02432274 NCT03742193 NCT04690231 NCT04824352	1 1 1 1 1
		Sunitinib	NCT03900793 NCT03277924	1 1
		Regorafenib	NCT04698785 NCT04055220 NCT04803877 NCT02389244 NCT02048371	1 2 2 2 2
		Apatinib	NCT03742193 NCT04690231 NCT04824352	2 2 2
		Cabozantinib	NCT05019703 NCT04661852 NCT02867592	2 2 2
Therapies targeting the mTOR pathway	PI3K (mTOR)	Samotolisib	NCT03213678	2
Immunotherapy	PDL-1/PD-1	ZKAB001	NCT03676985 NCT04359550	2 3
		Avelumab	NCT03006848	2
		Camreluzimab	NCT04294511	2
		Nivolumab	NCT03628209 NCT02500797	1 2
		Durvalumab	NCT04668300	2
	GD2	Dinutuximab	NCT02484443	2
	HER2	Trastuzumab	NCT04616560	2

Therapies targeting cell cycle and genome maintenance

The most common alterations include *TP53* and *RB1*. TP53 and RB1 are key players in genome maintenance and controlling cell cycle. Drugs that target recurrent alterations should be based on a distinction between cancerous and normal cells. Although mutations that lead to overexpression of *TP53* can be used to distinguish between cancerous and normal cells, the nuclear localization and lack of enzymatic activity of p53 makes it a rather difficult target for drugs (30). However, drugs that can reactivate the wild-type state of p53 mutant forms by induction of conformational changes, such as APR-246, seem promising and have progressed to clinical trials (31-33), although not in osteosarcoma.

RB1, when dephosphorylated and activated, blocks cell cycle progression by blocking cells from entering S-phase of the cell cycle (34). Proteins within the Rb-pathway are often affected in osteosarcoma patients, which include alterations in *CDK4*, *CDK6*, *CDKN2A* and *CDKN2B*. Drugs that prevent the phosphorylation, and thus inactivation of Rb, are currently strategies for targeting the Rb-pathway. CDK4 inhibitors block Rb phosphorylation and thereby cell proliferation. Currently clinical trials are ongoing to test CDK4 inhibitors in sarcomas, including osteosarcoma, with altered CDK4 expression (35, 36).

Recently, whole exome sequencing revealed that osteosarcoma shows a mutational profile that is reminiscent of tumours that are deficient in *BRCA*1/2, genes that are involved in the DNA homologous repair pathway (19). Osteosarcoma shows features of BRCAness, which is a mutational profile consisting of loss-of-heterozygosity, a specific combination of single nucleotide alterations and genomic instability. BRCAness could suggest sensitivity to PARP inhibitors such as talazoparib (19). Talazoparib has shown success *in vitro* where it reduced osteosarcoma cell viability, although this effect was less compared to *BRCA* negative breast cancer cell lines for which PARP inhibitor treatment is already the standard therapeutic option (37, 38). Clinical trials are currently ongoing to test PARP inhibitors olaparib and talazoparib in osteosarcoma (39, 40) (NCT04901702; NCT03233204).

Therapies targeting receptor tyrosine kinases (RTKs)

Tyrosine kinase inhibitors (TKIs) are a class of drugs that target molecules essential for cell signaling pathways. Tyrosine kinases that have been reported to be affected in osteosarcoma, include EGFR, VEGFR, PDGFR and IGF1R, (41). In particular, the genomic region 4q12 that contains tyrosine kinases *KIT*, *KDR* and *PDGFRA* showed amplification in 20% of osteosarcoma patients, indicating that broad spectrum TKIs could be a promising candidate drug for osteosarcoma patients (42). Previous clinical trials in which TKIs were administered have already shown promise in osteosarcoma patients, and currently 13 more registered clinical trials are ongoing (43). Insulin growth factor receptor 1 (IGF1R) is also considered a receptor tyrosine kinase. The IGF signaling pathway, that plays a role in bone homeostasis, was shown to be overexpressed in osteosarcoma (15, 44). Although a clinical trial that included osteosarcoma patients did not show significant benefit of treatment with IGF 1R inhibitor

Robatumumab (45), selecting patients based on IGF1R expression levels was hypothesized to increase the response (46).

Therapies targeting the mTOR pathway

The mTOR pathway plays a key role in energy metabolism, which is highly active in cancer cells (47), often through PI3K and Akt signaling. Activation of the mTOR pathway leads to increased cell proliferation and cell cycle progression, and a decrease in autophagy, thereby promoting tumour growth. In osteosarcoma, recurrent alterations have been identified in the mTOR/PI3K/Akt pathway (18). It was discovered that inhibiting mTOR, in combination with 3-phosphoglycerate dehydrogenase (PHGDH) inhibition, attenuated cell proliferation in osteosarcoma cells and could serve as a novel therapeutic target (48). Rapamycin, an inhibitor of the mTOR signaling pathway, was found to inhibit osteosarcoma cell proliferation in an *in vitro* model, and decreased tumour growth in a mouse model (49). Combination therapies with chemotherapeutics have also been investigated for osteosarcoma: in osteosarcoma cells, the combination of cisplatin together with rapamycin increased apoptosis and autophagy activity (50). mTOR inhibition has also been tested in a clinical trial for osteosarcoma patients, in which the mTOR inhibitor temsirolimus was administered together with IGF1R inhibitor cixutumumab, but this did not improve outcome (51).

Immunotherapy

In recent years immunotherapy has shown success in various cancer types. Immunotherapy is mainly aimed at stimulating the activity of the immune system or inhibiting the anti-immune activity of cancer cells. Many studies have been published in which immunotherapy was investigated in osteosarcoma and several attempts have been made to test immunotherapies in clinical trials in osteosarcoma, but until now with limited success (52, 53). For example, in the EURAMOS-1 clinical trial in which immunostimulatory IFN-α2b was tested, this did not lead to improvement in overall survival (54). However, a phase 3 clinical study in osteosarcoma was successful in which muramyl tripeptide (MTP), a drug that activates monocytes and macrophages, was tested in osteosarcoma patients. MTP in combination with conventional chemotherapy improved overall survival (53). One method to inhibit the anti-immune response of cancer cells is to inhibit the immune checkpoint response, in which the immune system is prevented to target cancerous cells. PD-1 and PD-L1 are immune checkpoint molecules, and are often the target of immune checkpoint inhibitors. PD-L1 is expressed in osteosarcomas, which suggests sensitivity to immune checkpoint inhibitors (55). Immune checkpoint inhibitors targeting PD-1 and PD-L1 include ZKAB001, avelumab, camreluzimab, nivolumab and durvalumab and are currently being tested in clinical trials (**Table 1**). Other checkpoints may also be active in osteosarcoma, e.g. TIM3 which is overexpressed in osteosarcoma tissue (56), and thereby potential targets for therapy.

Immunotherapy may also involve the use of antibodies targeting cell surface proteins that are overexpressed in cancer cells. The binding of antibodies to cell surface proteins can recruit immune cells leading to cytotoxicity of cancer cells. An example is GD2, which is overexpressed in osteosarcoma (57). Dinutuximab, a monoclonal antibody targeting GD2 that induces immune cell-mediated cytotoxicity, is currently being tested in a phase 2 clinical trial for osteosarcoma patients (NCT02484443). Another example is trastuzumab, a monoclonal antibody targeting HER2, which is currently also being tested in a phase 2 clinical trial (NCT04616560).

Chimeric Antigen Receptor (CAR) T-cell therapy is a type of immunotherapy in which the receptors of T-cells, derived from the patient or from a healthy donor, are genetically engineered to target cell surface proteins of cancer cells. CAR T-cell therapy has delivered promising results in leukemia, and could also be a novel therapeutic strategy for osteosarcoma patients (58).

In vitro models of bone-forming tumours

Good representative *in vitro* models are essential for pre-clinical testing of novel targeted treatments. There is a plethora of cell models available for osteosarcoma, including cell-of-origin based models, cell models derived from patient material, or from xenografts (59). Typically cell models involve the culture of cells, either directly derived from patient material or from animal tumor tissue, onto a plastic surface. The cells are cultured as a monolayer onto a two-dimensional surface and as such lack the three-dimensional environment the cells have originated from. Since the three-dimensional environment is lacking, it could be less representative for the *in vivo* situation. This could influence results obtained from drug testing in these cell models. In recent years an increase in studies was seen in which cells are instead cultured in a three-dimensional environment, where cells do have the interaction with other cells and the microenvironment (60).

Cell of origin

Osteoid osteoma, osteoblastoma and osteosarcoma are tumours of mesenchymal origin. For osteoid osteoma and osteoblastoma no cell models have been described. The presence of trabeculae of woven bone surrounding active osteoblasts, could indicate that it arises from osteoblast, or its progenitor the mesenchymal stem cell (61). Mesenchymal stem cells are undifferentiated cells but have the capacity to differentiate into osteoblasts, adipocytes, chondrocytes or myocytes. For osteosarcoma the proposed cell of origin is a topic of debate (62). There are studies that suggest osteoblasts are the cell of origin, or that osteosarcoma originates from mesenchymal stem cells.
The evidence from studies that suggest that osteoblasts are the cell of origin of osteosarcoma is mostly based on mouse models. Studies have shown that mice develop osteosarcoma when

Trp53 is deleted in osteoblast cells, throughout different stages of differentiation, by utilizing promotors that are specific to cells of the osteoblast lineage (63, 64).
Other studies have been published that mesenchymal stem cells rather than osteoblast are the cell-of-origin. Since mesenchymal stem cells are the progenitor cells of bone-forming osteoblasts, it is likely that bone-forming tumours arise during the differentiation process of mesenchymal stem cells. An overview of the differentiation of mesenchymal stem cells towards the osteogenic lineage is shown in **Figure 1**. Mesenchymal stem cells originating from mice are reported to spontaneously transform *in vitro*, which showed aneuploidy and loss of *Cdkn2a* similar to human osteosarcoma (65, 66). Furthermore, mice injected with transformed murine mesenchymal stem cells formed undifferentiated pleomorphic sarcoma or osteosarcoma (65, 67, 68). In human mesenchymal stem cells *in vitro* spontaneous transformation towards osteosarcoma has not been reported, but genetic manipulation of these cells by deletion of *TP53* or *RB1* has led to malignant transformation (69). In mouse studies, injection of mesenchymal stem cells carrying a deletion of *TP53* and RB1, or a combination of *MYC* overexpression and *CDKN2A* loss led to the formation of osteosarcoma (70, 71).

Figure 1. Mesenchymal stem cells differentiate towards osteoblast. During each stage of osteogenic differentiation different transcription factors and osteogenic markers play a role. Figure is adapted from reference (72). Templates adapted from Servier Medical Art, licensed under a Creative Commons attribution 3.0 Unported License.

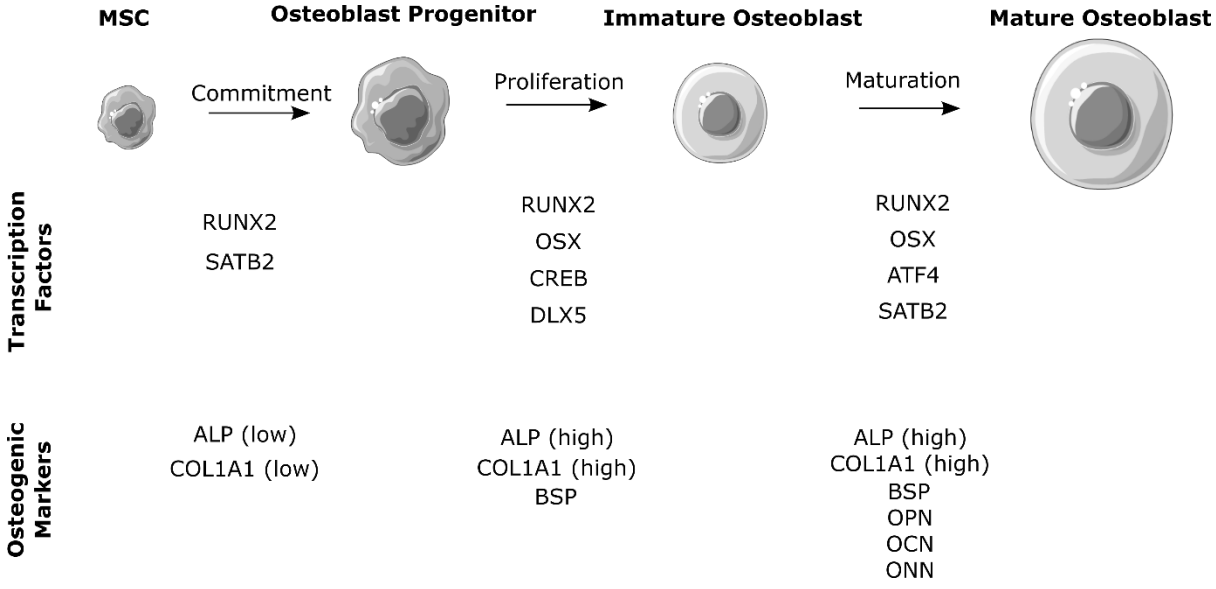

Cell lines

Among the most often used cell models are cultured cell lines, which have originated from patient material. Osteosarcoma cell lines are widely used not only to study osteosarcoma but also for general cell biology research applications, as osteosarcoma cell lines are among the human cell lines that are easily transfected (59). The ease of culture and high growth speed of osteosarcoma cell lines could also explain the exponential rise in publications using osteosarcoma cell lines (29). Among the most commonly used osteosarcoma cell lines there is high heterogeneity in metastatic potential, differentiation capacity and *in vivo* tumorigenicity, which also reflects the heterogeneity observed in osteosarcoma patients (73).

Cell lines can either be derived from human osteosarcoma or from animals. One animal model in particular is of great interest for studying human osteosarcoma: dogs. The incidence of osteosarcoma in dogs is 10 times higher compared to humans, and most often occur in large dog breeds (74). Since osteosarcoma is a rare bone tumour in humans, this makes dogs an attractive alternative model to study pathogenesis and for pre-clinical drug testing. Previous studies have already shown that osteosarcoma cell lines and tumours derived from dogs show similar genetic alterations compared to human osteosarcoma, including alterations in *TP53* (75, 76).

3D models for mesenchymal tumours

3D models are cell models in which cultured cells are not in direct contact with a plastic culture surface. The cells are not cultured in monolayer, and therefore cells can interact with other cells and produce extra-cellular matrix, which characterizes mesenchymal tumours and distinguishes them from epithelial tumours. It was previously shown that response to drugs also heavily relies on these interactions (77), illustrating the importance of 3D models. Moreover, larger 3D cultures show oxygen and nutrient gradients which resemble the oxygen and nutrient gradients found in tumours.

Many different types of 3D cell models for tumour cells have been developed. In general, 3D tumour models can be grown as organoids or as spheroids, also called multicellular tumour spheroids (MCTS) (78) or in scaffolds. Tumour organoids are clusters of different cell types that are present in the original tumour, for example cancer associated fibroblasts and tumour cells, whereas tumour spheroids only consist of tumour cells. Although tumour organoid models have gained popularity as a 3D model, in the case of mesenchymal tumours the tumour cells are mostly surrounded by self-produced extra-cellular matrix, which makes the organoid model less suitable. Instead, the spheroid model in which tumour cells can be grown on their own is most often used (60). Multicellular tumour spheroids have successfully been generated for osteosarcoma cells, and shown response to chemotherapeutic drugs, such as doxorubicin, although they were more resistant compared to 2D cultures (79). The transition

of 2D cultured cells into 3D by generating multicellular tumour spheroids, in which cells form aggregates without touching the culture plastic, can be done with different methods. An overview is shown in **Figure 2,** and can be divided by scaffold-free models or scaffold-based models. Scaffold-free models include liquid overlay culture or hanging droplet culture (80). With liquid overlay cultures, cells are seeded onto a non-adherent surface and form spheroids. The hanging droplet method involves the generation of droplets of cells on a surface that is placed upside-down, resulting in the formation of spheroids by gravitational forces. In 3D cultures that make use of a scaffold, the scaffolds are generated from biomaterials and typically contain elements that are also found in the extra-cellular matrix. Studies have been published where scaffolds have successfully been generated based on collagen, alginate, hyaluronic acid, hydroxyapatite or a combination of aforementioned materials (81, 82).

Not only is the 3D culture method important, the type of cell to use for 3D culture is of equal importance. Typically, in 3D culture studies cells that have been previously cultured in 2D are transitioned into a 3D environment. However, cell lines can change over time after extensive culturing in 2D, including chromosomal rearrangement or mutations (83). To overcome this problem, cells can also be cultured into 3D straight from the source material, such as a primary tumour, and therefore has not come into contact with a plastic culture surface. Since many different types of 3D culture exist, it remains challenging to identify the best and most representative culture method for a complex and heterogenous tumour such as osteosarcoma (84).

Figure 2. Overview of different types of 3D culture. Cells can be cultured in 3D either with or without a scaffold. Scaffold-free models can be generated by the hanging droplet method, in which cells are dropped onto a surface and placed upside down to form spheroids, or by the liquid overlay method, where cells are seeded onto a non-adherent surface to form spheroids. In scaffold-based models, cells are cultured inside structures made from biomaterials, for example collagen. For each method, advantages and disadvantages are described. Figure adapted from https://cytosmart.com/resources/spheroids

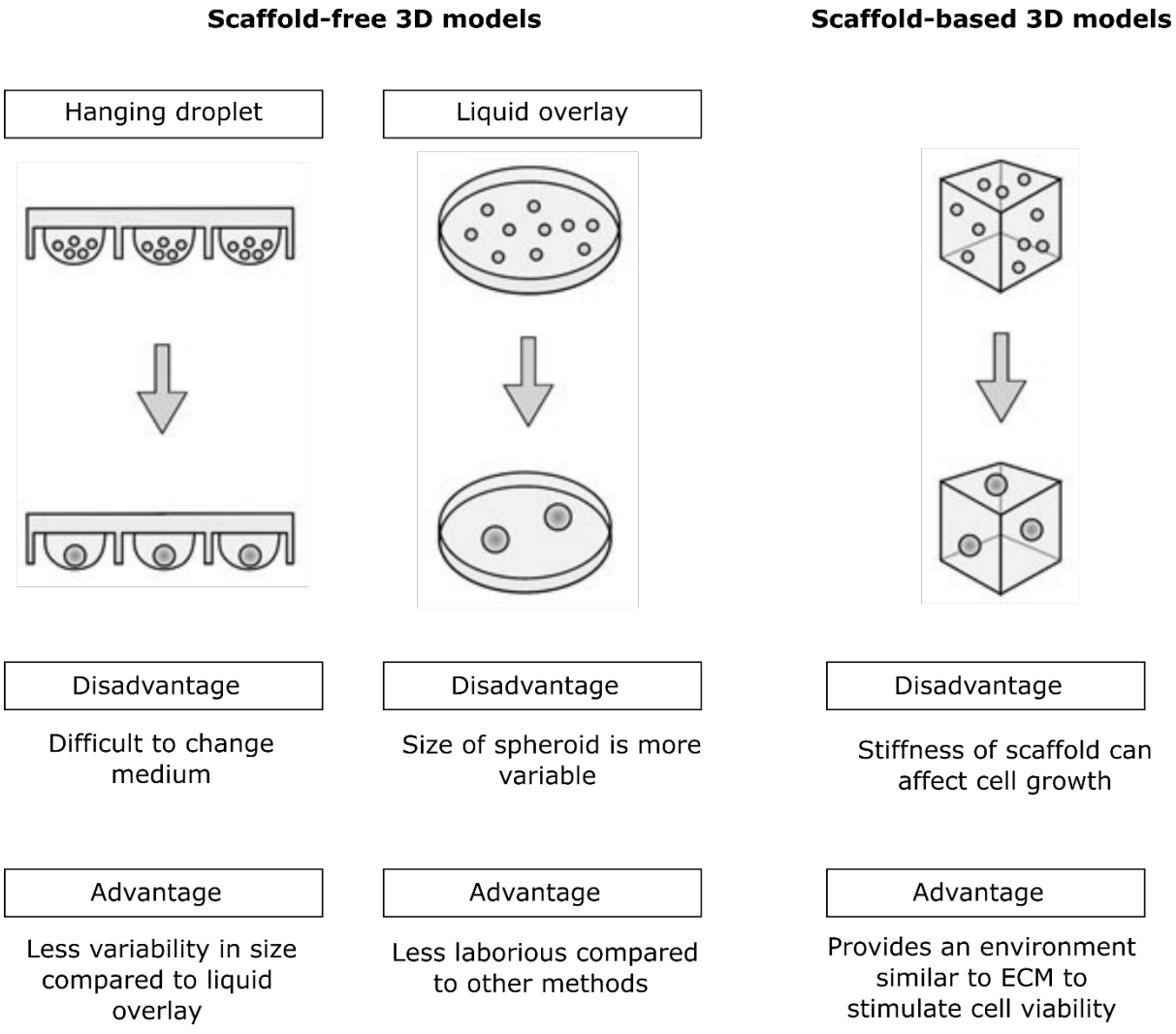

Aim and outline of this thesis

The aim of this thesis is to study the pathogenesis of osteoid osteoma, osteoblastoma and osteosarcoma by generating *in vitro* models, and utilize these models to understand tumorigenesis and to discover novel therapeutic options for osteosarcoma. In **chapter 2** all novel insights within the molecular pathology, clinical presentation and histology of osteoid osteoma, osteoblastoma and osteosarcoma are summarized and reviewed.

In the first part of this thesis, the development of *in vitro* models to study the pathogenesis of bone-forming tumours of the skeleton is described. In **chapter 3** a mesenchymal stem cell-based model for osteoid osteoma and osteoblastoma has been generated. In this model, mesenchymal stem cells overexpress a truncated form of FOS protein, which is a recurrent alteration in osteoid osteoma and osteoblastoma. The proliferation rate and osteogenic differentiation capacity of these cells have been determined, in order to investigate the role of FOS in the pathogenesis of osteoid osteoma and osteoblastoma. In **chapter 4** another mesenchymal stem cell-based model is described, in which spontaneously transformed murine and canine mesenchymal stem cells show similarities to sarcomas with complex genomics, with many copy number alterations and aneuploidy. Furthermore, these transformed cells formed (osteo) sarcoma after subcutaneous injection in a mouse model. This model has been used to identify the driver events in sarcoma with complex genomics.

In the second part of this thesis, different *in vitro* models of osteosarcoma are used to identify novel therapeutic strategies. In **chapter 5** the murine mesenchymal stem cell model for osteosarcoma from chapter 4 is used in which loss of *CDKN2A* and/or *CDKN2B* has been discovered. In this chapter it was investigated whether loss of *CDKN2A* and/or *CDKN2B* is an early event in osteosarcoma genesis. Furthermore, since loss of this locus can indicate that cells are sensitive to CDK4/CDK6 inhibition, the sensitivity of osteosarcoma cells to CDK4/CDK6 inhibitor palbociclib was investigated, which could be used in osteosarcoma patients with intact Rb and that show loss of p16 or overexpression of CDK4/CDK6. **Chapter 6** describes a potential novel therapeutic strategy for osteosarcoma patients with low *NAPRT* expression. Using both 2D and 3D cultured osteosarcoma cell line models, the sensitivity of cells to NAMPT inhibitor FK866 was tested, which targets the NAD salvage synthesis pathway. **Chapter 7** shows the development of osteosarcoma patient-derived 3D cultures, which have been used to test genome-informed targeted therapy for osteosarcoma. Finally, the thesis is summarized and discussed in **chapter 8**.

References

1. Lam SW, van Ijzendoorn DGP, Cleton-Jansen AM, Szuhai K, Bovée JVMG. Molecular Pathology of Bone Tumors. The Journal of Molecular Diagnostics. 2019;21(2):171-82.
2. WHO classification of tumours of soft tissue and bone, 5th edition. Lyon, France: WHO Classification of Tumours Editorial Board; 2020.
3. Frassica FJ, Waltrip RL, Sponseller PD, Ma LD, McCarthy EF, Jr. Clinicopathologic features and treatment of osteoid osteoma and osteoblastoma in children and adolescents. The Orthopedic clinics of North America. 1996;27(3):559-74.
4. Jaffe HL. Osteoid-osteoma. Proceedings of the Royal Society of Medicine. 1953;46(12):1007-12.
5. Jaffe H. Osteoid osteoma: a benign osteoblastic tumor composed of osteoid and atypical bone. Archives of Surgery. 1935;31(5):709-28.
6. Fittall MW, Mifsud W, Pillay N, Ye H, Strobl AC, Verfaillie A, et al. Recurrent rearrangements of FOS and FOSB define osteoblastoma. Nat Commun. 2018;9(1):2150.
7. van IJzendoorn DG, de Jong D, Romagosa C, Picci P, Benassi MS, Gambarotti M, et al. Fusion events lead to truncation of FOS in epithelioid hemangioma of bone. Genes Chromosomes Cancer. 2015;54(9):565-74.
8. Huang SC, Zhang L, Sung YS, Chen CL, Krausz T, Dickson BC, et al. Frequent FOS Gene Rearrangements in Epithelioid Hemangioma: A Molecular Study of 58 Cases With Morphologic Reappraisal. The American journal of surgical pathology. 2015;39(10):1313-21.
9. Lam SW, Cleven AHG, Briaire-de Bruijn IH, Schreuder WH, Kroon HM, Savci-Heijink DC, et al. FOS Rearrangement and Expression in Cementoblastoma. The American journal of surgical pathology. 2021;45(5):690-3.
10. Lam SW, Cleven AHG, Kroon HM, Briaire-de Bruijn IH, Szuhai K, Bovee J. Utility of FOS as diagnostic marker for osteoid osteoma and osteoblastoma. Virchows Arch. 2020;476(3):455-63.
11. Amary F, Markert E, Berisha F, Ye H, Gerrand C, Cool P, et al. FOS Expression in Osteoid Osteoma and Osteoblastoma: A Valuable Ancillary Diagnostic Tool. The American journal of surgical pathology. 2019;43(12):1661-7.
12. Shaulian E, Karin M. AP-1 in cell proliferation and survival. Oncogene. 2001;20.
13. Ozanne BW, Spence HJ, McGarry LC, Hennigan RF. Transcription factors control invasion: AP-1 the first among equals. Oncogene. 2007;26(1):1-10.
14. Stephens PJ, Greenman CD, Fu B, Yang F, Bignell GR, Mudie LJ, et al. Massive genomic rearrangement acquired in a single catastrophic event during cancer development. Cell. 2011;144(1):27-40.
15. Behjati S, Tarpey PS, Haase K, Ye H, Young MD, Alexandrov LB, et al. Recurrent mutation of IGF signalling genes and distinct patterns of genomic rearrangement in osteosarcoma. Nat Commun. 2017;8:15936.
16. Helman LJ, Meltzer P. Mechanisms of sarcoma development. Nat Rev Cancer. 2003;3(9):685-94.
17. Chen X, Bahrami A, Pappo A, Easton J, Dalton J, Hedlund E, et al. Recurrent somatic structural variations contribute to tumorigenesis in pediatric osteosarcoma. Cell Rep. 2014;7(1):104-12.
18. Perry JA, Kiezun A, Tonzi P, Van Allen EM, Carter SL, Baca SC, et al. Complementary genomic approaches highlight the PI3K/mTOR pathway as a common vulnerability in osteosarcoma. Proc Natl Acad Sci U S A. 2014;111(51):E5564-73.
19. Kovac M, Blattmann C, Ribi S, Smida J, Mueller NS, Engert F, et al. Exome sequencing of osteosarcoma reveals mutation signatures reminiscent of BRCA deficiency. Nat Commun. 2015;6:8940.
20. Kneisl JS, Simon MA. Medical management compared with operative treatment for osteoid-osteoma. The Journal of bone and joint surgery American volume. 1992;74(2):179-85.

21. Goto T, Shinoda Y, Okuma T, Ogura K, Tsuda Y, Yamakawa K, et al. Administration of nonsteroidal anti-inflammatory drugs accelerates spontaneous healing of osteoid osteoma. Archives of orthopaedic and trauma surgery. 2011;131(5):619-25.
22. Atesok KI, Alman BA, Schemitsch EH, Peyser A, Mankin H. Osteoid osteoma and osteoblastoma. The Journal of the American Academy of Orthopaedic Surgeons. 2011;19(11):678-89.
23. Lucas DR, Unni KK, McLeod RA, O'Connor MI, Sim FH. Osteoblastoma: clinicopathologic study of 306 cases. Hum Pathol. 1994;25(2):117-34.
24. Berry M, Mankin H, Gebhardt M, Rosenberg A, Hornicek F. Osteoblastoma: a 30-year study of 99 cases. Journal of surgical oncology. 2008;98(3):179-83.
25. Ta HT, Dass CR, Choong PF, Dunstan DE. Osteosarcoma treatment: state of the art. Cancer metastasis reviews. 2009;28(1-2):247-63.
26. Ferrari S, Smeland S, Mercuri M, Bertoni F, Longhi A, Ruggieri P, et al. Neoadjuvant chemotherapy with high-dose Ifosfamide, high-dose methotrexate, cisplatin, and doxorubicin for patients with localized osteosarcoma of the extremity: a joint study by the Italian and Scandinavian Sarcoma Groups. J Clin Oncol. 2005;23(34):8845-52.
27. Smeland S, Bielack SS, Whelan J, Bernstein M, Hogendoorn P, Krailo MD, et al. Survival and prognosis with osteosarcoma: outcomes in more than 2000 patients in the EURAMOS-1 (European and American Osteosarcoma Study) cohort. Eur J Cancer. 2019;109:36-50.
28. Ottaviani G, Jaffe N. The epidemiology of osteosarcoma. Cancer Treat Res. 2009;1552(3).
29. Peterse EFP, van Leeuwen TN, Cleton-Jansen AM. A researcher's perspective on the quantity of osteosarcoma in vitro studies. J Bone Oncol. 2017;7:29-31.
30. Duffy MJ, Synnott NC, O'Grady S, Crown J. Targeting p53 for the treatment of cancer. Seminars in cancer biology. 2020.
31. Bykov VJN, Eriksson SE, Bianchi J, Wiman KG. Targeting mutant p53 for efficient cancer therapy. Nat Rev Cancer. 2018;18(2):89-102.
32. Duffy MJ, Synnott NC, Crown J. Mutant p53 as a target for cancer treatment. Eur J Cancer. 2017;83:258-65.
33. Perdrix A, Najem A, Saussez S, Awada A, Journe F, Ghanem G, et al. PRIMA-1 and PRIMA-1(Met) (APR-246): From Mutant/Wild Type p53 Reactivation to Unexpected Mechanisms Underlying Their Potent Anti-Tumor Effect in Combinatorial Therapies. Cancers (Basel). 2017;9(12).
34. Weinberg R. The Retinoblastoma Protein and Cell Cycle Control. Cell. 1995;81:323-30.
35. Trial of Palbociclib in Second Line of Advanced Sarcomas With CDK4 Overexpression: Identifier NCT03242382; [Available from: https://clinicaltrials.gov/ct2/show/study/NCT03242382.
36. Abemaciclib for Bone and Soft Tissue Sarcoma With Cyclin-Dependent Kinase (CDK) Pathway Alteration: Identifier NCT04040205; [Available from: https://clinicaltrials.gov/ct2/show/NCT04040205.
37. Engert F, Kovac M, Baumhoer D. Osteosarcoma cells with genetic signatures of BRCAness are susceptible to the PARP inhibitor talazoparib alone or in combination with chemotherapeutics. Oncotarget. 2017;8(30):48794-806.
38. Holme H, Gulati A, Brough R, Fleuren EDG, Bajrami I, Campbell J, et al. Chemosensitivity profiling of osteosarcoma tumour cell lines identifies a model of BRCAness. Scientific Reports. 2018;8(1).
39. Study of Onivyde With Talazoparib or Temozolomide in Children With Recurrent Solid Tumors and Ewing Sarcoma: Identifier NCT04901702; [
40. Olaparib in Treating Patients With Relapsed or Refractory Advanced Solid Tumors, Non-Hodgkin Lymphoma, or Histiocytic Disorders With Defects in DNA Damage Repair Genes (A Pediatric MATCH Treatment Trial): Identifier NCT03233204; [
41. Rettew AN, Getty PJ, Greenfield EM. Receptor tyrosine kinases in osteosarcoma: not just the usual suspects. Advances in experimental medicine and biology. 2014;804:47-66.

42. Suehara Y, Alex D, Bowman A, Middha S, Zehir A, Chakravarty D, et al. Clinical Genomic Sequencing of Pediatric and Adult Osteosarcoma Reveals Distinct Molecular Subsets with Potentially Targetable Alterations. Clin Cancer Res. 2019;25(21):6346-56.
43. Tian Z, Niu X, Yao W. Receptor Tyrosine Kinases in Osteosarcoma Treatment: Which Is the Key Target? Front Oncol. 2020;10:1642.
44. Burrow S, Andrulis IL, Pollak M, Bell RS. Expression of insulin-like growth factor receptor, IGF-1, and IGF-2 in primary and metastatic osteosarcoma. Journal of surgical oncology. 1998;69(1):21-7.
45. Anderson PM, Bielack SS, Gorlick RG, Skubitz K, Daw NC, Herzog CE, et al. A phase II study of clinical activity of SCH 717454 (robatumumab) in patients with relapsed osteosarcoma and Ewing sarcoma. Pediatr Blood Cancer. 2016;63(10):1761-70.
46. Ameline B, Kovac M, Nathrath M, Barenboim M, Witt O, Krieg AH, et al. Overactivation of the IGF signalling pathway in osteosarcoma: a potential therapeutic target? J Pathol Clin Res. 2021;7(2):165-72.
47. Ren L, Hong ES, Mendoza A, Issaq S, Hoang CT, Lizardo M, et al. Metabolomics uncovers a link between inositol metabolism and osteosarcoma metastasis. Oncotarget. 2017;8.
48. Rathore R, Caldwell KE, Schutt C, Brashears CB, Prudner BC, Ehrhardt WR, et al. Metabolic compensation activates pro-survival mTORC1 signaling upon 3-phosphoglycerate dehydrogenase inhibition in osteosarcoma. Cell Rep. 2021;34(4):108678.
49. Zhang J, Yu XH, Yan YG, Wang C, Wang WJ. PI3K/Akt signaling in osteosarcoma. Clin Chim Acta. 2015;444:182-92.
50. Xie ZG, Xie Y, Dong QR. Inhibition of the mammalian target of rapamycin leads to autophagy activation and cell death of MG63 osteosarcoma cells. Oncol Lett. 2013;6(5):1465-9.
51. Wagner LM, Fouladi M, Ahmed A, Krailo MD, Weigel B, DuBois SG, et al. Phase II study of cixutumumab in combination with temsirolimus in pediatric patients and young adults with recurrent or refractory sarcoma: a report from the Children's Oncology Group. Pediatr Blood Cancer. 2015;62(3):440-4.
52. Müller CR, Smeland S, Bauer HC, Saeter G, Strander H. Interferon-alpha as the only adjuvant treatment in high-grade osteosarcoma: long term results of the Karolinska Hospital series. Acta Oncol. 2005;44(5):475-80.
53. Meyers PA, Schwartz CL, Krailo MD, Healey JH, Bernstein ML, Betcher D, et al. Osteosarcoma: the addition of muramyl tripeptide to chemotherapy improves overall survival--a report from the Children's Oncology Group. J Clin Oncol. 2008;26(4):633-8.
54. Bielack SS, Smeland S, Whelan JS, Marina N, Jovic G, Hook JM, et al. Methotrexate, Doxorubicin, and Cisplatin (MAP) Plus Maintenance Pegylated Interferon Alfa-2b Versus MAP Alone in Patients With Resectable High-Grade Osteosarcoma and Good Histologic Response to Preoperative MAP: First Results of the EURAMOS-1 Good Response Randomized Controlled Trial. J Clin Oncol. 2015;33(20):2279-87.
55. Koirala P, Roth ME, Gill J, Piperdi S, Chinai JM, Geller DS, et al. Immune infiltration and PD-L1 expression in the tumor microenvironment are prognostic in osteosarcoma. Sci Rep. 2016;6:30093.
56. Pu F, Chen F, Zhang Z, Qing X, Lin H, Zhao L, et al. TIM-3 expression and its association with overall survival in primary osteosarcoma. Oncol Lett. 2019;18(5):5294-300.
57. Poon VI, Roth M, Piperdi S, Geller D, Gill J, Rudzinski ER, et al. Ganglioside GD2 expression is maintained upon recurrence in patients with osteosarcoma. Clin Sarcoma Res. 2015;5(1):4.
58. Lin Z, Wu Z, Luo W. Chimeric Antigen Receptor T-Cell Therapy: The Light of Day for Osteosarcoma. Cancers (Basel). 2021;13(17).
59. Mohseny AB, Hogendoorn PC, Cleton-Jansen AM. Osteosarcoma models: from cell lines to zebrafish. Sarcoma. 2012;2012:417271.
60. De Luca A, Raimondi L, Salamanna F, Carina V, Costa V, Bellavia D, et al. Relevance of 3d culture systems to study osteosarcoma environment. J Exp Clin Cancer Res. 2018;37(1):2.

61. Tepelenis K, Skandalakis GP, Papathanakos G, Kefala MA, Kitsouli A, Barbouti A, et al. Osteoid Osteoma: An Updated Review of Epidemiology, Pathogenesis, Clinical Presentation, Radiological Features, and Treatment Option. In vivo (Athens, Greece). 2021;35(4):1929-38.
62. Mutsaers AJ, Walkley CR. Cells of origin in osteosarcoma: mesenchymal stem cells or osteoblast committed cells? Bone. 2014;62:56-63.
63. Walkley CR, Qudsi R, Sankaran VG, Perry JA, Gostissa M, Roth SI, et al. Conditional mouse osteosarcoma, dependent on p53 loss and potentiated by loss of Rb, mimics the human disease. Genes Dev. 2008;22(12):1662-76.
64. Mutsaers AJ, Ng AJ, Baker EK, Russell MR, Chalk AM, Wall M, et al. Modeling distinct osteosarcoma subtypes in vivo using Cre:lox and lineage-restricted transgenic shRNA. Bone. 2013;55(1):166-78.
65. Mohseny AB, Szuhai K, Romeo S, Buddingh EP, Briaire-de Bruijn I, de Jong D, et al. Osteosarcoma originates from mesenchymal stem cells in consequence of aneuploidization and genomic loss of Cdkn2. J Pathol. 2009;219(3):294-305.
66. Tolar J, Nauta AJ, Osborn MJ, Panoskaltsis Mortari A, McElmurry RT, Bell S, et al. Sarcoma Derived from Cultured Mesenchymal Stem Cells. Stem Cells. 2007;25(2):371-9.
67. Xu S, De Becker A, De Raeve H, Van Camp B, Vanderkerken K, Van Riet I. In vitro expanded bone marrow-derived murine (C57Bl/KaLwRij) mesenchymal stem cells can acquire CD34 expression and induce sarcoma formation in vivo. Biochem Biophys Res Commun. 2012;424(3):391-7.
68. Zhou YF, Bosch-Marce M, Okuyama H, Krishnamachary B, Kimura H, Zhang L, et al. Spontaneous transformation of cultured mouse bone marrow-derived stromal cells. Cancer Res. 2006;66(22):10849-54.
69. Li N, Yang R, Zhang W, Dorfman H, Rao P, Gorlick R. Genetically transforming human mesenchymal stem cells to sarcomas: changes in cellular phenotype and multilineage differentiation potential. Cancer. 2009;115(20):4795-806.
70. Rubio R, Gutierrez-Aranda I, Saez-Castillo AI, Labarga A, Rosu-Myles M, Gonzalez-Garcia S, et al. The differentiation stage of p53-Rb-deficient bone marrow mesenchymal stem cells imposes the phenotype of in vivo sarcoma development. Oncogene. 2013;32(41):4970-80.
71. Shimizu T, Ishikawa T, Sugihara E, Kuninaka S, Miyamoto T, Mabuchi Y, et al. c-MYC overexpression with loss of Ink4a/Arf transforms bone marrow stromal cells into osteosarcoma accompanied by loss of adipogenesis. Oncogene. 2010;29(42):5687-99.
72. Amarasekara DS, Kim S, Rho J. Regulation of Osteoblast Differentiation by Cytokine Networks. Int J Mol Sci. 2021;22(6).
73. Mohseny AB, Machado I, Cai Y, Schaefer KL, Serra M, Hogendoorn PC, et al. Functional characterization of osteosarcoma cell lines provides representative models to study the human disease. Lab Invest. 2011;91(8):1195-205.
74. Fenger JM, London CA, Kisseberth WC. Canine osteosarcoma: a naturally occurring disease to inform pediatric oncology. Ilar j. 2014;55(1):69-85.
75. Gola C, Giannuzzi D, Rinaldi A, Iussich S, Modesto P, Morello E, et al. Genomic and Transcriptomic Characterization of Canine Osteosarcoma Cell Lines: A Valuable Resource in Translational Medicine. Frontiers in veterinary science. 2021;8:666838.
76. Gardner HL, Sivaprakasam K, Briones N, Zismann V, Perdigones N, Drenner K, et al. Canine osteosarcoma genome sequencing identifies recurrent mutations in DMD and the histone methyltransferase gene SETD2. Commun Biol. 2019;2:266.
77. Bissell MJ, Radisky D. Putting tumours in context. Nat Rev Cancer. 2001;1(1):46-54.
78. Gunti S, Hoke ATK, Vu KP, London NR, Jr. Organoid and Spheroid Tumor Models: Techniques and Applications. Cancers (Basel). 2021;13(4).
79. Rimann M, Laternser S, Gvozdenovic A, Muff R, Fuchs B, Kelm JM, et al. An in vitro osteosarcoma 3D microtissue model for drug development. Journal of biotechnology. 2014;189:129-35.

80. Raghavan S, Mehta P, Horst EN, Ward MR, Rowley KR, Mehta G. Comparative analysis of tumor spheroid generation techniques for differential in vitro drug toxicity. Oncotarget. 2016;7(13):16948-61.
81. Akeda K, Nishimura A, Satonaka H, Shintani K, Kusuzaki K, Matsumine A, et al. Three-dimensional alginate spheroid culture system of murine osteosarcoma. Oncol Rep. 2009;22(5):997-1003.
82. Bassi G, Panseri S, Dozio SM, Sandri M, Campodoni E, Dapporto M, et al. Scaffold-based 3D cellular models mimicking the heterogeneity of osteosarcoma stem cell niche. Sci Rep. 2020;10(1):22294.
83. Lorsch JR, Collins FS, Lippincott-Schwartz J. Cell Biology. Fixing problems with cell lines. Science (New York, NY). 2014;346(6216):1452-3.
84. Chow T, Wutami I, Lucarelli E, Choong PF, Duchi S, Di Bella C. Creating In Vitro Three-Dimensional Tumor Models: A Guide for the Biofabrication of a Primary Osteosarcoma Model. Tissue Engineering Part B: Reviews. 2020.

Chapter 2

What's new in bone forming tumours of the skeleton?

Natasja Franceschini, Suk Wai Lam, Anne-Marie Cleton-Jansen and Judith V.M.G. Bovée

Published: *Virchows Arch. 2020; 476(1):147*

Abstract

Bone tumours are difficult to diagnose and treat, as they are rare and over 60 different subtypes are recognized. The emergence of next-generation sequencing has partly elucidated the molecular mechanisms behind these tumours, including the group of bone forming tumours (osteoma, osteoid osteoma, osteoblastoma and osteosarcoma). Increased knowledge on the molecular mechanism could help to identify novel diagnostic markers and/or treatment options.

Osteoid osteoma and osteoblastoma are bone forming tumours without malignant potential that have overlapping morphology. They were recently shown to carry *FOS* and – to a lesser extent - *FOSB* rearrangements suggesting that these tumours are closely related. The presence of these rearrangements could help discriminate these entities from other lesions with woven bone deposition. Osteosarcoma is a malignant bone forming tumour for which different histological subtypes are recognized. High grade osteosarcoma is the prototype of a complex karyotype tumour, and extensive research exploring its molecular background has identified phenomena like chromothripsis and kataegis, and some recurrent alterations. Due to lack of specificity, this has not led to a valuable novel diagnostic marker so far. Nevertheless, these studies have also pointed towards potential targetable drivers of which the therapeutic merit remains to be further explored.

Introduction

Bone tumours are rare and therefore considered difficult to diagnose and treat. They comprise a heterogeneous group of tumours, where most subtypes have a distinct clinical and histological presentation.
Histologically, over 60 different bone tumours are recognized. Some are difficult to separate as there can be extensive morphological and even immunohistochemical overlap. Distinction is important as these tumours differ in clinical behaviour and thus in required treatment. In recent years, many papers have been published unravelling the molecular background of several bone tumours, mostly using deep sequencing techniques. From the molecular point of view, these tumours can be roughly divided in two main groups, as a conceptual framework (1): tumours can either have a simple or complex karyotype. The group of tumours with a simple karyotype are usually monomorphic, and driven by a specific mutation or translocation. The tumours with complex karyotype are more often pleomorphic, show aneuploidy, with many copy number alterations and (random) translocations and mutations. The group of skeletal tumours that are characterized by bone deposition contains osteoma, osteoid osteoma, osteoblastoma and osteosarcoma (**Table 1**). Osteoma is benign and composed of mature lamellar bone, has a simple karyotype, occurs in patients with Gardner's syndrome and as a consequence is caused by a germline mutation in the *APC* gene. Osteoid osteoma and osteoblastoma are histologically identical, have a simple karyotype and deep sequencing studies have recently unravelled a recurrent translocation (2). This is in contrast with high grade osteosarcoma, for which a complex karyotype showing aneuploidy, multiple copy number alterations, (random) translocations and mutations is the hallmark (3). This review will focus on osteoid osteoma/osteoblastoma and high grade osteosarcoma, as examples for simple karyotype, translocation driven, versus complex karyotype tumours, respectively.

Osteoid osteoma and osteoblastoma

Novel *FOS* and *FOSB* rearrangements were recently found in osteoid osteoma and osteoblastoma (2). These tumours account for 3% and 1% of all primary bone tumours, respectively (4). These two entities are histologically similar, and only slightly differ in their clinical presentation. At present they are arbitrarily divided by tumour size below or above 2 cm in diameter, although the recent finding that they share the same molecular alteration might suggest that they represent the same disease (4-7).

Clinical presentation

Osteoid osteoma and osteoblastoma typically present during the second decade of life, with men being overrepresented (male to female ratio 2:1) (4). Osteoid osteoma is usually located at the long bones in the lower extremity, but other commonly described sites

involve the spine, upper extremity, hands, feet, and pelvis (4, 5, 7, 8). The most prominent clinical symptom of osteoid osteoma is frequent and severe night pain that responds adequately to nonsteroidal anti-inflammatory drugs (NSAIDs) (4, 5). Osteoblastoma is larger in size, and the majority are localized in the posterior column of the spine (4, 5, 9), resulting in neurologic symptoms as a recurring sign (4). Pain is frequently present, but in contrast to osteoid osteoma does not respond to administration of NSAIDs (4, 5). Both osteoid osteoma and osteoblastomas have no malignant potential, although osteoblastoma can behave as a locally aggressive tumour (4). For radiologists, the diagnosis of osteoid osteoma is usually straight forward, showing a characteristic oval radiolucency (nidus) with surrounding sclerosis, while osteoblastoma can be accompanied by a more broad differential diagnosis depending on its location, including aneurysmal bone cyst, giant cell tumour of bone, and osteosarcoma (4, 10).

Table 1. Clinical features, radiology, karyotype, and molecular pathology of osteoma, osteoid osteoma, osteoblastoma and conventional osteosarcoma.

	OSTEOMA	**OSTEOID OSTEOMA**	**OSTEOBLASTOMA**	**CONVENTIONAL OSTEOSARCOMA**
CLINICAL FEATURES	● Benign ● Mostly found incidentally ● Located at bone surface	● Benign ● <2 cm in size ● Located in long bones	● Locally aggressive ● >2 cm in size ● Located in posterior column of spine	● Malignant ● Located at metaphysis of long bones
RADIOLOGY	Homogenous and sharply demarcated tumour	Oval radiolucency (nidus) with surrounding sclerosis	Often lytic lesion , may be alike aneurysmal bone cyst	Lytic, sclerotic or mixed lesion, often expanding into surrounding soft tissue
KARYOTYPE	Simple karyotype	Simple karyotype	Simple karyotype	Complex karyotype
MOLECULAR PATHOLOGY	Associated with Gardner's syndrome: germline *APC* mutation	*FOS* - and to a lesser extent *FOSB* - translocations	*FOS* - and to a lesser extent *FOSB* - translocations	Chromothripsis and kateagis with most often alterations in *TP53*

Histology

Osteoid osteoma and osteoblastoma are histologically indistinguishable (11) (**Fig. 1A, B**). Both tumours are composed of irregular trabeculae of woven bone, lined with active osteoblasts. In osteoid osteoma, the central area of the lesion (nidus) is sharply demarcated, and surrounded by hyper-vascularized sclerotic bone. In between the trabeculae there is loose vascularized stroma (7, 8). Osteoblastoma can show slightly more haphazardly arranged trabeculae (6).

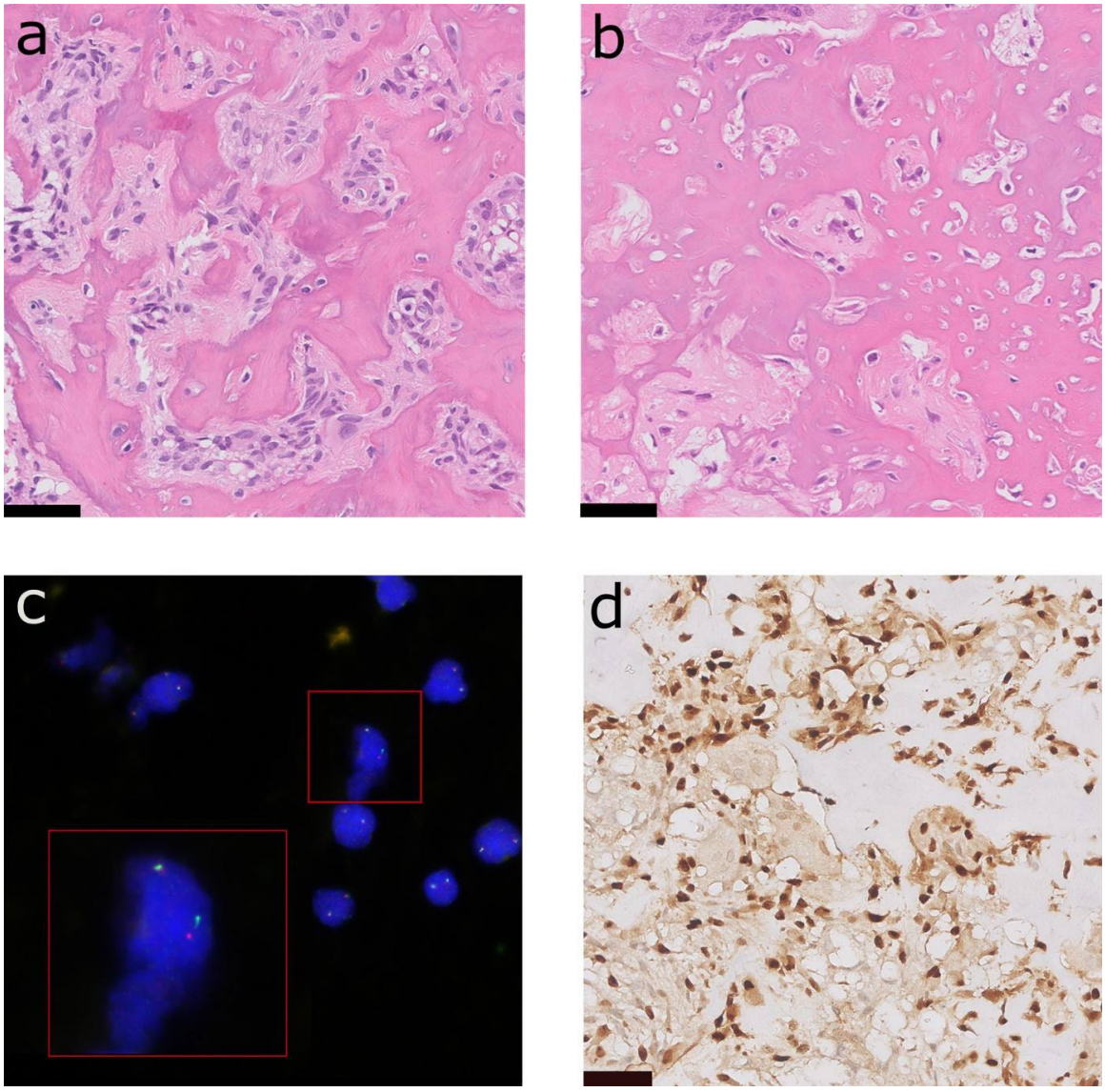

Fig. 1 Osteoid osteoma and osteoblastoma. **A.** Osteoid osteoma, and **B.** Osteoblastoma show identical morphology at hematoxylin and eosin staining, with deposition of woven bone by osteoblast-like tumor cells. **C.** Fluorescence in-situ hybridization (FISH) showing *FOS* rearrangement in osteoblastoma. **D.** Immunohistochemical staining for FOS in osteoblastoma showing nuclear overexpression in the tumor cells. Scale bar is 50 µm

Molecular pathology

Before the elucidation of the genetic background of osteoid osteoma and osteoblastoma, clonal chromosome aberrations were reported in two osteoblastomas, with structural alterations involving 22q13.1 (12), and only non-recurrent rearrangements were found using cytogenic studies (13). In 2018, in a quiet genomic background with paucity of somatic alterations, recurrent *FOS* and – to a lesser extent - *FOSB* rearrangements were found in both osteoid osteoma and osteoblastoma using RNA sequencing, demonstrating that both tumours were similar at the molecular level. In 5 out of 6 cases, *FOS* rearrangements were present, while the remaining case showed rearrangements involving its paralogue, *FOSB*. All *FOS* breakpoints were exonic, and involved exon 4. Rearrangement partners were both introns of others genes (*ANKH, KIAA1199, MYO1B*), or intergenic regions (2). Equivalent to *FOS* rearranged epithelioid hemangioma (14, 15), stop codons were encountered at, or early after the break points, leading to truncation of the protein with retention of the leucine zipper, and therefore its function as a transcription factor. Functional studies in epithelioid hemangioma demonstrated that the truncated protein was more resistant to degradation (16). In the *FOSB* rearranged osteoblastoma, rearrangement resulted in an in frame fusion connecting *PPP1R10* to *FOSB*, leading to altered signalling, due to promotor swapping (2). Strikingly, *FOSB* fusions were also involved in pseudomyogenic hemangioendothelioma and atypical epithelioid hemangioma, resulting in promoter swapping (17, 18). As genetic alterations in these vascular tumours are identical to those found in osteoid osteoma and osteoblastoma, one can speculate that a comparable molecular mechanism of tumorigenesis is operable in osteoid osteoma and osteoblastoma.

These novel molecular findings have provided new tools to improve diagnostic accuracy, as both fluorescence in-situ hybridization (FISH) and immunohistochemical staining can detect *FOS* rearrangements (**Fig. 1C, D**). Fluorescence in-situ hybridization (FISH) was performed in an independent cohort and showed in the majority of cases rearrangements involving *FOS* and to a lesser extent *FOSB* (2). In a follow-up study immunohistochemistry showed strong and diffuse nuclear staining in the majority (79%) of osteoid osteomas and osteoblastomas, using a FOS antibody against the N-terminus (19). However, a previously published small study cohort demonstrated that osteoid osteoma and osteoblastoma lacked strong nuclear expression of FOS, indicating variability in sensitivity between different antibodies (20). In terms of specificity, strong nuclear expression of FOS has been detected in a subset of other bone forming tumours, and was only rarely present in osteosarcoma (2, 20). Notably, in mouse models the *c-fos* oncogene caused osteosarcoma, when fused with a highly active promotor and the *v-fos* 3' untranslated region (21). This is intriguing as in human tumours *FOS* and *FOSB* rearrangements have so far only been identified in vascular and bone forming tumours lacking malignant potential (14, 15, 17, 18).

Osteosarcoma

Osteosarcoma is the most common primary malignant tumour of the bone (22). The 5-year overall survival for osteosarcoma patients is 71% and has not improved in the last decades, clearly indicating that novel therapeutic strategies are needed (23). Fortunately, many papers have been published gradually unravelling the pathogenesis of osteosarcoma, which might help develop new therapeutic targets.

Clinical presentation

Primary high grade osteosarcoma occurs most often in young children and adolescents, but there is a second peak at a later age, often secondary to radiation or Paget's disease (24). Osteosarcoma has a slight male predominance (25). Patients with osteosarcoma often show signs of localized deep pain, especially manifest at night, developed over a longer period of a few weeks to months. This could also be in combination with limited mobility, or localized warmth. A small palpable mass can be present, which is tender during physical examination (26).

For diagnosis of conventional osteosarcoma, a radiograph is made in two planes, in which the lesion appears as lytic, sclerotic or mixed lytic and sclerotic. This lesion often expands into the surrounding soft tissue, with periosteal reaction and destruction of cortical bone (27). MRI- or CT-imaging may provide additional information, guiding the subsequent biopsy of the lesion (27).

Histology

The presence of osteoid, the unmineralized extracellular matrix produced by the tumour cells, is a hallmark of osteosarcoma and visible as a pink dense structure in hematoxylin and eosin stained sections (**Fig. 2A**). Mineralization can occur. Osteosarcoma can arise in the medulla (central) or at the bone surface. Different osteosarcoma subtypes are recognized, based on their clinical presentation in combination with histological and molecular features (**Table 2**) (25). High grade central osteosarcoma is the most common subtype, and most papers published over the last decade, as well as this review, focus on this subtype.

Germline predisposition to osteosarcoma

Certain hereditary syndromes predispose to osteosarcoma, such as Li-Fraumeni syndrome (mutations in *TP53* or, less frequently, *CHEK2*), Retinoblastoma (mutations in *RB1*), and Rothmund-Thomson syndrome (mutations in *RECQL4*) (28-30). Other hereditary syndromes with germline mutations in RecQ Like Helicases, including RAPADILINO syndrome, Baller-Gerold syndrome, Werner syndrome and Bloom syndrome, also have an increased risk for osteosarcoma (31, 32). Another hereditary syndrome in which a helicase is mutated is ATR-X syndrome (Alpha-thalassemia mental retardation syndrome). Patients with ATR-X syndrome show intellectual disability and skeletal abnormalities. Recently, two patients have been reported with ATR-X syndrome that developed osteosarcoma (33, 34).

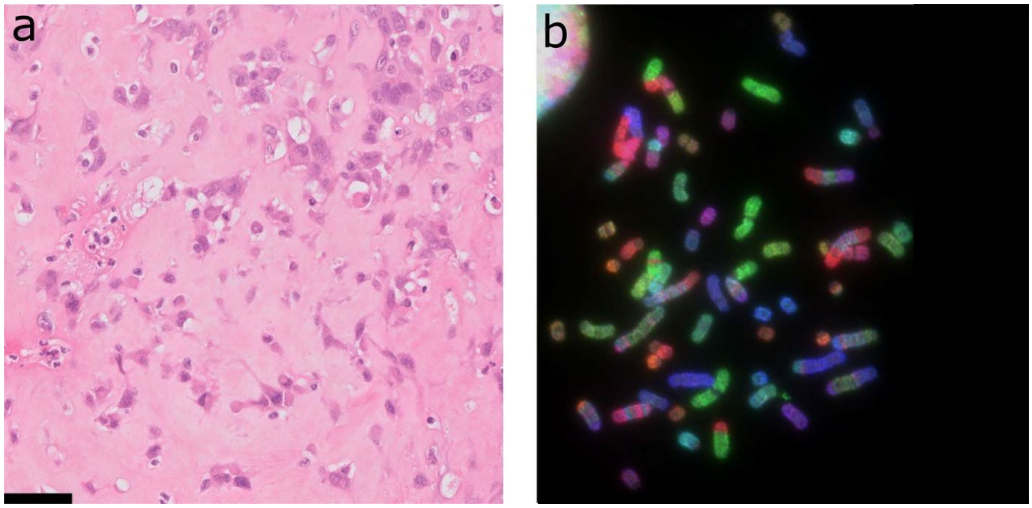

Fig. 2 High grade osteosarcoma. **A.** Conventional osteoblastic osteosarcoma showing atypical cells with abundant deposition of osteoid (hematoxylin and eosin staining). Scale bar is 50 µm. **B.** Combined binary ratio fluorescence in-situ hybridization (COBRA-FISH) (35) showing complex numerical and structural changes which is characteristic of high grade osteosarcoma.

Molecular alterations in osteosarcoma

High grade osteosarcoma is characterized by a complex karyotype with many amplifications, deletions and (random) translocations (Fig. 2B) . This complex genome hampers identification of the driver genes causing genome instability: very few recurrent alterations have been identified in osteosarcoma.

One mechanism explaining the genomic instability in osteosarcoma is chromothripsis, the shattering of one or a few chromosomes into small fragments that are stitched together in a random order and orientation. Chromothripsis occurs in 3% of all cancers and in 30% of osteosarcomas (36). It was first discovered by Stephens et al in chronic lymphocytic leukemia, chordoma and osteosarcoma (36) and later studies have confirmed chromothripsis in osteosarcoma (3, 37, 38). Exome sequencing shows a relatively low mutational burden in osteosarcoma ranging from 0.3-1.2 mutations per mega base, however there is a pattern of localized hypermutation called kataegis in 50% of the tumours (3, 39). These point mutations are non-recurrent, haphazard and cannot be considered as driver genes. Further hampering the identification of driver genes is that no benign precursor of osteosarcoma is known. This is in contrast with for instance colorectal cancer, in which a benign precursor can be used to investigate multi-step progression behind tumorigenesis.

Nevertheless, recent next-generation sequencing studies have revealed known and novel recurrent genetic alterations in osteosarcoma (**Table 3**). Most genes that were found to be altered are involved in maintaining genomic stability. Among the most commonly altered genes in osteosarcoma are the main players in maintaining genome stability: *TP53* and *RB1*.

Table 2. Osteosarcoma subtypes

SUBTYPE	LOCATION	GRADE	HISTOLOGY
LOW GRADE CENTRAL OSTEOSARCOMA	Medulla	Low grade	Spindle cells with low-grade nuclear atypia and well-formed neoplastic woven bone trabeculae, and 12q13 amplification
PAROSTEAL OSTEOSARCOMA	Surface	Low grade	spindle cell proliferation, often with cartilaginous differentiation, and 12q13 amplification
PERIOSTEAL OSTEOSARCOMA	Surface (typically underneath the periosteum)	Intermediate grade	Predominantly chondroblastic bone-forming sarcoma
CONVENTIONAL OSTEOSARCOMA -FIBROBLASTIC -CHONDROBLASTIC -OSTEOBLASTIC	Medulla	High-grade	High grade sarcoma in which the tumour cells produce bone. Tumour cells can be fibroblastic, chondroblast- or osteoblast-like
SMALL CELL OSTEOSARCOMA	Medulla	High-grade	Small cells with scant cytoplasm, associated with variable osteoid formation; may resemble Ewing sarcoma
TELANGIECTATIC OSTEOSARCOMA	Medulla	High-grade	Osteosarcoma composed of blood-filled or empty cystic spaces closely simulating aneurysmal bone cyst
HIGH GRADE SURFACE OSTEOSARCOMA	Surface	High grade	Similar to conventional osteosarcoma

Table 3. Overview of recurrent alterations found in conventional osteosarcoma

GENE	TYPE OF ALTERATION	SOMATIC/GERMLINE	FUNCTION	FREQUENCY IN SPORADIC OS	LITERATURE
TP53	Translocation; Deletion; Mutation	Germline (Li-fraumeni syndrome) and somatic	Genome stability; cell cycle control	47% – 90%	(3, 37, 39, 40)
RB1	Mutation; Deletion	Germline (retinoblastoma) and somatic	Genome stability; cell cycle control	29% – 47%	(3, 39, 40)
MYC	Amplification	Somatic	Cell proliferation	39%	(41)
CCNE1	Amplification	Somatic	Cell cycle control	33%	(41)
DLG2	Deletion	Somatic	Cell signaling	29% - 52%	(3, 42)
COPS3	Amplification	Somatic	Signal transduction	20% - 39%	(37, 39)
AURKB	Amplification	Somatic	Cell cycle	13%	(41)
PTEN	Mutation; Deletion; Copy number alteration	Somatic	Cell cycle control	12% - 50%	(37, 39, 40)
CDKN2A	Deletion	Somatic	Cell cycle control	15%	(40)
ATRX	Mutation; Deletion	Germline (ATR-X syndrome) and somatic	Genome stability; chromatin remodeling; ALT	10% - 29%	(3, 33, 34, 37, 39, 40)
CDKN2A	Mutation; Deletion	Somatic	Cell cycle control	10%	(37)
CDK4	Amplification	Somatic	Regulates RB activity	9% - 11%	(41, 43)
MDM2	Amplification	Somatic	Regulates P53 activity	5% - 12%	(39, 43)
IGF1R	Mutation; Amplification	Somatic	Bone growth and development	5%	(37)
AKT	Amplification	Somatic	Cell proliferation; apoptosis	5%	(41, 44, 45)
RECQL4	Mutation	Germline (Rothmund-Thomson syndrome)	Genome stability	0%	(31)

TP53 and RB1

Mutations in *TP53* can be found in germline or can be sporadic. Previously, using immunohistochemistry or sequencing of the DNA binding domain of *TP53*, mutations were detected in only 20% of osteosarcomas (46). Interestingly, whole genome sequencing studies reveal a much higher percentage (47-90%) of osteosarcomas harbouring *TP53* alterations (3, 37, 39, 40). This difference can be explained by the notion that most *TP53* alterations involve structural alterations, which most often consist of translocations in the first intronic region of *TP53*, which is 10 kb in length. These alterations can only be detected with whole genome sequencing (47).
The second most frequently altered gene in osteosarcoma is *RB1* (Retinoblastoma 1), involved in blocking cells from entering S-phase of the cell cycle (48). Loss of Rb function in osteosarcoma therefore leads to a loss in Rb blockade of cell division. In addition to germline mutations, somatic mutations in *RB1* were identified in 29-47% of osteosarcomas (3, 40).

The importance of *TP53* and *RB1* in osteosarcoma genesis is illustrated by the fact that patients with germline mutations in *TP53* and *RB1* are highly susceptible to cancer and frequently develop sarcomas. Different *in vitro* and *in vivo* studies confirm the important role of *TP53* and *RB1* mutations in sarcoma genesis (49-51). For example, homozygous deletion of *TP53* and *RB1* in osteogenic differentiated murine MSCs gives rise to osteosarcoma when injected into mice (50), while heterozygous deletion of *TP53* is sufficient to induce osteosarcoma in a mouse model (49).

Regulators of p53 and Rb activity

MDM2 (mouse double minute 2 homolog) regulates p53 activity by ubiquitinating p53 protein leading to proteasomal degradation of p53 (52). Up to 12% of high grade osteosarcomas have amplification of the *MDM2*-gene at 12q13-15, but this is much higher (67%) in low-grade central osteosarcoma and parosteal osteosarcoma (43, 53) (Table 2). The *CDK4*-gene (cyclin dependent kinase 4) is located within the same region at 12q13-15 (54) and regulates Rb activity by phosphorylating Rb, resulting in deactivation of Rb. *CDK4* and *MDM2* are often co-amplified and overexpressed in osteosarcoma. *CDK4* is amplified in 67-100% of low-grade osteosarcomas, but rarely in high grade osteosarcoma (9%)(43, 53, 55). As the percentage of *CDK4* and *MDM2* amplifications in low grade central osteosarcoma and parosteal osteosarcoma are much higher than in high grade osteosarcoma, most likely the *CDK4/MDM2* positive high grade tumours represent progression from low grade osteosarcoma (55). Rb activity is also regulated by p16, which normally inhibits both CDK4 and CDK6. P16 is encoded by the *CDKN2A* gene at chromosome 9p21.3, that also encodes for p14. Homozygous deletion of the *CDKN2A* locus, which is associated with poor prognosis in osteosarcoma, eradicates both expression of $p16^{Ink4A}$ and $p14^{ARF}$, of which the latter is a negative regulator of MDM2 (40, 56-58). Therefore, deletion of p16 and p14, similar to co-amplification of *CDK4* and *MDM2*, leads to inactivation of both the p53 and Rb pathway.

Other genome maintenance pathways

In addition to the p53 and Rb pathway, also other pathways involved in maintaining genome stability can be affected by mutations, both in sporadic as well as hereditary osteosarcoma. For instance, *ATRX* mutations can be found both as germline or somatic mutations (59), which is in contrast to mutations in RecQ Like Helicases where only germline mutations have been identified. Around 29% of osteosarcomas harbor somatic mutations in *ATRX* (3). The role of *ATRX* mutations in osteosarcoma genesis is largely unknown. *ATRX* is involved in chromatin remodelling and plays an important role in maintenance of chromosome stability (60). Loss-of-function mutations in *ATRX* can lead to activation of the alternative lengthening of telomeres (ALT) pathway, maintaining the length of chromosome-ends (61). ALT is found in 59% of osteosarcomas, which is much higher as compared to other cancers such as carcinomas (5-15%) (62).

DNA repair is essential in maintaining genome stability. For instance, homologous recombination, the DNA repair pathway in which BRCA plays an important role, is crucial in maintaining genome stability. A recent whole exome sequencing (WES) study revealed that a subset of osteosarcomas resemble features of *BRCA* mutant tumours (40). These tumours show loss of heterozygosity, genomic instability and a mutation signature of substitutions and deletions that is also found in breast cancers with *BRCA1/2* mutations. Around 80% of osteosarcomas show this BRCAness signature (40). As this signature is linked to defects in homologous recombination, this vulnerability might be exploited with PARP inhibitors based on the principle of synthetic lethality. Indeed, different *in vitro* studies with osteosarcoma cell lines show that osteosarcoma cells are sensitive to PARP inhibitors (63, 64). These results are promising, suggesting a possible new therapeutic strategy for osteosarcoma. However, further investigation on homologous recombination deficiency and PARP inhibitor sensitivity in osteosarcoma is needed.

Hormonal pathways

Although the genes that play a role in genome stability are among the most frequently mutated genes in osteosarcoma (*RB1, TP53, CDK4, MDM2, ATRX*), these genes function in essential cell survival pathways. Therefore these genes are difficult to specifically target in the treatment of osteosarcoma. Fortunately, also mutations in other genes are frequently found that are easier to target as they are involved in hormonal pathways. For example, mutations in genes involved in IGF (insulin-like growth factor) signaling, including the IGF1 receptor (*IGF1R*), were identified in around 7-14% of osteosarcomas, with many of these genes having altered activity compared to normal human osteoblasts or mesenchymal stem cells (37, 65). The IGF signaling pathway is known to be important in normal bone growth, bone development, and bone metabolism and it is therefore not surprising that it might also play a role in osteosarcoma pathogenesis (66, 67). These findings provide a rationale to explore anti-IGFR therapy as a treatment strategy for a subset of osteosarcomas.

The estrogen hormonal pathway is also altered in osteosarcoma. Healthy osteoblasts normally express estrogen receptor alpha (ERα), but this is lacking in osteosarcoma (68). Until recently the mechanism behind the inactivation of estrogen receptor in osteosarcoma was not known. In a recent study it was found that ERα was hypermethylated in osteosarcoma, which can be ameliorated by the DNA methyltransferase inhibitor DAC (69). DAC could re-express ERα and subsequently restored defective osteogenic differentiation and inhibited proliferation in osteosarcoma cells. This study illustrates that epigenetic alterations such as hypermethylation of genes are also important in osteosarcoma genesis.

Conclusion

There is an ongoing shift from traditional cancer classification based solely on histopathology towards incorporation of molecular pathology in routine diagnostics, which ultimately can aid diagnostic decision making. Among the group of bone forming tumours of the skeleton, the use of deep sequencing has unravelled the molecular background of osteoid osteoma and osteoblastoma. The discovery of *FOS* and *FOSB* rearrangements found in osteoid osteoma and osteoblastoma have not only given insight in tumorigenesis, but have also provided the bone tumour pathologist with a novel diagnostic tool to improve diagnostic accuracy.
For high grade osteosarcoma, due to its complex genomic background, no specific, recurrent genetic alteration has been found that can explain tumorigenesis, or can be used for diagnosis or treatment. Even though the number of publications on drugs that allegedly inhibit osteosarcoma growth has exponentially increased over the past few years, these claims are often based on *in vitro* studies including one single cell line (70). Most of these publications are from Chinese institutes and often consist of investigations on the effect of traditional medicine on osteosarcoma. The remarkable increase of these studies is most probably the corollary of the convenient tissue culture properties of osteosarcoma cell lines and obscures findings of real significance.

Nevertheless, in the last years several deep sequencing studies have been published that contribute towards the understanding of osteosarcoma pathogenesis. These next-generation sequencing studies have revealed underlying mechanisms, such as chromothripsis and kataegis, as well as a number of genes and pathways associated with osteosarcoma, especially those involved in genome maintainance (*TP53, RB1, ATRX* and homologous recombination) or hormonal signalling (IGF and ER signalling). The results from these studies could be the stepping stone towards the development of novel diagnostics/prognostic markers or treatment options. Since most of the alterations that were identified are not recurrent and involved in crucial processes in the cell such as genome stability, cell cycle, and DNA repair, it will be a huge challenge for the coming decade to translate these findings into novel treatment options. In contrast to targeting genes involved in maintaining genome stability, such as *TP53* and *RB1*, targeting the hormonal pathways, especially IGF and estrogen, seems more promising.

Acknowledgements

The authors would like to thank Dr. K. Szuhai, Department of Cell and Chemical Biology, Leiden University Medical Center, for providing figure 2B.

References

1. Lam SW, van Ijzendoorn DGP, Cleton-Jansen AM, Szuhai K, Bovée JVMG. Molecular Pathology of Bone Tumors. The Journal of Molecular Diagnostics. 2019;21(2):171-82.
2. Fittall MW, Mifsud W, Pillay N, Ye H, Strobl AC, Verfaillie A, et al. Recurrent rearrangements of FOS and FOSB define osteoblastoma. Nat Commun. 2018;9(1):2150.
3. Chen X, Bahrami A, Pappo A, Easton J, Dalton J, Hedlund E, et al. Recurrent somatic structural variations contribute to tumorigenesis in pediatric osteosarcoma. Cell Rep. 2014;7(1):104-12.
4. Atesok KI, Alman BA, Schemitsch EH, Peyser A, Mankin H. Osteoid osteoma and osteoblastoma. The Journal of the American Academy of Orthopaedic Surgeons. 2011;19(11):678-89.
5. Greenspan A. Benign bone-forming lesions: osteoma, osteoid osteoma, and osteoblastoma. Clinical, imaging, pathologic, and differential considerations. Skeletal radiology. 1993;22(7):485-500.
6. Schajowicz F, Lemos C. Osteoid osteoma and osteoblastoma. Closely related entities of osteoblastic derivation. Acta orthopaedica Scandinavica. 1970;41(3):272-91.
7. Jaffe HL. Osteoid-osteoma. Proceedings of the Royal Society of Medicine. 1953;46(12):1007-12.
8. Jaffe HL. "Osteoid-osteoma": a bening osteoblastic tumor composed of osteoid and atypical bone. Arch Surg. 1935;31(5):709-28.
9. Cerase A, Priolo F. Skeletal benign bone-forming lesions. Eur J Radiol. 1998;27 Suppl 1:S91-7.
10. Kroon HM, Schurmans J. Osteoblastoma: clinical and radiologic findings in 98 new cases. Radiology. 1990;175(3):783-90.
11. Frassica FJ, Waltrip RL, Sponseller PD, Ma LD, McCarthy EF, Jr. Clinicopathologic features and treatment of osteoid osteoma and osteoblastoma in children and adolescents. The Orthopedic clinics of North America. 1996;27(3):559-74.
12. Nord KH, Nilsson J, Arbajian E, Vult von Steyern F, Brosjo O, Cleton-Jansen AM, et al. Recurrent chromosome 22 deletions in osteoblastoma affect inhibitors of the Wnt/beta-catenin signaling pathway. PLoS One. 2013;8(11):e80725.
13. Giannico G, Holt GE, Homlar KC, Johnson J, Pinnt J, Bridge JA. Osteoblastoma characterized by a three-way translocation: report of a case and review of the literature. Cancer Genet Cytogenet. 2009;195(2):168-71.
14. van IJzendoorn DGP, de Jong D, Romagosa C, Picci P, Benassi MS, Gambarotti M, et al. Fusion events lead to truncation of FOS in epithelioid hemangioma of bone. Genes Chromosomes Cancer. 2015;54(9):565-74.
15. Huang SC, Zhang L, Sung YS, Chen CL, Krausz T, Dickson BC, et al. Frequent FOS Gene Rearrangements in Epithelioid Hemangioma: A Molecular Study of 58 Cases With Morphologic Reappraisal. The American journal of surgical pathology. 2015;39(10):1313-21.
16. van IJzendoorn DGP, Forghany Z, Liebelt F, Vertegaal AC, Jochemsen AG, Bovee J, et al. Functional analyses of a human vascular tumor FOS variant identify a novel degradation mechanism and a link to tumorigenesis. J Biol Chem. 2017;292(52):21282-90.
17. Walther C, Tayebwa J, Lilljebjorn H, Magnusson L, Nilsson J, von Steyern FV, et al. A novel SERPINE1-FOSB fusion gene results in transcriptional up-regulation of FOSB in pseudomyogenic haemangioendothelioma. J Pathol. 2014;232(5):534-40.
18. Antonescu CR, Chen HW, Zhang L, Sung YS, Panicek D, Agaram NP, et al. ZFP36-FOSB fusion defines a subset of epithelioid hemangioma with atypical features. Genes Chromosomes Cancer. 2014;53(11):951-9.
19. Lam SW, Cleven AH, Briaire-de Bruijn IH, Bovee JVMG. Utility of FOS and FOSB immunohistochemistry in osteoid osteoma and osteoblastoma. Lab Invest. 2019;99(1):18.

20. Franchi A, Calzolari A, Zampi G. Immunohistochemical detection of c-fos and c-jun expression in osseous and cartilaginous tumours of the skeleton. Virchows Arch. 1998;432(6):515-9.
21. Grigoriadis AE, Schellander K, Wang Z, Wagner EF. Osteoblasts are target cells for transformation in c-fos transgenic mice. The journal of Cell Biology. 1993;122(3):685-701.
22. Mirabello L, Troisi RJ, Savage SA. Osteosarcoma incidence and survival rates from 1973 to 2004: data from the Surveillance, Epidemiology, and End Results Program. Cancer. 2009;115(7):1531-43.
23. Smeland S, Bielack SS, Whelan J, Bernstein M, Hogendoorn P, Krailo MD, et al. Survival and prognosis with osteosarcoma: outcomes in more than 2000 patients in the EURAMOS-1 (European and American Osteosarcoma Study) cohort. Eur J Cancer. 2019;109:36-50.
24. Ottaviani G, Jaffe N. The epidemiology of osteosarcoma. Cancer Treat Res. 2009;1552(3).
25. Osteogenic tumors. In: Fletcher C, Bridge JA, Hogendoorn P, Mertens F, editors. WHO classification of tumours of soft tissue and bone, 4th. Lyon: IARC; 2013.
26. Widhe B, Widhe T. Initial Symptoms and Clinal Features in Osteosarcoma and Ewing Sarcoma. The Journal of Bone and Joint Surgery. 2000;82(5).
27. Casali PG, Bielack S, Abecassis N, Aro HT, Bauer S, Biagini R, et al. Bone sarcomas: ESMO–PaedCan–EURACAN Clinical Practice Guidelines for diagnosis, treatment and follow-up†. Annals of Oncology. 2018;29(Supplement_4):iv79-iv95.
28. Ruijs MWG, Broeks A, Menko FH, Ausems MGEM, Wagner A, Oldenburg R, et al. The contribution of CHEK2 to the TP53-negative Li-Fraumeni phenotype. Hereditary Cancer in Clinical Practice. 2009;7(1).
29. Ruijs MWG, Verhoef S, Rookus MA, Pruntel R, van der Hout AH, Hogervorst FBL, et al. TP53 germline mutation testing in 180 families suspected of Li-Fraumeni syndrome: mutation detection rate and relative frequency of cancers in different familial phenotypes. Journal of Medical Genetics. 2010;47(6):421-8.
30. Marees T, Moll AC, Imhof SM, de Boer MR, Ringens PJ, van Leeuwen FE. Risk of second malignancies in survivors of retinoblastoma: more than 40 years of follow-up. J Natl Cancer Inst. 2008;100(24):1771-9.
31. Hameed M, Mandelker D. Tumor Syndromes Predisposing to Osteosarcoma. Adv Anat Pathol. 2018;25:217-22.
32. Dietschy T, Shevelev I, Stagljar I. The molecular role of the Rothmund-Thomson-, RAPADILINO- and Baller-Gerold-gene product, RECQL4: recent progress. Cell Mol Life Sci. 2007;64(7-8):796-802.
33. Ji J, Quindipan C, Parham D, Shen L, Ruble D, Bootwalla M, et al. Inherited germline ATRX mutation in two brothers with ATR-X syndrome and osteosarcoma. American Journal of Medical Genetics Part A. 2017;173(5):1390-5.
34. Smolle MA, Heitzer E, Geigl JB, Al Kaissi A, Liegl-Atzwanger B, Seidel MG, et al. A novel mutation in ATRX associated with intellectual disability, syndromic features, and osteosarcoma. Pediatr Blood Cancer. 2017;64(10).
35. Szuhai K, Tanke HJ. COBRA: combined binary ratio labeling of nucleic-acid probes for multi-color fluorescence in situ hybridization karyotyping. Nat Protoc. 2006;1(1):264-75.
36. Stephens PJ, Greenman CD, Fu B, Yang F, Bignell GR, Mudie LJ, et al. Massive genomic rearrangement acquired in a single catastrophic event during cancer development. Cell. 2011;144(1):27-40.
37. Behjati S, Tarpey PS, Haase K, Ye H, Young MD, Alexandrov LB, et al. Recurrent mutation of IGF signalling genes and distinct patterns of genomic rearrangement in osteosarcoma. Nat Commun. 2017;8:15936.
38. Smida J, Xu H, Zhang Y, Baumhoer D, Ribi S, Kovac M, et al. Genome-wide analysis of somatic copy number alterations and chromosomal breakages in osteosarcoma. Int J Cancer. 2017;141(4):816-28.

39. Perry JA, Kiezun A, Tonzi P, Van Allen EM, Carter SL, Baca SC, et al. Complementary genomic approaches highlight the PI3K/mTOR pathway as a common vulnerability in osteosarcoma. Proc Natl Acad Sci U S A. 2014;111(51):E5564-73.
40. Kovac M, Blattmann C, Ribi S, Smida J, Mueller NS, Engert F, et al. Exome sequencing of osteosarcoma reveals mutation signatures reminiscent of BRCA deficiency. Nat Commun. 2015;6:8940.
41. Sayles LC, Breese MR, Koehne AL, Leung SG, Lee AG, Liu HY, et al. Genome-Informed Targeted Therapy for Osteosarcoma. Cancer Discov. 2019;9(1):46-63.
42. Shao YW, Wood GA, Lu J, Tang QL, Liu J, Molyneux S, et al. Cross-species genomics identifies DLG2 as a tumor suppressor in osteosarcoma. Oncogene. 2019;38(2):291-8.
43. Mejia-Guerrero S, Quejada M, Gokgoz N, Gill M, Parkes RK, Wunder JS, et al. Characterization of the 12q15MDM2and 12q13-14CDK4amplicons and clinical correlations in osteosarcoma. Genes, Chromosomes and Cancer. 2010:NA-NA.
44. Kuijjer ML, van den Akker BEWM, Hilhorst R, Mommersteeg M, Buddingh EP, Serra M, et al. Kinome and mRNA expression profiling of high-grade osteosarcoma cell lines implies Akt signaling as possible target for therapy. BMC Medical Genomics. 2014;7(4).
45. Baranski Z, Booij TH, Kuijjer ML, de Jong Y, Cleton-Jansen AM, Price LS, et al. MEK inhibition induces apoptosis in osteosarcoma cells with constitutive ERK1/2 phosphorylation. Genes and Cancer. 2015;6(11):503-12.
46. Radig K, Schneider-Stock R, Oda Y, Neumann W, Mittler U, Roessner A. Mutation spectrum of p53 gene in highly malignant human osteosarcomas. Gen Diagn Pathol. 1996;142(1):25-32.
47. Macintyre G, Ylstra B, Brenton JD. Sequencing Structural Variants in Cancer for Precision Therapeutics. Trends in Genetics. 2016;32(9):530-42.
48. Weinberg R. The Retinoblastoma Protein and Cell Cycle Control. Cell. 1995;81:323-30.
49. Walkley CR, Qudsi R, Sankaran VG, Perry JA, Gostissa M, Roth SI, et al. Conditional mouse osteosarcoma, dependent on p53 loss and potentiated by loss of Rb, mimics the human disease. Genes Dev. 2008;22(12):1662-76.
50. Rubio R, Gutierrez-Aranda I, Saez-Castillo AI, Labarga A, Rosu-Myles M, Gonzalez-Garcia S, et al. The differentiation stage of p53-Rb-deficient bone marrow mesenchymal stem cells imposes the phenotype of in vivo sarcoma development. Oncogene. 2013;32(41):4970-80.
51. Wang J-Y, Wu P-K, Chen PC-H, Lee C-W, Chen W-M, Hung S-C. Generation of Osteosarcomas from a Combination of Rb Silencing and c-Myc Overexpression in Human Mesenchymal Stem Cells. STEM CELLS Translational Medicine. 2017;6(2):512-26.
52. Freedman DA, Levine AJ. Functions of the MDM2 oncoprotein. Cellular and Molecular Life Sciences. 1999;55:96-107.
53. Yoshida A, Ushiku T, Motoi T, Shibata T, Beppu Y, Fukayama M, et al. Immunohistochemical analysis of MDM2 and CDK4 distinguishes low-grade osteosarcoma from benign mimics. Mod Pathol. 2010;23(9):1279-88.
54. Wunder JS, Eppert K, Burrow SR, Gogkoz N, Bell RS, Andrulis IL. Co-amplification and overexpression of CDK4, SAS and MDM2 occurs frequently in human parosteal osteosarcomas. Oncogene. 1999;18:783-8.
55. Dujardin F, Binh MB, Bouvier C, Gomez-Brouchet A, Larousserie F, Muret A, et al. MDM2 and CDK4 immunohistochemistry is a valuable tool in the differential diagnosis of low-grade osteosarcomas and other primary fibro-osseous lesions of the bone. Mod Pathol. 2011;24(5):624-37.
56. Mohseny AB, Szuhai K, Romeo S, Buddingh EP, Briaire-de Bruijn I, de Jong D, et al. Osteosarcoma originates from mesenchymal stem cells in consequence of aneuploidization and genomic loss of Cdkn2. J Pathol. 2009;219(3):294-305.
57. Mohseny AB, Tieken C, van der Velden PA, Szuhai K, de Andrea C, Hogendoorn PC, et al. Small deletions but not methylation underlie CDKN2A/p16 loss of expression in conventional osteosarcoma. Genes Chromosomes Cancer. 2010;49(12):1095-103.

58. Park Y-B, Park MJ, Kimura K, Shimizu K, Lee SH, Yokota J. Alterations in the Ink4a/ARF locus and their effects on the growth of human osteosarcoma cell lines. Cancer Genetics and Cytogenetics. 2002;133:105-11.
59. Helman LJ, Meltzer P. Mechanisms of sarcoma development. Nat Rev Cancer. 2003;3(9):685-94.
60. De La Fuente R, Baumann C, Viveiros MM. Role of ATRX in chromatin structure and function: implications for chromosome instability and human disease. Reproduction. 2011;142(2):221-34.
61. Yost KE, Clatterbuck Soper SF, Walker RL, Pineda MA, Zhu YJ, Ester CD, et al. Rapid and reversible suppression of ALT by DAXX in osteosarcoma cells. Sci Rep. 2019;9(1):4544.
62. Henson JD, Reddel RR. Assaying and investigating Alternative Lengthening of Telomeres activity in human cells and cancers. FEBS Lett. 2010;584(17):3800-11.
63. Engert F, Kovac M, Baumhoer D. Osteosarcoma cells with genetic signatures of BRCAness are susceptible to the PARP inhibitor talazoparib alone or in combination with chemotherapeutics. Oncotarget. 2017;8(30):48794-806.
64. Holme H, Gulati A, Brough R, Fleuren EDG, Bajrami I, Campbell J, et al. Chemosensitivity profiling of osteosarcoma tumour cell lines identifies a model of BRCAness. Scientific Reports. 2018;8(1).
65. Kuijjer M, Peterse EFP, Van den Akker BEWM, I.H. B-dB, Serra M, Meza-Zepeda LA, et al. IRIGF1R signaling as potential target for treatment of high-grade osteosarcoma. BMC Cancer. 2013;13(245).
66. Conover CA. Insulin-like growth factor-binding proteins and bone metabolism. Am J Physiol Endocrinol Metab. 2008;294(1):E10-4.
67. McCarthy TL, Centrella M. Local IGF-I expression and bone formation. Growth Horm IGF Res. 2001;11(4):213-9.
68. Dohi O, Hatori M, Suzuki T, Ono K, Hosaka M, Akahira J, et al. Sex steroid receptors expression and hormone-induced cell proliferation in human osteosarcoma. Cancer Sci. 2008;99(3):518-23.
69. Lillo Osuna MA, Garcia-Lopez J, El Ayachi I, Fatima I, Khalid AB, Kumpati J, et al. Activation of Estrogen Receptor Alpha by Decitabine Inhibits Osteosarcoma Growth and Metastasis. Cancer Res. 2019;79(6):1054-68.
70. Peterse EFP, van Leeuwen TN, Cleton-Jansen AM. A researcher's perspective on the quantity of osteosarcoma in vitro studies. J Bone Oncol. 2017;7:29-31.

Part I

In vitro models of bone-forming tumours

Chapter 3

Truncated FOS reduces osteogenic differentiation capacity in osteoid osteoma and osteoblastoma

Natasja Franceschini, Suk-Wai Lam, Brendy van den Akker, David van IJzendoorn, Harald Mikkers, Anne-Marie Cleton-Jansen, Karoly Szuhai, and Judith V.M.G. Bovée

Abstract

Osteoid osteoma and osteoblastoma are non-malignant bone-forming tumours of the skeleton, characterized by the presence of irregular trabeculae of woven bone. Rearrangements in *FOS,* and less frequently *FOSB*, have recently been identified in osteoid osteoma and osteoblastoma. Identical rearrangements in *FO*S were previously detected in epithelioid hemangioma, where this leads to truncation of the FOS protein in the C-terminal domain causing increased protein stability due to impaired degradation. Since FOS plays a role in osteogenic differentiation, we investigated the effect of FOS truncation on osteogenic differentiation and proliferation in an *in vitro* model for osteoid osteoma and osteoblastoma. In this model, fetal mesenchymal stem cells have been transduced to overexpress truncated (FOSΔ) or full-length FOS as a comparison. Osteogenic differentiation - assessed by measuring mineralization, ALP expression and ALP activity - and proliferation rate were reduced in cells overexpressing truncated FOS (FOSΔ), or FOS with a deletion (FOSΔ376-377) or mutation (FOSL376N) in the C-terminal domain, compared to wild-type mesenchymal stem cells. In contrast, cells overexpressing full-length FOS showed increased proliferation and almost completely lost mineralization. These results demonstrate that the balance between differentiation and proliferation can be disrupted by changes in FOS expression, which may explain the indolent growth and formation of woven bone observed in osteoid osteoma and osteoblastoma.

Introduction

Osteoid osteoma and osteoblastoma are bone-forming tumours of the skeleton. Whereas osteoid osteomas are small in size (<2 cm) and benign, osteoblastomas are larger and can be locally aggressive (1). Despite differences in clinical presentation, the histology of these entities is identical. Both osteoid osteoma and osteoblastoma are composed of trabeculae of woven bone, which can show various degrees of mineralization of the matrix (1). These trabeculae are lined by plump osteoblast-like cells. Another benign tumour that shows morphological similarities to osteoid osteoma and osteoblastoma, but differs in clinical presentation, is cementoblastoma (2). This odontogenic tumour is characterized by the presence of immature cementum-like matrix containing activated cementoblasts, that are indistinguishable from osteoblasts.

Recently it was discovered that osteoid osteoma and osteoblastoma show overexpression of FOS or FOSB due to frequent rearrangements in *FOS* (87%) and – less frequent – *FOSB* (2%) (3). In cementoblastoma, rearrangements in *FOS* and overexpression of FOS have also been identified (2). For osteoid osteoma and osteoblastoma, the rearrangements in *FOS* involve exon 4, leading to a truncation of the FOS protein, as stop-codons are introduced near the breakpoints (**Figure 1A**). Rearrangements leading to truncation of FOS at the same exon in the gene have been previously identified in epithelioid haemangioma (4). Under normal conditions, FOS is a short-lived protein and its levels and stability are highly regulated by different mechanisms both on the RNA stability and post-translational level, including control via the 3'-UTR region, ubiquitin-dependent or ubiquitin-independent proteasomal degradation, and phosphorylation (5-11).
In epithelioid haemangioma, it was shown that truncated FOS was more resistant to proteasomal degradation, caused by the absence of a highly conserved destabilizing element (LLAL region) within the last four amino acids in the C-terminus of FOS in cells expressing truncated FOS (FOSΔ). The LLAL region acted as a signal for proteasomal degradation, causing cells carrying a mutation (FOSL376N) or deletion (FOSΔ376-377) within the LLAL region to sustain expression of FOS protein (4, 12).
Therefore the truncation of FOS found in osteoid osteoma, osteoblastoma and cementoblastoma lead to stabilization and thus sustained expression of FOS protein. Similar to epithelioid hemangioma, these tumours show strong nuclear expression of FOS in the tumour cells, and therefore overexpression of FOS can be used as a diagnostic tool (13, 14)(**Figure 1B)**.

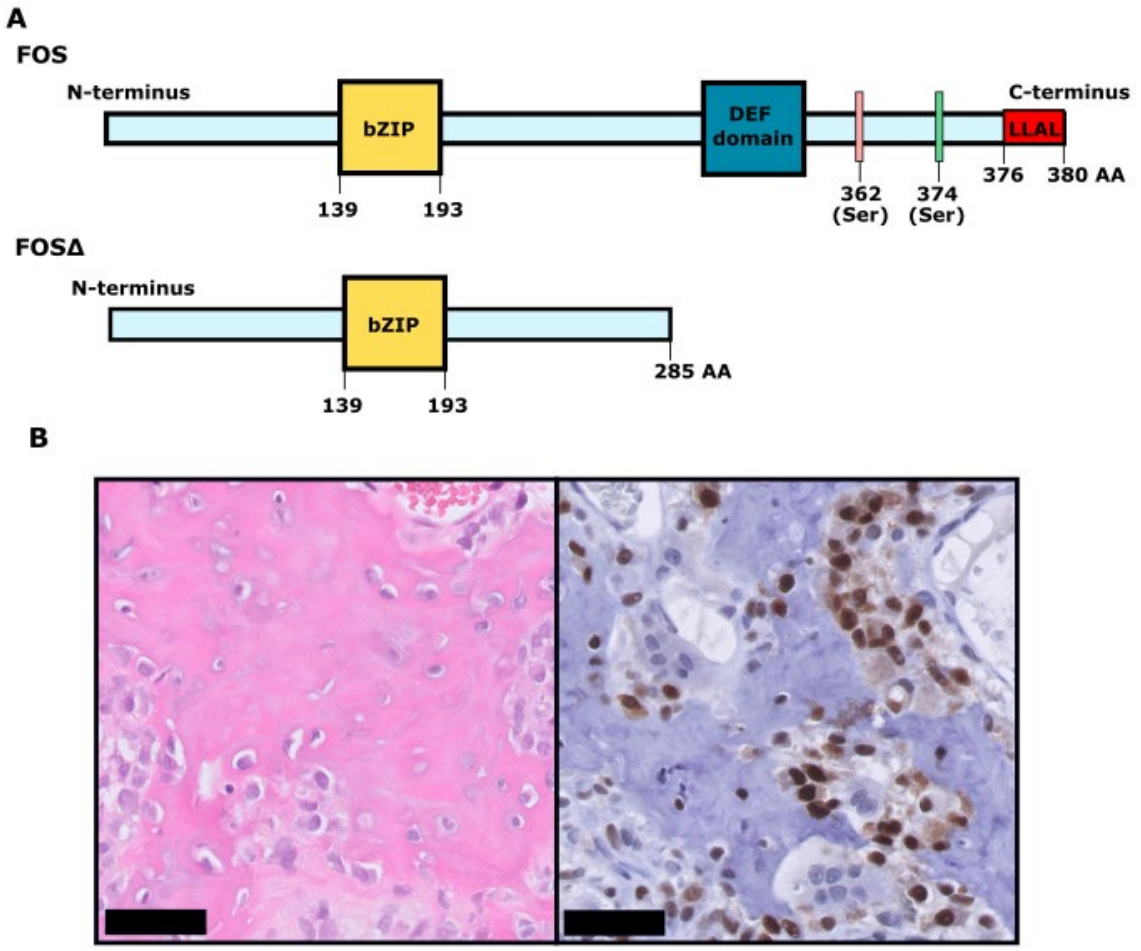

Figure 1. FOS is truncated and overexpressed in osteoid osteoma, osteoblastoma and cementoblastoma. **(A)** Schematic overview of full-length FOS protein (380 amino acids), and the truncated FOS (FOSΔ, 285 amino acids) protein found in osteoid osteoma, osteoblastoma, cementoblastoma and epithelioid haemangioma. Basic-region Leucine Zipper (bZIP) domain, DEF domain (binding site for MAPK) and the LLAL region within the C-terminus of FOS are indicated. The LLAL region is closely located to the phosphorylation sites Ser362 and Ser374. Figure adapted from (4) and (15). (**B**) Haematoxylin and eosin staining demonstrating immature woven bone deposited by osteoblasts (left panel) and FOS immunohistochemical staining (right) depicting overexpression of FOS in osteoid osteoma. Scale bar represents 50 µm.

FOS can form a heterodimer with JUN family proteins, to form the AP-1 complex, and act as a transcription factor. The AP-1 complex is involved in cell growth control and cell transformation, and a plethora of other essential cellular processes (16-18). Sustained FOS expression is sufficient for the transformation of cells (19). Interestingly, transgenic mice overexpressing FOS in bone develop osteosarcoma, although FOS overexpression itself is rarely identified in human osteosarcoma (13, 14, 20-22). The AP-1 complex and FOS also play a role in osteogenic differentiation. During osteogenic differentiation, the expression of FOS increases, which in turn further upregulates other genes involved in osteogenic differentiation (23, 24). For example, the promotors of key osteogenic genes such as alkaline phosphatase, collagen I and osteocalcin all have an AP-1 site (24). AP-1 has previously been

identified as a driver of tumorigenesis in vascular tumours epithelioid hemangioma and pseudomyogenic haemangioendothelioma, that contain similar *FOS,* or *FOSB,* rearrangements (4). It was found that HUVECs expressing truncated FOS displayed increased endothelial sprouting without changing proliferation. These results suggest AP-1 could be driving tumorigenesis both in the vascular as well as in the osteogenic lineage.

This study aims to investigate how alterations in FOS affect osteogenic differentiation and proliferation in osteoid osteoma and osteoblastoma. We hypothesized that truncation of FOS deregulates osteogenic differentiation and/or maturation and possibly proliferation leading to the characteristic presence of immature woven bone in these tumours. Since mesenchymal stem cells are the most likely progenitor cells of osteogenic tumours (25), fetal mesenchymal stem cells (fMSCs) were transduced to overexpress truncated FOS, or full-length FOS as a comparison. We carried out functional analysis of these fMSCs to assess osteogenic differentiation and proliferation. fMSCs overexpressing full-length FOS almost completely lost osteogenic differentiation capacity, whereas osteogenic differentiation was mildly impaired in fMSCs expressing truncated FOS. Furthermore, the proliferation of fMSCs expressing truncated FOS was decreased, whereas fMSCs expressing full-length FOS showed increased proliferation. These differences in osteogenic differentiation and proliferation appeared to be caused specifically by the LLAL region in the C-terminal domain of FOS, as fMSCs expressing FOS protein without the C-terminal proteasomal degradation signal showed similar impairment of proliferation and differentiation as fMSCs expressing FOS with larger truncated regions. Thus, these results demonstrate that the C-terminal domain of FOS protein plays an important role in the balance between osteogenic differentiation and proliferation and that its loss may explain the presence of woven bone and the indolent growth of osteoid osteoma and osteoblastoma.

Materials and Methods

Cell culture

Fetal mesenchymal stem cells (fMSCs) were derived from the femurs of a 22-week-old deceased fetus (abortion with unknown medical cause). fMSCs were collected based on individual written (parental) informed consent after approval by the Medical Ethics Committee of the Leiden University Medical Center (reference number: P08-087). The experiments involving human materials were performed in accordance with the principles outlined in the Declaration of Helsinki (World Medical Association). fMSCs (passage number between 5 and 13) were cultured in αMEM (Gibco) supplemented with 10% FBS, 1% non-essential amino acids (Gibco) and 1% pen/strep (Gibco) in a humidified incubator, with 5% CO_2 and at 37 °C. Cells were tested for mycoplasma.

Lentiviral transduction

FOS constructs have been generated as described previously (4). Briefly, four human FOS cDNAs were used, either containing full-length FOS (FOS FL), a FOS isoform lacking the C-terminal 95 amino acids but including the bZIP domain (FOSΔ, **Figure 1A**), a FOS isoform with a mutation (FOSL376N) or a deletion (FOSΔ376-377) within the C terminal four amino acids (LLAL) containing helical region. These cDNAs were C-terminally fused in-frame with a FLAG tag and cloned into the pLV lentiviral vector, under control of a CMV promotor. For transfection, lentivirus together with polybrene (8 µg/ml) was added to fMSCs. The next day, a medium containing lentivirus was removed and transduced cells were selected with puromycin (5 ng/ml).

Osteogenic differentiation

Cells were seeded at 5000 cells/cm^2 for osteogenic differentiation. One day after seeding, cells were treated with osteogenic compounds: β-glycerophosphate (5 mM, Sigma-Aldrich), dexamethasone (0.1 µM, Sigma-Aldrich), and ascorbate-2-phosphate (0.15 mM, Sigma-Aldrich). Medium with osteogenic compounds was refreshed twice a week. As a negative control, cells were cultured without any osteogenic compounds. Osteogenic differentiation was performed at least three times in independent experiments, by three independent researchers.

Alkaline phosphatase activity assay

After ten days of osteogenic differentiation, cells were lysed with PBS/Triton 0.1% and incubated with pNPP (P7998, Sigma-Aldrich) for 4 minutes. The reaction was stopped with NaOH. Absorption at 405 nm was measured using a microplate reader (Infinite M Plex, Tecan Group Ltd., Zürich, Switzerland). Experiments were performed in triplicate at least three times.

RT-PCR

After one, two or three weeks of osteogenic differentiation, RNA was isolated using Trizol according to the manufacturer's instructions. cDNA synthesis was performed using iScript cDNA Synthesis Kit (1708890, Bio-rad) according to the manufacturer's instructions. For RT-qPCR, iQ SYBR Green Supermix (1708880, Bio-rad) and a Thermal Cycler (Bio-rad) were used, with primers for osteogenic markers *ALPL, COL1A1, SPARC, RUNX2, SPP1* and *BGLAP*. *GAPDH* was used as a reference gene. A list of primers used can be found in **Table 1**. Relative gene expression levels to reference genes were determined with the following formula: $2^{\text{Ct value reference gene – Ct value gene of interest.}}$ Experiments were performed at least two times in duplicate.

Table 1. List of primers

Gene	Forward primer	Reverse primer
ALPL	TCACTCTCCGAGATGGTGGT	GCCTGCTTGGCTTTTCCTTC
COL1A1	AAGACGAAGACATCCCACCAAT	GTCACAGATCACGTCATCGCA
SPARC	CTGGACTACATCGGGCCTTG	CAGGACGTTCTTGAGCCAGT
RUNX2	CCCTGAACTCTGCACCAAGT	GGCTCAGGTAGGAGGGGTAA
SPP1	TTCGCAGACCTGACATCCAG	ACGGCTGTCCCAATCAGAAG
BGLAP	CCTCACACTCCTCGCCCTAT	GCTTGGACACAAAGGCTGCAC
GAPDH	TTCCAGGAGCGAGATCCCT	CACCCATGACGAACATGGG
FOS	GAGAAAAGGAGAATCCGAAGG	GTCAGAGGAAGGCTCATTGC

Alizarin Red staining

After three weeks of osteogenic differentiation, mineralization was determined by Alizarin Red staining. Cells were fixed for 1 hour in cold ethanol and incubated with Alizarin Red S staining solution (2 g Alizarin Red S (02100375, MP Biomedicals, Thermo Fisher Scientific, Waltham, MA, USA) in 60 mL water, pH 4.2) for 5 minutes. For quantification, Alizarin Red staining was rinsed with water and 10% acetic acid was added to each well for 30 minutes. Acetic acid solution containing cells was transferred to a microcentrifuge tube and vortexed. Samples were heated at 85 °C for 10 minutes and centrifuged at 12000 rpm for 15 minutes. The supernatant of each sample was transferred to a 96-well plate and 10% ammonium hydroxide was added to each well to neutralize the acid. Absorbance at 405 nm was measured using a microplate reader (Infinite M Plex, Tecan Group Ltd.). Experiments were performed in triplicate at least three times.

Proliferation assays

To determine proliferation, cells were seeded at 1500 cells per well of a 96-well plate. One, two, three, four or five days after seeding, cells were washed with PBS and incubated with Presto Blue cell viability reagent (Invitrogen, Thermo Fisher Scientific) for 60 minutes and measured using a microplate reader (Infinite M Plex, Tecan Group Ltd.). After read-out, cells were fixed with 4% formaldehyde and stained with 2 µg/mL Hoechst (Invitrogen, Thermo Fisher Scientific). Nuclei were counted using the Cellomics ArrayScan VTI HCS 700 and HCS Studio Cell Analysis Software (Thermo Fisher Scientific). Experiments were performed at least three times in triplicate.

Statistical analysis

All statistical analyses were performed using GraphPad Prism V.9. For multiple comparisons between groups, a Kruskal–Wallis test was used. Groups were compared to pLV. Comparisons were considered statistically significant using a significance level of 5%.

Results

Mesenchymal stem cells expressing truncated FOS have reduced osteogenic differentiation capacity

Fetal mesenchymal stem cells (fMSCs) transduced with constructs containing full-length FOS or truncated FOS (FOSΔ), both showed overexpression of FOS at mRNA level (**Figure 2A**). These cells were used to determine the effect of FOS truncation on osteogenic differentiation. After culture in osteogenic medium, Alizarin Red staining revealed that fMSCs expressing truncated FOS showed a reduction of mineralization ($P = 0.02$), whereas fMSCs expressing full-length FOS lost osteogenic differentiation capacity, almost completely lacking mineralization ($P \leq 0.0001$) (**Figure 2B**). The expression levels of osteogenic markers during three weeks of osteogenic differentiation were variable. Osteogenic markers *BGLAP, OPN* and *RUNX2* showed hardly any expression in fMSCs and therefore no difference between the different constructs could be determined (**Figure S1**). Gene expression of *SPARC* and *COL1A1* was induced upon osteogenic differentiation but with no marked difference between wild-type fMSCs and fMSCs overexpressing FOS (full length or truncated) (**Figure S1**). *ALPL* RNA expression and ALP activity showed a trend towards reduction in fMSCs overexpressing truncated FOS compared to wild-type fMSCs (pLV), although this was not statistically significant ($P = 0.2$ for *ALPL* expression and $P = 0.1$ for ALP activity) (**Figure 2C, 2D**). fMSCs overexpressing full length FOS further reduced *ALPL* expression (although not significant, $P = 0.2$) and ALP activity ($P \leq 0.0001$) compared to wild-type fMSCs (pLV) (**Figure 2C, 2D**).

Mesenchymal stem cells expressing truncated FOS show decreased proliferation

Since sustained expression of FOS is known to induce transformation of cells (19, 26), the proliferation rate of fMSCs expressing full length or truncated FOS was determined. Cell viability, as well as nuclei count, was assessed over a period of five days (**Figure 3A, 3B**). fMSCs expressing truncated FOS (FOSΔ) showed lower proliferation rates compared to wild-type fMSCs ($P \leq 0.05$), whereas fMSCs expressing full-length FOS showed an increase in proliferation rate ($P \leq 0.05$).

Mutations or deletions in the C-terminal region of FOS protein impair osteogenic differentiation capacity similar to truncated FOS

Proliferation rate and osteogenic differentiation capacity were determined for additional FOS constructs to explore whether disruption of the C-terminal region of FOS protein can explain the changes in proliferation and osteogenic differentiation in fMSCs expressing truncated FOS. fMSCs expressing FOSL376N or FOSΔ376-377, which are both alterations located within the LLAL region of the C-terminus of FOS, showed similarly diminished proliferation rate (**Figure 4A**) and osteogenic differentiation capacity as fMSCs expressing truncated FOS (FOSΔ), as measured by mineralization content (**Figure 4B**) and alkaline phosphatase activity (**Figure 4C**). These results indicate that disruption of the helical region within the C-terminus of FOS impairs osteogenic differentiation capacity.

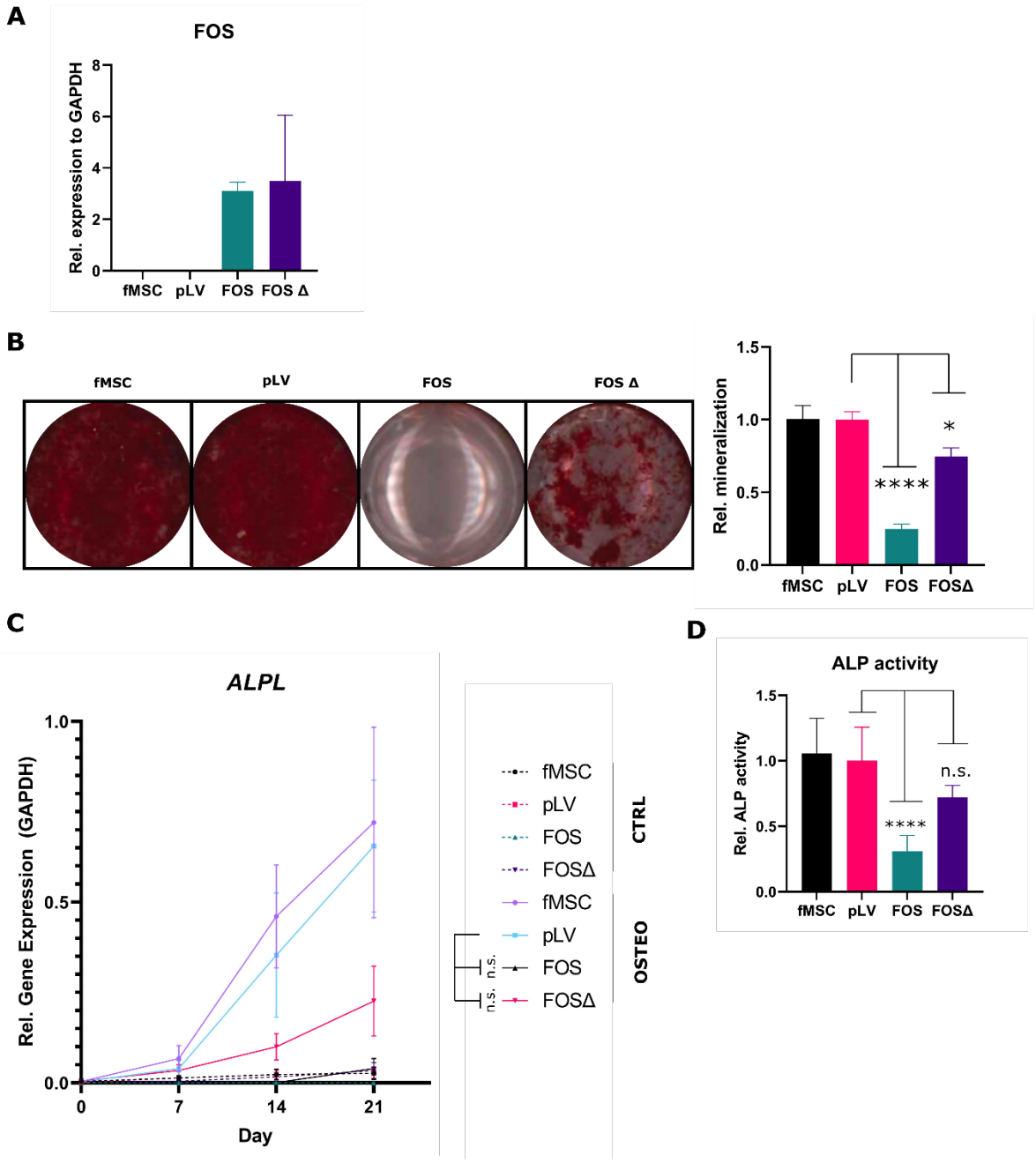

Figure 2. Osteogenic differentiation is reduced upon overexpression of truncated FOS. (**A**) FOS mRNA was overexpressed in fMSCs transduced with full-length FOS (FOS) or truncated FOS (FOSΔ). Each bar represents the mean of two experiments performed in duplicate ± standard deviation. (**B)** fMSCs expressing truncated FOS (FOSΔ) show reduced mineralization, while mineralization is almost completely absent in fMSCs expressing full-length FOS (FOS). For each condition, one representative image is shown. Mineralization was quantified relative to empty vector transduced fMSCs (pLV) and each bar represents the mean of three experiments performed in triplicate ± standard deviation. Groups were compared to pLV, using the Kruskal – Wallis test. * = P ≤ 0.05; **** = P ≤ 0.0001. (**C**) Expression of osteogenic marker *ALPL* is induced during osteogenic differentiation. Representative data from one experiment is shown. Statistical analysis was performed based on the mean of three experiments performed by two independent researchers in duplicate that all showed a similar trend as to the data shown. (**D**) Alkaline phosphatase activity was determined in fMSCs, relative to empty vector transduced fMSC (pLV). Each bar represents the mean of four experiments performed in triplicate ± standard deviation. Groups were compared to pLV, using the Kruskal – Wallis test. * = P ≤ 0.05 ; **** = P ≤ 0.0001; n.s. = not statistically significant, p > 0.05

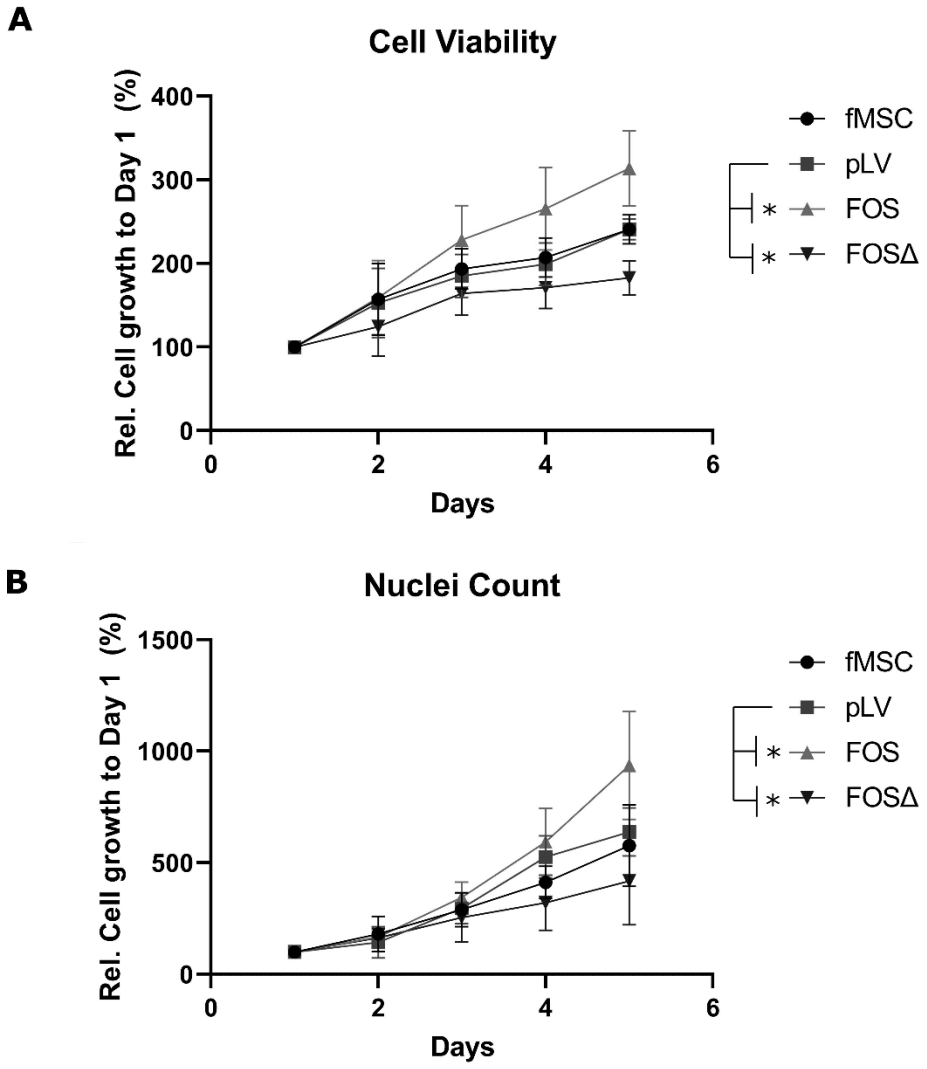

Figure 3. The proliferation rate of fMSCs with the various constructs. Both cell viability (**A**) and nuclei count (**B**) was reduced in fMSCs expressing truncated FOS (FOSΔ) compared to untransduced (fMSC) and empty vector transduced (pLV) fMSCs, whereas this was increased in cells expressing full-length FOS Each data point represents the mean of three experiments performed in triplicate ± standard deviation. Groups were compared to pLV. * = $P \leq 0.05$

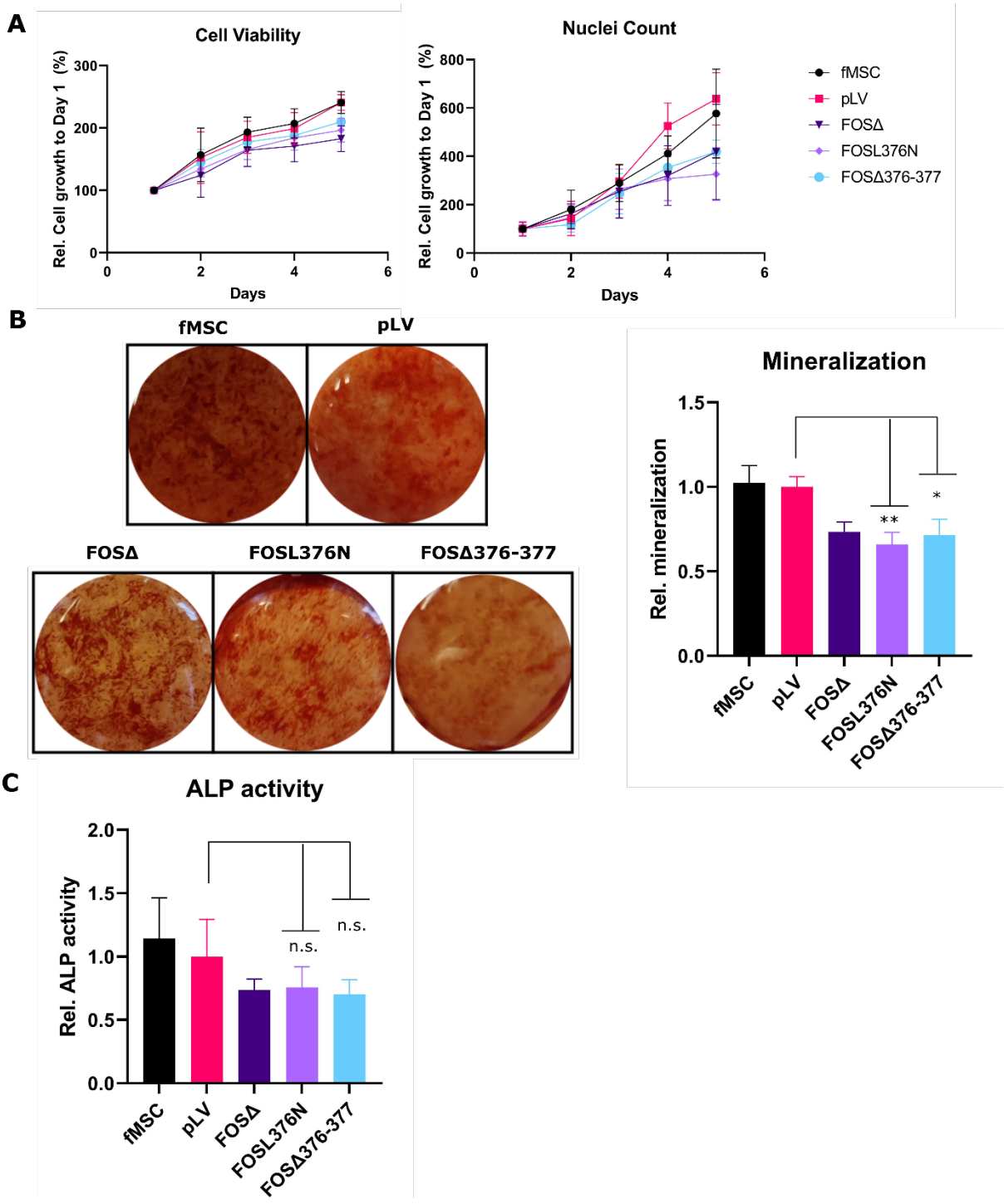

Figure 4. Osteogenic differentiation capacity and proliferation of fMSCs expressing FOS harbouring alterations in LLAL region. (**A**) Cell viability and nuclei count showed a similar proliferation rate in fMSCs expressing truncated FOS (FOSΔ), FOS with a deletion (FOSΔ376-377) or mutation (FOSL376N) in the LLAL region of the C-terminal domain. (**B**) Mineralization, as measured by Alizarin Red staining of FOSL376N or FOSΔ376-377, is similar to truncated FOS (FOSΔ). One representative image per condition is shown. Mineralization was quantified relative to empty vector transduced fMSCs (pLV) and each bar represents the mean of three experiments performed in triplicate ± standard deviation. (**C**) Alkaline phosphatase activity was determined in fMSCs, relative to empty vector transduced fMSCs (pLV), which was comparable among fMSCs expressing truncated FOS (FOSΔ), FOS with a deletion (FOSΔ376-377) or mutation (FOSL376N) in the LLAL region of the C-terminal domain. Each bar represents the mean of three experiments performed in triplicate ± standard deviation. Groups were compared to pLV using the Kruskal – Wallis test. ** = P ≤ 0.01; * = P ≤ 0.05; n.s. = not statistically significant, p > 0.05

Discussion

Osteoid osteoma, osteoblastoma and cementoblastoma show frequent rearrangements of the *FOS*- gene with various fusion partners that lead to truncation of the FOS protein. The truncation was previously identified in epithelioid hemangioma and was shown to cause resistance to protein degradation resulting in overexpression of the truncated FOS protein (4).

In this study, we investigated how truncated FOS affects osteogenic differentiation, since osteoid osteoma, osteoblastoma and cementoblastoma are characterized by the presence of immature woven bone. To investigate this, fMSCs transduced with lentiviral vectors driving expression of truncated FOS were compared to wild-type fMSCs and fMSCs overexpressing full-length FOS. In fMSCs expressing truncated FOS, mineralization was reduced, and alkaline phosphatase expression and activity showed a trend towards reduction, compared to wild-type fMSCs. Not only fMSCs expressing truncated FOS, but also fMSCs expressing FOS with a disrupted helical region of the C-terminus (FOSL376N and FOSΔ376-377) show similar results. As the helical region of FOS contains a signal for proteasomal degradation, these results suggest that the disruption of the helical region impairs osteogenic differentiation.

It was previously shown that cells expressing FOS constructs with a disrupted helical region of the C-terminus (FOSL376N and FOSΔ376-377) have impaired proteasomal degradation (4). Combined with our results, this suggests that sustained expression of FOS, either by truncation of FOS or disruption of the helical region in the C-terminus of FOS, causes the impairment of osteogenic differentiation and proliferation.
Interestingly, fMSCs that overexpress full-length FOS completely lost osteogenic differentiation capacity, which is in line with previous results that showed that human mesenchymal stem cells expressing FOS lost both osteogenic and adipogenic differentiation (27). The difference in osteogenic differentiation and proliferation as a result of overexpression of full-length FOS or truncated FOS in fMSCs is interesting. It is known that sustained expression of full-length FOS leads to the transformation of cells (19, 26). In line with this, we observed that fMSCs expressing full-length FOS increased proliferation compared to fMSCs expressing truncated FOS and wildtype cells, which is in line with a previous study using MSCs (27). As differentiation and proliferation are carefully balanced cellular processes (28), it is not surprising that the same fast-growing cells lose osteogenic differentiation capacity. The difference in proliferation and differentiation observed in fMSCs expressing truncated or full-length FOS is in line with the phenotypical difference between osteosarcoma, a malignant bone tumour, and the non-malignant bone-forming tumours osteoid osteoma and osteoblastoma (1). Osteoid osteoma and osteoblastoma have a limited growth capacity with reduced proliferation as compared to osteosarcoma and can show non-mineralized and mineralized woven bone (1). In fMSCs expressing truncated FOS, we observed slower proliferation rates compared to full-length FOS, and reduced osteogenic

differentiation capacity. Thus, fMSCs overexpressing truncated FOS can explain the more indolent growth with the presence of organized, immature woven bone observed in osteoid osteoma and osteoblastoma. These data suggest that the definitive phenotype is a careful balance between differentiation and proliferation.
A small subset of osteoid osteoma and osteoblastoma lack alterations in FOS (29). Instead, there is a subgroup that shows *FOSB* rearrangements, or loss of *NF2* (3, 29). Truncation of FOSB would likely lead to similar changes in osteogenic differentiation since both FOS and FOSB can form parts of the A.P1 complex. However, further research is needed to elucidate how FOSB and NF2 contribute to the formation of osteoid osteoma and osteoblastoma.

Another open question remains how (truncation of) FOS is able to confer these cellular changes in osteoid osteoma and osteoblastoma. FOS protein levels and protein stability are tightly regulated, and one of these regulatory processes involve phosphorylation of FOS. Phosphorylation of FOS leads to increased stability, and several phosphorylation sites at the C-terminus of FOS are binding sites for kinases of the RSK or the MAPK protein family such as ERK, JNK and p38 (30, 31). A previous study has shown that phosphorylation of FOS by RSK or MAPK usually start at Ser362 and Ser374 in the C-terminus which facilitates further phosphorylation of FOS (32). In this study we have used fetal MSCs overexpressing truncated FOS lacking the phosphorylation sites near the C-terminus. It is possible that changes in the phosphorylation status can confer changes in RSK or MAPK signalling, which alters cellular processes and ultimately leads to osteoid osteoma and osteoblastoma. Unfortunately, it was not possible to further explore this in the current study due to the lack of reliable antibodies detecting phosphorylated FOS.

In conclusion, we have demonstrated that overexpression of truncated FOS reduces osteogenic differentiation and proliferation in fMSCs. This may explain the indolent growth of osteoid osteoma and osteoblastoma and the presence of immature woven bone in these tumours.

Acknowledgements

The authors would like to thank Hans Baelde, and Pauline Wijers-Koster for technical assistance and discussion.

References

1. WHO classification of tumours of soft tissue and bone, 5th edition. Lyon, France: WHO Classification of Tumours Editorial Board; 2020.
2. Lam SW, Cleven AHG, Briaire-de Bruijn IH, Schreuder WH, Kroon HM, Savci-Heijink DC, et al. FOS Rearrangement and Expression in Cementoblastoma. The American journal of surgical pathology. 2021;45(5):690-3.
3. Fittall MW, Mifsud W, Pillay N, Ye H, Strobl AC, Verfaillie A, et al. Recurrent rearrangements of FOS and FOSB define osteoblastoma. Nat Commun. 2018;9(1):2150.
4. van IDGP, Forghany Z, Liebelt F, Vertegaal AC, Jochemsen AG, Bovee J, et al. Functional analyses of a human vascular tumor FOS variant identify a novel degradation mechanism and a link to tumorigenesis. J Biol Chem. 2017;292(52):21282-90.
5. Ferrara P, Andermarcher E, Bossis G, Acquaviva C, Brockly F, Jariel-Encontre I, et al. The structural determinants responsible for c-Fos protein proteasomal degradation differ according to the conditions of expression. Oncogene. 2003;22(10):1461-74.
6. Stancovski I, Gonen H, Orian A, Schwartz AL, Ciechanover A. Degradation of the Proto-Oncogene Product c-Fos by the Ubiquitin Proteolytic System In Vivo and In Vitro: Identification and Characterization of the Conjugating Enzymes. Molecular and Cellular Biology. 1995;15:7106-16.
7. Han XR, Zha Z, Yuan HX, Feng X, Xia YK, Lei QY, et al. KDM2B/FBXL10 targets c-Fos for ubiquitylation and degradation in response to mitogenic stimulation. Oncogene. 2016;35(32):4179-90.
8. Adler J, Reuven N, Kahana C, Shaul Y. c-Fos proteasomal degradation is activated by a default mechanism, and its regulation by NAD(P)H:quinone oxidoreductase 1 determines c-Fos serum response kinetics. Mol Cell Biol. 2010;30(15):3767-78.
9. Sasaki T, Kojima H, Kishimoto R, Ikeda A, Kunimoto H, Nakajima K. Spatiotemporal regulation of c-Fos by ERK5 and the E3 ubiquitin ligase UBR1, and its biological role. Mol Cell. 2006;24(1):63-75.
10. Bossis G, Ferrara P, Acquaviva C, Jariel-Encontre I, Piechaczyk M. c-Fos proto-oncoprotein is degraded by the proteasome independently of its own ubiquitinylation in vivo. Mol Cell Biol. 2003;23(20):7425-36.
11. Acquaviva C, Salvat C, Brockly F, Bossis G, Ferrara P, Piechaczyk M, et al. Cellular and viral Fos proteins are degraded by dierent proteolytic systems. Oncogene. 2001;20:942-50.
12. Campbell KM, Terrell AR, Laybourn PJ, Lumb KJ. Intrinsic Structural Disorder of the C-Terminal Activatin Domain from the bZIP Transcription Factor FOS. Biochemistry. 2000;39:2708-13.
13. Lam SW, Cleven AHG, Kroon HM, Briaire-de Bruijn IH, Szuhai K, Bovee J. Utility of FOS as diagnostic marker for osteoid osteoma and osteoblastoma. Virchows Arch. 2020;476(3):455-63.
14. Amary F, Markert E, Berisha F, Ye H, Gerrand C, Cool P, et al. FOS Expression in Osteoid Osteoma and Osteoblastoma: A Valuable Ancillary Diagnostic Tool. The American journal of surgical pathology. 2019;43(12):1661-7.
15. Ofir R, Dwarki VJ, Rashid D, Verma IM. Phosphorylation of the C terminus of Fos protein is required for transcriptional transrepression of the c-fos promotor. Nature. 1990;348.
16. Shaulian E, Karin M. AP-1 in cell proliferation and survival. Oncogene. 2001;20.
17. Karin M, Liu ZG, Zandi E. AP-1 function and regulation. Current Opinion in Cell Biology. 1997;9(2):240-6.
18. Ozanne BW, Spence HJ, McGarry LC, Hennigan RF. Transcription factors control invasion: AP-1 the first among equals. Oncogene. 2007;26(1):1-10.
19. Miao GG, Curran T. Cell Transformation by c-fos Requires an Extended Period of Expression and Is Independent of the Cell Cycle. Molecular and Cellular Biology. 1994;14(6):4295-310.
20. Grigoriadis AE, Schellander K, Wang Z, Wagner EF. Osteoblasts are target cells for transformation in c-fos transgenic mice. The journal of Cell Biology. 1993;122(3):685-701.

21. Wang ZQ, Lian J, Schellander K, Wagner EF, Grigoriadis AE. c-fos-induced Osteosarcoma Formation in Transgenic Mice: Cooperativity with c-jun and the role of endogenous c-fos. Cancer Research. 1995;55:6244-51.
22. Franchi A, Calzolari A, Zampi G. Immunohistochemical detection of c-fos and c-jun expression in osseous and cartilaginous tumours of the skeleton. Virchows Arch. 1998;432:515-9.
23. Kang X, Sun Y, Zhang Z. Identification of key transcription factors - gene regulatory network related with osteogenic differentiation of human mesenchymal stem cells based on transcription factor prognosis system. Exp Ther Med. 2019;17(3):2113-22.
24. McCabe LR, Banerjee C, Kundu R, Harrison RJ, DObner PR, Stein JL, et al. Developmental Expression and Activities of specific FOS and Jun proteins are functionally related to Osteoblast Maturation. Endocrinology. 1996;137(10):4398-408.
25. Mohseny AB, Szuhai K, Romeo S, Buddingh EP, Briaire-de Bruijn I, de Jong D, et al. Osteosarcoma originates from mesenchymal stem cells in consequence of aneuploidization and genomic loss of Cdkn2. J Pathol. 2009;219(3):294-305.
26. Miller AD, Curran T, Verma IM. c-fos protein van induce cellular transformation: a novel mechanism of activation of a cellular oncogene. Cell. 1984;36:51-60.
27. Abarrategi A, Gambera S, Alfranca A, Rodriguez-Milla MA, Perez-Tavarez R, Rouault-Pierre K, et al. c-Fos induces chondrogenic tumor formation in immortalized human mesenchymal progenitor cells. Sci Rep. 2018;8(1):15615.
28. Ruijtenberg S, van den Heuvel S. Coordinating cell proliferation and differentiation: Antagonism between cell cycle regulators and cell type-specific gene expression. Cell Cycle. 2016;15(2):196-212.
29. Saba KH, Cornmark L, Hofvander J, Magnusson L, Nilsson J, van den Bos H, et al. Loss of NF2 defines a genetic subgroup of non-FOS-rearranged osteoblastoma. J Pathol Clin Res. 2020;6(4):231-7.
30. Tanos T, Marinissen MJ, Leskow FC, Hochbaum D, Martinetto H, Gutkind JS, et al. Phosphorylation of c-Fos by members of the p38 MAPK family. Role in the AP-1 response to UV light. J Biol Chem. 2005;280(19):18842-52.
31. Monje P, Hernandez-Losa J, Lyons RJ, Castellone MD, Gutkind JS. Regulation of the transcriptional activity of c-Fos by ERK. A novel role for the prolyl isomerase PIN1. J Biol Chem. 2005;280(42):35081-4.
32. Chen RH, Abate C, Blenis J. Phosphorylation of the c-Fos transrepression domain by mitogen-activated protein kinase and 90-kD ribosomal S6 kinase. Proc Natl Acad Sci U S A. 1993;90:10952-6.

Supplementary Figures

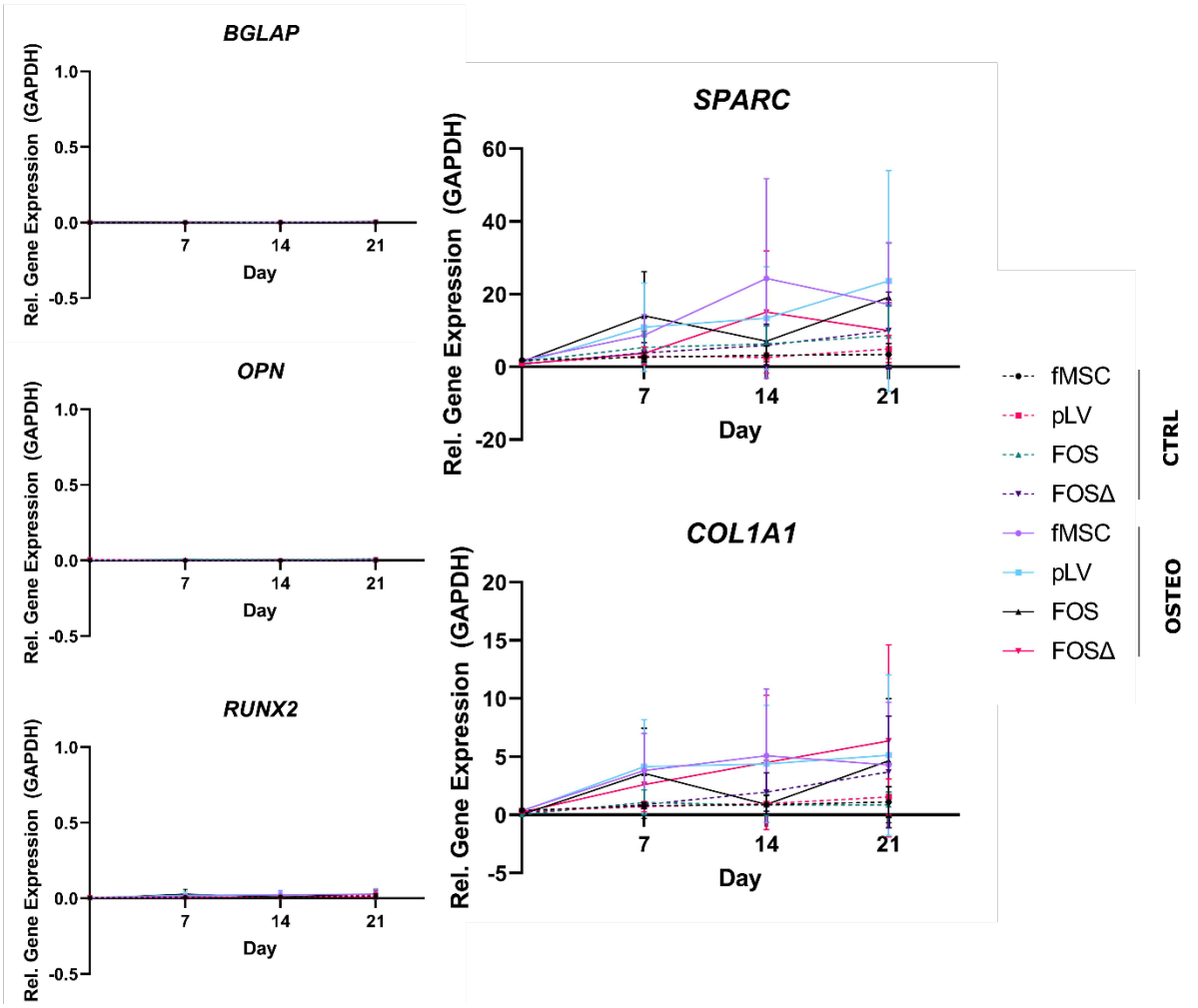

Figure S1. Gene expression of osteogenic markers *BGLAP*, *OPN* and *RUNX2* showed nearly undetectable levels in fMSCs. Gene expression of *COL1A1* and *SPARC* was highly variable.

Chapter 4

Transformed canine and murine mesenchymal stem cells as a model for sarcoma with complex genomics

Natasja Franceschini, Bas Verbruggen, Marianna A. Tryfonidou, Alwine B. Kruisselbrink, Hans Baelde, Karin E. de Visser, Anne-Marie Cleton-Jansen and Judith V.M.G. Bovée

Published: *Cancers. 2021; 13(5):1126*

Abstract

Sarcomas are rare mesenchymal tumors with a broad histological spectrum, but they can be divided into two groups based on molecular pathology: sarcomas with simple or complex genomics. Tumors with complex genomics can have aneuploidy and copy number gains and losses, which hampers the detection of early, initiating events in tumorigenesis. Often, no benign precursors are known, which is why good models are essential. The mesenchymal stem cell (MSC) is the presumed cell of origin of sarcoma. In this study, MSCs of murine and canine origin are used as a model to identify driver events for sarcomas with complex genomic alterations as they transform spontaneously after long-term culture. All transformed murine but not canine MSCs formed sarcomas after subcutaneous injection in mice. Using whole genome sequencing, spontaneously transformed murine and canine MSCs displayed a complex karyotype with aneuploidy, point mutations, structural variants, inter-chromosomal translocations, and copy number gains and losses. Cross-species analysis revealed that point mutations in *Tp53/Trp53* are common in transformed murine and canine MSCs. Murine MSCs with a cre-recombinase induced deletion of exon 2-10 of *Trp53* transformed earlier compared to wild-type murine MSCs, confirming the contribution of loss of p53 to spontaneous transformation. Our comparative approach using transformed murine and canine MSCs points to a crucial role for p53 loss in the formation of sarcomas with complex genomics.

Introduction

Sarcomas represent a large group of mesenchymal tumors with a diverse histological spectrum. Based on histology, ~70 subtypes are recognized (1). However, based on their molecular alterations, sarcomas can be roughly divided into two groups, where tumors either have simple or complex genomics (2). Sarcomas with simple genomics are mutation or translocation driven, whereas sarcomas with complex genomics often have multiple alterations such as mutations, translocations, and copy number alterations.

For many sarcoma subtypes, in particular sarcomas with simple genomics, the molecular pathology has been unraveled in more detail over the last years, which has led to the identification of diagnostic as well as prognostic and predictive biomarkers (2). In contrast, in tumors with complex genomics, such as osteosarcoma or undifferentiated (pleomorphic) sarcoma, the identification of relevant markers is more difficult. They often have few recurrent alterations, and as a consequence no specific molecular diagnostic markers or targets for therapy are currently available (2-4).

Osteosarcoma is a high-grade bone-forming neoplasm that often shows chromoanagenesis (chromothripsis and chromoplexy), in which a single catastrophic event results in fragmentation of chromosomes that are randomly rearranged (1, 5-7). Therefore, recurrent alterations in sporadic osteosarcoma are not frequently identified. However, in recent years many next-generation sequencing (NGS) studies have been published showing that alterations in genes such as *TP53* and *RB1* are most common, followed by alterations in *MYC, CCNE1, DLG2, COPS3, PTEN, ATRX,* and *MDM2* (3, 5, 8-15).

Undifferentiated (pleomorphic) sarcoma is a heterogenous high-grade sarcoma that can occur in soft tissue as well as bone, lacking any line of differentiation (1). It is a diagnosis of exclusion (1). In undifferentiated (pleomorphic) sarcoma in soft tissue, recent NGS studies identified recurrently altered genes such as *ATRX, RB1, ATM, KDR* and *PIK3CA*, but most often *TP53* (16-19).

We and others have shown previously that murine MSCs transform spontaneously after long-term culturing, and form sarcoma when injected in mice (20-23). These transformed murine MSCs showed many similarities with sarcomas with complex genomics, such as extensive aneuploidy. Unlike murine MSCs, human bone marrow derived MSCs do not transform spontaneously in vitro after long-term culture (24).

In the current study, an alternative approach was used to investigate the initiation of sarcomas with complex genomics by employing not only murine but also canine MSCs. Canines too develop osteosarcoma, with a similar clinical and biological presentation as human osteosarcoma (25, 26) and we show here for the first time that canine MSCs can undergo spontaneous transformation.

Using this cross-species approach, the aim was to identify driver genes among the plethora of genetic alterations in sarcoma with complex genomics. Whole genome sequencing was applied to identify single nucleotide variants, structural variants, and copy number

alterations. Cross-species analysis revealed that *TP53/Trp53* point mutations are common in late passage canine and murine MSCs, indicating a crucial role for loss of p53 in the initiation of sarcomas with complex genomics.

Materials and Methods

Mesenchymal Stem Cell Isolation and Cell Culture

Murine bone-marrow-derived mesenchymal stem cells (MSCs) were isolated by collecting the femurs and tibia from surplus C57BL/6J (*n* = 6), NMRI (*n* = 3), FVB mice (*n* = 1) (kindly gifted by Dr. Paul Krimpenfort), or Kcre/P53f (FVB) (*n* = 4) (27) mice between 24–27 weeks old (B6_4, B6_7, B6_10, NMRI_2, NMRI_3, NMRI_9, FVB WT, P53_1, P53_2). Bones were flushed with MSC-medium (αMEM (BE12-169F, Lonza, Switzerland) supplemented with 15% Performance plus Fetal Bovine Serum (16000044, Gibco, Invitrogen Life-Technologies, Scotland, UK), 1% Penicllin-Streptromycin (15140122, Gibco), and 1% Glutamax (35050061, Gibco) and bone marrow cells were resuspended in 75 µL of DNAse (1.33 mg/mL, 11284932001, Sigma-Aldrich, Saint Louis, MO, USA). Cells were washed in 10 mL erythrocyte lysis buffer (NH_4Cl (8.4 g/L), $KHCO_3$ (1 g/L); pH = 7.4, in-house hospital pharmacy). All bone marrow cells per mouse were seeded in one T75 flask, and the medium was refreshed twice per week to wash away non-adherent cells. After 10 days, cells were trypsinized to collect all adherent cells.

Early passage (P0 or P1) bone-marrow derived MSCs from dogs (canine MSCs) were isolated as described previously (28). These cells were isolated from the proximal humerus of a Rottweiler (*n* = 1) (OSBMSC1), diagnosed with metastatic conventional osteosarcoma in the distal radius and treated by amputation and chemotherapy, or Labrador Retrievers (*n* = 5) (MSC_492, MSC_490, MSC_447, MSC_446, MSC_405), that were euthanized for unrelated experiments between the age of 2–4 months (29), which was approved by the Ethics Committee of the Utrecht University (DEC 2009.III.06.050). Canine MSCs from Labrador Retrievers were selected based on having positive tri-lineage differentiation capacity, as published elsewhere (manuscript under submission). Canine MSCs were also cultured in MSC-medium.

All MSCs were cultured at 37 °C with 5% CO_2 in a humidified incubator, and were tested regularly for mycoplasm. Once cells reached near-confluence (80–90%), cells were passaged with a ratio of 1:3. Every passage, cells were counted with a Bürker-Türk counting chamber to determine cumulative population doublings and any residual cells were frozen.

Transformation Analysis of Mesenchymal Stem Cells

To verify transformation of late passage MSCs karyotyping, soft agar anchorage independent growth assay, Multicolour Combined binary ratio labelling (COBRA) FISH and DNA content analysis were performed.

For karyotyping, late passage canine or murine MSCs were seeded at 6000 cells/cm^2 in 6-well plates. After cells reached 70–80% confluence, cells were washed twice with serum-free MSC-

medium and incubated for 25 min at 37 °C with 1 mL Calyculin A (80 nM, C-3987, LC Laboratories, Woburn, MA, USA). All cells were incubated with 7.5 mL KCl (0.075 M, P9541, Sigma-Aldrich) for 12 min at 37 °C. Cells were then centrifuged 3× for 8 min at 120 rcf. After each centrifugation, the pellet was fixed by adding 8 mL of methanol: acetic acid in a ratio of 4:1. Finally, 12 µL of cell suspension was added on a glass slide inside a humidified chamber (55% humidity at 25 °C). Slides were air-dried and stained with DAPI for microscopic counting of metaphase chromosomes.

For COBRA FISH, metaphase chromosomes harvested from bone-marrow-derived MSCs (passage 9, during crisis, and passage 10, after transformation) from one C57BL/6J mouse were hybridized using a mouse whole chromosome painting probe set as described in detail previously (30). Images were collected and analyzed using ColorProc software tool, as described previously (30).

For soft agar anchorage independent growth assay, non-tissue culture treated 6-well plates (351146, Corning, New York, NY, USA) were coated with a bottom layer of 0.7% agarose (dissolved in medium) (16520050, Invitrogen). Late passage canine or murine MSCs were seeded at 20,000 cells per well in 0.35% agarose (dissolved in medium) on top of the bottom layer. Plates were incubated at 37 °C for 3–4 weeks and imaged with GelCount (Oxford Optronix, Milton, United Kingdom).

For DNA content analysis, late passage (P34) and early passage (P1) canine MSCs of the transformed canine MSC culture (OSBMSC1) were analyzed using a standard LSRII (BD Biosciences, San Jose, CA, USA) flow cytometer according to the Vindelov method, without the use of chicken or trout reference nuclei, using the blue 488 nm laser for excitation and a 610/20 nm bandpass filter for collecting propidium iodide (PI) fluorescence. At least 10,000 single cell events were collected using the DNA PI area versus width signals (31).

Whole Genome Sequencing and Data Analysis of Early Passage and Transformed Late Passage MSCs

For whole genome sequencing (WGS), early (OSBMSC1, passage 5 and 6) and transformed late (OSBMSC1, passage 34 and 42) passage canine MSCs, and normal tissue from the Rottweiler were collected for DNA isolation. For murine MSCs, early (B6_4 passage 2, B6_7 passage 2, B6_10 passage 3) and late (B6_4 passage 10, B6_7 passage 15, B6_10 passage 13) passage MSCs from three different C57BL/6J mice were collected for DNA isolation. For DNA isolation, the Wizard Genomic DNA purification kit (A1125, Promega, Madison, WI, USA) was used according to the manufacturer's instructions. DNA samples were checked for degradation by gel electrophoresis. Whole genome sequencing was performed by BGI Europe using the BGISEQ-500 platform, with 150 bp paired-end reads and 30× coverage.

Adapters were trimmed from the raw sequencing reads, using cutadapt v1.10 (32) followed by quality trimming with sickle 1.33 (33) with default parameters. The cleaned reads were aligned to the mouse reference genome, GRCm38 (GCA_000001305.2), or to the dog reference genome, CanFam 3.1 (GCA_000002285.2), with bwa mem 0.7.15-r1140 (34) with default parameters. Duplicates were marked with Picard tools 2.9.0 and base quality score

recalibration and indel realignment were performed with GenomeAnalysisTK 3.7.0q following GATK Best Practices recommendations (35-37).

Somatic SNVs and small Indels for the murine MSCs were identified by comparing the early passage samples for each individual with their respective late passage samples. For the canine MSCs, early passage samples and late passage samples were matched with the normal tissue sample. Three variant callers were applied: Mutect2 v4.0.11.0 (35), Strelka v2.9.10-0 (38) and Varscan v2.4.3 (39), all with default settings, removing those that did not pass the quality filters of the respective callers. The variants were annotated using ANNOVAR (version: 2018-04-16) (40) and filtered for non-synonymous exonic variants with an allele frequency ≥ 0.2. Human orthologs for *M. musculus* or *C.I. familiaris* genes with variants retrieved from Ensembl Genes 97 using biomaRt v2.38.0 (41). The human orthologs for each identified variant were called using COBALT (42, 43). Pathogenicity of a variant was determined by ClinVar (44). For TP53 analysis, transcript variant 1 was used (NM_000546.5).

Copy number variations were identified through Varscan v.2.4.3 copynumber with a minimal segment size of 1000 and maximum segment size of 10,000. Segments were adjusted for GC content by Varscan v.2.4.3 copycaller. Segments were assembled into larger regions of equal log2 ratio using circular binary segmentation with the DNAcopy 1.56.0 (45) package in R 3.5.2 (46). For canine MSCs, copy ratios were determined by comparing late passage or early passage canine MSCs to normal tissue. For murine MSCs, late passage MSCs were compared to early passage MSCs. Genes spanning multiple segments were assigned the average log2 ratio of the segments. For structural variant calling, we used three different structural variant discovery tools: Delly v0.8.1 (47), manta v2.9.10-0 (48) and lumpy-sv v0.3.0-2 (49). Structural variants called in the three callers were merged with SURVIVOR v1.0.6 (50), keeping those that were shared by at least two SV callers with a breakpoint window of 1000 bp. The SVs were annotated with SURVIVOR_ant 0.1.0.

Sanger sequencing was used to evaluate the presence or absence of *TP53/Trp53* mutations in DNA samples from all transformed murine MSCs, OSBMSC1 MSCs passage 34, passage 42, and tumor tissue from the same dog. Forward and reverse primers were designed to flank the identified mutation in *TP53* or exons 4, 5, 6, 7 and 8 (**Table S4** available online).

Trilineage Differentiation

Early and late canine or murine MSCs were seeded at 5000 cells/cm^2 or 15,000 cells/cm^2 for osteogenic or adipogenic differentiation, respectively. Cells were refreshed with medium twice per week for three weeks. Medium was supplemented with osteogenic differentiation compounds: β-glycerophosphate (5 mM, G6251, Sigma-Aldrich), dexamethasone (0.1 µM, D8893, Sigma-Aldrich), and ascorbate-2-phosphate (0.15 mM, A8960, Sigma-Aldrich), or with adipogenic differentiation compounds: dexamethasone (0.25 µM), ascorbate-2-phosphate (0.15 mM), indomethacin (50 µM, I7378, Sigma-Aldrich), and 1-methyl-3-isobtylxantine (0.5 mM, I5879, Sigma-Aldrich). After three weeks, cells were harvested for RNA isolation or fixed with cold ethanol for 1 h. Alizarin Red S staining solution (2 g Alizarin Red S (02100375, MP Biomedicals, Thermo Fisher Scientific, MA, USA) in 60 mL water, pH 4.2) or Oil Red O staining

solution (0.3 g Oil Red (105230, Merck Millipore, Burlington, MA, USA) in 60 mL isopropanol) for osteogenic or adipogenic differentiation, respectively, was added for 5 min and washed with water until solution was clear for imaging.

For chondrogenic differentiation, late passage canine or murine MSCs were seeded as pellets in a U-shaped 96-well plate (0.5×10^6 cells per well) and cultured in DMEM high glucose (31966, Gibco), supplemented with proline (40 µg/mL, P5607, Sigma-Aldrich), 1% Penicllin-Streptromycin, ITS+ premix (5 µg/mL insulin, 5 µg/mL transferrin, 5 ng/mL selenious acid, 354351, Corning), ascorbate-2-phosphate (0.15 mM), dexamethasone (0.1 µM), TGFb3 (10 ng/mL, 243B3, R&D Systems, Minneapolis, MN, USA), refreshed twice per week. After 4 weeks, cell pellets were fixed with 4% PFA for 30 min, paraffin embedded, and sections were stained with toluidine blue staining solution (0.5 g Azur B (A4043, Sigma Aldrich) in 50 mL MQ, 0.5 g toluidine blue (115930, Merck Millipore) in 25 mL MQ, 0.5 g sodium tetraborate (1330434, Merck Millipore) in 25 mL).

Reverse Transcriptase Quantitative PCR (RT-qPCR)

RNA isolation was done using Trizol (15596026, Invitrogen) according to the manufacturer's instructions, followed by cDNA synthesis using iScript cDNA Synthesis Kit (1708890, Bio-rad, Hercules, CA, USA) according to the manufacturer's instructions. Species specific primers for osteogenic markers (*RUNX2, SPARC, SPP1, BGLAP*) and housekeeping genes (*RPL8, B2MG*) were used (**Table S4** available online). RT-qPCR was performed using iQ SYBR Green Supermix (1708880, Bio-rad) and a Bio-rad Thermal Cycler according to the manufacturer's instructions. Relative gene expression levels to housekeeping genes *RPL8* and *B2MG* were determined with the following formula: $2^{(\text{Ct value housekeeping genes} - \text{Ct value gene of interest})}$.

Cre-Mediated KO of Trp53 Exon 2-10 in Murine MSCs

Passage 1 MSCs from Kcre/P53f (FVB) mice were seeded with 500,000 cells per T25 flask. The next day, cells were washed twice with PBS and cre-recombinase (3 or 6 µM) (SCR508, Merck-Milipore) was added and incubated for 1 h at 37 °C. Hereafter, cells were washed twice with PBS and replaced with normal MSC-medium. After 2 weeks, DNA was isolated using the Wizard Genomic DNA purification Kit (A1125, Promega) according to the manufacturer's instructions. PCR was performed using primers flanking the loxP sites in *Trp53* (Table S4). PCR product size was checked by DNA gel electrophoresis. In DNA samples where *Trp53* exons 2-10 are excised, the expected PCR product size is 612 bp, whereas *Trp53* wild-type DNA samples should yield no PCR product.

Western Blotting

Whole cell lysates were made by scraping cells with Hot SDS buffer (1% SDS, 10 mM EDTA, 10 mM Tris pH 7.4) containing protease inhibitor cocktail (11697498001, Roche, Basel, Switzerland) and phosphatase inhibitor cocktail (04906837001, Roche, Basel Switzerland) and incubating lysates for 5 min at 100 °C. Protein concentration of lysates was measured using a microplate reader (Infinite M Plex, Tecan, Switzerland).

Samples (10 µg protein per lane) were loaded on 10% acrylamide gels, and blotted using the Trans-blot Turbo Transfer System (Bio-rad). Blots were blocked in 5% non-fat dry milk in 0.1% Tween-20/PBS for 1 h at RT. Primary antibodies (GAPDH (5174, Cell Signaling, Leiden, The Netherlands), Histon H3 (4499, Cell Signaling), P53 (2524, Cell Signaling)) were incubated overnight at 4 °C. After washing blots with 0.1% Tween/PBS, blots were incubated with secondary antibodies, anti-mouse (7076, Cell Signaling) and anti-rabbit (7074, Cell Signaling), for 1 h at RT. Blots were developed with SuperSignal West Pico PLUS Chemiluminescent Substrate (34579, Thermo Fisher Scientific) using the ChemiDoc Touch Imaging System (Bio-rad). Band intensity was calculated using ImageLab software. Protein expression was determined relative to GAPDH.

In Vivo Tumour Formation

Athymic mice, 6-weeks old, (BALB/c *nu/nu*) were purchased (*n* = 15) from Jackson (Janvier-labs, France), and housed at the animal facility of the Leiden University Medical Center. BALB/c *nu/nu* mice (*n* = 3 per MSC-line) were injected subcutaneously with 50 µL of 0.5×10^6 cells (transformed B6_4, B6_7, B6_10 or OSBMSC1 MSCs) resuspended in PBS/Cultrex BME (1:1 mix) (3433010R1, R&D Systems, Minneapolis MN, USA), under isoflurane anesthetics. Tumor size was measured bi-weekly by calliper. Tumor volume was determined with the following formula: ½ (length × width^2)(51).

Luciferase transduced transformed canine MSCs (OSBMSC1), were injected intratibially with 5×10^5 cells in 10 µL PBS/Cultrex BME (1:1 mix) under isoflurane anesthetics. Every week, tumor growth was measured by non-invasive bioluminescent imaging (BLI) on the IVIS Spectrum Xenogen (Perkin Elmer, Waltham, MA, USA) and quantified In photons/sec/cm^2/sr after intraperitoneal injection of D-luciferin (150 mg/kg, Synchem UG&CO, Felsberg, Germany). Before the end of the experiment, under injection of anesthetics, microCT (Skyscan 1076 Micro CT scanner, Bruker, Billerica, MA, USA) was performed. Mice were sacrificed by CO_2 before tumor size reached 1 cm^3 or after 12 weeks. Tumors, lung, and liver tissues were excised and a half was processed for embedding in paraffin, the other half was fresh frozen. Sections were made of formalin-fixed paraffin-embedded tissue and stained with H&E.

Statistical Analysis

Survival plots were generated using GraphPad Prism 7 software by performing a Kaplan–Meyer analysis. A *t*-test was used to analyze differences in gene expression in samples treated with normal medium or osteogenic medium. To compare densitometry readings of Western blot samples treated with or without cisplatin (3 or 10 µM), an ANOVA test followed by a Dunnett's test was performed. Comparisons were considered statistically significant using a significance level of 5%.

Results

All Murine MSCs Transform Spontaneously after Long-Term In Vitro Culture

Bone-marrow derived MSCs were isolated from two strains (C57BL/6J and NMRI) and differentiation capacity towards the osteogenic and adipogenic lineage was evaluated. There were two out of three MSC cultures that showed both osteogenic and adipogenic differentiation capacity, while the third (B6_4) only showed osteogenic differentiation (**Figure S1** available online). Due to the limited amount of early passage untransformed cells, not all differentiation assays could be performed for all cultures. Long-term cultured MSCs underwent spontaneous transformation after 57–74 days, which was accompanied by an increased growth rate (**Figure 1A**) and morphological changes: late passage murine MSCs have an increased nuclear to cytoplasm ratio compared to early passage murine MSCs (**Figure 1B**). We could confirm the transformation by karyotyping of all late passage murine MSCs, as most late passage cells harbored typically between 74–216 chromosomes, whereas early passage cells mostly have the normal amount of 40 chromosomes (**Figure 1B**). Soft agar assay demonstrated anchorage independent growth in three out of six late passage murine MSC cultures (**Figure S2** available online).

Infrequent Spontaneous Transformation of Canine MSCs after Long-Term In Vitro Culture

Not only murine MSCs, but also one MSC culture derived from the seven-year-old Rottweiler (OSBMSC1) escaped a crisis phase after long-term in vitro culture, followed by rapid cell growth (**Figure 1C**). However, the spontaneous transformation of canine MSCs seemed to be a rare event, as we did not observe transformation in the five other canine MSC cultures isolated from the Labrador Retrievers (**Figure S3** available online). Similar to the murine MSC late passage cultures, late passage MSCs of OSBMSC1 showed an abnormal chromosome number between 91–100 chromosomes, whereas normal chromosome number should be 78 (**Figure 1B**). Morphological changes in transformed canine MSCs were less evident compared to transformed murine MSCs (**Figure 1B**). Aneuploidy in the late passage canine MSCs from OSBMSC1 was also evident from DNA content analysis by DNA flow cytometry (**Figure 1D**).

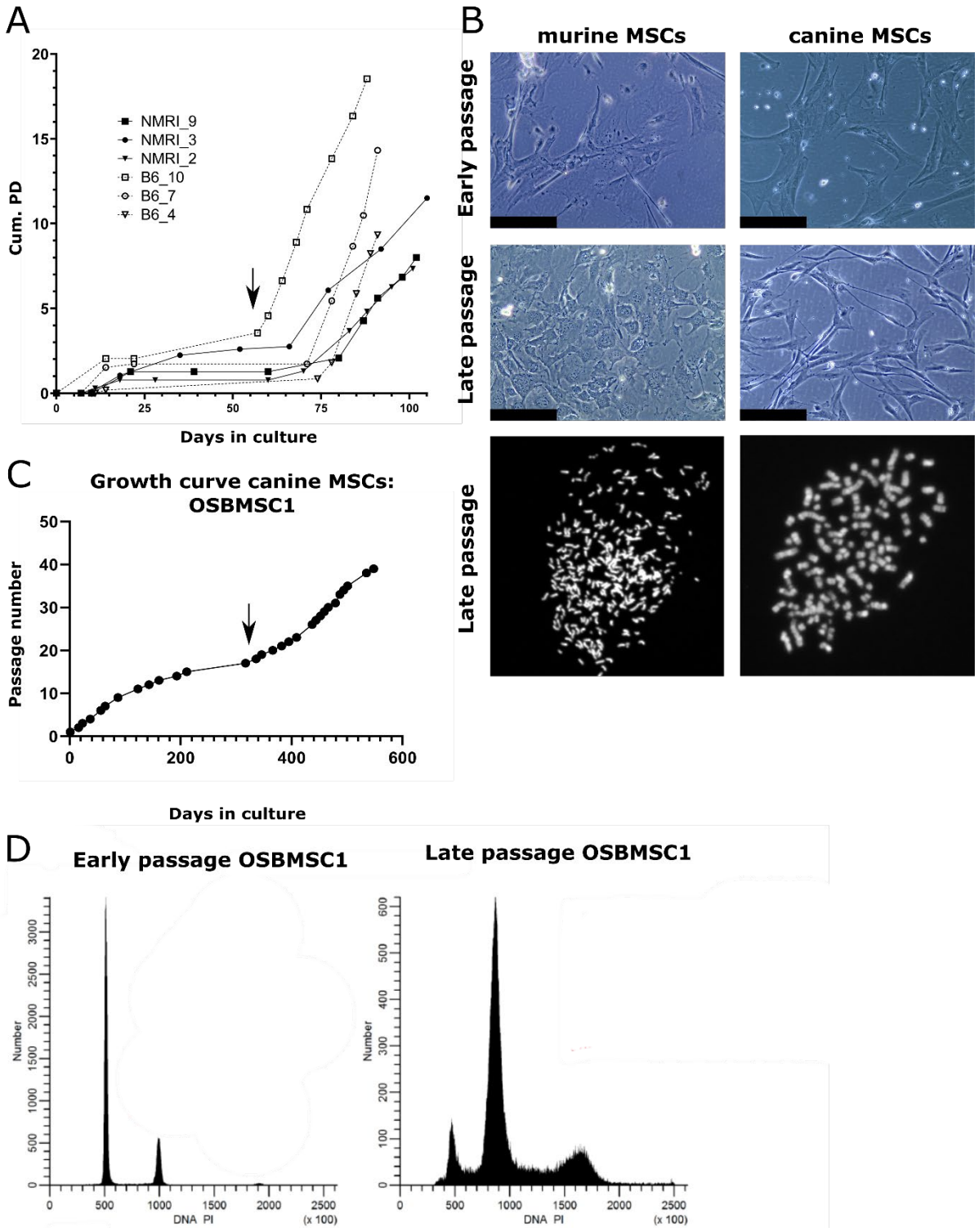

Figure 1. Mesenchymal stem cells (MSCs) from dogs and mice transform spontaneously after long-term culture. (**A**) MSCs isolated from NMRI or C57BL/6J mice undergo spontaneous transformation after long-term in vitro culture based on cumulative population doubling (Cum. PD). Example of transformation event in B6_10 is indicated by an arrow. (**B**) Representative images of murine and canine MSCs. Late passage murine MSCs show a higher nuclear to cytoplasm ratio, as evident from the nuclear enlargement, compared to early passage MSCs. Scalebar represents 100 µm. Karyotyping showed late passage MSCs have an increased number of chromosomes per cell after DAPI staining, as murine and canine cells normally have 40 or 78 chromosomes, respectively. (**C**) MSCs isolated from a 7-year-old Rottweiler transform spontaneously after long-term ex vivo culture (OSBMSC1), indicated with an arrow, at each data point, cells were trypsinized and passaged. (**D**) DNA content analysis by flow cytometry shows that late passage canine MSCs OSBMSC1 have become aneuploid.

Clonal Expansion of Murine MSCs Prior to Transformation Event

The transformation event likely occurred during a period where no expansion of cells was observed, (lag-phase of **Figure 1A**). MSCs derived from bone marrow of one C57BL/6J mouse were harvested and molecular karyotyped by COBRA-FISH at the crisis phase at passage 9. There were 19 cells suitable for analysis and showed a ploidy of 3n (**Figure 2 A–C**). Eighteen of the nineteen cells showed structural chromosomal rearrangements, deletions and/or translocations and the presence of centromeric fragments. Random structural changes involving deletion and translocations were observed in all chromosomes except for 17, 19, and X, with alterations in chromosomes 3, 7, 6, and 4 being the most frequent. One cell showed the karyotype: 3n, XXX, der(18)t(4;18)x2, del(3), der(7)t(3;7) (**Figure 2C**). This karyotype was also seen in the next passage (passage 10) after crisis, in which 15/22 cells showed clonal expansion of a dominantly 3n cell population carrying der(18)t(4;18),der(7)t(3;7) (**Figure 2 D–F**). From these 15 cells, 7 had additional alterations, indicating the formation of subclones. Within the non-clonal cells, one cell was identified with a complex chromosome break, chromosome rearrangement, and acentric fragment, indicating the presence of genomic instability (**Figure 2F**).

Transformed Murine and Canine MSCs Display Variable Mesenchymal Differentiation Capacity

The trilineage differentiation capacity of transformed late passage murine MSCs was highly variable: four out of six murine MSC cultures (B6_4, B6_10, NMRI_2, NMRI_3) could differentiate towards the osteogenic lineage, three out of six cultures (B6_7, B6_10, NMRI_3) could differentiate towards the adipogenic lineage, and two out of six cultures (B6_4 and B6_7) showed chondrogenic differentiation (**Figure 3A**). The transformed canine MSCs did not show any trilineage differentiation capacity under the conditions studied (**Figure 3B**), but by RT-qPCR analysis, most osteogenic markers (*BGLAP*, *RUNX2*, and *SPP1*) were significantly upregulated (**Figure 3C**).

Transformed Murine MSCs Form Tumours with Variable Growth Rate and Histology In Vivo

To confirm tumorigenicity of transformed MSCs, we injected three (B6_4, B6_7, B6_10) transformed murine MSCs and the transformed canine MSCs (OSBMSC1) subcutaneously in mice, in triplicate. Within 21–82 days, eight out of nine mice that were injected with transformed murine MSCs developed tumors (**Figure 4A–C**). No metastases were found in liver or lung tissue. All mice injected with MSCs from B6_7 and B6_10 had to be sacrificed due to tumor formation, but mice injected with MSCs from B6_4 were only sacrificed at the end of the study (81 days). However, numbers were too small to conduct meaningful statistical analysis. (**Figure 4B**). The growth rate, tumor size, and histological spectrum of tumors was variable between the lines. A total of two out of three mice injected with murine MSCs B6_4 developed very slow growing and small tumors (0.005 cm^3).

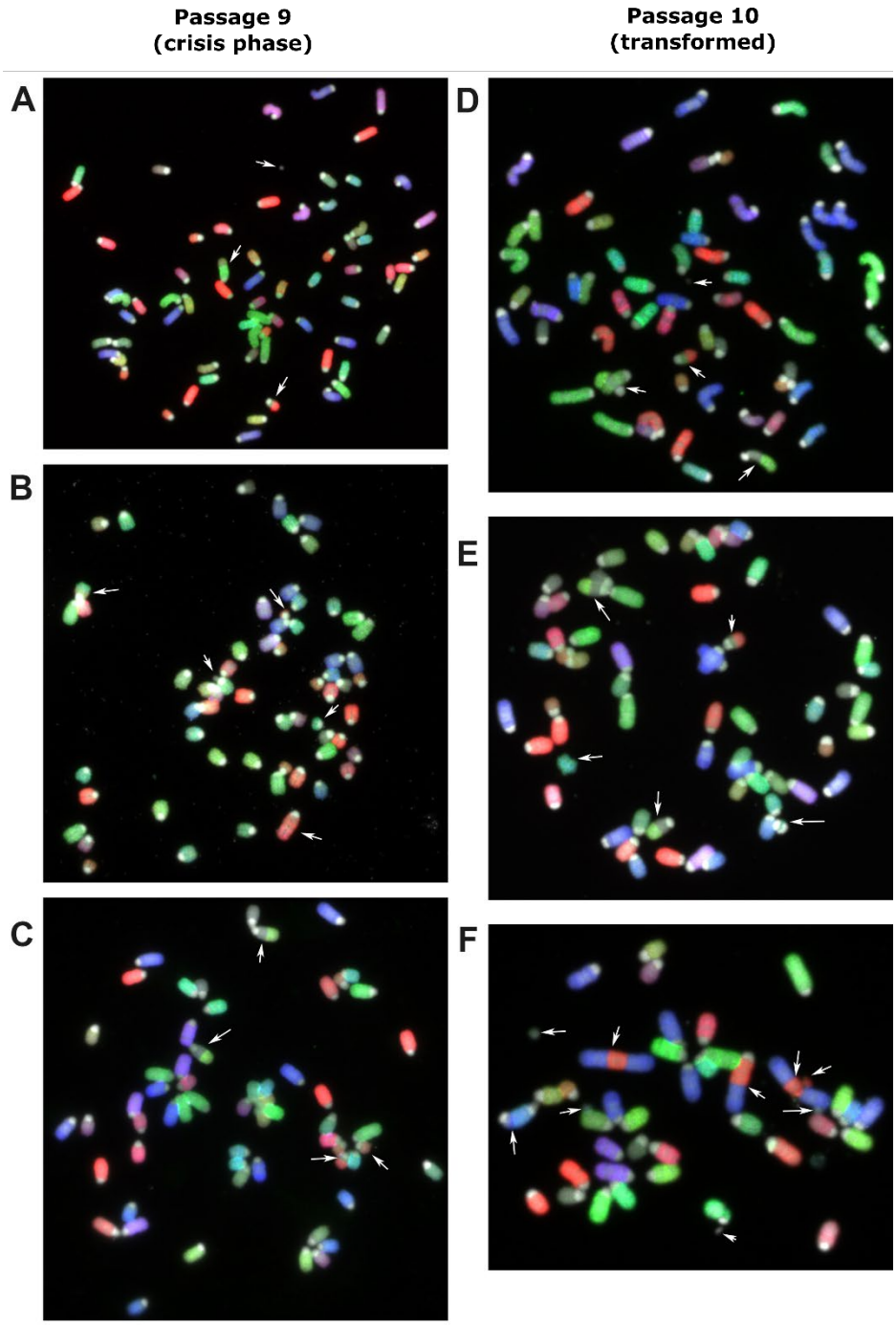

Figure 2. Murine MSC derived from bone marrow of a C57BL/6J mouse was harvested and molecular karyotyped at crisis phase at passage 9 (**A**–**C**) and the next passage (P10) after transformation (**D**–**F**) using COBRA-FISH. In all panels, both numerical and structural chromosomal alterations are visible. Arrows indicate involved chromosomes and rearranged chromosomes are listed per panel from top to bottom and from left to right: (**A**) Centromeric fragment, der(4)t(4;7), der(7)t(3;7), (**B**) der(16)t(13;16), del(3), centromeric fragment, del(13), der(3)t(3;12), (**C**) der(18)t(4;18), der(18)t(4;18), del(3), der(7)t(3;7), (**D**) centromeric fragment, der(7)t(3;7), der(18)t(4;18), der(18)t(4;18), (**E**) der(7)t(3;7), der(18)t(4;18), ace(17), der(18)t(4;18), dic(17;17), (**F**) centromeric fragment, acentric chromosome from chromosome 2-3-2 fusion, der(3)t(2;3), acentric chromosome from chromosome 2-3-2 fusion, fragment of chromosome 3, centromeric fragment, centromeric fragment, dic(5;11), centromeric fragment. COBRA-RGB-color images were superimposed with DAPI (grey) to visualize chromosome centromeric regions. Magnification 630x.

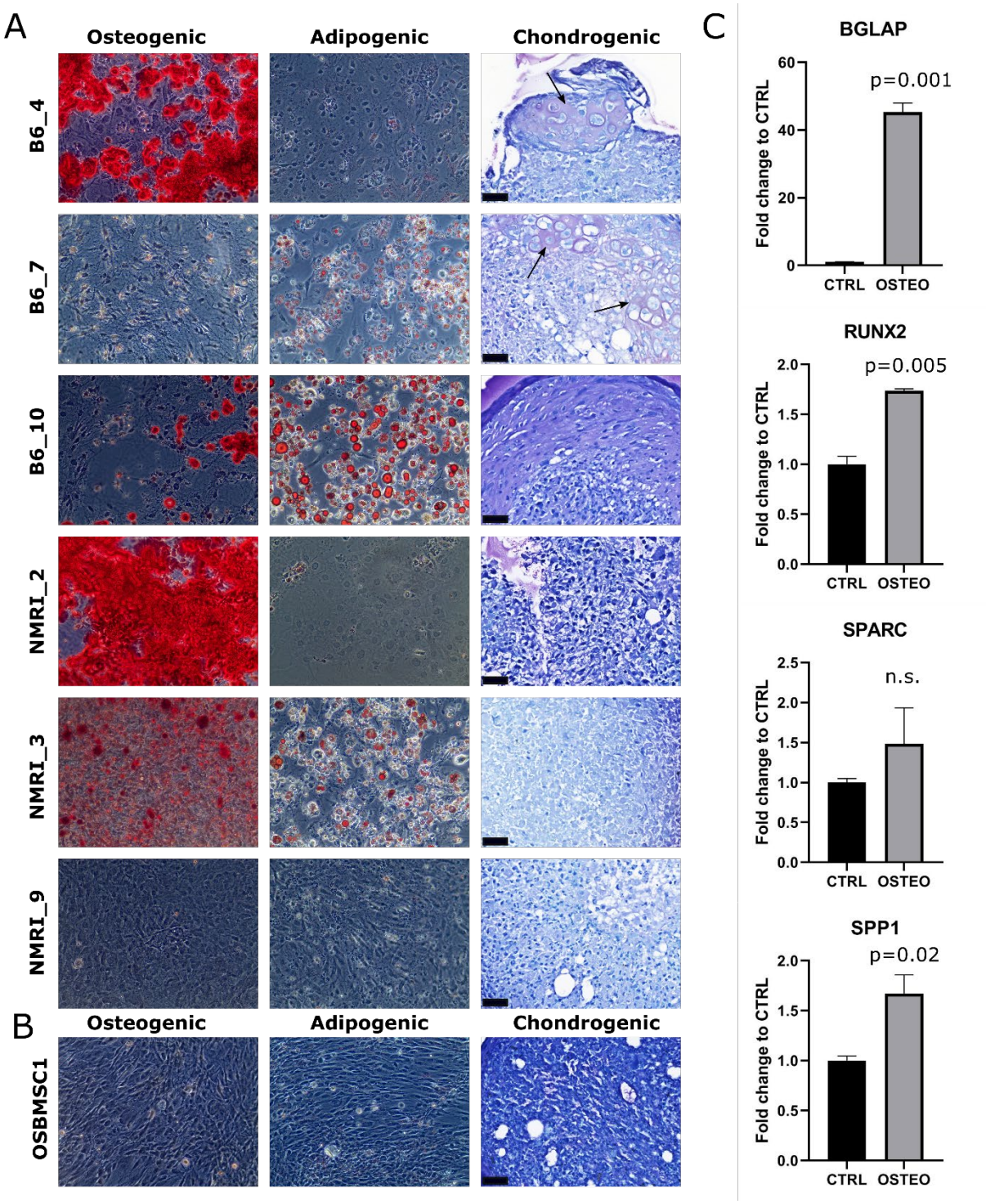

Figure 3. Trilineage differentiation of late passage murine and canine MSCs. Osteogenic, adipogenic and chondrogenic differentiation of (**A**) late passage murine MSCs (Please add scale bar or magnification.) and (**B**) late passage canine MSCs of OSBMSC1 was assessed by Alizarin Red (Magnification 100x), Oil Red O (Magnification 100x), and Toluidine Blue staining, respectively, and was highly variable among donors. For Toluidine Blue staining, arrows indicate metachromatic staining, indicative for cartilaginous matrix. Scale bar represents 40 µm. (**C**) Osteogenic gene expression markers (BGLAP, RUNX2, SPP1) were significantly upregulated in late passage OSBMSC1 treated with osteogenic stimuli for 3 weeks (OSTEO), compared to non-treated MSCs (CTRL). Bars represent the mean of one experiment performed in triplicate ± standard deviation.

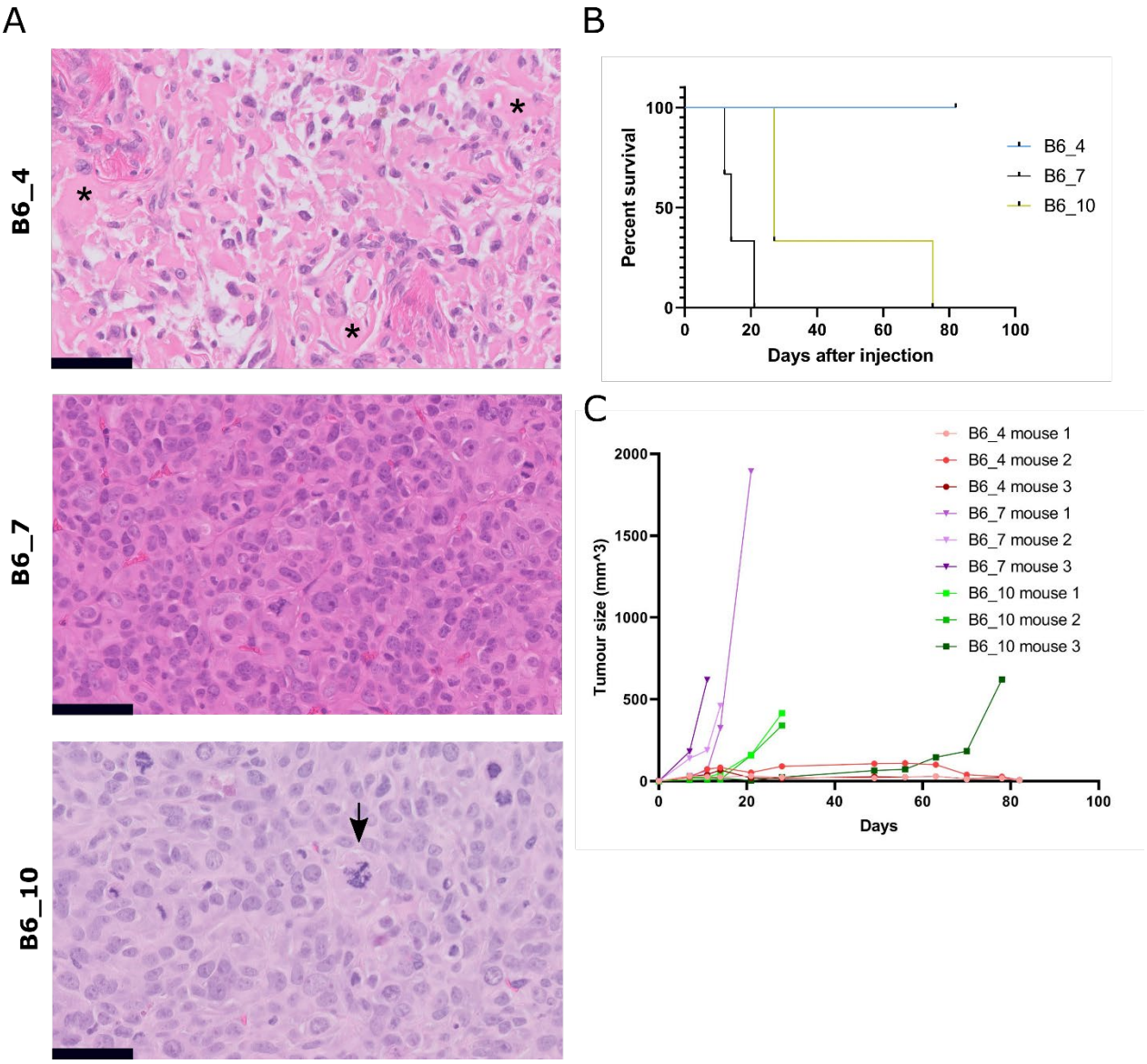

Figure 4. Subcutaneous injection of transformed murine MSCs result in tumor formation with variable histology. (**A**) H&E staining of tumors formed after subcutaneous injection of transformed murine MSCs (B6_4, B6_7, B6_10). Tumor B6_4 displayed a moderately cellular and pleomorphic tumor with deposition of amorphous eosinophilic extracellular matrix, suggestive of osteoid (indicated with asterisks). In contrast, tumors B6_7 and B6_10 were more cellular, pleomorphic, with a high number of mitoses, and morphologically lack any differentiation. Atypical mitosis were present, indicated with an arrow in B6_10. Tumor volumes for B6_4, B6_7 and B6_10 were 0.005 cm^3 (*n* = 2), 0.4–1.1 cm^3 (*n* = 3) and 0.3–0.6 cm^3 (*n* = 3), respectively. Scalebar represents 50 µm. (**B**) Number of days after subcutaneous injection when mice were sacrificed due to an increase in tumor volume. (**C**) Tumor size measured by calliper of each mouse after subcutaneous injection of transformed murine MSCs (t = 0).

Both tumors were moderately cellular, pleomorphic, with deposition of an amorphous eosinophilic matrix strongly suggestive of osteoid, thereby resembling human osteosarcoma (**Figure 4A**). Interestingly, this MSC culture did not show any colonies with the soft agar assay (**Figure S2** available online). On the contrary, all mice injected with murine MSCs B6_7 developed the fastest growing and largest tumors (0.4–1.1 cm^3) after 12–21 days and showed colonies with the soft agar assay. All mice injected with MSCs from B6_10 developed tumors after 27–74 days, and all tumors were similar in size (0.4–0.6 cm^3) and histology as the tumors from B6_7. Histologically, all six tumors from B6_7 and B6_10 showed a highly cellular, pleomorphic and mitotically active proliferation of large undifferentiated cells, suggesting resemblance to human undifferentiated (pleomorphic) sarcoma. Mice that were injected with transformed canine MSCs, either subcutaneously or intratibially, did not develop any tumors. We did observe luciferase activity after intratibial injection, supporting initial engraftment, but this signal decreased over time.

Transformed Murine and Canine MSCs Have Numerous Structural Variants and Copy Number Alterations

To study the complex genomics in transformed murine and canine MSCs in more detail, copy number alterations and structural variants were determined for three murine MSC cultures (B6_4, B6_7 and B6_10), by comparing late passage MSCs with early passage MSCs, and the canine MSC culture (OSBMSC1), by comparing canine MSCs with normal tissue from the same dog, using WGS. For murine MSCs, all transformed late passage samples show numerous copy number alterations across the entire genome (**Figure 5A**). Although late passage MSCs from B6_7 harbored a large deletion in chromosome 4, including the *Cdkn2a* and *Cdkn2b* gene (**Table S1** available online), no recurrent copy number alterations were found. Furthermore, no deviations in whole chromosomes were identified in early passage murine MSCs (**Figure S4** available online).

For canine MSCs, in the early passage MSCs there were two apparent copy number alterations: a duplication of chromosome 20, and a small regional duplication in chromosome 4 (**Figure 5B**). After transformation, aneuploidy was apparent in the copy ratio plots. The copy ratios for P34 show that the abnormalities in chromosomes 4 and 20 were retained, but in addition a myriad of other chromosomes showed changes in copy ratio (**Figure 5B**).

For murine MSCs, the number of structural variants was limited (**Figure 5C**). No recurrent structural variants were identified between the different mice. Furthermore, the number of variants varied between the different samples. This was apparent in the number of inter chromosomal translocations in the samples, with no translocations detected in B6_4, only one translocation in B6_7 between chromosome 9 and X, and translocations between chromosome 1 and 5 and chromosome 3 and 7 in B6_10 (**Figure S5A** available online).

For canine MSCs, the overall number of structural variants increased dramatically after MSC transformation (**Figure 5D**). Whereas the structural variations in the early passages were

limited to two deletions and two inversions, in the late passage, samples a progression in the number of structural variants was observed. The increase in structural variations like translocations highlight the emergence of a complex karyotype upon MSC transformation (**Figure S5B** available online). However, structural variants found in transformed canine MSCs were not observed in the orthologous genomic regions in transformed murine MSCs.

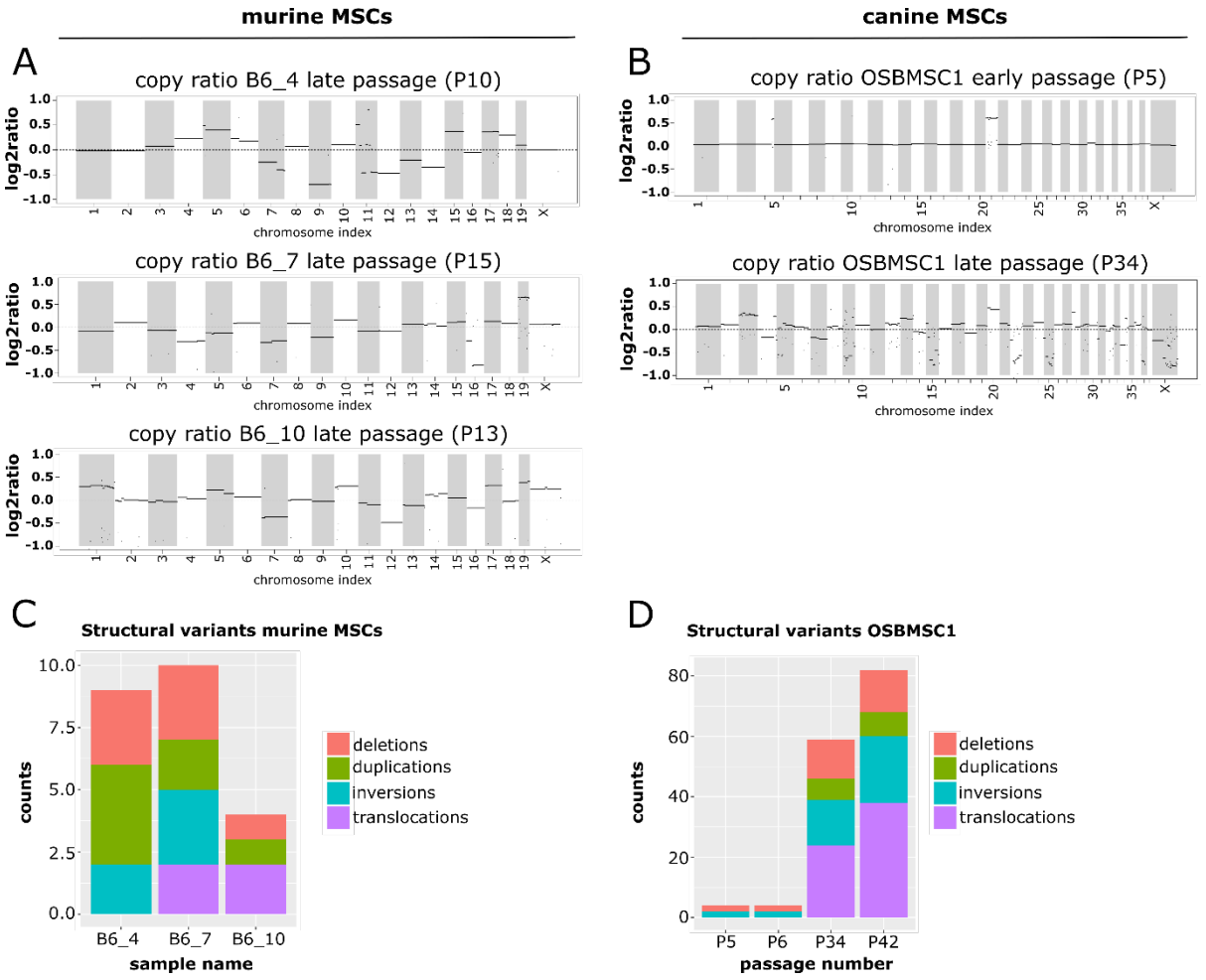

Figure 5. Late passage murine and canine MSCs show a complex molecular karyotype after whole-genome sequencing. Segmented copy ratios are shown for (**A**) late passage murine MSCs and (**B**) early and late passage canine MSCs. Positive copy ratios indicate a gain of genomic materials, whereas negative ratios indicate losses. The total number of structural variants in (**C**) late passage murine MSCs and (**D**) early and late passage canine MSCs.

Cross-Species Analysis Reveal TP53/Trp53 Mutation as a Common Single-Nucleotide Variant in Transformed Murine and Canine MSCs

To search for common driver alterations (SNVs) that may play a role in the initiation of sarcomas with a complex genome, whole genome sequences from three murine and one canine MSC line, before and after spontaneous transformation, were compared.

The SNV with the highest allele frequency in late passage murine MSCs of mouse B6_4 and B6_10, and the only SNV overlapping between different mice (**Figure 6A, Table S2** available online), was a non-synonymous point mutation in *Trp53*. This point mutation in murine MSCs was a T > A/L191H and a T > G/L191R variant in mouse B6_4 and B6_10, respectively (**Figure 6B**). This mutation was confirmed by Sanger sequencing in B6_4 and B6_10 transformed MSCs (**Figure S6** available online), which was not present in B6_7. No other mutations in *Trp53* in the same exon or in the most commonly mutated (52) exons, 4, 5, 7, and 8 were identified in other transformed murine MSCs (NMRI_2, NMRI_3, NMRI_9) (**Figure S6** available online). Using COBALT (42), the identified variants were shown to be orthologous to the human *TP53* variant L194H or L194R, both reported to be likely pathogenic according to ClinVar. As cisplatin treatment causes DNA damage and activates the p53 pathway, functionality of p53 was assessed by treating murine MSCs with PBS or cisplatin (3 or 10 μM). MSCs from B6_4 and B6_10 treated with cisplatin only slightly increased p53 expression (1.2–2.1 fold). This was in contrast with MSCs from B6_7, where cisplatin treatment increased the expression of p53 over 3-fold (**Figure 6C**), although this was not statistically significant.

In late passage canine MSCs, we identified more SNVs and small indels compared to early passage MSCs (**Figure 6A**). In the transformed MSCs, the variant with the highest allele frequency was in *TP53*, with an allele frequency of almost 1, indicating loss of the WT allele (**Figure 6B; Table S3** available online). This was an A668T/C230S variant. C230 is located in the *TP53* DNA-binding domain and as the amino acid introduces a cysteine it is likely that the variant has a negative impact on the functioning of p53. Using COBALT, this variant is orthologous to the human *TP53* variant C242S and reported to be likely pathogenic according to ClinVar (rs1057519982). As the canine MSCs have been isolated from a dog with osteosarcoma, the question remained whether the transformed cells could originate from a micrometastasis from the original tumor. The *TP53* mutation we identified in the transformed/late passage MSCs was absent in the tumor and in the healthy tissue of the dog (**Figure S7** available online) and has not been identified previously in NGS studies of osteosarcoma in canine patients (53, 54).

Aside from *TP53*, the only gene with a variant that was present at an allele frequency over 0.75 in both P34 and P42 OSBMSC1 is *UNC80* C1145G/P382R. The protein encoded by *UNC80* is part of the sodium leak ion channel (*NALCN*) (55). Variants in *NALCN* and *UNC80* have been linked to many diseases, including several types of cancer (55, 56). However, the P382R variant is not located in any Pfam or InterPro annotated domains, therefore its impact on protein function is more difficult to assess.

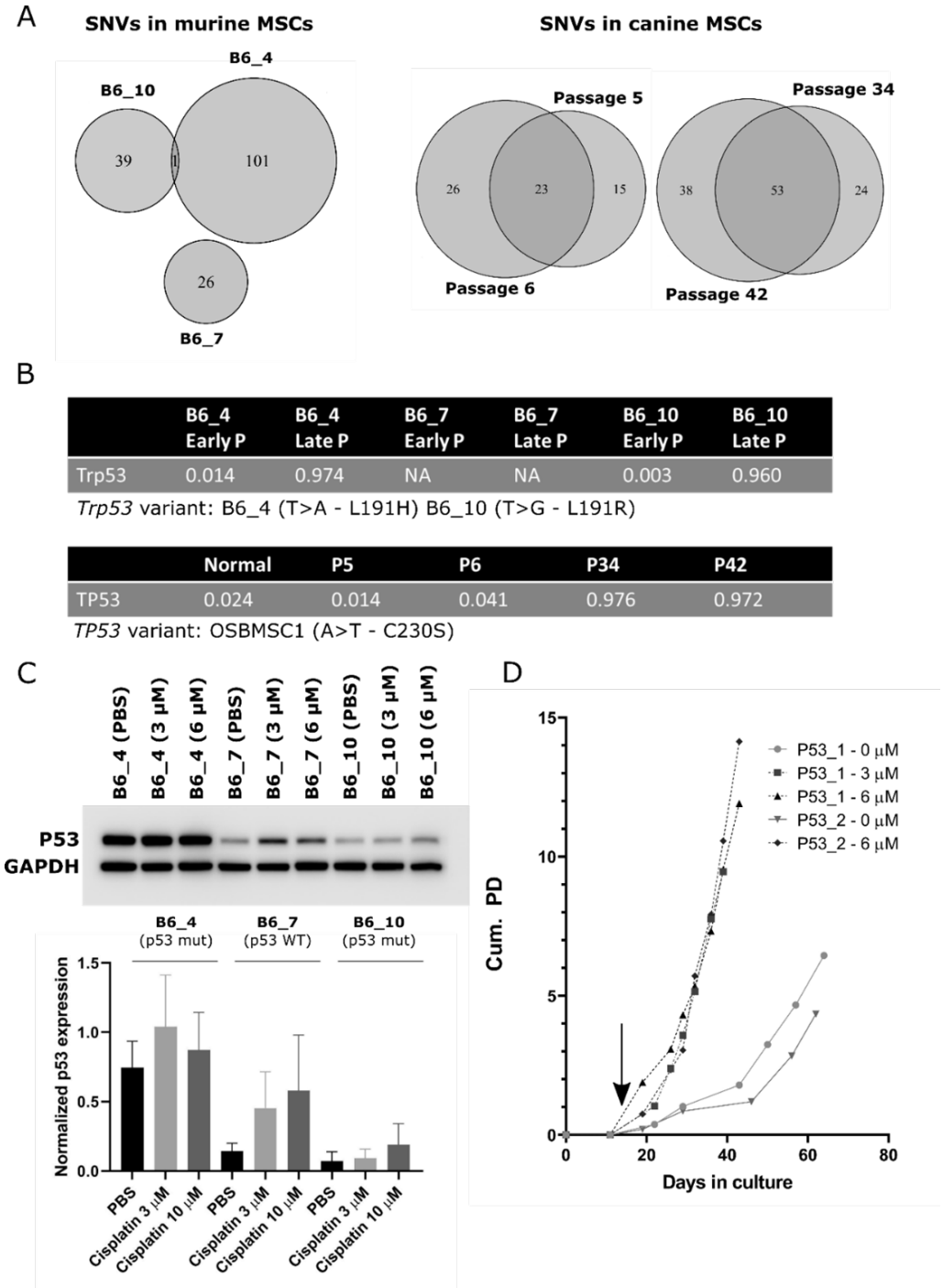

	B6_4 Early P	B6_4 Late P	B6_7 Early P	B6_7 Late P	B6_10 Early P	B6_10 Late P
Trp53	0.014	0.974	NA	NA	0.003	0.960

Trp53 variant: B6_4 (T>A - L191H) B6_10 (T>G - L191R)

	Normal	P5	P6	P34	P42
TP53	0.024	0.014	0.041	0.976	0.972

TP53 variant: OSBMSC1 (A>T - C230S)

Figure 6. Point mutations in *TP53/Trp53* are a common single nucleotide variant (SNV) in transformed murine and canine MSCs. Venn diagrams depicting the total number of SNVs and small indels in (**A**) late passage murine MSCs and early and late passage canine MSCs. (**B**) Single nucleotide variant in *Trp53* or *TP53* was the SNV with the highest allele frequency in late passage murine and canine MSCs. (**C**) Western blot showing p53 protein expression in late passage murine MSCs, treated with PBS or cisplatin (3 and 10 μM). Murine MSCS with WT p53 (B6_7) increase p53 expression over 3-fold, whereas murine MSCS with mutant p53 (B6_4 and B6_10) increase p53 expression only 1.2–2.1 fold, indicating p53 function is partially impaired in these cells. GAPDH was used as a loading control. Quantification of relative p53 protein expression to GAPDH is depicted on the bottom panel. Statistical analysis was performed based on three independent experiments, but here only one representative blot is shown. No changes in protein expression were statistically significant. Whole blots with densitometry readings can be found in Figure S9. (**D**) Murine MSCs from Kcre/p53f mice were treated with cre-recombinase (3 or 6 μM) at day 11 (indicated by black arrow) inducing immediate transformation, whereas non-treated MSCS transform later. At each data point, cells were trypsinized and counted to calculate cumulative population doubling (Cum. PD).

Murine MSCs with a KO of P53 Transform Earlier Compared to WT Murine MSCs

As both murine and canine transformed MSCs had acquired *TP53/Trp53* alterations upon transformation, we further investigated the role of *TP53/Trp53* in spontaneous malignant transformation. We created a KO of *Trp53* in murine MSCs, in which exon 2-10 are flanked by Lox-sites, by in vitro treatment with cre-recombinase. We observed that MSCs treated with 3 or 6 µM cre-recombinase, transformed immediately after treatment, whereas non-treated murine MSCs transformed after 60 days, comparable with MSCs from mice of other WT strains (**Figures 6D and 1A**). KO of *Trp53* was confirmed by Western blotting and PCR (**Figure S8A,B** available online). Transformed *Trp53* KO MSCs showed a complex karyotype with aneuploidy (**Figure S8C** available online). To exclude that cre-recombinase treatment itself has an effect on cell expansion, we treated MSCs from FVB WT mice with cre-recombinase, which did not have an effect on expansion rate (**Figure S8D** available online). These results confirm that p53 plays an important role in the spontaneous transformation of MSCs and the generation of a complex genome.

Discussion

The pathogenesis of sarcomas with complex genomics is notoriously difficult to study, especially if no benign precursor is known, e.g., for osteosarcoma. Here we use MSCs from mice and a dog that spontaneously transform in vitro, to pinpoint, among the huge amount of genetic alterations, those genes, including *TP53*/*Trp53*, that are involved in the initiation of sarcomas with complex genomics.

There is an interesting difference between species, where human MSCs never transform in vitro (24), canine MSCs occasionally transform, and murine MSCs always show a spontaneous transformation. We and others have shown that all bone-marrow-derived murine MSCs, independent of strain or age, eventually transform (20-23). For the first time, we now also observed spontaneous transformation in canine MSCs. In contrast to murine MSCs, the phenomenon is rarer in canine MSCs, as only one out of six canine MSC cultures transformed spontaneously, even though cultures were kept for over 150 days. Of note, the canine MSCs that transformed were isolated from an old Rottweiler (7 years) with osteosarcoma, whereas the other donors were Labrador Retrievers, much younger (4–5 months) and without osteosarcoma, so transformation of MSCs in dogs might be age and breed dependent. Furthermore, we excluded that the transformed MSC cultures from the Rottweiler originated from a micrometastasis from the osteosarcoma, as the TP53 mutation that was found in the transformed canine MSCs, was absent in the primary tumor, although we cannot completely rule out that Sanger sequencing missed a subclonal presence of the mutation in the tumor. The difference in transformation between species might also be explained by inbreeding. The mice used in this study were inbred mouse strains, resulting in a more homozygous genome, such that it could possibly cause more frequent spontaneous transformation compared to dogs or humans.

After subcutaneous injection of transformed murine MSCs, mice formed tumors with variable growth rate and histology. The tumors with a slower growth rate showed osteogenic differentiation, and are histologically identical to human high- grade osteosarcoma. The faster growing tumors were highly cellular and pleomorphic, morphologically lacking any line of differentiation, suggesting resemblance to human undifferentiated (pleomorphic) sarcoma, although immunohistochemical markers commonly used to rule out specific lines of differentiation, for instance myogenic differentiation, could not be applied on the mouse tissue because these antibodies are of mouse origin, rendering stainings non-specific. As the histology of the tumors is diverse after subcutaneous injection, it is possible that additional (epi)genetic factors determine the definitive histological subtype or that it is determined by the micro environment, which would have to be studied in an orthotopic model. In contrast to murine MSCs, the transformed canine MSCs did not form tumors in athymic mice, both subcutaneously and intratibially. It might be that canine cells have difficulty engrafting in a mouse microenvironment, however, previously published studies reported the successful growth of (adipose-derived) MSCs and osteosarcoma cell lines from canine origin in immune deficient mice, both subcutaneously and intratibially (57, 58).

Transformed murine and canine MSCs show translocations, copy number alterations, and an increased number of single nucleotide variants and structural variants in later passages, resembling the genomic alterations in sarcomas with complex genomics. By COBRA-FISH karyotyping, we identified that prior to the transformation event, cells showed both numerical and structural changes with non-clonal random rearrangements and a strikingly high number of centromeric fragments indicating major loss of chromosomal material. After the crisis phase, a clonal expansion of a successor clone was seen with further rearrangements, but with non-clonal variants. In the non-clonal related cells, however, a great genomic instability was depicted by observing chromosomal breaks, chromosomal rearrangement, and acentric fragments that would be leading to further genomic rearrangement or could be lethal for the next cell generation.

The cross-species approach, described in the present study, enabled us not only to investigate single cells during the crisis phase, but also to compare earlier non-transformed passages of the same mouse or dog with cells after transformation, creating the opportunity to identify genes and pathways involved in the formation of sarcomas with complex genomics. We identified point mutations in *TP53/Trp53*, with loss of heterozygosity in the late passages. The important role of p53 in spontaneous transformation is further evident from the murine MSCs that transformed immediately after the induction of a deletion of exon 2-10 of *Trp53*. Taken together, our unique cross species model has identified an important role for *TP53* in the formation of sarcomas with complex genomics. The importance of *TP53* for the malignant transformation process has been found in other cancer types (59-61). Our results are also in line with the hypothesis (62) that *TP53* mutations are early events and selected for in ectodermal and mesodermal-derived tumors, such as sarcomas, in contrast to tumors from endodermal origin, such as colon cancer, in which *TP53* mutations are the last to occur.

In sarcomas with complex genomics, such as undifferentiated sarcoma and osteosarcoma, alterations in *TP53* and/or the p53 pathway are frequently found: 22–66% in UPS and 47–90% in sporadic osteosarcoma [5,9,10,17,18,63]. Previous studies have shown a link between *TP53* alterations and chromoanagenesis, characteristic for complex genomics sarcomas such as osteosarcoma, but the precise mechanism is unknown (7, 63-65). *TP53* alterations are not the only causative factor for chromoanagenesis, since there are also tumors with chromoanagenesis with intact *TP53,* and tumors with aberrant *TP53* that do not show chromoanagenesis (66, 67). In this study, we have confirmed an important role for *TP53* in the initiation of sarcomas with complex genomics, as two out of three murine MSCs carried alterations in *TP53*. This indicates, however, that also other alterations besides *TP53* can be involved. In a previous study (20), we have shown that transformed murine MSCs isolated from C57BL6/J or BALBC mice had a homozygous deletion in the locus containing *Cdkn2a* and *Cdkn2b*. These transformed murine MSCs formed osteosarcoma when injected subcutaneously into mice. In this study, we also identified a large deletion in the same gene in late passage MSCs from mouse B6_7. In osteosarcoma, alterations in *RB1* are identified in 29–47% of tumors (5, 8-10). RB1 activity is regulated by p16 and p15, proteins encoded by *CDKN2A* and *CDKN2B*, respectively. Moreover, mice with a conditional deletion of either *Tp53* or both *Tp53* and *Rb1* developed osteosarcomas (68). In our COBRA-FISH karyotyping data, we also observed frequent rearrangements in chromosome 4, carrying the *Cdkn2a* and *Cdkn2b* genes. This all further supports the involvement of different pathways besides p53 towards the transformation of sarcoma with complex genomics.

Conclusion

In summary, we have shown that transformed murine and canine MSCs provide a unique cross-species model for the identification of driver events in sarcomas with complex genomics. Spontaneously transformed murine MSCs show a plethora of genomic alterations, including copy number alterations, structural variants and point mutations, and form sarcomas in mice after subcutaneous injection. A cross-species analysis revealed that loss of p53 is a driver event in the formation of sarcomas with complex genomics.

Acknowledgments

The authors would like to thank Wim Corver for the flow cytometric DNA content analysis; Paul Krimpenfort for providing the WT FVB mice; Alex Mohseny, Melissa van Pel, Leon Mei, Marieke Kuijjer and Michelle Teunissen for helpful discussions; Daniela Salvatori and Nelleke Verhave for help with writing the project license application for animal procedures; Inge Briaire-de Bruijn, Pauline Wijers-Koster, and Brendy van den Akker for technical assistance; Ivo Que for the MicroCT imaging.

References

1. WHO classification of tumours of soft tissue and bone, 5th edition. Lyon, France: WHO Classification of Tumours Editorial Board; 2020.
2. Lam SW, van Ijzendoorn DGP, Cleton-Jansen AM, Szuhai K, Bovée JVMG. Molecular Pathology of Bone Tumors. The Journal of Molecular Diagnostics. 2019;21(2):171-82.
3. Franceschini N, Lam SW, Cleton-Jansen AM, Bovée JVMG. What's new in bone forming tumours of the skeleton? Virchows Arch. 2020;476(1):147-57.
4. Jain S, Xu R, Prieto VG, Lee P. Molecular classification of soft tissue sarcomas and its clinical applications. Int J Clin Exp Pathol. 2010;3(4):416-29.
5. Behjati S, Tarpey PS, Haase K, Ye H, Young MD, Alexandrov LB, et al. Recurrent mutation of IGF signalling genes and distinct patterns of genomic rearrangement in osteosarcoma. Nat Commun. 2017;8:15936.
6. Stephens PJ, Greenman CD, Fu B, Yang F, Bignell GR, Mudie LJ, et al. Massive genomic rearrangement acquired in a single catastrophic event during cancer development. Cell. 2011;144(1):27-40.
7. Cortes-Ciriano I, Lee JJ, Xi R, Jain D, Jung YL, Yang L, et al. Comprehensive analysis of chromothripsis in 2,658 human cancers using whole-genome sequencing. Nat Genet. 2020;52(3):331-41.
8. Chen X, Bahrami A, Pappo A, Easton J, Dalton J, Hedlund E, et al. Recurrent somatic structural variations contribute to tumorigenesis in pediatric osteosarcoma. Cell Rep. 2014;7(1):104-12.
9. Kovac M, Blattmann C, Ribi S, Smida J, Mueller NS, Engert F, et al. Exome sequencing of osteosarcoma reveals mutation signatures reminiscent of BRCA deficiency. Nat Commun. 2015;6:8940.
10. Perry JA, Kiezun A, Tonzi P, Van Allen EM, Carter SL, Baca SC, et al. Complementary genomic approaches highlight the PI3K/mTOR pathway as a common vulnerability in osteosarcoma. Proc Natl Acad Sci U S A. 2014;111(51):E5564-73.
11. Sayles LC, Breese MR, Koehne AL, Leung SG, Lee AG, Liu HY, et al. Genome-Informed Targeted Therapy for Osteosarcoma. Cancer Discov. 2019;9(1):46-63.
12. Shao YW, Wood GA, Lu J, Tang QL, Liu J, Molyneux S, et al. Cross-species genomics identifies DLG2 as a tumor suppressor in osteosarcoma. Oncogene. 2019;38(2):291-8.
13. Ji J, Quindipan C, Parham D, Shen L, Ruble D, Bootwalla M, et al. Inherited germline ATRX mutation in two brothers with ATR-X syndrome and osteosarcoma. American Journal of Medical Genetics Part A. 2017;173(5):1390-5.
14. Smolle MA, Heitzer E, Geigl JB, Al Kaissi A, Liegl-Atzwanger B, Seidel MG, et al. A novel mutation in ATRX associated with intellectual disability, syndromic features, and osteosarcoma. Pediatr Blood Cancer. 2017;64(10).
15. Mejia-Guerrero S, Quejada M, Gokgoz N, Gill M, Parkes RK, Wunder JS, et al. Characterization of the 12q15MDM2and 12q13-14CDK4amplicons and clinical correlations in osteosarcoma. Genes, Chromosomes and Cancer. 2010:NA-NA.
16. Movva S, Wen W, Chen W, Millis S. Multi-platform profiling of over 2000 sarcomas: Identifcation of biomarkers and novel therapeutic targets. Oncotarget. 2015;6(14).
17. Lewin J, Garg S, Lau BY, Dickson BC, Traub F, Gokgoz N, et al. Identifying actionable variants using next generation sequencing in patients with a historical diagnosis of undifferentiated pleomorphic sarcoma. Int J Cancer. 2018;142(1):57-65.
18. Zheng B, Qu Y, Wang J, Shi Y, Yan W. Pathogenic and Targetable Genetic Alterations in Resected Recurrent Undifferentiated Pleomorphic Sarcomas Identified by Targeted Next-generation Sequencing. Cancer Genomics Proteomics. 2019;16(3):221-8.
19. Steele CD, Tarabichi M, Oukrif D, Webster AP, Ye H, Fittall M, et al. Undifferentiated Sarcomas Develop through Distinct Evolutionary Pathways. Cancer Cell. 2019;35(3):441-56 e8.

20. Mohseny AB, Szuhai K, Romeo S, Buddingh EP, Briaire-de Bruijn I, de Jong D, et al. Osteosarcoma originates from mesenchymal stem cells in consequence of aneuploidization and genomic loss of Cdkn2. J Pathol. 2009;219(3):294-305.
21. Xu S, De Becker A, De Raeve H, Van Camp B, Vanderkerken K, Van Riet I. In vitro expanded bone marrow-derived murine (C57Bl/KaLwRij) mesenchymal stem cells can acquire CD34 expression and induce sarcoma formation in vivo. Biochem Biophys Res Commun. 2012;424(3):391-7.
22. Zhou YF, Bosch-Marce M, Okuyama H, Krishnamachary B, Kimura H, Zhang L, et al. Spontaneous transformation of cultured mouse bone marrow-derived stromal cells. Cancer Res. 2006;66(22):10849-54.
23. Tolar J, Nauta AJ, Osborn MJ, Panoskaltsis Mortari A, McElmurry RT, Bell S, et al. Sarcoma Derived from Cultured Mesenchymal Stem Cells. Stem Cells. 2007;25(2):371-9.
24. Buddingh EP, Ruslan SEN, Reijnders CMA, Szuhai K, Kuijjer ML, Roelofs H, et al. Mesenchymal stromal cells of osteosarcoma patients do not show evidence of neoplastic changes during long-term culture. Clinical Sarcoma Research. 2015;5(1).
25. Withrow SJ, Wilkins RM. Cross talk from pets to people: translational osteosarcoma treatments. ILAR Journal. 2010;51(3):208-13.
26. Kirpensteijn J, Kik M, Teske E, Rutteman GR. TP53 gene mutations in canine osteosarcoma. Vet Surg. 2008;37(5):454-60.
27. Jonkers J, Meuwissen R, van der Gulden H, Peterse H, van der Valk M, Berns A. Synergistic tumor suppressor activity of BRCA2 and p53 in a conditional mouse model for breast cancer. Nat Genet. 2001;29(4):418-25.
28. Malagola E, Teunissen M, van der Laan LJ, Verstegen MM, Schotanus BA, van Steenbeek FG, et al. Characterization and Comparison of Canine Multipotent Stromal Cells Derived from Liver and Bone Marrow. Stem Cells Dev. 2016;25(2):139-50.
29. Lau SF, Hazewinkel HA, Grinwis GC, Wolschrijn CF, Siebelt M, Vernooij JC, et al. Delayed endochondral ossification in early medial coronoid disease (MCD): a morphological and immunohistochemical evaluation in growing Labrador retrievers. Vet J. 2013;197(3):731-8.
30. Szuhai K, Tanke HJ. COBRA: combined binary ratio labeling of nucleic-acid probes for multi-color fluorescence in situ hybridization karyotyping. Nat Protoc. 2006;1(1):264-75.
31. Vindelov LL, Christensen IJ, Nissen NI. A Detergent-Trypsin Method for the Preparation of Nuclei for Flow Cytometric DNA analysis. Cytometry. 1983;3(5):323-7.
32. Martin M. Cutadapt removes adapter sequences from high-throughput sequencing reads. EMBnet. 2011;17(1).
33. Joshi NA, Fass JN. Sickle: A sliding-window, adaptive, quality-based trimming tool for FastQ files

(Version 1.33). [Software]. 2011.
34. Li H, Durbin R. Fast and accurate short read alignment with Burrows-Wheeler transform. Bioinformatics. 2009;25(14):1754-60.
35. McKenna A, Hanna M, Banks E, Sivachenko A, Cibulskis K, Kernytsky A, et al. The Genome Analysis Toolkit: a MapReduce framework for analyzing next-generation DNA sequencing data. Genome Res. 2010;20(9):1297-303.
36. DePristo MA, Banks E, Poplin R, Garimella KV, Maguire JR, Hartl C, et al. A framework for variation discovery and genotyping using next-generation DNA sequencing data. Nat Genet. 2011;43(5):491-8.
37. Van der Auwera GA, Carneiro MO, Hartl C, Poplin R, Del Angel G, Levy-Moonshine A, et al. From FastQ data to high confidence variant calls: the Genome Analysis Toolkit best practices pipeline. Current protocols in bioinformatics. 2013;43:11.0.1-33.
38. Kim S, Scheffler K, Halpern AL, Bekritsky MA, Noh E, Kallberg M, et al. Strelka2: fast and accurate calling of germline and somatic variants. Nature methods. 2018;15(8):591-4.

39. Koboldt DC, Zhang Q, Larson DE, Shen D, McLellan MD, Lin L, et al. VarScan 2: somatic mutation and copy number alteration discovery in cancer by exome sequencing. Genome Res. 2012;22(3):568-76.
40. Wang K, Li M, Hakonarson H. ANNOVAR: functional annotation of genetic variants from high-throughput sequencing data. Nucleic Acids Research. 2010;38(16):e164-e.
41. Durinck S, Spellman PT, Birney E, Huber W. Mapping identifiers for the integration of genomic datasets with the R/Bioconductor package biomaRt. Nat Protoc. 2009;4(8):1184-91.
42. Papadopoulos JS, Agarwala R. COBALT: constraint-based alignment tool for multiple protein sequences. Bioinformatics. 2007;23(9):1073-9.
43. COBALT [Available from: https://www.ncbi.nlm.nih.gov/tools/cobalt/re_cobalt.cgi.
44. ClinVar [Available from: https://www.ncbi.nlm.nih.gov/clinvar/.
45. Seshan VE, Olshen A. DNAcopy: DNA copy number data analysis. R package version 1560. 2019.
46. RCoreTeam. R: A language and environment for statistical computing. R Foundation for Statistical Computing. 2014.
47. Rausch T, Zichner T, Schlattl A, Stütz AM, Benes V, Korbel JO. DELLY: structural variant discovery by integrated paired-end and split-read analysis. Bioinformatics. 2012;28(18):i333-i9.
48. Chen X, Schulz-Trieglaff O, Shaw R, Barnes B, Schlesinger F, Källberg M, et al. Manta: rapid detection of structural variants and indels for germline and cancer sequencing applications. Bioinformatics. 2015;32(8):1220-2.
49. Layer RM, Chiang C, Quinlan AR, Hall IM. LUMPY: a probabilistic framework for structural variant discovery. Genome Biology. 2014;15(6):R84.
50. Jeffares DC, Jolly C, Hoti M, Speed D, Shaw L, Rallis C, et al. Transient structural variations have strong effects on quantitative traits and reproductive isolation in fission yeast. Nature Communications. 2017;8:14061.
51. Tomayko MM, Reynold CP. Determination of subcutaneous tumor size in athymic (nude) mice. Cancer Chemotherapy and Pharmacology. 1989;24:148-54.
52. IARC TP53 Database [Available from: https://p53.iarc.fr/.
53. Gardner HL, Sivaprakasam K, Briones N, Zismann V, Perdigones N, Drenner K, et al. Canine osteosarcoma genome sequencing identifies recurrent mutations in DMD and the histone methyltransferase gene SETD2. Commun Biol. 2019;2:266.
54. Sakthikumar S, Elvers I, Kim J, Arendt ML, Thomas R, Turner-Maier J, et al. SETD2 Is Recurrently Mutated in Whole-Exome Sequenced Canine Osteosarcoma. Cancer Res. 2018;78(13):3421-31.
55. Cochet-Bissuel M, Lory P, Monteil A. The sodium leak channel, NALCN, in health and disease. Front Cell Neurosci. 2014;8:132-.
56. Hu B, Shi C, Jiang H, Qin S. Identification of novel therapeutic target genes and pathway in pancreatic cancer by integrative analysis. Medicine (Baltimore). 2017;96(42):e8261-e.
57. Requicha JF, Carvalho PP, Anjos Pires M, Isabel Dias M. Evaluation of Canine Adipose-derived Stem Cells in a Healthy Mice Subcutaneous Model. Journal of Stem Cell Research & Therapy. 2016;6(9).
58. Scott MC, Tomiyasu H, Garbe JR, Cornax I, Amaya C, O'Sullivan MG, et al. Heterotypic mouse models of canine osteosarcoma recapitulate tumor heterogeneity and biological behavior. Dis Model Mech. 2016;9(12):1435-44.
59. Rivlin N, Brosh R, Oren M, Rotter V. Mutations in the p53 Tumor Suppressor Gene: Important Milestones at the Various Steps of Tumorigenesis. Genes & Cancer. 2011;2(4):466-74.
60. Mantovani F, Collavin L, Del Sal G. Mutant p53 as a guardian of the cancer cell. Cell Death Differ. 2019;26(2):199-212.
61. Walerych D, Napoli M, Collavin L, Del Sal G. The rebel angel: mutant p53 as the driving oncogene in breast cancer. Carcinogenesis. 2012;33(11):2007-17.

62. Levine AJ. p53: 800 million years of evolution and 40 years of discovery. Nat Rev Cancer. 2020;20(8):471-80.
63. Rausch T, Jones DT, Zapatka M, Stutz AM, Zichner T, Weischenfeldt J, et al. Genome sequencing of pediatric medulloblastoma links catastrophic DNA rearrangements with TP53 mutations. Cell. 2012;148(1-2):59-71.
64. Hermsen R, Toonen P, Kuijk E, Youssef SA, Kuiper R, van Heesch S, et al. Lack of major genome instability in tumors of p53 null rats. PLoS One. 2015;10(3):e0122066.
65. Muller PA, Vousden KH. Mutant p53 in cancer: new functions and therapeutic opportunities. Cancer Cell. 2014;25(3):304-17.
66. Cohen A, Sato M, Aldape K, Mason CC, Alfaro-Munoz K, Heathcock L, et al. DNA copy number analysis of Grade II-III and Grade IV gliomas reveals differences in molecular ontogeny including chromothripsis associated with IDH mutation status. Acta Neuropathol Commun. 2015;3:34.
67. Mehine M, Kaasinen E, Makinen N, Katainen R, Kampjarvi K, Pitkanen E, et al. Characterization of uterine leiomyomas by whole-genome sequencing. N Engl J Med. 2013;369(1):43-53.
68. Walkley CR, Qudsi R, Sankaran VG, Perry JA, Gostissa M, Roth SI, et al. Conditional mouse osteosarcoma, dependent on p53 loss and potentiated by loss of Rb, mimics the human disease. Genes Dev. 2008;22(12):1662-76

Part II

Utilizing in vitro models to identify novel treatment options in osteosarcoma

Chapter 5

A murine mesenchymal stem cell model for initiating events in osteosarcomagenesis points to CDK4/CDK6 inhibition as a therapeutic target

Natasja Franceschini, Raffaele Gaeta, Paul Krimpenfort, Inge Briaire-de Bruijn, Alwine B. Kruisselbrink, Karoly Szuhai, Ieva Palubeckaitė, Anne-Marie Cleton-Jansen and Judith V.M.G. Bovée

Published: *Lab. Invest. 2021;*

Abstract

Osteosarcoma is a high-grade bone-forming neoplasm, with a complex genome. Tumours frequently show chromothripsis, many deletions, translocations and copy number alterations. Alterations in the p53 or Rb pathway are the most common genetic alterations identified in osteosarcoma. Using spontaneously transformed murine mesenchymal stem cells (MSCs) which formed sarcoma after subcutaneous injection into mice, it was previously demonstrated that p53 is most often involved in the transformation towards sarcomas with complex genomics, including osteosarcoma. In the current study, not only loss of p53 but also loss of $p16^{Ink4a}$ is shown to be a driver of osteosarcomagenesis: murine MSCs with deficient $p15^{Ink4b}$, $p16^{Ink4a}$, or $p19^{Arf}$ transform earlier compared to wild-type murine MSCs. Furthermore, in a panel of nine spontaneously transformed murine MSCs, alterations in $p15^{Ink4b}$, $p16^{Ink4a}$, or $p19^{Arf}$ were observed in eight out of nine cases. Alterations in the Rb/p16 pathway could indicate that osteosarcoma cells are vulnerable to CDK4/CDK6 inhibitor treatment. Indeed, using two-dimensional (n=7) and three-dimensional (n=3) cultures of human osteosarcoma cell lines, it was shown that osteosarcoma cells with defective $p16^{INK4A}$ are sensitive to the CDK4/CDK6 inhibitor palbociclib after 72-hour treatment. A tissue microarray analysis of 109 primary tumour biopsies revealed a subset of patients (20-23%) with intact Rb, but defective p16 or overexpression of CDK4 and/or CDK6. These patients might benefit from CDK4/CDK6 inhibition, therefore our results are promising and might be translated to the clinic.

Introduction

Osteosarcoma is the most common malignant mesenchymal tumour of the bone in children and adolescents and characterized by osteoid formation. Compared to other cancer types driven by a specific mutation , osteosarcomas show highly complex genomes with a relatively high occurrence of chromoanagenesis, such as chromothripsis (1-3). Recurrent alterations are rare, but most often osteosarcomas harbour loss-of-function alterations in *TP53* (47-90%) (1, 4, 5). The second most common alteration inactivates *RB1* (29-47%) (4, 5), a tumour suppressor gene controlling cell cycle progression (6). Other regulators of the cell cycle pathway are also often affected in osteosarcoma. *CDK4* is amplified in 10% of high-grade osteosarcomas, and together with *CDK6* directly controls Rb activity by phosphorylation of Rb (7-9). Upstream of the Rb pathway, $p15^{INK4B}$ and $p16^{INK4A}$ can inhibit CDK4 and CDK6 activity (6). $p15^{INK4b}$ is transcribed from the *CDKN2B* gene, whereas $p16^{INK4A}$, and its alternate reading frame $p14^{ARF}$ ($p19^{Arf}$ in mouse), is transcribed from the *CDKN2A* gene (a schematic overview of the locus is depicted in **Supplementary Figure S1** available online). $p14^{ARF}$ / $p19^{Arf}$ is involved in activating p53-dependent growth arrest (10). *CDKN2B* and *CDKN2A* are adjacent loci on the genome and are often co-deleted. Somatic alterations in both genes have been identified in 14-19% of osteosarcomas and also often in other tumour types (11, 12). In particular, deletions of *CDKN2A* are clinically relevant, as loss of $p16^{INK4A}$ is correlated with poor overall survival and poor response to chemotherapy (13-18).
We previously demonstrated that murine and canine mesenchymal stem cells (MSCs) spontaneously transform *in vitro* and can be used to model driver or initiating events involved in the development of sarcomas with complex genomics, including osteosarcoma (19). We showed that spontaneously transformed murine MSCs harbour point mutations in *Trp53* and/or copy number alterations in *Cdkn2a* and *Cdkn2b*. Upon inactivation of *Trp53*, murine MSCs transformed earlier compared to wild-type, confirming the contribution of loss of p53 to spontaneous transformation and development of sarcomas with a complex genome.

In the current study, we investigate the role of the *Cdkn2a/Cdkn2b* genes in the spontaneous transformation of murine MSCs towards osteosarcoma. We show that murine MSCs with deficient $p15^{Ink4b}$, $p16^{Ink4a}$, or $p19^{Arf}$ transform earlier compared to wild-type MSCs. Furthermore, we demonstrate that the defective cell cycle regulation pathway caused by $p16^{INK4A}$ inactivation can be therapeutically exploited using the selective CDK4/CDK6 inhibitor palbociclib in both 2D and 3D *in vitro* culture models of osteosarcoma cell lines. Our study demonstrates that 20-23% of primary osteosarcoma biopsies showed intact Rb, but defective $p16^{INK4A}$ or overexpression of CDK4 and/or CDK6, indicating potential benefit from CDK4/CDK6 inhibition in almost one quarter of osteosarcoma patients.

Materials and Methods

Cell culture

Murine bone-marrow derived mesenchymal stem cells (MSCs) were isolated as described previously (19), from surplus C57BL/6J (B6_4, B6_5, B6_7, B6_10), surplus NMRI (NMRI_2, NMRI_3, NMRI_9) mice, or C57BL/6J mice kindly gifted by Dr. Melissa van Pel (BM42, BM91). Growth curves, differentiation capacity, in vivo growth capacity and a detailed genomic analysis using whole genome sequencing have been described elsewhere for B6_4, B6_7, B6_10 (19). Additional murine MSCs were isolated from surplus FVB mice and mice with deficient $p15^{Ink4b}$ (Ink4b -/-), $p16^{Ink4a}$ (Ink4a -/-), $p15^{Ink4b}$ and $p16^{Ink4a}$ (Ink4ab -/-), or $p19^{Arf}$ (Arf -/-) mice. Mice with deficient $p15^{Ink4b-}$ (Ink4b -/-) and $p16^{Ink4a}$ (Ink4a -/-) were generated as described previously (20) (**Supplementary Figure S1** available online). Genetic knockout was confirmed at the protein level by Western blotting and for Ink4ab -/- mice also at the DNA level by PCR using 5'GCAGTGTTGCAGTTTGAACCC 3' as a forward primer and 5'TGTGGCAACTGATTCAGTTGG 3' as a reverse primer (20). All murine MSCs were cultured in alpha MEM (Gibco, Invitrogen Life Technologies, Scotland, UK) supplemented with 15% Performance plus fetal bovine serum (FBS) (Gibco), 1% Pen/Strep (Gibco), and 1% Glutamax (Gibco) at 37 °C with 5% CO_2 in a humidified incubator and were tested regularly for mycoplasma. Each passage cells were trypsinized and counted with a Bürker-Türk counting chamber to calculate population doublings.

Human osteosarcoma cell lines 143B, MG63, MHM, SAOS2, ZK58, HAL and KPD were cultured in RPMI 1640 (Gibco), supplemented with 10% FBS, in a humidified incubator at 37 °C and 5% CO_2. Human cell lines were retrieved from the EuroBoNet consortium (21) and were regularly STR profiled using the GenePrint 10 system kit (Promega, Madison, WI, USA) and tested for mycoplasma. For the generation of multi-cellular tumour spheroids (MCTS) of osteosarcoma cell lines (protocol adapted from (22)), cells were suspended in medium combined with methylcellulose (0.24% (w/v) dissolved in DMEM), and seeded into a 1% agarose coated 96-well plate for seven days before the start of an experiment.

Drug treatment

For 2D cultures, human osteosarcoma cell lines or murine MSCs were seeded (between 3000 – 6000 cells per well) into 96-well plates and after 24 hours treated with PBS or Palbociclib (dissolved in PBS, PD-0332991, Selleckchemicals, Houston, TX, USA) in concentrations ranging from 0.01 µM to 100 µM. Cells were fixed three days after treatment with 4% formaldehyde and stained with 2 µg/ml Hoechst (Invitrogen Life Technologies, Thermo Fisher Scientific, MA, USA) and nuclei were counted with the Cellomics ArrayScan VTI HCS 700 and HCS Studio Cell Analysis Software (Thermo Fisher Scientific). For MCTS, cells were treated with PBS or palbociclib in concentrations ranging from 0.1 µM to 100 µM. Cells were incubated three days after treatment with PrestoBlue cell viability reagent (Invitrogen Life Technologies) for 90 minutes and fluorescence was measured using a microplate reader (Infinite M Plex, Tecan

Group Ltd., Zürich, Switzerland). After read-out, MCTS were fixed in 4% formaldehyde containing Alcian Blue (1:400) and paraffin embedded. To determine cell viability relative to PBS control, dose response curves were made using Graphpad Prism 8 software, after correcting for background reads and normalized growth rates of each cell line, as described previously (23).

Transformation analysis of mesenchymal stem cells

Late passage (> passage 8) murine MSCs were subjected to metaphase analysis and the soft agar anchorage independent growth assay as described previously (19). In short, for metaphase harvest murine MSCs were seeded and treated with Calyculin A (80 nM, LC Laboratories, Woburn, MA, USA). Hereafter, cells were washed, incubated with KCl (0.075 M) and fixed with methanol/glacial acetic acid in a ratio of 4:1. The cell suspension was dropped onto a slide and stained with DAPI for microscopic counting of metaphase chromosomes. For the soft agar anchorage independent growth assay, a cell suspension of 50,000 cells were seeded into a top layer of 0.35% agarose, on top of a bottom layer of 0.7% agarose in non-tissue culture treated 6-well plates and incubated in a humidified incubator at 37 °C with 5% CO_2 for 4 weeks, after which cells were imaged with GelCount (Oxford Optronix, Milton, UK). Previously transformed cells (B6_10) (19) were taken along as a positive control.

Western blotting

For p15, p16, Rb and GAPDH western blots, whole cell Hot-SDS lysates of murine MSCs or osteosarcoma cell lines were collected as described previously (19). For p19 and Histon H3 western blots, nuclear lysates were made by washing cells twice with cold PBS, followed by the addition of PBS-Triton X (0.5%) for 10 minutes, while shaking on ice. Cells were centrifuged twice, washed with PBS-Triton X (0.5%) and the pellet was resuspended in Hot-SDS buffer (1% SDS, 10 mM EDTA, 10 mM Tris pH 7.4) containing protease inhibitor cocktail (Roche, Basel, Switzerland) and phosphatase inhibitor cocktail (Roche). Protein concentrations of lysates were determined with the Biorad DC™ protein assay kit (Bio-rad, Hercules, CA, USA) according to the manufacturer's protocol, measured with a microplate reader (Infinite M Plex, Tecan Group Ltd.).

Sample loading, blotting and quantification were performed as previously described (19). Blots were stained for p15 (1:500, Abcam, Cambridge, UK), p16 (1:1000, clone JC8, Immunologic, WellMed BV, Duiven, The Netherlands), p19 (1:5000, clone ab80, Abcam), Rb (1:500, clone G3-245, BD Pharmingen, San Diego, CA, USA), Histon H3 (1:1000, Cell Signalling, Leiden, The Netherlands), or GAPDH (1:3000, Cell Signalling). Blots were developed with SuperSignal
West Pico PLUS Chemiluminescent Substrate (Thermo Fisher Scientific) using the
ChemiDoc Touch Imaging System (Bio-rad).

Immunohistochemistry

Tissue micro array construction

For this study five osteosarcoma tissue micro arrays (TMA) were used, that contain FFPE samples of primary tumour biopsies, primary tumour resections, local relapses and metastases of 158 patients (not all sample types were available for each patient). Clinicopathological details can be found in **Supplementary Table S1**. Good histological response to chemotherapy was defined as ≥ 90% tumour necrosis after chemotherapy (24). The construction of one of the TMAs has been described previously (cohort 2) (25, 26). For the construction of TMAs for cohorts 1,3, and 4, punches (1.0 mm (cohort 3) or 1.5 mm (cohort 1and 4)) of FFPE samples were placed into an acceptor block using the TMA master (3DHISTECH, Budapest, Hungary). For each tumour, three tissue-cores were present in the same block. For cutting sections, the tape transfer system (39475205, Leica Biosystems, Wetzlar, Germany) was used. Each TMA also contained other tissue types as internal controls for immunohistochemistry.

Immunohistochemical staining

Slides of each TMA or slides containing sections (4 µm) of paraffin embedded MCTS were stained with haematoxylin and eosin (H&E) or used for immunohistochemical staining after deparaffinisation and rehydration. TMA sections were stained for CDK6 (151213, Abbiotec, San Diego, CA, USA), CDK4 (12790, clone D9G3E, Cell Signaling) or Rb (554136, clone G3245, BD Pharmingen). MCTS sections were stained for Rb, Ki67 (clone D2H10, Cell Signaling), cleaved caspase 3 (Cell Signaling), and SATB2 (clone CL0276, Sigma). For CDK6, SATB2, Ki67 and cleaved caspase 3 staining, antigen retrieval was performed by incubation in 10 mM citrate buffer (pH 6) for 10 minutes and cooling down for 2 hours. For CDK4 and Rb staining, antigen retrieval was performed in Tris-EDTA (pH 9). Sections were incubated with primary antibody (Ki67, 1:1600; cleaved caspase 3, 1:800; CDK4, 1:4000; CDK6, 1:100; Rb, 1:2000, SATB2, 1:10) overnight at 4 °C. The next day, sections were incubated with BrightVision one step detection system poly-HRP anti-mouse/rabbit (VWRKDPVO110HRP, Immunologic) for 30 minutes. Sections were then washed with PBS and DAB+ Chromogen (K3468, Dako, Agilent Technologies, CA, USA) was added to each slide for 10 minutes. Slides were counterstained with haematoxylin, dehydrated and mounted.

Immunohistochemical scoring

For TMAs two independent observers (N.F. and R.G.) scored each core semi-quantitatively based on the intensity of the staining and percentage of positive cells, as described previously (27). For intensity, a value of 1 (weak), 2 (moderate), or 3 (strong) was given, and for the percentage of positive cells, a value of 1 (0-24%), 2 (25-49%), 3 (50-74%), or 4 (75-100%). For CDK4 and Rb the staining was nuclear, but for CDK6 both nuclear and cytoplasmic staining was evaluated. Tumours were regarded as positive if the sum of scores for intensity and percentage of positive cells was ≥ 4 for CDK4 (27). Tumours were classified as CDK6 high when

the sum of cytoplasmic and nuclear scores for CDK6 was ≥ 7 (28). Tumours with a sum of scores equal to 0, yet with a positive internal control, were regarded as negative for Rb staining. In case of discrepancies between the two observers, slides were reviewed by a third observer (J.V.M.G.B.) to reach a consensus. For quantification of MCTS, the number of positive cells of cleaved caspase 3 and Ki67 stainings was determined using QuPath Software v.0.2.3 on three different sections on each slide (29).

Statistical analysis

For statistical comparisons between two groups, a student t-test was performed. Correlation analysis was performed using Spearman's correlation. Comparisons between survival curves were performed using the Log-rank (Mantel-Cox) test. All statistical analyses were performed using GraphPad Prism v.8. Comparisons were considered statistically significant using a significance level of 5%.

Results

Loss of CDKN2A/CDKN2B is frequent in spontaneously transformed murine MSCs

We previously identified a large deletion in the *Cdkn2a/Cdkn2b* locus in one of three transformed murine MSC cultures (B6_7), that formed sarcoma *in vivo* (19), for which the *Cdkn2a/Cdkn2b* locus is shown in **Fig 1A**. To evaluate the relevance of *Cdkn2a* and *Cdkn2b* loss we used a larger panel of nine spontaneously transformed murine MSCs, originating from different strains (C57BL/6J or NMRI), for expression of $p15^{Ink4b}$, $p16^{Ink4a}$ and $p19^{Arf}$ at the protein level. Transformation of six out of nine murine MSC lines have been described elsewhere (B6_4, B6_7, B6_10, NMRI_2, NMRI_3, NMRI_9)(19). For the additional three lines, the transformation event was confirmed by karyotyping (B6_5, BM42, BM91; **Supplementary Figure S2** available online). Transformed murine MSC line B6_7 indeed showed loss of protein expression of $p15^{Ink4b}$, $p16^{Ink4a}$ and $p19^{Arf}$. Furthermore, loss of $p15^{Ink4b}$, $p16^{Ink4a}$ or $p19^{Arf}$ is a common event, as six out of nine MSCs have lost $p15^{Ink4b}$ expression, and six out of nine MSCs have lost $p19^{Arf}$ expression (**Fig 1B**). Eight out of nine MSCs show loss of $p16^{Ink4a}$ expression. However, in this western blot loss of $p16^{Ink4a}$ protein expression is not always indicative for $p16^{Ink4a}$ deletion on genomic level, illustrated for instance by murine MSC line B6_4 that has intact $p16^{Ink4a}$ based on whole-genome sequencing data (**Fig 1B**)(19), but does not show $p16^{Ink4a}$ protein expression.

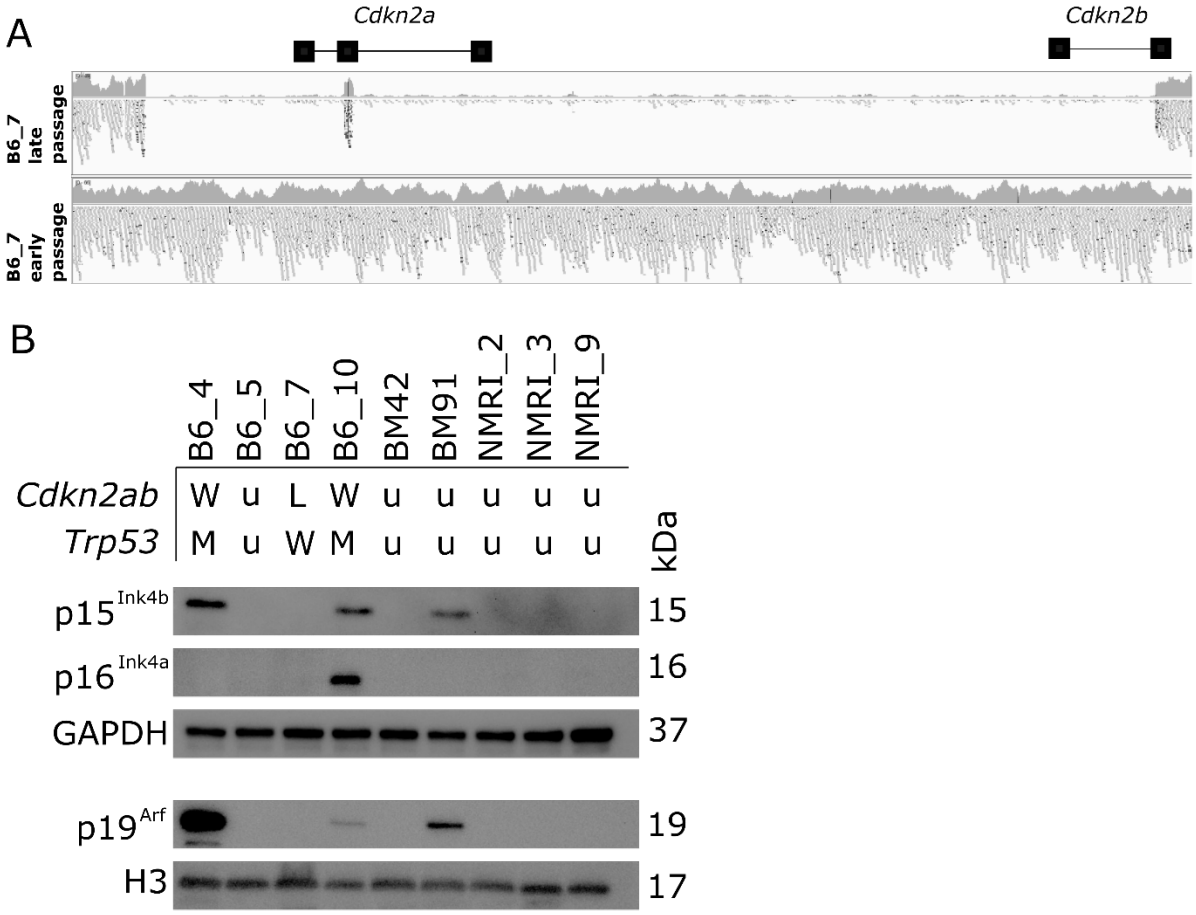

Figure 1. Transformed murine MSCs of different mouse strains frequently show loss of protein expression of $p15^{Ink4b}$, $p16^{Ink4a}$ and $p19^{Arf}$. (**A**) IGV viewer showing a homozygous deletion including both *Cdkn2a* and *Cdkn2b* genes in transformed (late passage) murine MSC B6_7. Early passage cells (P2) were collected prior to the transformation event, whereas late passage cells (P15) were collected after spontaneous transformation. (**B**) Western blot depicting protein expression of $p15^{Ink4b}$, $p16^{Ink4a}$, $p19^{Arf}$ in transformed murine MSCs from C57BL/6J (B6_4, B6_7, B6_10, BM42, BM91) or NMRI mice (NMRI_2, NMRI_3, NMRI_9). GAPDH or Histon H3 was used as a loading control. The size of each band is indicated in kDa. The genomic status of genes *Cdkn2a*, *Cdkn2b*, and *Trp53* is indicated for transformed murine MSCs as described previously (19). M = point mutation, W = wildtype, L = homozygous loss, u = no genomic status available.

Murine MSCs deficient for p16^{Ink4a} and deficient for p15^{Ink4b} transform earlier compared to wildtype MSCs

To evaluate whether loss of p16^{Ink4a} and p15^{Ink4b} or both is important in the spontaneous transformation of murine MSCs, MSCs from mice with loss of p16^{Ink4a} (Ink4a -/-), loss of p15^{Ink4b} (Ink4b -/-), or both (Ink4ab -/-) were cultured long-term to observe when transformation would occur (for a schematic overview of the knockout mice used in this study see **Supplementary Figure S1** available online). Murine MSCs from Ink4a -/-, Ink4b -/- or Ink4ab -/- mice transformed earlier (after 25-46 days) compared to wild-type murine MSCs (after 64-76 days) (**Fig 2A**). As the *Cdkn2a* gene also encodes an alternative reading frame, p19^{Arf}, murine MSCs with a loss of p19^{Arf} were cultured and also shown to transform earlier (after 23 days) compared to wildtype MSCs (after 61 days) (**Fig 2B**). For all knockout mice, the knockout was confirmed by western blotting and for mice with deficient p16^{Ink4a}; p15^{Ink4b} (Ink4ab -/-) mice also at the DNA level by PCR (**Supplementary Figure S3** available online). Transformation of murine MSCs was confirmed by metaphase analysis (**Fig 2C**), as late passage MSCs had higher than the normal modal number of 40 chromosomes. However, none of the knockout MSCs showed soft agar anchorage independent growth (**Fig 2D**). These results show that loss of p16^{Ink4a} and/or p15^{Ink4b} enhanced proliferation and genomic alterations suggesting transformation.

Transformed murine MSCs with loss of p16^{Ink4a} and p15^{Ink4b} are sensitive to palbociclib

Within the Rb pathway, the Ink4 proteins inhibit CDK4/CDK6 activity, thereby inhibiting cell cycle progression. Therefore loss of p16^{Ink4a} and p15^{Ink4b} could make cells more vulnerable to CDK4/CDK6 inhibitors to decrease uncontrolled cell proliferation. To investigate this in our murine mesenchymal stem cell model, transformed murine MSCs, in which p16^{Ink4a} and p15^{Ink4b} loss was confirmed, were treated with the CDK4/CDK6 inhibitor palbociclib. Murine MSCs in which whole-genome sequencing previously confirmed loss of p16^{Ink4a} and p15^{Ink4b} (B6_7) (19) were more sensitive to palbociclib, with an IC_{50} of 0.5 µM compared to transformed MSCs that have intact p16^{Ink4a} and p15^{Ink4b} (B6_4 and B6_10), with IC_{50} values of 3.6 and 10.3 µM, respectively (**Fig 3A**). To determine whether the increased sensitivity was caused by loss of p16^{Ink4a} and p15^{Ink4b}, murine MSCs isolated from Ink4ab$^{-/-}$ mice were treated with palbociclib (**Fig 3B**). MSCs from Ink4ab$^{-/-}$ mice showed the highest sensitivity to palbociclib, with IC_{50} values between 0.8 – 1.2 µM, compared to wild-type MSCs, with an IC_{50} of 8.3 µM, suggesting that loss of p16^{Ink4a} and p15^{Ink4b} increases sensitivity to palbociclib.

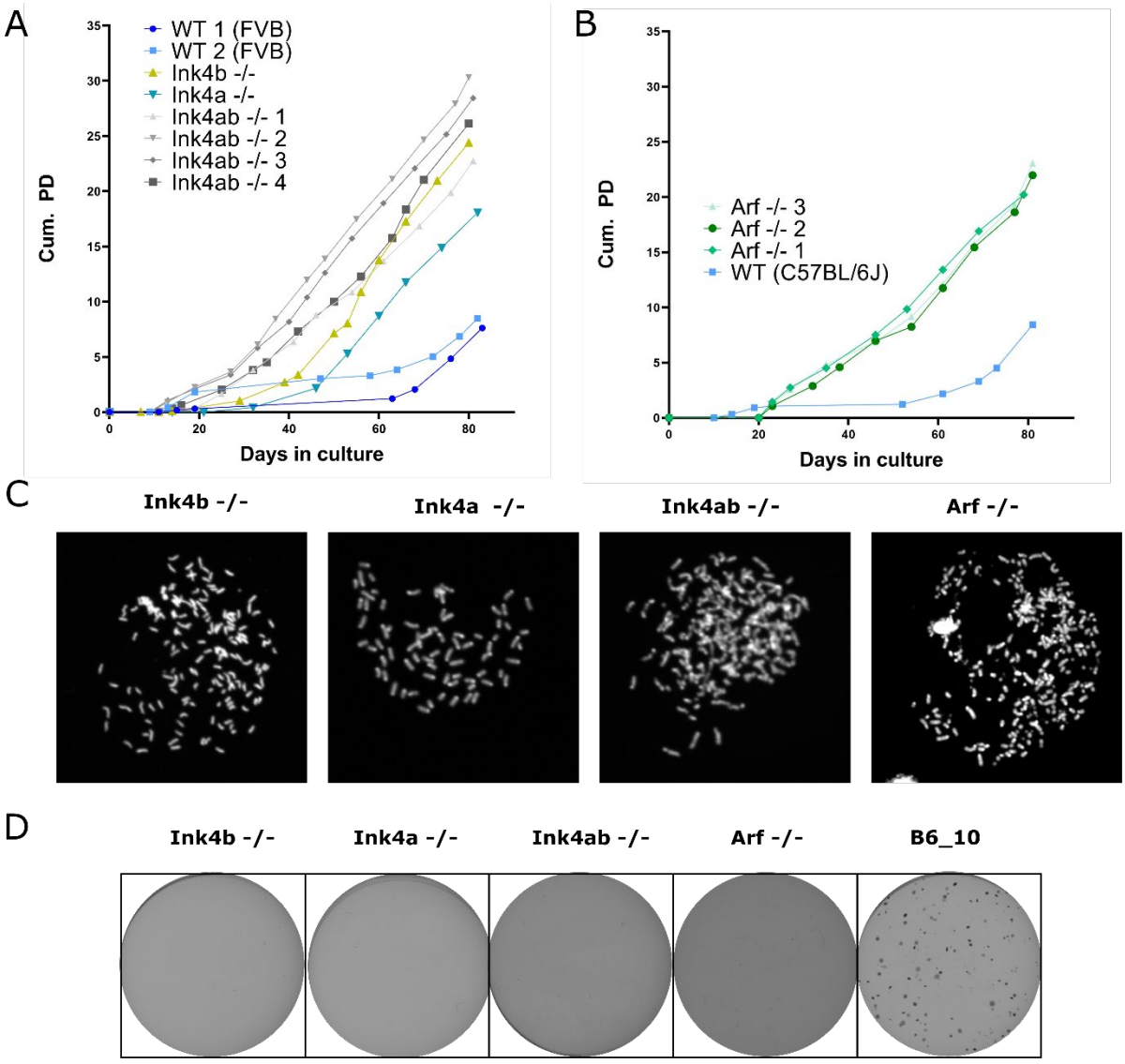

Figure 2. Murine MSCs isolated from (**A**) Ink4a$^{-/-}$ (n=1), Ink4b$^{-/-}$ (n=1), Ink4ab$^{-/-}$ (n=4) (**B**) or Arf$^{-/-}$ (n=3) transform earlier compared to wild-type MSCs from FVB or C57BL/6J mice, based on cumulative population doublings (Cum. PD.). Each datapoint represents a passage of the cell culture. (**C**) Metaphase analysis of murine MSCs from Ink4a$^{-/-}$, Ink4b$^{-/-}$, Ink4ab$^{-/-}$, or Arf$^{-/-}$ mice showed abnormal chromosome numbers, higher than the normal modal number of 40. (**D**) Soft agar anchorage independent growth assay of murine MSCs from Ink4a$^{-/-}$, Ink4b$^{-/-}$, Ink4ab$^{-/-}$, or Arf$^{-/-}$ mice showed no colony formation. Transformed murine MSCs from B6_10 were used as a positive control.

A

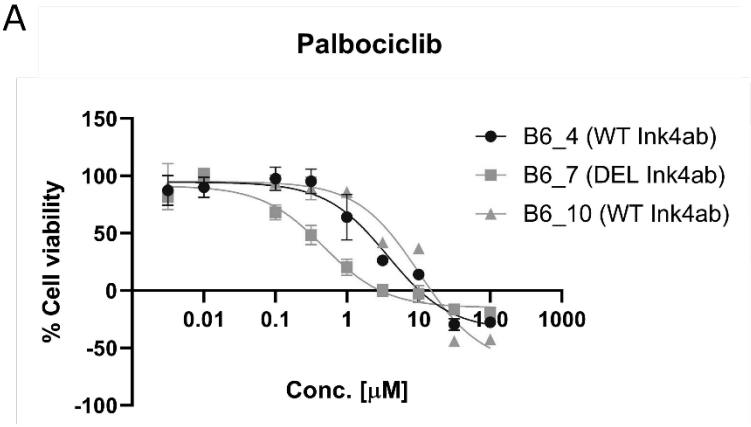

Cell line	IC50 (μM)
B6_4	3.6
B6_7	0.5
B6_10	10.3

B

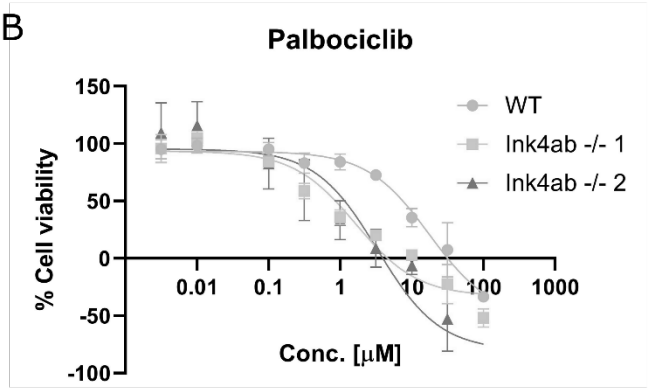

Cell line	IC50 (μM)
WT	8.3
Ink4ab -/- 1	0.8
Ink4ab -/- 2	1.2

Figure 3. Transformed murine MSCs are sensitive to CDK4/CDK6 inhibitor palbociclib. Murine MSCs (**A**) that have spontaneously transformed after long-term culture (B6_4, wildtype (WT) Ink4ab; B6_7, deletion (DEL) of Ink4ab; B6_10, wildtype (WT) Ink4ab) or (**B**) MSCs from Ink4ab$^{-/-}$ mice after transformation were treated with palbociclib for 72 hours after which relative cell viability and IC_{50} values were determined. Wildtype MSCs were derived from FVB mice. Data points represent the mean of three experiments performed ± standard deviation.

Human osteosarcoma cell lines are sensitive to palbociclib

Osteosarcoma cell lines were treated with palbociclib in 2D cultures and IC_{50} values were determined (**Fig 4A**). A highly variable dose-dependent response to palbociclib in all osteosarcoma cell lines was observed. As the efficacy of CDK4/CDK6 inhibition relies on the presence of intact Rb, the Rb status of each osteosarcoma cell line was determined by western blot. All osteosarcoma cell lines (143B, MG63, MHM, HAL and KPD), except for SAOS2 and ZK58, showed Rb expression (**Fig 4B**). SAOS2 and ZK58, with loss of Rb, indeed showed the highest IC_{50} of palbociclib compared to other osteosarcoma cell lines. However, the difference in IC_{50} value between ZK58 and other osteosarcoma cell lines with intact Rb was smaller than for SAOS2. The expression status of other proteins involved in the p16-Rb pathway was investigated, including $p16^{INK4A}$, CDK4 and CDK6. $p16^{INK4A}$ protein expression of each cell line was based on immunohistochemical expression published previously (21) (**Fig 1B**). The p16 immunohistochemical status of each cell line was combined with the IC_{50} values from the current study. Although osteosarcoma cells with loss of $p16^{INK4A}$ showed on average a lower IC_{50} to palbociclib (1.4 μM) than cells with normal $p16^{INK4A}$ expression (4.1 μM), this difference was not statistically significant (p=0.3) (**Fig 4C**). *CDK4* and *CDK6* RNA expression levels were

derived from a previously published dataset (30), and correlation analysis was performed using IC_{50} values from the current study. There was no correlation between *CDK4* and *CDK6* RNA expression and sensitivity to palbociclib in osteosarcoma cell lines (**Fig 4D**).

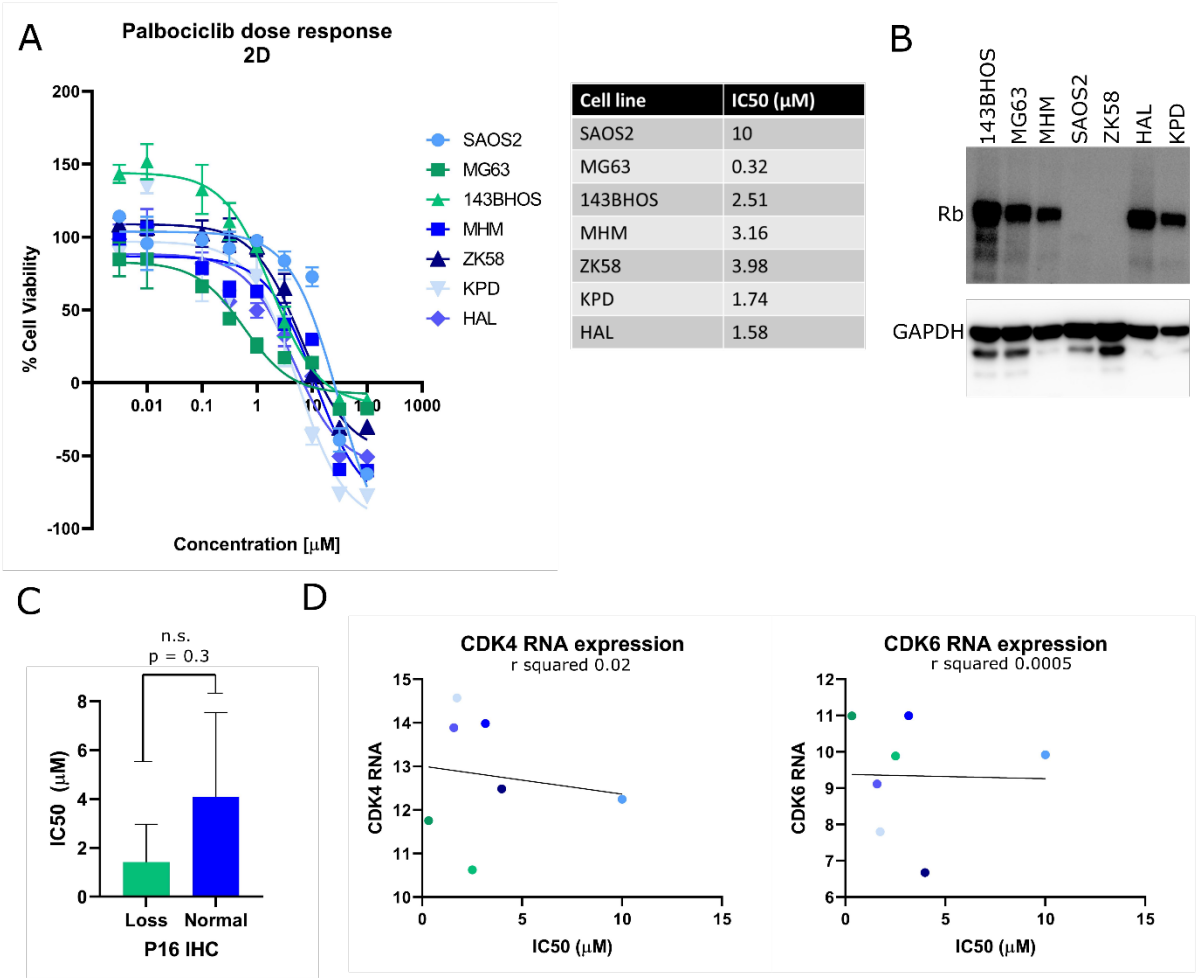

Figure 4. 2D cultures of human osteosarcoma cell lines are sensitive to CDK4/CDK6 inhibitor palbociclib. (**A**) Osteosarcoma cell lines were treated with palbociclib for 72 hours after which relative cell viability and IC_{50} values were determined. Cell lines MG63 and 143BHOS (green) have loss of p16, whereas other OS cell lines have intact p16 (blue). Data points represent the mean of three experiments performed ± standard deviation. (**B**) Western blot showing expression levels of Rb in osteosarcoma cell lines. GAPDH was used as a loading control. (**C**) p16 protein expression status of each osteosarcoma cell line as published (21) was correlated with IC_{50} values from the current study. n.s. = not statistically significant. (**D**) CDK4 and CDK6 RNA expression levels as published elsewhere (30) of each cell line did not correlate with IC_{50} values from the current study. Each dot represents one cell line.

3D cultures of osteosarcoma are also sensitive to palbociclib

Since 2D cultures might be less representative for the *in vivo* situation compared to 3D cultures, as demonstrated in previous studies (31-33), the response to palbociclib in 3D cultures of osteosarcoma cell lines was investigated. Multi-cellular tumour spheroids (MCTS) of three osteosarcoma cell lines were generated (MHM, SAOS2 and MG63) and histological analysis showed the morphological heterogeneity that is also seen in primary tumours (**Fig 5A**). MCTS of SAOS2 and MHM show areas suggestive of extracellular matrix deposition and tumour cells were focally positive for SATB2, a marker for osteogenic differentiation (**Fig 5A**). MCTS of all osteosarcoma cell lines showed a dose-dependent decrease in cell viability after treatment with palbociclib (**Fig 5B**). The IC_{50} values of 3D cultures were higher compared to 2D cultures (**Fig 5B**). In MCTS of osteosarcoma cell lines MHM and MG63, palbociclib treatment significantly reduced the percentage of proliferating cells and increased apoptosis as evident from Ki67 and cleaved caspase 3 staining, respectively (**Fig 5C**).

Protein expression of Rb, CDK4 and CDK6 in osteosarcoma patient primary tumour tissue

To estimate which percentage of osteosarcoma patients might be eligible for palbociclib treatment, the expression levels of proteins in the p16-Rb pathway, including Rb, CDK4, CDK6 and p16, was determined in primary tumour tissue of 109 patients using TMA (**Table 1; Fig 6A**). As Rb status determines the efficacy of CDK4/CDK6 inhibition (34, 35), first Rb expression was evaluated. 36.4% of the osteosarcomas have lost expression of Rb. As palbociclib directly inhibits CDK4 and CDK6, protein expression levels of CDK4 and CDK6 were determined. 23.7% of primary tumours were CDK4 positive and 44.8% were CDK6 high. p16 scores have been determined in a previous study in osteosarcoma patients (cohort 2), where 20.5 % of osteosarcoma patients showed loss of p16 (13).

As a combination of Rb expression and CDK4/CDK6 expression or loss of p16 expression are expected to imply sensitivity to CDK4/CDK6 inhibition, the combination scores were determined (**Table 1**). Of the primary tumour biopsies, 22.7% of the tumours were positive for both Rb and CDK4, 52.9% were positive for Rb and CDK6, and 43.1% was positive for Rb, and CDK4 or CDK6. In cohort 2, 13.3% of the primary tumour biopsies were positive for Rb, but lost p16 expression. In total, between 20.0% and 23.3% of the tumours are $Rb^{positive}/p16^{negative}$, $Rb^{positive}/CDK4^{positive}$, or $Rb^{positive}/CDK6^{high}$, which corresponds to the group of patients that might benefit from CDK4/CDK6 inhibitor treatment.

A previous study showed that p16 loss was prognostic for poor overall survival in osteosarcoma patients (13). In the current study, CDK6 scores were found to be prognostic for overall survival, where patients with overexpression of CDK6 have a worse overall survival compared to those patients with low CDK6 expression (**Fig 6B**). For Rb and CDK4 expression there was no significant difference in survival (**Supplementary Fig S4** available online). Neither Rb, CDK4, or CDK6 scores are prognostic for metastasis-free survival (**Supplementary Fig S4** available online) or response to chemotherapy (not shown).

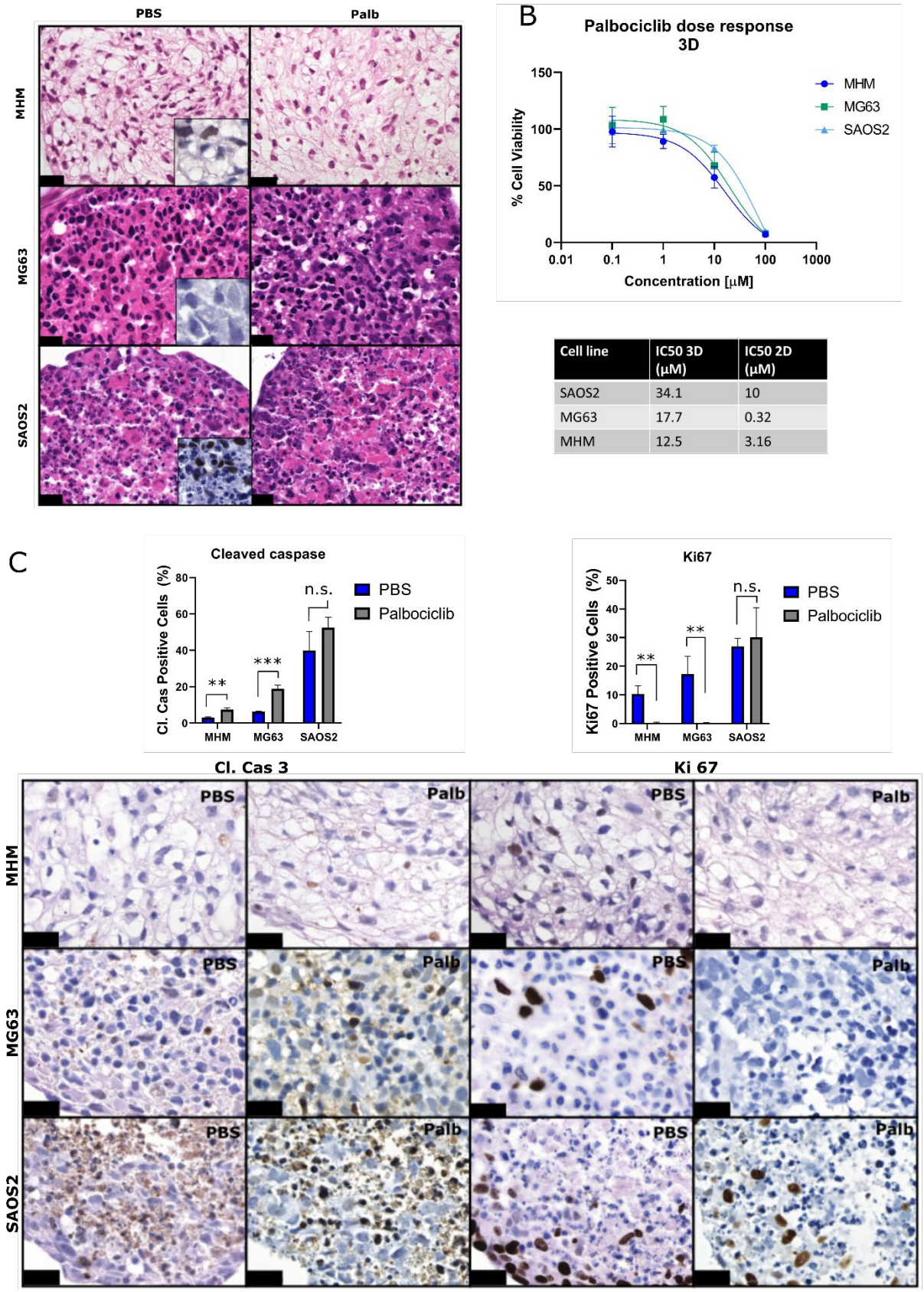

Cell line	IC50 3D (µM)	IC50 2D (µM)
SAOS2	34.1	10
MG63	17.7	0.32
MHM	12.5	3.16

Figure 5. 3D cultured MCTS of osteosarcoma cell lines are also sensitive to palbociclib. (**A**) Hematoxylin and eosin staining of osteosarcoma MCTS treated with palbociclib for 72 hours. Scalebar represents 20 µm. Inset shows SATB2 staining. (**B**) Relative cell viability and IC_{50} values were

determined after treatment with palbociclib. (**C**) Cleaved caspase 3 and Ki67 staining and quantification of 3D cultured MCTS of OS cell lines treated with 10 µM palbociclib (Palb) or PBS. Scale bar represents 20 µm. n.s. = not statistically significant, ** = p ≤ 0.01, *** = p ≤ 0.001.

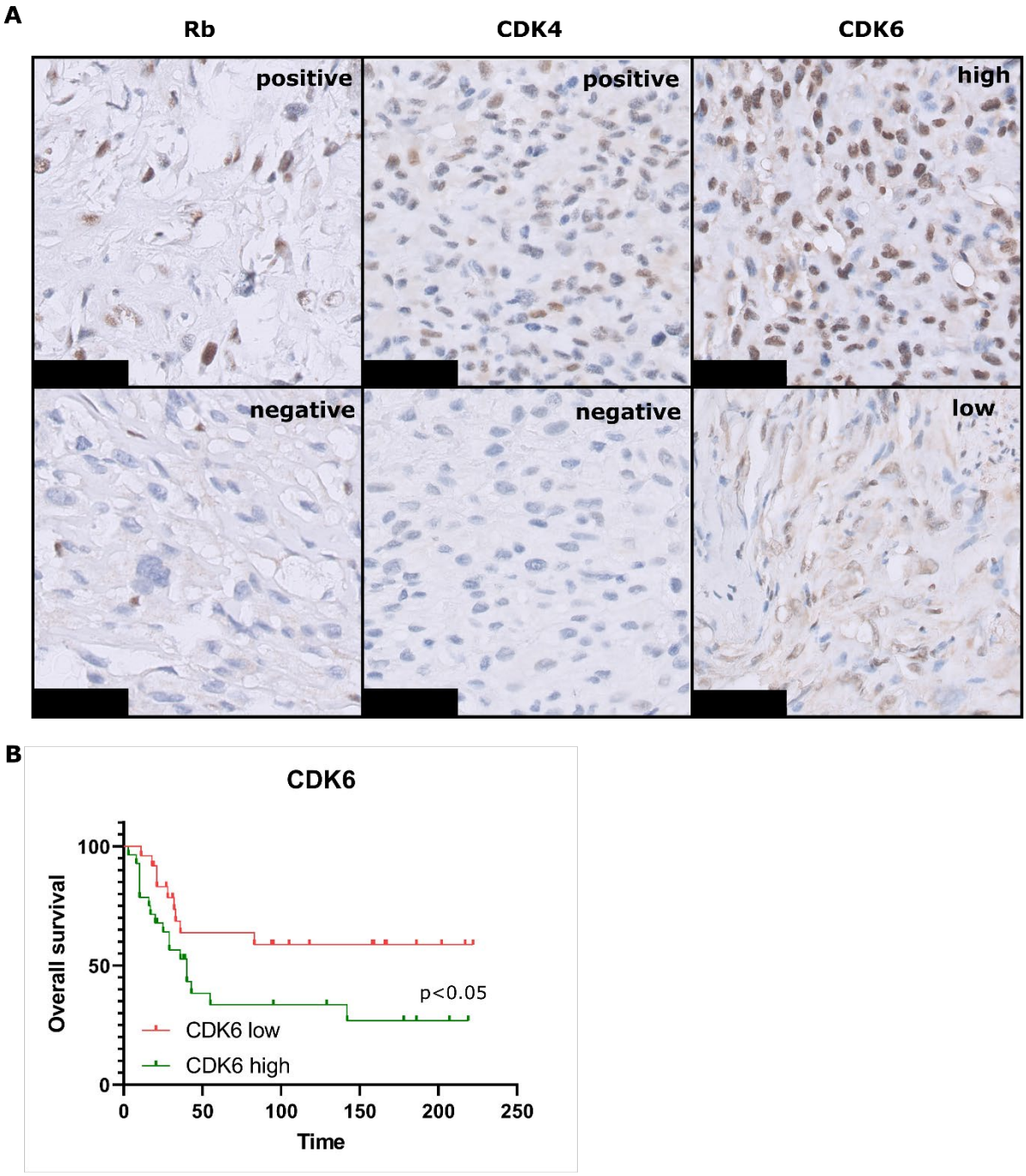

Figure 6. Immunohistochemistry of osteosarcoma tissue micro array (**A**) Example of immunohistochemical staining of Rb, CDK4, or CDK6, scored as positive or negative in tissue micro-arrays of osteosarcoma. Scale bar represents 50 µm. (**B**) Kaplan-Meier curves of overall survival in osteosarcoma patients, based on CDK6 scores.

Table 1. Overview of immunohistochemical expression of Rb, CDK4, and CDK6, combined with previously published (13) p16 protein expression results, in tissue micro-arrays of osteosarcoma

	PRIMARY TUMOUR BIOPSY	PRIMARY TUMOUR RESECTION	LOCAL RECURRENCE	METASTASIS
RB	**Total (n=66)**	**Total (n=68)**	**Total (n=9)**	**Total (n=38)**
POSITIVE	42 (63.6%)	42 (61.7%)	6 (66.7%)	32 (84.2%)
NEGATIVE	24 (36.4%)	26 (38.2%)	3 (33.3%)	6 (15.8%)
CDK4	**Total (n=76)**	**Total (n=77)**	**Total (n=9)**	**Total (n=38)**
POSITIVE	18 (23.7%)	15 (19.5%)	4 (44.4%)	7 (18.4%)
NEGATIVE	58 (76.3%)	62 (80.5%)	5 (55.6%)	31 (81.6%)
CDK6	**Total (n=58)**	**Total (n=56)**	**Total (n=7)**	**Total (n=26)**
HIGH	26 (44.8%)	32 (57.1%)	6 (85.7%)	12 (46.2%)
LOW	32 (56.2%)	24 (42.8%)	1 (14.3%)	14 (53.8%)
COMBINATION STATUS				
$RB^{POSITIVE}$ AND $CDK4^{POSITIVE}$	15/66 (22.7 %)			
$RB^{POSITIVE}$ AND $CDK6^{POSITIVE}$	27/51 (52.9%)			
$RB^{POSITIVE}$ AND $CDK4^{POSITIVE}$ AND $CDK6^{POSITIVE}$	6/51 (11.8%)			
$RB^{POSITIVE}$ AND $CDK4^{POSITIVE}$ OR $CDK6^{POSITIVE}$	22/51 (43.1%)			
P16 (COMBINATION) STATUS				
$RB^{POSITIVE}$ AND $P16^{NEGATIVE}$	4/30 (13.3%)			
$RB^{POSITIVE}$/$P16^{NEGATIVE}$ OR $RB^{POSITIVE}$/$CDK4^{POSITIVE}$	6/30 (20.0%)			
$RB^{POSITIVE}$/$P16^{NEGATIVE}$ OR $RB^{POSITIVE}$/$CDK6^{POSITIVE}$	7/30 (23.3%)			

Discussion

Transformed murine MSCs provide an excellent model to identify drivers of transformation in osteosarcoma. In addition to p53 alterations (19), transformed murine MSCs also frequently lose expression of $p15^{Ink4b}$, $p16^{Ink4a}$ and $p19^{Arf}$. However, the protein expression status did not always correspond to the genomic status, as is evident for MSC line B6_4 with loss of $p16^{Ink4a}$ protein expression without concomitant genomic alterations at the *CDKN2A* locus. Alternative mechanisms of $p16^{Ink4a}$ protein expression loss, such as promotor methylation may be active. Nevertheless, the loss of expression of $p15^{Ink4b}$, $p16^{Ink4a}$ and $p19^{Arf}$ in murine MSCs, reflects the genomic status of human osteosarcoma where alterations in $p15^{INK4B}$, $p16^{INK4A}$, or $p14^{ARF}$ are also frequently found (4, 5, 7, 8, 25).

This study shows that loss of either $p15^{Ink4b}$, $p16^{Ink4a}$, or $p19^{Arf}$ in the murine MSC model accelerates transformation. Using the same murine MSC model , we have previously published that these transformed murine MSCs, including those with loss of *CDKN2A/CDKN2B*, show hallmarks of osteosarcoma with a highly complex genome and many copy number alterations (19). Although chromothripsis could not be evaluated in the current study, not all human osteosarcomas show signs of chromothripsis either, since this only occurs in ~30% of cases (2). In another study, we have demonstrated that mice injected with transformed murine MSCs, all with loss of *CDKN2A/CDKN2B*, formed osteosarcoma, with evident osteoid formation by atypical tumour cells (13). Thus, our results combined with previously published results, suggest that loss of *CDKN2A/CDKN2B* is an early driver event in osteosarcoma. Loss of genes in the Rb-p16 pathway is indeed considered as an early event in the transformation towards osteosarcoma (7, 36, 37). The exact interplay with alterations in the p53 pathway is currently unknown, and since not all late passage murine MSCs with known loss of $p16^{Ink4a}$ or p53 could form colonies in soft agar, it is not yet known which combination of genomic alterations are required for transformation. This would warrant further investigation.

Loss of $p16^{INK4A}$ protein expression as a result of homozygous loss of the *CDKN2A* genomic region has previously been shown to correlate with poor prognosis as well as a poor response to neoadjuvant chemotherapy in osteosarcoma patients (13-18, 25, 38). Thus, studying the loss of $p16^{INK4A}$ in osteosarcoma is clinically relevant and gives a rationale for exploring the Rb-p16 pathway as a novel therapeutic option. Cells with loss of $p16^{INK4A}$ are hypothesized to be more sensitive to CDK4/CDK6 inhibition. Therefore, we investigated the sensitivity to CDK4/CDK6 inhibitor palbociclib in osteosarcoma cells. We confirmed that both 2D and 3D cultures of osteosarcoma cells show a dose-dependent decrease in cell viability after palbociclib treatment. This is in line with other *in vitro* studies showing that pan-CDK or specific CDK4/CDK6 inhibition in osteosarcoma resulted in growth inhibition of cells and increased senescence and/or apoptosis (39, 40).

In the current study, 2D cultures were more sensitive compared to 3D cultures. The difference in sensitivity is not surprising and could be explained by the formation of tight intercellular

contacts within MCTS which may hamper drug penetration (41). In general, the concentrations of palbociclib used in the current study, especially in 3D, are higher compared to concentrations used in the clinic for treatment of HER-2 negative breast cancer and in breast cancer cell lines *in vitro* (42). However, we have treated the cells with a single dose, whereas in the clinic multiple doses are administered. Moreover, the IC_{50} values determined in the current study are in a comparable concentration range when compared to other *in vitro* studies in osteosarcoma cells using palbociclib (39, 40). Thus, our data support previous findings that CDK4/CDK6 inhibition might be a new targeted treatment strategy for osteosarcoma patients (40, 43). However, more research is needed to investigate the efficacy of palbociclib for osteosarcoma patients, and whether there are any adverse effects. For the treatment of breast cancer, it was reported that the adverse effects of palbociclib include neutropenia, leukopenia or anaemia (42, 44).

Currently, two phase 2 clinical trials are ongoing which include advanced cases of sarcoma that overexpress CDK4, including osteosarcoma, for palbociclib treatment or similar CDK4/CDK6 inhibitors (45, 46). One of these studies was also designed to test the utility of CDK4 expression in predicting tumour response to CDK inhibitors, but this study did not evaluate whether patients show loss of $p16^{INK4A}$ or intact Rb. In the current study sensitivity to palbociclib did not correlate with CDK4 expression in osteosarcoma cells.

Not only CDK4, but also CDK6 was evaluated as a prognostic and predictive biomarker in our study. Interestingly, about half of the osteosarcoma patients (44.8%) showed overexpression of CDK6 which was associated with a worse overall survival. In this group of patients palbociclib could be beneficial to improve outcome. Palbociclib is most effective when Rb is intact, which was the case in approximately half (52.9%) of the patients with CDK6 overexpression. The expression status of CDK4 and CDK6 is important to consider, since it was recently published that palbociclib selectively dissociates p21 from cyclin D1-CDK4-p21 complexes and not of cyclin D1-CDK6-p21 complexes, which could affect drug sensitivity and resistance (47).

Another subgroup of osteosarcoma patients that might benefit from CDK4/CDK6 inhibition, include patients with intact Rb, but loss of p16 expression. The *in vitro* study confirms that osteosarcoma cell lines with intact Rb and/or loss of p16 are more sensitive to palbociclib compared to osteosarcoma cell lines with loss of Rb and/or intact p16. Furthermore, osteosarcoma cell lines with loss of p16 staining by immunohistochemistry showed a trend towards higher sensitivity to palbociclib compared to cells without loss of p16. The immunohistochemical study on the tissue microarray indicates that 13.3% of the patients falls within this category of intact Rb and loss of p16 that may benefit from palbociclib treatment. Taken together, our results illustrate that there is a clear subset of osteosarcoma patients (20-23%) for which CDK4/CDK6 inhibition might be promising and that loss of p16 protein expression or overexpression of CDK6, combined with intact Rb, may serve as a biomarker to select eligible patients.

In conclusion, this study demonstrated that our model of transformed murine MSCs provide a valuable tool to identify targets for therapy and the identification of biomarkers for osteosarcoma patients. Our results illustrate that loss of *CDKN2A* and/or *CDKN2B* are early events in the development of osteosarcoma, and that these events can be targeted by CDK4/CDK6 inhibition, which might be used as a novel therapeutic option in approximately 20-23% of the patients.

Acknowledgements

The authors would like to thank Melissa van Pel for providing murine MSCs; Pauline Wijers-Koster and Brendy van den Akker for technical assistance; Marieke Kuijjer and René Zwartbol for the generation of the TMAs; Michiel van de Sande for the clinical data used in the tissue micro arrays; Dirk-Jan Moes for discussions about the physiological concentration range of palbociclib.

References

1. Behjati S, Tarpey PS, Haase K, Ye H, Young MD, Alexandrov LB, et al. Recurrent mutation of IGF signalling genes and distinct patterns of genomic rearrangement in osteosarcoma. Nat Commun. 2017;8:15936.
2. Stephens PJ, Greenman CD, Fu B, Yang F, Bignell GR, Mudie LJ, et al. Massive genomic rearrangement acquired in a single catastrophic event during cancer development. Cell. 2011;144(1):27-40.
3. Cortes-Ciriano I, Lee JJ, Xi R, Jain D, Jung YL, Yang L, et al. Comprehensive analysis of chromothripsis in 2,658 human cancers using whole-genome sequencing. Nat Genet. 2020;52(3):331-41.
4. Perry JA, Kiezun A, Tonzi P, Van Allen EM, Carter SL, Baca SC, et al. Complementary genomic approaches highlight the PI3K/mTOR pathway as a common vulnerability in osteosarcoma. Proc Natl Acad Sci U S A. 2014;111(51):E5564-73.
5. Kovac M, Blattmann C, Ribi S, Smida J, Mueller NS, Engert F, et al. Exome sequencing of osteosarcoma reveals mutation signatures reminiscent of BRCA deficiency. Nat Commun. 2015;6:8940.
6. Weinberg R. The Retinoblastoma Protein and Cell Cycle Control. Cell. 1995;81:323-30.
7. Sayles LC, Breese MR, Koehne AL, Leung SG, Lee AG, Liu HY, et al. Genome-Informed Targeted Therapy for Osteosarcoma. Cancer Discov. 2019;9(1):46-63.
8. Mejia-Guerrero S, Quejada M, Gokgoz N, Gill M, Parkes RK, Wunder JS, et al. Characterization of the 12q15MDM2and 12q13-14CDK4amplicons and clinical correlations in osteosarcoma. Genes, Chromosomes and Cancer. 2010:NA-NA.
9. Burkhart DL, Sage J. Cellular mechanisms of tumour suppression by the retinoblastoma gene. Nat Rev Cancer. 2008;8(9):671-82.
10. Sherr CJ, Weber JD. The ARF/p53 pathway. Curr Opin Genet Dev. 2000;10(1):94-9.
11. Miller CW, Aslo A, Campbell MJ, Kawamata N, Lampkin BC, Koeffler HP. Alterations of the p15, p16 and p18 Genes in Osteosarcoma. Cancer Genetics and Cytogenetics. 1996;86:136-42.
12. Tsuchiya T, Sekine K, Hinohara S, Namiki T, Nobori T, Kaneko Y. Analysis of the p16INK4, p14ARF, p15, TP53, and MDM2 Genes and Their Prognostic Implications in Osteosarcoma and Ewing Sarcoma. Cancer Genetics and Cytogenetics. 2000;120:91-8.
13. Mohseny AB, Szuhai K, Romeo S, Buddingh EP, Briaire-de Bruijn I, de Jong D, et al. Osteosarcoma originates from mesenchymal stem cells in consequence of aneuploidization and genomic loss of Cdkn2. J Pathol. 2009;219(3):294-305.

14. Righi A, Gambarotti M, Sbaraglia M, Sisto A, Ferrari S, Dei Tos AP, et al. p16 expression as a prognostic and predictive marker in high-grade localized osteosarcoma of the extremities: an analysis of 357 cases. Hum Pathol. 2016;58:15-23.
15. Kosemehmetoglu K, Ardic F, Karslioglu Y, Kandemir O, Ozcan A. p16 expression predicts neoadjuvant tumor necrosis in osteosarcomas: reappraisal with a larger series using whole sections. Hum Pathol. 2016;50:170-5.
16. Bu J, Li H, Liu L, Ouyang Y, Guo H, Li X, et al. P16Ink4a overexpression and survival in osteosarcoma patients: a meta analysis. Int J Clin Exp Pathol

2014;7(9).
17. Borys D, Canter RJ, Hoch B, Martinez SR, Tamurian RM, Murphy B, et al. P16 expression predicts necrotic response among patients with osteosarcoma receiving neoadjuvant chemotherapy. Hum Pathol. 2012;43(11):1948-54.
18. Maitra A, Roberts H, Weinberg A, Geradts J. Loss of p16ink4a expression correlates with decreased survival in pediatric osteosarcomas

Int J Cancer. 2001;95.
19. Franceschini N, Verbruggen B, Tryfonidou MA, Kruisselbrink AB, Baelde H, de Visser KE, et al. Transformed murine and canine mesenchymal stem cells as a model for sarcoma with complex genomics. Cancers. 2021;13(5).
20. Krimpenfort P, Ijpenberg A, Song JY, van der Valk M, Nawijn M, Zevenhoven J, et al. p15Ink4b is a critical tumour suppressor in the absence of p16Ink4a. Nature. 2007;448(7156):943-6.
21. Ottaviano L, Schaefer KL, Gajewski M, Huckenbeck W, Baldus S, Rogel U, et al. Molecular characterization of commonly used cell lines for bone tumor research: a trans-European EuroBoNet effort. Genes Chromosomes Cancer. 2010;49(1):40-51.
22. Zhang W, Li C, Baguley BC, Zhou F, Zhou W, Shaw JP, et al. Optimization of the formation of embedded multicellular spheroids of MCF-7 cells: How to reliably produce a biomimetic 3D model. Anal Biochem. 2016;515:47-54.
23. Hafner M, Niepel M, Chung M, Sorger PK. Growth rate inhibition metrics correct for confounders in measuring sensitivity to cancer drugs. Nature methods. 2016;13(6).
24. WHO classification of tumours of soft tissue and bone, 5th edition. Lyon, France: WHO Classification of Tumours Editorial Board; 2020.
25. Mohseny AB, Tieken C, van der Velden PA, Szuhai K, de Andrea C, Hogendoorn PC, et al. Small deletions but not methylation underlie CDKN2A/p16 loss of expression in conventional osteosarcoma. Genes Chromosomes Cancer. 2010;49(12):1095-103.
26. Buddingh EP, Kuijjer ML, Duim RA, Burger H, Agelopoulos K, Myklebost O, et al. Tumor-infiltrating macrophages are associated with metastasis suppression in high-grade osteosarcoma: a rationale for treatment with macrophage activating agents. Clin Cancer Res. 2011;17(8):2110-9.
27. Schrage YM, Lam S, Jochemsen AG, Cleton-Jansen AM, Taminiau AH, Hogendoorn PC, et al. Central chondrosarcoma progression is associated with pRb pathway alterations: CDK4 down-regulation and p16 overexpression inhibit cell growth in vitro. J Cell Mol Med. 2009;13(9A):2843-52.
28. Gong W, Wang L, Zheng Z, Chen W, Du P, Zhao H. Cyclin-dependent kinase 6 (CDK6) is a candidate diagnostic biomarker for early non-small cell lung cancer. Translational Cancer Research. 2020;9(1):95-103.
29. Bankhead P, Loughrey MB, Fernandez JA, Dombrowski Y, McArt DG, Dunne PD, et al. QuPath: Open source software for digital pathology image analysis. Sci Rep. 2017;7(1):16878.
30. Kresse SH, Rydbeck H, Skarn M, Namlos HM, Barragan-Polania AH, Cleton-Jansen AM, et al. Integrative analysis reveals relationships of genetic and epigenetic alterations in osteosarcoma. PLoS One. 2012;7(11):e48262.
31. Chow T, Wutami I, Lucarelli E, Choong PF, Duchi S, Di Bella C. Creating In Vitro Three-Dimensional Tumor Models: A Guide for the Biofabrication of a Primary Osteosarcoma Model. Tissue Engineering Part B: Reviews. 2020.

32. De Luca A, Raimondi L, Salamanna F, Carina V, Costa V, Bellavia D, et al. Relevance of 3d culture systems to study osteosarcoma environment. J Exp Clin Cancer Res. 2018;37(1):2.
33. Gao S, Shen J, Hornicek F, Duan Z. Three-dimensional (3D) culture in sarcoma research and the clinical significance. Biofabrication. 2017;9(3):032003.
34. Sherr CJ, Beach D, Shapiro GI. Targeting CDK4 and CDK6: From Discovery to Therapy. Cancer Discov. 2016;6(4):353-67.
35. Guha M. Cyclin-dependent kinase inhibitors move into Phase III. Nat Rev Drug Discov. 2012;11(12):892-4.
36. Kovac M, Ameline B, Ribi S, Kovacova M, Cross W, Barenboim M, et al. The early evolutionary landscape of osteosarcoma provides clues for targeted treatment strategies. J Pathol. 2021.
37. Mohseny AB, Hogendoorn PC, Cleton-Jansen AM. Osteosarcoma models: from cell lines to zebrafish. Sarcoma. 2012;2012:417271.
38. Tang Y, Yang C, Guo Z, Fu Y, Yu X, Liu B, et al. P16 protein expression as a useful predictive biomarker for neoadjuvant chemotherapy response in patients with high-grade osteosarcoma. Medicine (Baltimore). 2017;96(19).
39. Zhou Y, Shen JK, Yu Z, Hornicek FJ, Kan Q, Duan Z. Expression and therapeutic implications of cyclin-dependent kinase 4 (CDK4) in osteosarcoma. Biochim Biophys Acta Mol Basis Dis. 2018;1864(5 Pt A):1573-82.
40. Perez M, Galván SM, García MP, Marín JJ, Carnero A. Efficacy of CDK4 inhibition against sarcomas depends on their levels of CDK4 and p16ink4 mRNA. Oncotarget. 2015;6(30).
41. Gong X, Lin C, Cheng J, Su J, Zhao H, Liu T, et al. Generation of Multicellular Tumor Spheroids with Microwell-Based Agarose Scaffolds for Drug Testing. PLoS One. 2015;10(6):e0130348.
42. Cristofanilli M, Turner NC, Bondarenko I, Ro J, Im S-A, Masuda N, et al. Fulvestrant plus palbociclib versus fulvestrant plus placebo for treatment of hormone-receptor-positive, HER2-negative metastatic breast cancer that progressed on previous endocrine therapy (PALOMA-3): final analysis of the multicentre, double-blind, phase 3 randomised controlled trial. The Lancet Oncology. 2016;17(4):425-39.
43. Delmore JE, Issa GC, Lemieux ME, Rahl PB, Shi J, Jacobs HM, et al. BET bromodomain inhibition as a therapeutic strategy to target c-Myc. Cell. 2011;146(6):904-17.
44. Finn RS, Martin M, Rugo HS, Jones S, Im SA, Gelmon K, et al. Palbociclib and Letrozole in Advanced Breast Cancer. N Engl J Med. 2016;375(20):1925-36.
45. Trial of Palbociclib in Second Line of Advanced Sarcomas With CDK4 Overexpression: Identifier NCT03242382; [Available from: https://clinicaltrials.gov/ct2/show/study/NCT03242382.
46. Abemaciclib for Bone and Soft Tissue Sarcoma With Cyclin-Dependent Kinase (CDK) Pathway Alteration: Identifier NCT04040205; [Available from: https://clinicaltrials.gov/ct2/show/NCT04040205.
47. Pack LR, Daigh LH, Chung M, Meyer T. Clinical CDK4/6 inhibitors induce selective and immediate dissociation of p21 from cyclin D-CDK4 to inhibit CDK2. Nat Commun. 2021;12(1):3356.

Chapter 6

Targeting the NAD salvage synthesis pathway as a novel therapeutic strategy for osteosarcomas with low NAPRT expression

Natasja Franceschini, Jan Oosting, Maud Tamsma, Bertine Niessen, Inge Briaire-de Bruijn, Brendy van den Akker, Alwine B. Kruisselbrink, Ieva Palubeckaite, Judith V.M.G. Bovée and Anne-Marie Cleton-Jansen

Published: *Int. J. Mol. Sci. 2021; 22(12):6273*

Abstract

For osteosarcoma (OS), the most common primary malignant bone tumor, overall survival has hardly improved over the last four decades. Especially for metastatic OS, novel therapeutic targets are urgently needed. A hallmark of cancer is aberrant metabolism, which justifies targeting metabolic pathways as a promising therapeutic strategy. One of these metabolic pathways, the NAD+ synthesis pathway, can be considered as a potential target for OS treatment. Nicotinamide phosphoribosyltransferase (NAMPT) is the rate-limiting enzyme in the classical salvage pathway for NAD+ synthesis, and NAMPT is overexpressed in OS. In this study, five OS cell lines were treated with the NAMPT inhibitor FK866, which was shown to decrease nuclei count in a 2D in vitro model without inducing caspase-driven apoptosis. The reduction in cell viability by FK866 was confirmed in a 3D model of OS cell lines (n = 3). Interestingly, only OS cells with low nicotinic acid phosphoribosyltransferase domain containing 1 (NAPRT1) RNA expression were sensitive to NAMPT inhibition. Using a publicly available (Therapeutically Applicable Research to Generate Effective Treatments (TARGET)) and a previously published dataset, it was shown that in OS cell lines and primary tumors, low NAPRT1 RNA expression correlated with NAPRT1 methylation around the transcription start site. These results suggest that targeting NAMPT in osteosarcoma could be considered as a novel therapeutic strategy, where low NAPRT expression can serve as a biomarker for the selection of eligible patients.

Introduction

Osteosarcoma is the most common high-grade malignant tumor of the bone, primarily diagnosed in children and adolescents (1). Histologically, conventional osteosarcoma is characterized by the presence of osteoblast-like neoplastic cells that produce osteoid (1). The current treatment strategy consists of a combination of (neo)adjuvant chemotherapy and surgery, which has greatly improved the outcome for osteosarcoma patients since its introduction, with a 5-year overall survival rate of 71% (2). However, in the last four decades, the survival rates have not improved (2) despite the high number of in vitro studies using cell lines (3). Targeting the aberrant metabolism which hallmarks many tumors (4, 5) is a likely option for osteosarcoma. A previously published study illustrated the importance of metabolism in OS as metastatic OS cells were found to be highly metabolically active, and therefore targeting metabolism in OS can be a potential novel therapy (6). Furthermore, it was shown that both the inhibition of mTOR—a key regulator of metabolism, and the inhibition of 3-phosphoglycerate dehydrogenase (PHGDH)—the rate-limiting enzyme of serine biosynthesis, attenuated cell proliferation in OS cells and can therefore serve as a novel therapeutic target (7-9). The NAD+ synthesis pathway is a metabolic pathway often upregulated in tumors as cancer cells need to maintain a high level of NAD+ required for cell survival processes (10, 11). NAD+ is an essential co-enzyme central to many metabolic processes such as aerobic glycolysis, the citric acid cycle, oxidative phosphorylation, fatty acid metabolism, and anti-oxidant metabolism (12). NAD+ can be synthesized de novo, or via the alternative salvage or classical salvage pathway (12, 13) (**Figure 1**). In the alternative salvage pathway, NAD+ synthesis is catalyzed by the enzyme nicotinic acid phosphoribosyltransferase domain containing 1 (NAPRT1), whereas in the classical salvage pathway, it is catalyzed by the enzyme nicotinamide phosphoribosyltransferase (NAMPT). Cancer cells rely mostly on the classical NAD+ synthesis pathway as de novo synthesis from amino acids is inefficient and the alternative pathway is often inactive due to the lack of expression of NAPRT1 (13, 14). In osteosarcoma, NAMPT is overexpressed as compared to that found in normal bone (15). Targeting NAMPT could therefore potentially be a novel therapeutic option for osteosarcoma patients; consequently, the main aim of this study is to test the sensitivity of osteosarcoma cells to NAMPT inhibition.

In a recent study, a connection between NAMPT and osteogenic differentiation was discovered (16), in which NAMPT expression increased during osteogenic differentiation in osteoblasts. As the hallmark of osteosarcoma is the production of the osteogenic matrix (osteoid) by tumor cells (1), we further investigated whether NAMPT inhibition would be affecting osteogenic differentiation and mineralization in osteosarcoma.

In this study, it was discovered that cell viability of osteosarcoma cells decreased after treatment with the NAMPT inhibitor FK866, in both 2D cultured and 3D cultured cells. More importantly, only OS cells with a low expression of NAPRT1, and as such depending more on the classical salvage pathway for NAD+ synthesis, were sensitive to NAMPT inhibition. Low NAPRT1 expression in primary tumor samples of osteosarcoma correlated with the

methylation of the NAPRT1 promotor. Therefore, low NAPRT expression could serve as a potential biomarker for the selection of osteosarcoma patients who could benefit from treatments that inhibit NAMPT.

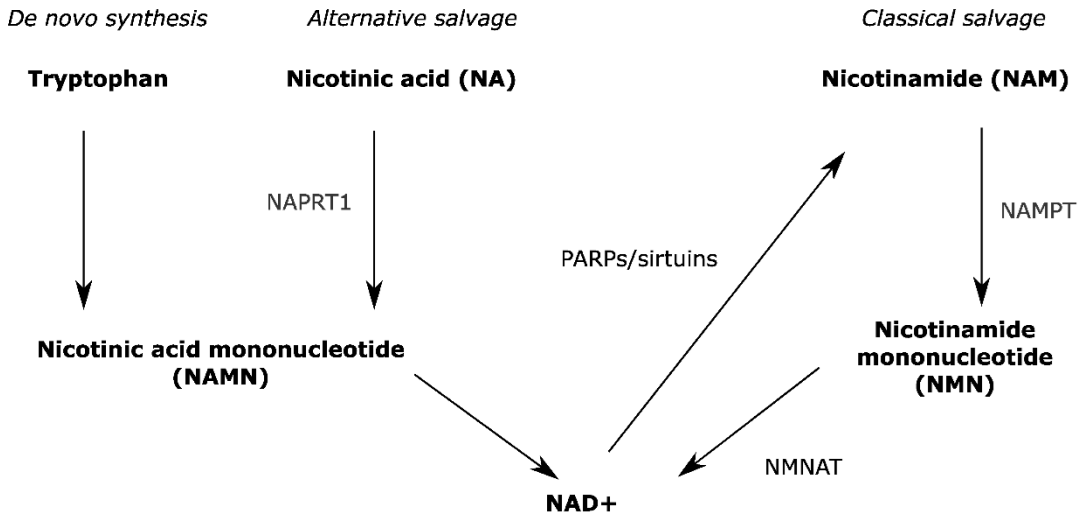

Figure 1. Simplified overview of the NAD+ synthesis pathway. NAD+ is synthesized by de novo synthesis, the alternative salvage pathway, or the classical salvage pathway. NAMPT and NAPRT1 are the rate-limiting enzymes of the classical salvage and alternative salvage pathways, respectively. NMNAT = Nicotinamide mononucleotide adenylyltransferase 1

Material and Methods

Cell Culture

For 2D cell culture, the osteosarcoma cell lines KPD, MHM, MG63, ZK58, SAOS2, U2OS, and 143B were cultured in RPMI 1640 medium (Gibco, Invitrogen Life-Technologies, Scotland, UK), supplemented with 10% Fetal Bovine Serum (Gibco). Cell lines were retrieved from the EuroBoNet consortium (17). For 3D cell culture, osteosarcoma cell lines MHM, MG63, and ZK58 were cultured in αMEM (Gibco) supplemented with 10% FBS. To create multi-cellular tumor spheroids (MCTS) (protocol adapted from (18)), cells were suspended in a medium containing methylcellulose (0.24% (*w*/*v*)) dissolved in DMEM, and were seeded in 1% agarose coated 96-well plates for seven days before the start of an experiment. All cells were cultured in a humidified incubator, with 5% CO_2 and at 37 °C. Cell lines were regularly STR-profiled using the GenePrint 10 system kit (Promega, Madison, WI, USA) and tested for mycoplasm.

Drug Treatment

Cells were seeded and treated after 24 h (2D cell culture) or after seven days (3D cell culture) with 0.1% DMSO as a non-treated sample or FK866 (F8557, Sigma-Aldrich, Saint Louis, MO, USA, dissolved in DMSO) in concentrations ranging from 0.1–1000 nM. For NAD+ rescue experiments, NAD+ (10127965001, Sigma-Aldrich, dissolved in RPMI 1640) was added at the same time as FK866 (10 nM for 2D culture experiments, 30 nM for 3D culture experiments), with a concentration of 10, 50, or 100 µM. Dose range was determined based on a previous

study (19). After 72 h of treatment, nuclear count or cell viability was determined. For nuclear count, cells were fixed with 4% formaldehyde, stained with 2 µg/mL Hoechst (H1399, Invitrogen Life Technologies), and nuclei were counted with the Cellomics ArrayScan VTI HCS 700 and HCS Studio Cell Analysis Software (Thermo-Fisher Scientific, Waltham, MA, USA). For cell viability assays, MCTS or 2D cultured cells were incubated with the Presto Blue cell viability reagent (A13262, Invitrogen Life Technologies) for 90 min (MCTS) or 60 min (2D cultured cells) and measured using a microplate reader (Infinite M Plex, Tecan Group Ltd., Zürich, Switzerland). After a read-out of MCTS, pellets were fixed with 4% formaldehyde containing Alcian Blue (1:200) and paraffin embedded. Cell viability was determined relative to untreated control. Each datapoint was corrected for background reads and normalized to cell number at Day 0 (before treatment) to correct for growth rate in each cell line, as described in (20). Dose response curves were created using the GraphPad Prism version 8 (GraphPad Software, La Jolla, CA, USA). Dose response studies were performed at least two times in triplicate.

Cell Cycle Analysis

MG63, SAOS2, and ZK58 cells were seeded in 6-well plates and treated for 48 h the next day with 5 (MG63 and SAOS2) or 60 nM (ZK58) of FK866, or 0.1% DMSO. Drug dose was defined as the IC75 determined in a 72 h exposure in 2D. Adherent cells were trypsinized and collected with supernatant. Cells were centrifuged, washed with PBS, and fixed in cold methanol for at least 20 min, as described in (21). Cells were stained for 30 min with DAPI in PBS/1% Bovine serum albumin/0.05% Tween and stored at 4 °C overnight. At least 10,000 single cell events were measured with the NucleoCounter NC-250 (Chemometec, Lillerød, Denmark), and analyzed using Winlist 3D Version 8, and Modfit Version 4.1.7 (Verity Software House, Topsham, ME, USA).

Western Blotting

Whole cell Hot-SDS lysates were obtained as described previously (22) for MG63, SAOS2, and ZK58. Cells were treated with 0.1% DMSO, FK866 (5 nM (MG63 and SAOS2), 60 nM (ZK58)), or ABT-737 (5 µM) and doxorubicin (1 µM) for 48 h, as a positive control for the induction of apoptosis (23). The supernatant of the treated cells was collected in the same lysate sample. Protein concentrations of lysates were determined with the Bio-rad DCTM protein assay kit (5000111, Bio-rad, Hercules, CA, USA) according to the manufacturer's protocol and measured with a microplate reader (Infinite M Plex, Tecan Group Ltd., Zürich, Switzerland). Sample loading, blotting, and quantification were performed, as previously described (22). Blots were stained for PARP (1:1000, clone 46D11, Cell Signaling Technology, Leiden, The Netherlands), caspase 3 (1:1000, clone 8G10, Cell Signaling Technology), and gel-loading control α-tubulin (1:30,000, clone DM1A, Sigma-Aldrich).

Immunohistochemistry

Sections (4µm) of paraffin-embedded multicellular tumor spheroids were made; after deparaffinization and rehydration, these were used for immunohistochemical staining for Ki67 (1:1600, clone D2H10, Cell Signaling) and cleaved caspase 3 (Cleaved caspase 3 (Asp175), 1:800, Cell Signaling). Antigen retrieval was performed by incubating sections in citrate buffer (10 mM, pH 6) for 10 min and cooling down for 2 h. Sections were incubated with primary antibody overnight at 4 °C. The next day, sections were incubated with the BrightVision one step detection system poly-HRP anti-mouse/rabbit (VWRKDPVO110HRP, Immunologic, WellMed B.V., Duiven, The Netherlands) for 30 min at room temperature. Sections were washed with PBS and DAB+ Chromogen (K3468, Dako, Agilent Technologies, Carpinteria, CA, USA) was added to each slide for 10 min. Slides were counterstained with hematoxylin, dehydrated, and mounted. For quantification of the stained sections, the percentage of Ki67 or cleaved caspase 3 positive cells was determined using QuPath Software v.0.2.3 on three different sections on each slide (24).

Osteogenic Differentiation

The OS cell line ZK58 was seeded at 5000 cells/cm^2 for osteogenic differentiation. One day after seeding, αMEM medium supplemented with 10% FBS was added, containing either 0.1% DMSO or FK866 (25 nM), with or without osteogenic differentiation compounds (β-glycerophosphate (5 mM, Sigma-Aldrich), dexamethasone (0.1 µM, Sigma-Aldrich), and ascorbate-2-phosphate (0.15 mM, Sigma-Aldrich)). Four or seven days after the addition of the osteogenic differentiation medium, cell viability was determined with Presto Blue. ALP activity was determined after four days of differentiation by lysing of cells with PBS/Triton 0.1% and incubating with pNPP (P7998, Sigma-Aldrich) for 4 min. Absorption at 405 nm was measured using a microplate reader (Infinite M Plex, Tecan). ALP activity in mU was corrected for number of cells of each well. To assess mineralization, osteogenic differentiation was terminated after 21 days, and cells were stained with Alizarin Red S solution (2 g Alizarin Red S (02100375, MP Biomedicals, Thermo Fisher Scientific) in 60 mL water, pH 4.2) for 5 min. To determine the gene expression of osteogenic markers, RNA was harvested after four or seven days of differentiation using Trizol (15596026, Invitrogen Life Technologies) according to the manufacturer's instructions, followed by cDNA synthesis and reverse transcriptase quantitative PCR, described in detail in the next section.

Reverse Transcriptase Quantitative PCR (RT-qPCR)

RNA was isolated from OS cell lines KPD, MHM, MG63, ZK58, SAOS2, U2OS, and 143B using Trizol according to the manufacturer's instructions. cDNA synthesis was performed using iScript cDNA Synthesis Kit (1708890, Bio-rad) according to the manufacturer's instructions. For the RT-qPCR, iQ SYBR Green Supermix (1708880, Bio-rad) and a Thermal Cycler (Bio-rad) were used with primers for osteogenic markers (*ALPL, COL1A1, SPARC, RUNX2, SPP1*), *NAMPT*, *NAPRT,* or housekeeping genes that were found to show stable expression in mesenchymal tumors (*CAPNS1, SRPR*) (Table 1) (25). Gene expression levels' relation to housekeeping genes were determined with the following formula: $2^{\wedge (\text{Ct value housekeeping genes} - \text{Ct value gene of interest})}$.

Table 1. List of primer sequences used in this study.

Gene	Forward Primer	Reverse Primer
ALPL	TCACTCTCCGAGATGGTGGT	GCCTGCTTGGCTTTTCCTTC
COL1A1	AAGACGAAGACATCCCACCAAT	GTCACAGATCACGTCATCGCA
SPARC	CTGGACTACATCGGGCCTTG	CAGGACGTTCTTGAGCCAGT
RUNX2	CCCTGAACTCTGCACCAAGT	GGCTCAGGTAGGAGGGGTAA
SPP1	TTCGCAGACCTGACATCCAG	ACGGCTGTCCCAATCAGAAG
NAMPT	GGAGCATCTGCTCACTTGGT	TCATGGTCTTTCCCCCAAGC
NAPRT	GCTGGAGTCAGTCCTCATCG	TATAGACGCCACCCAGGGAA
CAPNS1	ATGGTTTTGGCATTGACACATG	GCTTGCCTGTGGTGTCGC
SRPR	CATTGCTTTTGCACGTAACCAA	ATTGTCTTGCATGCGGCC

Expression and Methylation Analysis

Methylation and gene expression data generated by the Therapeutically Applicable Research to Generate Effective Treatments (TARGET) (https://ocg.cancer.gov/programs/target (accessed on 22-02-2021) initiative, phs000468, which include 86 osteosarcoma samples, were used in this study. Methylation data was obtained from osteosarcomas using Infinium 450 K Arrays. Probes within the complete genes, or 2000 bases around the transcription start site, of NAMPT and NAPRT1 were selected. For gene expression analysis, log2 (TPM) values of RNAseq data were used. All data used for this analysis are available on https://portal.gdc.cancer.gov/projects (accessed on 22-02-2021). For OS cell line methylation and gene expression analysis, methylation β-values and VSN-normalized gene expression data were obtained from a previously published dataset (GEO accession number GSE36002) (26). Correlation analysis between methylation levels and gene expression was performed using R.

Statistical Analysis

For statistical comparisons between two groups, a Student *t*-test was performed. For multiple comparisons between groups, a Kruskal–Wallis test was used. All statistical tests were performed on the GraphPad Prism 8.

Results

Osteosarcoma Cells Show Variable Sensitivity to NAMPT Inhibition

To assess whether NAMPT inhibition affects nuclei count and cell viability in osteosarcoma, five OS cell lines—MG63, MHM, SAOS, 143B, and ZK58—were treated for 72 h with the NAMPT inhibitor FK866 (**Figure 2A**). There was no marked difference between nuclei count and cell viability (**Figure S1A** available online). All OS cell lines showed a dose-dependent decrease in nuclei count after NAMPT inhibitor treatment, with IC_{50} values ranging from 3.0 to 26.7 nM, except for MHM which showed very limited sensitivity to NAMPT inhibition. There was marked variability in sensitivity to NAMPT inhibition: in order to define a biomarker for the NAMPT inhibitor sensitivity of OS cell lines, RNA expression levels of NAMPT and NAPRT1 as well as the NAMPT/NAPRT1 ratio were analyzed in a panel of seven OS cell lines. NAMPT and NAPRT1 expressions were highly variable in OS cell lines, as were NAMPT/NAPRT1 expression ratios (**Figure 2B**). Interestingly, MHM, the OS cell line which showed very limited sensitivity to NAMPT inhibition, showed the lowest NAMPT/NAPRT1 ratio and the highest NAPRT1 expression as compared to cell lines ZK58, SAOS2, 143B, and MG63.

To assess whether the effect of NAMPT inhibition on nuclei count was specifically due to the targeting of the NAD+ classical salvage pathway, treatment with the NAMPT inhibitor FK866 was supplemented with NAD+ in three OS cell lines with high (143B), medium (ZK58), or low (MHM) sensitivity to FK866. Although NAD+ itself reduced nuclei counts, NAD+ treatment rescued the inhibitory effect of the NAMPT inhibitor FK866 partially in OS cell lines 143B and ZK58 (**Figure 2C**). MHM cells showed limited sensitivity to FK866 treatment and an addition of NAD+ increased nuclei count in cells treated with FK866, although this was not statistically significant. To investigate whether FK866 reduced nuclei count by inducing apoptosis—as this was previously suggested to be how FK866 induced cell death (27)—OS cells that were sensitive to FK866 (MG63, SAOS2, ZK58) were treated with FK866. Apoptosis was subsequently measured by western blot of cleaved caspase 3 and cleaved PARP. OS cells treated for 48 h with FK866 showed decreased nuclei count (**Figure 2D**), but the same cells did not show any cleaved caspase 3 or cleaved PARP on western blot, indicating that FK866 did not induce apoptosis in these cells (**Figure 2E**). To investigate if FK866 has an effect on cell cycle progression, OS cells were treated with FK866. Marked changes in cell cycle progression were observed after FK866 treatment in the OS cell line MG63 as the percentage of cells in the G2-phase decreased, while the percentage of cells in the S-phase and the G1-phase increased (**Figure 2F**). However, two other OS cell lines, SAOS2 (FK866 sensitive) and ZK58 (relatively sensitive), did not show any changes in cell cycle progression after the FK866 treatment.

A

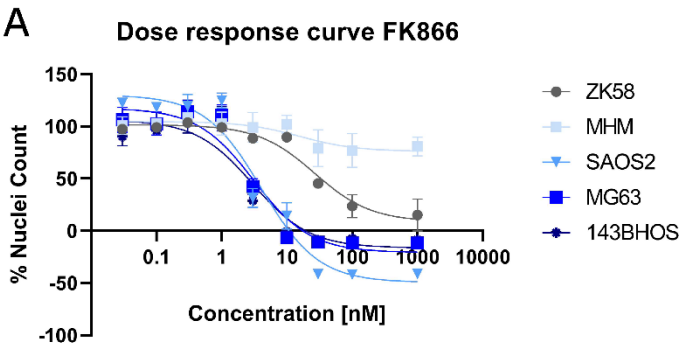

Cell line	IC50 (nM)
ZK58	26.7
MHM	N.D.
SAOS2	4.1
MG63	3.1
143BHOS	3.0

B

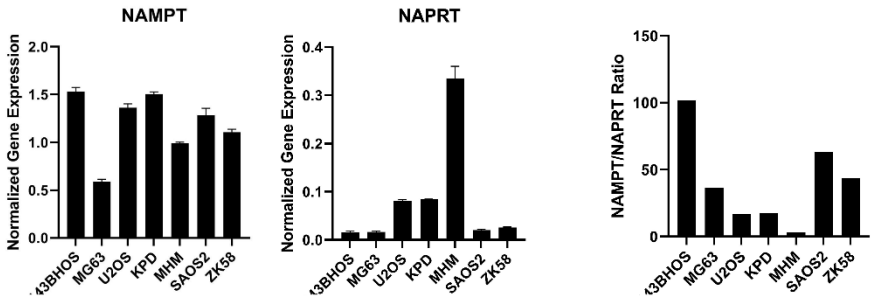

C

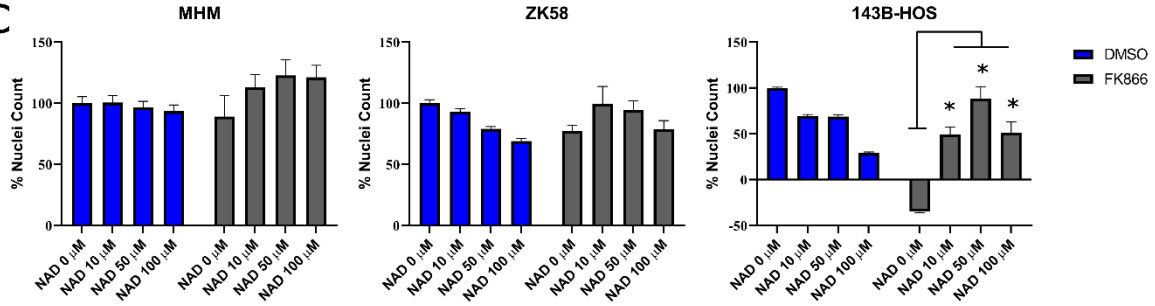

D

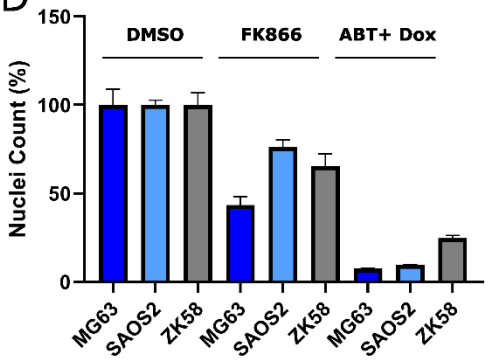

E

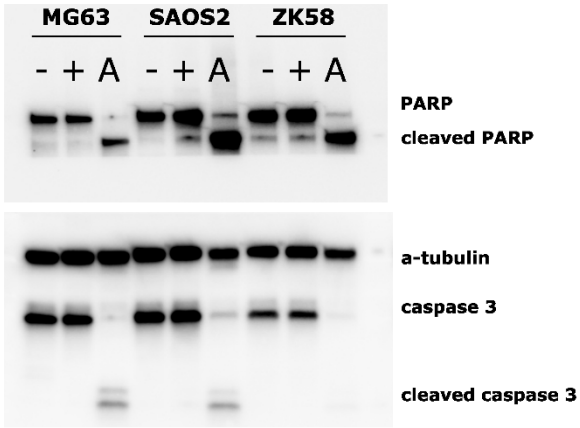

F

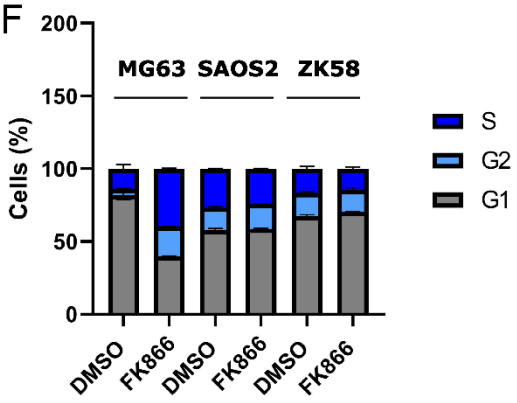

Figure 2. NAMPT inhibitor FK866 decreases cell viability in 2D cultured osteosarcoma cell lines. (**A**) Osteosarcoma cell lines were treated for 72 hours with NAMPT inhibitor FK866 after which cell relative cell viability and IC_{50} values were determined. Data points represent the mean of two experiments performed in triplicate ± standard deviation. (**B**) Gene expression of NAMPT and NAPRT1 in osteosarcoma cell lines. (**C**) NAD+ rescues the inhibitory effect of NAMPT inhibitor FK866 on cell viability. Bars represent the mean of two experiments performed in triplicate ± standard deviation. * = $p < 0.05$ (**D**) OS cells treated for 48 hours with FK866 reduced cell viability. Cells treated with ABT-737 and doxorubicin were used as a positive control for induction of apoptosis (23). Bars represent the mean of two experiments performed in triplicate ± standard deviation. (**E**) Westernblot for cleaved PARP and cleaved caspase 3 after 48 hour treatment with FK866 (+), or 0.1% DMSO (-). No increased apoptosis was observed in OS cell lines. OS cells treated with ABT-737 and doxorubicin (A) were used as a positive control for induction of apoptosis (23). Experiments were performed two times and one representative blot is shown. (**F**) Cell cycle analysis after 48 hour treatment with FK866 showed that treatment induced changes in cell cycle progression in MG63 cells, but not in SAOS2 and ZK58. Bars represent the mean of two experiments ± standard deviation.

3D Cultured Osteosarcoma Cells Are Also Sensitive to NAMPT Inhibition

As 3D cultured cells are often more representative of the in vivo situation compared to 2D cultured cells, multi-cellular tumor spheroids (MCTS) of the OS cell lines MHM, MG63, SAOS2 were generated and treated for 72 h with the NAMPT inhibitor FK866 to determine cell viability. 3D cultured OS cell lines were sensitive to the NAMPT inhibitor treatment (**Figure 3A**). The MHM cell line, which did not show sensitivity to the NAMPT inhibitor in 2D, also showed limited sensitivity in our 3D model compared to the other OS cell lines, with an IC_{50} of 292 nM (**Figure 3B**). In our 3D model of OS cell lines MG63 and SAOS2, NAD+ treatment also rescued the effect of FK866 treatment on cell viability (**Figure 3C**). Immunohistochemical staining of the multi-cellular tumor spheroids for Ki67 and Cleaved Caspase 3 showed no changes in apoptosis (**Figure 3D,E**), which was in line with the results obtained from the caspase 3 and PARP western blot in 2D (**Figure 2E**). However, a reduction of proliferating cells was observed in SAOS2 and MG63 after FK866 treatment (**Figure 3D,E**), whereas the insensitive MHM showed a slight increase of Ki67 positive cells.

FK866 Showed a Variable and Time-Dependent Effect on Osteogenic Differentiation in the OS Cell Line ZK58

A positive link between osteogenic differentiation in osteoblasts and NAMPT expression has recently been suggested (16). Therefore, to determine whether osteogenic differentiation is affected by NAMPT inhibition in OS, we used the OS cell line ZK58, the only cell line in our panel with a known osteogenic differentiation potential (28). ZK58 was treated for four or seven days with FK866 in an osteogenic differentiation medium. Only FK866 and not the osteogenic medium reduced cell viability in ZK58 (**Figure 4A**). Osteogenic differentiation was determined after four or seven days of treatment with FK866, by measuring ALP activity and the gene expression levels of a panel of osteogenic markers (COL1A1, ALPL, RUNX2, SPP1, SPARC). FK866 increased ALP activity, irrespective of the presence or absence of the osteogenic differentiation medium after four days of treatment (**Figure 4B**). The gene expression of several osteogenic markers was not affected by FK866 treatment after the four days; however, the in the case of SPP1, gene expression was increased by FK866 treatment irrespective of the culture medium (**Figure 4C**). After seven days of treatment with FK866,

changes in gene expression occurred. The osteogenic marker SPP1 was still upregulated after FK866 treatment, while other markers (COL1A1, ALPL, RUNX2) were downregulated (**Figure 4C**). The downregulation of osteogenic markers (SPP1, RUNX2, SPARC) was also observed in MCTS of ZK58 treated for seven days with FK866 (**Figure S1B** available online). To investigate the effect of NAMPT inhibition on mineralization, OS cells were treated for 21 days with FK866, after which mineralization was assessed with an Alizarin Red staining. FK866-treated cells showed no visible Alizarin Red staining around the cell population that remained, indicating that no mineralization had occurred (**Figure 4D**).

NAPRT Expression in Osteosarcomas Correlates Inversely with Methylation of the NAPRT Promotor

OS cell lines with low NAPRT1 expression exhibited the highest sensitivity to NAMPT inhibition. In addition, the low expression of NAPRT1 was previously found to be correlated with NAPRT1 promotor hypermethylation in chondrosarcomas (19). Thus, the methylation levels of NAPRT in OS cell lines were compared with the gene expression of NAPRT1. In a previous study, methylation arrays have been performed in osteosarcoma cell lines (26). Using this dataset, NAPRT1 promotor methylation was shown to correlate with decreased NAPRT1 expression in OS cell lines (**Figure 5A**).

NAPRT1/NAMPT expression and methylation were further investigated in a publicly available dataset of the Therapeutically Applicable Research to Generate Effective Treatments (TARGET) (https://ocg.cancer.gov/programs/target (accessed on 22-02-2021) initiative, comprising 86 osteosarcomas and includes data from whole genome RNA expression deep sequencing analyses and DNA methylation arrays. Methylation levels around the NAPRT1 transcription start site were determined; osteosarcomas showed variable levels of methylation around the transcription start site (Figure 5B). These results demonstrate that NAPRT1 and NAMPT expression in primary tumors is variable. There was no correlation between NAMPT and NAPRT1 expression levels in primary tumors (**Figure S1C** available online). The methylation level of NAPRT1 correlated inversely with NAPRT1 expression levels ($r^2 = 0.317$), but there was no correlation with parameters such as sex and the presence of metastasis (**Figure 5C**). In contrast, the NAMPT promotor was not methylated in any of the samples, and therefore no correlation between methylation and expression levels could be observed ($r^2 = 0.03$) (**Figure 5B,C**).

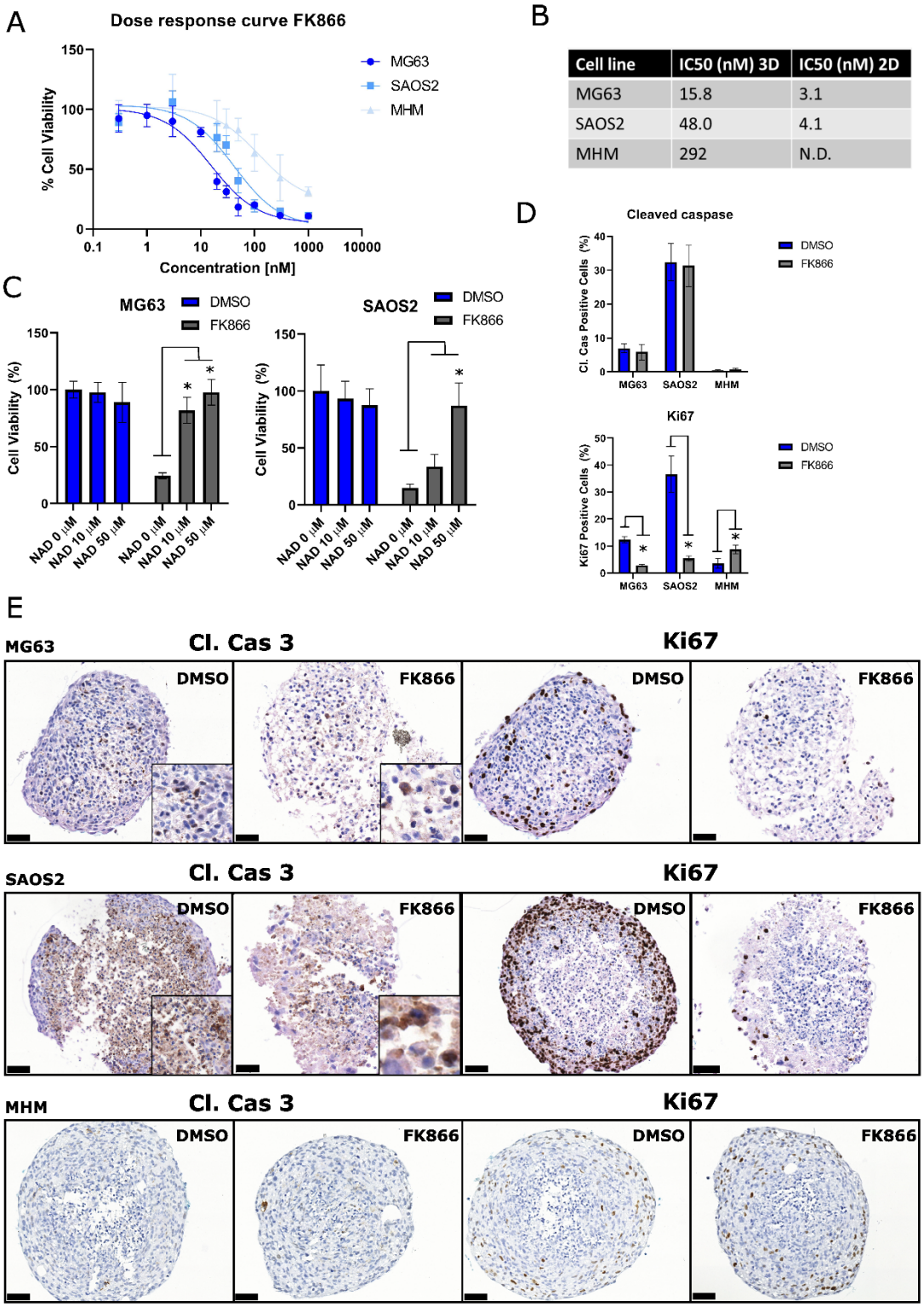

Cell line	IC50 (nM) 3D	IC50 (nM) 2D
MG63	15.8	3.1
SAOS2	48.0	4.1
MHM	292	N.D.

Figure 3. NAMPT inhibitor FK866 decreases cell viability in 3D cultured osteosarcoma cell lines. (**A**) Osteosarcoma multi-cellular tumor spheroids were treated for 72 hours with NAMPT inhibitor FK866 after which relative cell viability and (**B**) IC_{50} values were determined. Data points represent the mean of two experiments performed ± standard deviation. (**C**) NAD+ rescues the inhibitory effect of NAMPT inhibitor FK866 (30 nM) on cell viability in MG63 and SAOS2. Bars represent the mean of one experiment performed in triplicate ± standard deviation. * = $p < 0.05$ (**D**) Quantification and (**E**) representative images of Cleaved caspase 3 and Ki67 stained sections of 3D cultured osteosarcoma cells treated with DMSO or FK866 (30 nM). Scale bar represents 50 µm. * = $p < 0.05$.

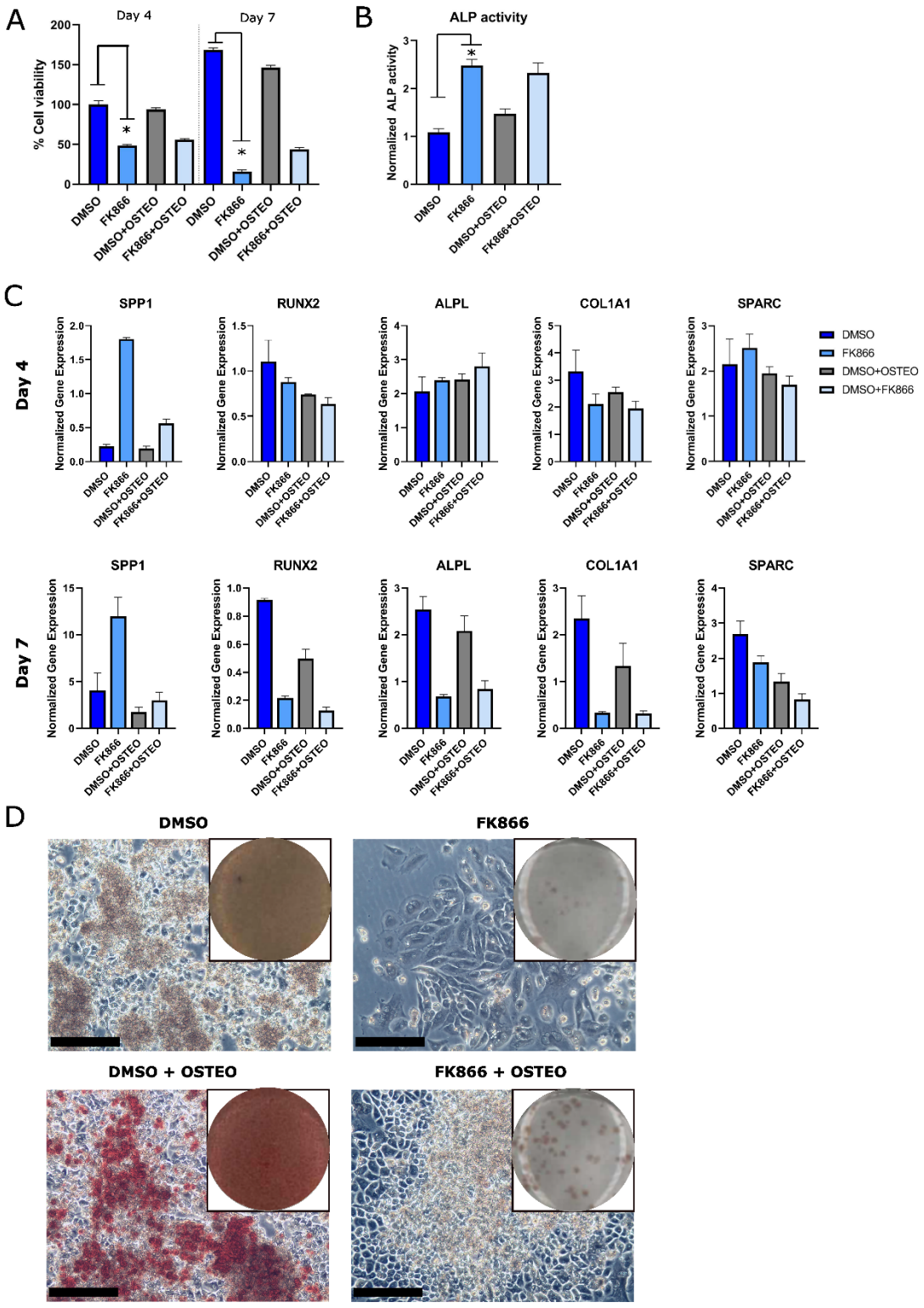

Figure 4. Effect of FK866 on osteogenic differentiation in OS cell line ZK58 is dependent on duration of treatment. All bars represent the mean of two experiments in triplicate ± standard deviation. * = $p < 0.05$. (**A**) Only FK866 treatment (25 nM) and not osteogenic medium affects cell viability. (**B**) ALP enzymatic activity increases after 4 days of FK866 treatment. (**C**) Osteogenic gene expression marker *SPP1* is upregulated after 4 or 7 days of FK866 treatment (25 nM), whereas markers *ALPL*, *COL1A1*, *SPARC* and *RUNX2* are downregulated after 7 days of treatment. (**D**) Mineralization was inhibited in FK866 (25 nM) treated OS cells, after 21 days of osteogenic differentiation. Of each condition one representative image is shown. Scale bar represents 100 µm.

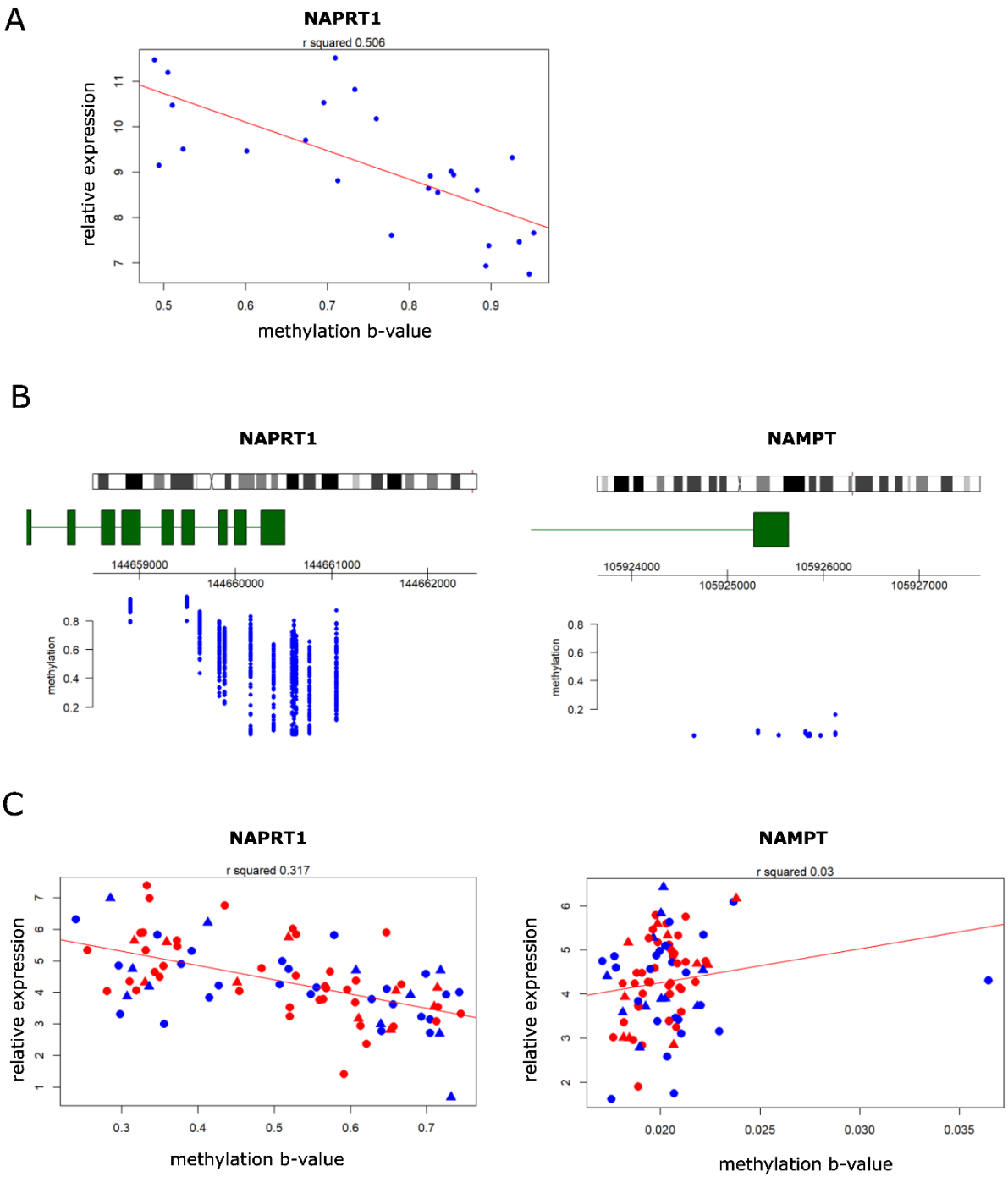

Figure 5. NAPRT promotor methylation correlates with low NAPRT1 expression in osteosarcoma. (**A**) In OS cell lines, methylation of NAPRT1 correlates with low expression of NAPRT1. (**B**) Transcription start site of NAPRT1, and not NAMPT, has areas of methylation in a subset of osteosarcoma tumours. (**C**) High methylation correlates with low expression of NAPRT1 in osteosarcomas. NAMPT gene expression does not correlate with methylation status. Red = male, blue = female, circle = non-metastatic, triangle = metastatic

Discussion

Despite the large number of next-generation sequencing studies identifying targets in osteosarcoma (29-31) and the high volume of in vitro studies (3), no novel therapeutic options for osteosarcoma have been brought to the clinic since the introduction of conventional chemotherapy. In this study, we investigated whether targeting the NAD+ metabolic pathway in osteosarcoma could be a novel therapeutic strategy for osteosarcoma patients. It was shown that osteosarcoma cell lines, both in 2D and 3D cell culture models, are sensitive to NAMPT inhibition by FK866.

We investigated whether NAMPT inhibition affected nuclear count and cell viability in osteosarcoma cell lines by inhibiting apoptosis, or by attenuating cell proliferation. In the current study, it was shown that apoptosis was not induced in OS cells after treatment with FK866. To investigate cell proliferation, cell cycle analysis and Ki67 staining was performed on FK866-treated OS cells. Ki67 staining showed that the number of proliferating cells was reduced by FK866 in two out of three OS cell lines, suggesting that FK866 inhibited cell proliferation. Cell cycle analysis showed that the percentage of MG63 cells in the G2 phase decreased after FK866 treatment, which could suggest a G2 arrest. The observed increased percentage of cells in the S-phase suggests an arrest in the S-phase in the middle of DNA duplication, given the decrease of nuclei count observed after FK866 treatment. Interestingly, only MG63 showed changes in cell cycle progression; the two other FK866-sensitive OS cell lines, SAOS2 and ZK58, did not exhibit such changes. So far, it remains unclear whether the changes in the cell cycle observed in MG63 are an exception. The effect of FK866 is variable among OS cell lines, which is in line with previous studies in literature that have investigated the mechanism of how FK866 reduces cell viability. Previous studies have shown that FK866 does not have an effect on cell cycle distribution (27), or on the contrary, that FK866 inhibits cell cycle progression (32). Similarly, it was demonstrated that FK866 either induced apoptosis ((27)) or that it did not induce caspase-driven apoptosis in cancer cell types with rapid ATP turnover (32, 33). Instead, these cells undergo oncosis-mediated cell death, characterized by cell swelling upon cell death (33, 34). Other mechanisms, such as autophagy, have also been suggested (35). Taken together, the current study underlines the fact that there is currently no consensus in the field on the exact mechanism of FK866 and that future studies should be performed to investigate this in more detail.

Osteosarcoma is characterized by tumor cells that produce an osteogenic matrix. As earlier studies suggested that NAMPT inhibits osteogenic differentiation in murine osteoblast and bone marrow-derived mesenchymal stem cells (16, 36), we investigated whether NAMPT also affected osteogenic differentiation in osteosarcoma cells. We indeed found that FK866 treatment inhibited mineralization in osteosarcoma cells, but this was not reflected in the RNA expression patterns and may also be attributed to the loss of cell viability. In contrast, the early osteogenic marker ALP was increased after a short-term FK866 treatment and may

indicate that inhibition of differentiation is mainly induced after a longer treatment with FK866.

We showed here for the first time that osteosarcoma cell lines are sensitive to NAD+ depletion by using NAMPT inhibition. In the sarcoma field, previous studies suggest that NAMPT inhibition could also be a potential novel therapeutic strategy in chondrosarcoma and Ewing sarcoma (19, 32). In chondrosarcoma, it was reported that low NAPRT1 expression correlated with increased sensitivity (19). This is in line with the current study, where NAMPT inhibition was only effective in osteosarcoma cell lines with low NAPRT1 expression. These cancer cells solely depend on NAMPT for NAD+ supply and therefore NAMPT inhibition will cause synthetic lethality in these cells. As the balance between the NAD synthesis pathways (de novo, classical, or alternative) is different in cancer cells as compared to normal tissue, targeting NAMPT can hence be a novel therapeutic strategy. Not only osteosarcoma but also other types of cancer generally lack NAPRT1 expression (37-39). In line with our results, it was previously shown that in gastric cancer cells with low NAPRT expression, cells were the most sensitive to NAMPT inhibition (40).

In the current study NAMPT inhibition was tested in both 2D and 3D cultured OS cells. It was demonstrated that multi-cellular tumor spheroids have a lower sensitivity to FK866 as compared to 2D cultured cells. It was previously shown that tight intercellular contacts can cause MCTS to have poor drug penetration (41), which could also explain the reduced sensitivity to FK866 in MCTS in the current study. An advantage of using MCTS as a model system is that these spheroids express features that occur in solid tumors, such as regions of hypoxia and necrosis (42). In a previously published study, an increase of apoptosis was observed in MCTS as compared to 2D cultured cells (41). Indeed, we observed apoptotic cells mainly in the core of spheroids, with a highly proliferative outer ring. Thus, it is suggested that MCTS are more representative, also in terms of metabolism (43), compared to 2D cultured cells. This makes OS MCTS an attractive model for further pre-clinical (metabolic) drug testing.

Despite promising results from this study, early clinical trials that have used FK866 in the same concentration range as what we have used (1–10 ng/mL) (44), showed dose-limiting hematological toxicities in patients with other cancer types (39, 44). The toxic effects are not surprising, as healthy tissue expresses both NAMPT and NAPRT1. Therefore, future trials should investigate the possibility of the co-administration of a NAMPT inhibitor with nicotinic acid (NA) to maintain high NAD levels in healthy tissue, or focus on patients in which NAPRT1 expression in the tumor is low in order to limit the dose of the NAMPT inhibitor needed. Pre-clinical studies indeed showed that mice in which the NAMPT inhibitor was co-administrated with NA rescued mortality and limited toxicities. Moreover, this co-administration strategy did not affect anti-tumor activity in xenograft models (45-47). Likewise, a combination therapy including the currently used chemotherapeutic agents should be considered.

The status of NAPRT1 expression could be a good biomarker to predict sensitivity to NAMPT inhibitor treatment. We identified that low NAPRT1 expression correlated with high promotor methylation. Our results are in line with a previous study, which concluded that low NAPRT1 expression by promotor methylation could act as a predictive biomarker for NAMPT inhibition

(48). The current study demonstrated that in most OS cell lines, NAPRT1 RNA expression was low, whereas NAMPT expression was high. In primary tumor samples, the OS the expression of NAPRT1 and NAMPT is variable; however, a subset of patients demonstrates low NAPRT1 in their tumors. With these results combined, it is highly likely that a subgroup of osteosarcoma patients that could benefit from NAMPT inhibition exists. However, future studies should explore co-administration with nicotinic acid or conventional chemotherapy. Furthermore, future studies should investigate if the use of lower doses of the NAMPT inhibitor in tumor tissue expressing low NAPRT1, by using in vivo models, could limit toxicities.

Acknowledgments

The authors would like to thank Pauline Wijers-Koster and Sanne Venneker for technical assistance and discussion

References

1. WHO classification of tumours of soft tissue and bone, 5th edition. Lyon, France: WHO Classification of Tumours Editorial Board; 2020.
2. Smeland S, Bielack SS, Whelan J, Bernstein M, Hogendoorn P, Krailo MD, et al. Survival and prognosis with osteosarcoma: outcomes in more than 2000 patients in the EURAMOS-1 (European and American Osteosarcoma Study) cohort. Eur J Cancer. 2019;109:36-50.
3. Peterse EFP, van Leeuwen TN, Cleton-Jansen AM. A researcher's perspective on the quantity of osteosarcoma in vitro studies. J Bone Oncol. 2017;7:29-31.
4. Boroughs LK, DeBerardinis RJ. Metabolic pathways promoting cancer cell survival and growth. Nat Cell Biol. 2015;17(4):351-9.
5. DeBerardinis RJ, Chandel NS. Fundamentals of cancer metabolism. Sci Adv. 2016;2.
6. Ren L, Hong ES, Mendoza A, Issaq S, Hoang CT, Lizardo M, et al. Metabolomics uncovers a link between inositol metabolism and osteosarcoma metastasis. Oncotarget. 2017;8.
7. Rathore R, Caldwell KE, Schutt C, Brashears CB, Prudner BC, Ehrhardt WR, et al. Metabolic compensation activates pro-survival mTORC1 signaling upon 3-phosphoglycerate dehydrogenase inhibition in osteosarcoma. Cell Rep. 2021;34(4):108678.
8. Wang D-w, Wu L, Cao Y, Yang L, Liu W, E X-q, et al. A novel mechanism of mTORC1-mediated serine/glycine metabolism in osteosarcoma development. Cellular Signalling. 2017;29:107-14.
9. Hu K, Dai HB, Qiu ZL. mTOR signaling in osteosarcoma: Oncogenesis and therapeutic aspects (Review). Oncol Rep. 2016;36(3):1219-25.
10. Chiarugi A, Dolle C, Felici R, Ziegler M. The NAD metabolome--a key determinant of cancer cell biology. Nat Rev Cancer. 2012;12(11):741-52.
11. Canto C, Menzies KJ, Auwerx J. NAD(+) Metabolism and the Control of Energy Homeostasis: A Balancing Act between Mitochondria and the Nucleus. Cell Metab. 2015;22(1):31-53.
12. Kennedy BE, Sharif T, Martell E, Dai C, Kim Y, Lee PW, et al. NAD(+) salvage pathway in cancer metabolism and therapy. Pharmacol Res. 2016;114:274-83.
13. Sampath D, Zabka TS, Misner DL, O'Brien T, Dragovich PS. Inhibition of nicotinamide phosphoribosyltransferase (NAMPT) as a therapeutic strategy in cancer. Pharmacol Ther. 2015;151:16-31.
14. Xiao Y, Elkins K, Durieux JK, Lee L, Oeh J, Yang LX, et al. Dependence of tumor cell lines and patient-derived tumors on the NAD salvage pathway renders them sensitive to NAMPT inhibition with GNE-618. Neoplasia. 2013;15(10):1151-60.
15. Meram AT, Alzubaidi Y, Cotelingam J, Ghali G, Lopez L, Coppola D, et al. Nicotinamide Phosphoribosyl Transferase Is Increased in Osteosarcomas and Chondrosarcomas Compared to Benign Bone and Cartilage. Anticancer Res. 2019;39(4):1761-5.
16. Li Y, He J, He X, Li Y, Lindgren U. Nampt expression increases during osteogenic differentiation of multi- and omnipotent progenitors. Biochemical and Biophysical Research Communications. 2013;434(1):117-23.
17. Ottaviano L, Schaefer KL, Gajewski M, Huckenbeck W, Baldus S, Rogel U, et al. Molecular characterization of commonly used cell lines for bone tumor research: a trans-European EuroBoNet effort. Genes Chromosomes Cancer. 2010;49(1):40-51.
18. Zhang W, Li C, Baguley BC, Zhou F, Zhou W, Shaw JP, et al. Optimization of the formation of embedded multicellular spheroids of MCF-7 cells: How to reliably produce a biomimetic 3D model. Anal Biochem. 2016;515:47-54.
19. Peterse EFP, van den Akker B, Niessen B, Oosting J, Suijker J, de Jong Y, et al. NAD Synthesis Pathway Interference Is a Viable Therapeutic Strategy for Chondrosarcoma. Mol Cancer Res. 2017;15(12):1714-21.
20. Hafner M, Niepel M, Chung M, Sorger PK. Growth rate inhibition metrics correct for confounders in measuring sensitivity to cancer drugs. Nature methods. 2016;13(6):`521-7.

21. van Haaften C, Boot A, Corver WE, van Eendenburg JD, Trimbos BJ, van Wezel T. Synergistic effects of the sesquiterpene lactone, EPD, with cisplatin and paclitaxel in ovarian cancer cells. J Exp Clin Cancer Res. 2015;34:38.
22. Franceschini N, Verbruggen B, Tryfonidou MA, Kruisselbrink AB, Baelde H, de Visser KE, et al. Transformed murine and canine mesenchymal stem cells as a model for sarcoma with complex genomics. Cancers. 2021;13(5).
23. Baranski Z, de Jong Y, Ilkova T, Peterse EFP, Cleton-Jansen AM, Van de Water B, et al. Pharmacological inhibition of Bcl-xL sensitizes osteosarcoma to doxorubicin. Oncotarget. 2015;6.
24. Bankhead P, Loughrey MB, Fernandez JA, Dombrowski Y, McArt DG, Dunne PD, et al. QuPath: Open source software for digital pathology image analysis. Sci Rep. 2017;7(1):16878.
25. Rozeman LB, Hameetman L, Cleton-Jansen AM, Taminiau AH, Hogendoorn PC, Bovee JV. Absence of IHH and retention of PTHrP signalling in enchondromas and central chondrosarcomas. J Pathol. 2005;205(4):476-82.
26. Kresse SH, Rydbeck H, Skarn M, Namlos HM, Barragan-Polania AH, Cleton-Jansen AM, et al. Integrative analysis reveals relationships of genetic and epigenetic alterations in osteosarcoma. PLoS One. 2012;7(11):e48262.
27. Hasmann M, Schemainda I. FK866, a Highly Specific Noncompetitive Inhibitor of Nicotinamide Phosphoribosyltransferase, Represents a Novel Mechanism for Induction of Tumor Cell Apoptosis. Cancer Research. 2003;63.
28. Mohseny AB, Machado I, Cai Y, Schaefer KL, Serra M, Hogendoorn PC, et al. Functional characterization of osteosarcoma cell lines provides representative models to study the human disease. Lab Invest. 2011;91(8):1195-205.
29. Perry JA, Kiezun A, Tonzi P, Van Allen EM, Carter SL, Baca SC, et al. Complementary genomic approaches highlight the PI3K/mTOR pathway as a common vulnerability in osteosarcoma. Proc Natl Acad Sci U S A. 2014;111(51):E5564-73.
30. Kovac M, Blattmann C, Ribi S, Smida J, Mueller NS, Engert F, et al. Exome sequencing of osteosarcoma reveals mutation signatures reminiscent of BRCA deficiency. Nat Commun. 2015;6:8940.
31. Behjati S, Tarpey PS, Haase K, Ye H, Young MD, Alexandrov LB, et al. Recurrent mutation of IGF signalling genes and distinct patterns of genomic rearrangement in osteosarcoma. Nat Commun. 2017;8:15936.
32. Mutz C, Schwentner R, Aryee D, Bouchar E, Mjia E, Hatch G, et al. EWS-FLI1 confers exquisite sensitivity to NAMPT inhibition in Ewing sarcoma cells. Oncotarget. 2017;8(15):24679-93.
33. Del Nagro C, Xiao Y, Rangell L, Reichelt M, O'Brien T. Depletion of the central metabolite NAD leads to oncosis-mediated cell death. J Biol Chem. 2014;289(51):35182-92.
34. Weerasinghe P, Buja LM. Oncosis: an important non-apoptotic mode of cell death. Exp Mol Pathol. 2012;93(3):302-8.
35. Billington RA, Genazzani AA, Travelli C, Condorelli F. NAD depletion by FK866 induces autophagy. Autophagy. 2008;4(3):385-7.
36. He X, He J, Shi Y, Pi C, Yang Y, Sun Y, et al. Nicotinamide phosphoribosyltransferase (Nampt) may serve as the marker for osteoblast differentiation of bone marrow-derived mesenchymal stem cells. Exp Cell Res. 2017;352(1):45-52.
37. Duarte-Pereira S, Pereira-Castro I, Silva S, Correia M, Neto C, da Costa L, et al. Extensive regulation of nicotinate phosphoribosyltransferase (NAPRT) expression in human tissues and tumors. Oncotarget. 2015;7(2).
38. Cole J, Guiot M, Gravel M, Bernier C, Shore G, Roulston A. Novel NAPRT specific antibody identifies small cell lung cancer and neuronal cancers as promising clinical indication for a NAMPT inhibitor/niacin co-administration strategy. Oncotarget. 2017;8(44).
39. Yaku K, Okabe K, Hikosaka K, Nakagawa T. NAD Metabolism in Cancer Therapeutics. Front Oncol. 2018;8:622.

40. Lee J, Kim H, Lee JE, Shin SJ, Oh S, Kwon G, et al. Selective Cytotoxicity of the NAMPT Inhibitor FK866 Toward Gastric Cancer Cells With Markers of the Epithelial-Mesenchymal Transition, Due to Loss of NAPRT. Gastroenterology. 2018;155(3):799-814 e13.
41. Gong X, Lin C, Cheng J, Su J, Zhao H, Liu T, et al. Generation of Multicellular Tumor Spheroids with Microwell-Based Agarose Scaffolds for Drug Testing. PLoS One. 2015;10(6):e0130348.
42. Schreiber-Brynzak E, Klapproth E, Unger C, Lichtscheidl-Schultz I, Goschl S, Schweighofer S, et al. Three-dimensional and co-culture models for preclinical evaluation of metal-based anticancer drugs. Invest New Drugs. 2015;33(4):835-47.
43. Lagies S, Schlimpert M, Neumann S, Waldin A, Kammerer B, Borner C, et al. Cells grown in three-dimensional spheroids mirror in vivo metabolic response of epithelial cells. Commun Biol. 2020;3(1):246.
44. Holen K, Saltz LB, Hollywood E, Burk K, Hanauske AR. The pharmacokinetics, toxicities, and biologic effects of FK866, a nicotinamide adenine dinucleotide biosynthesis inhibitor. Invest New Drugs. 2008;26(1):45-51.
45. Watson M, Roulston A, Belec L, Billot X, Marcellus R, Bedard D, et al. The small molecule GMX1778 is a potent inhibitor of NAD+ biosynthesis: strategy for enhanced therapy in nicotinic acid phosphoribosyltransferase 1-deficient tumors. Mol Cell Biol. 2009;29(21):5872-88.
46. Olesen UH, Thougaard AV, Jensen PB, Sehested M. A preclinical study on the rescue of normal tissue by nicotinic acid in high-dose treatment with APO866, a specific nicotinamide phosphoribosyltransferase inhibitor. Mol Cancer Ther. 2010;9(6):1609-17.
47. Beauparlant P, Bedard D, Bernier C, Chan H, Gilbert K, Goulet D, et al. Preclinical development of the nicotinamide phosphoribosyl transferase inhibitor prodrug GMX1777. Anticancer Drugs. 2009;20(5):346-54.
48. Shames DS, Elkins K, Walter K, Holcomb T, Du P, Mohl D, et al. Loss of NAPRT1 expression by tumor-specific promoter methylation provides a novel predictive biomarker for NAMPT inhibitors. Clin Cancer Res. 2013;19(24):6912-23.

Chapter 7

Osteosarcoma 3D patient derived cultures to test genome-informed personalized treatment options; a feasibility study

Natasja Franceschini, Ieva Palubeckaite, Sanne Venneker, Pauline Wijers-Koster, Cedrick Agaser, Inge Briaire-de Bruijn, Alwine B. Kruisselbrink, Brendy van den Akker, Hailiang Mei, Anne-Marie Cleton-Jansen, Hans Gelderblom, Michiel A.J. van de Sande and Judith V.M.G. Bovée

Abstract

Osteosarcoma is the most common malignant bone sarcoma, characterized by a complex karyotype. Current treatment for osteosarcoma consists of (neo) adjuvant chemotherapy and surgery, which has not improved survival in the last decades. Therefore there is urgent need for novel therapeutic options for osteosarcoma patients, in particular personalized and targeted treatment options. Potential novel therapies are often tested pre-clinically in 2D *in vitro* models, however, these models do not completely recapitulate the *in vivo* situation, whereas 3D models are more representative. In this study, we have established for the first time long-term primary osteosarcoma 3D cultures, either cultured as hydrogels or microsarcs, for the purpose of pre-clinical drug testing. For seven patients, whole-exome sequencing was performed of corresponding primary tumour tissue to identify potential targets for drug treatment. Three out of seven of the established primary osteosarcoma 3D cultures harboured the same genetic alterations as the primary tumours, while for the remaining four cultures no driver mutations were found to confirm these were tumour-derived. For two patients, the primary osteosarcoma 3D cultures were suitable to evaluate personalized treatment, after which cell viability was assessed and cultures were analysed by histology and immunohistochemistry. One primary osteosarcoma 3D culture with a homozygous loss of *CDKN2A* was sensitive to CDK4/CDK6 inhibitor palbociclib, while the other carried a *MYC* amplification and was sensitive to MYC inhibitor 10058-F4, although control cultures indicated the response was not predicted by the genetic biomarker. To compare sensitivity to drugs of primary osteosarcoma 3D cultures (hydrogels and microsarcs) with 2D cultures or 2D cells propagated in a 3D environment, a panel of potential novel treatment options for osteosarcoma was used and histology and cell viability were assessed. Drug treated osteosarcoma hydrogels and microsarcs were less sensitive to drugs compared to 2D cultured cells, or 2D cells cultured as multi-cellular tumour spheroids. These results demonstrate that long-term primary osteosarcoma 3D cultures are suitable to include in a pre-clinical pipeline when testing novel therapeutic options for osteosarcoma.

Introduction

Osteosarcoma, the most common bone sarcoma is most often diagnosed in children and young adults (<30 years), but also has a second peak of incidence in the elderly (1). Osteosarcoma patient five-year survival rates are as low as 30% in cases of recurrence or relapse. Treatment strategies have not significantly improved survival rates over the last decades. Current treatment consists of highly toxic neoadjuvant methotrexate-doxorubicin-cisplatin (MAP) treatment and surgical resection as no new, improved treatment options have been identified (2). An improved multimodal treatment strategy is critical to improve outcomes for these patients.

The rarity of recurring alterations in combination with the genomic complexity and inter-tumour heterogeneity of osteosarcoma poses a challenge to overcome for future identification of novel treatment options and the development of clinical trials. By performing comprehensive analysis of clinically relevant targetable alterations and tailoring treatment strategies in patient-derived xenograft (PDX) models, Sayles and colleagues demonstrated the potential efficacy of genome informed targeted therapy (3). This approach can be applied to other representative osteosarcoma models, such as 3D cell cultures, in order to gain more information on personalized treatment strategies for the disease.

In conventional osteosarcoma 3D culture methods, cells are initially cultured in monolayer on a treated plastic surface, and subsequently transferred to low attachment or scaffold-based 3D culture. This method allows for the evaluation of treatment response that is more representative of the *in vivo* situation as compared to conventional 2D cell lines (4, 5). *In vitro* models can be further improved when derived straight from patients and by maintaining cells in extracellular matrix-based scaffolds, using methods such as organoid culture (6). In general, sarcoma cells cultured in 2D are morphologically very different from the *in vivo* situation due to a lack of cell-cell and cell-matrix attachment, and cells are prone to dedifferentiation over time (7). Continuous culturing to establish cell lines can select for specific cells and introduce additional mutations, alter gene and protein expression, and thus may alter drug response (8-10). Recapitulating the *in vivo* environment as closely as possible ensures a more representative therapeutic outcome. Organoid-like long-term culture of metastatic osteosarcoma was previously established by adaptation of epithelial organoid culture methods to osteosarcoma samples (11). However, this method was not successful for generation of long-term primary osteosarcoma tumour patient-derived cultures.

In the present study we describe culture methods tailored to the osteosarcoma microenvironment. We were able to establish long-term osteosarcoma primary 3D cultures, regardless of osteosarcoma subtype or pre-treatment. The culture was established without use of organoid culture methods commonly used for epithelial cancers, avoiding non-representative cell behaviour and increasing cost effectiveness. Instead, collagen- based

hydrogels and osteogenic growth factors were used for osteosarcoma 3D cell culture propagation. Patient cells were propagated in hydrogels immediately after collection of patient material to prevent 2D culture-based dedifferentiation. Denser cell masses, termed microsarcs, were produced from hydrogel propagated cells in order to more sufficiently mimic *in vivo* osteosarcoma upon treatment. In addition, multi-cellular tumour spheroids (MCTS) were generated from 2D primary cultures of one patient to compare 3D models created after culture in 2D to the immediate 3D propagation models. The primary osteosarcoma 3D long-term cultures were used in this study to investigate whether these models can be used for personalized targeted treatment. For this purpose, whole-exome sequencing (WES) was performed on tumour tissue of seven osteosarcoma patients to detect targetable alterations, after which the 3D primary osteosarcoma cultures of two patients were treated with drugs targeting the alterations. Furthermore, the sensitivity to drugs was compared between conventional 2D cultures, 2D cells propagated in a 3D environment, and straight-from-patient derived 3D cultures. We demonstrate use and relevance of these osteosarcoma 3D culture models in the context of precision medicine to obtain more representative pre-clinical data and improve clinical outcomes for osteosarcoma patients.

Materials and Methods

Patient samples

All tumour tissue samples used for this study were derived from the bone and soft tissue tumour biobank of the Leiden University Medical Centre (BWD005/SH/sh) and obtained from patients undergoing surgical resection. The use of tumour tissue samples for this study was approved by the LUMC ethical review board (B.16.026). Written informed consent was obtained from all participants and the study was conducted according to the code for Proper Secondary Use of Human Tissue in the Netherlands. Relevant clinical information can be found in **Table 1**.

2D primary line production

Tissue samples were obtained directly from surgery and minced with razor blades and immersed in 3mL collagenase/dispase (1mg/mL) either at 37°C for two hours or at room temperature overnight. Once digested, the samples were washed twice with DMEM:F12 (#10565018, Gibco, Waltham, USA). The remaining pieces of tissue were squeezed using a glass pipette in order to suspend the cells. After washing, the cells were transferred into 75 ml culture flasks and cultured in αMEM (#LO BE12-169F, Lonza, Basel, Switzerland) supplemented with 10% foetal bovine serum (FBS), 100U/ml penicillin and 100µg/mL streptomycin (Life Technologies Limited) and 1% NEAAs (#11140050, Gibco, Waltham, USA). Cells were grown in a humidified incubator with 1% O_2 and 5% CO_2 and cultured until stably multiplying.

Table 1. Overview of osteosarcoma patient samples used in this study. M = male; F = female; SNV = single nucleotide variant; amp = amplification; NA = not applicable

Patient ID	L6558	L6565	L6581	L6620	L6621	L6647	L6727
Subtype	Conventional, telangiectatic	Conventional	Conventional	Conventional	Conventional chondroblastic	Conventional	Conventional, telangiectatic
Location	Fibula	Humerus	Lung	Humerus	Os ilium	Abdomen	Pelvis
Age	36	57	29	51	21	25	67
Gender	M	F	M	F	M	M	F
Tumour sample	primary	primary	metastasis	primary	primary	metastasis	primary
Neo-adjuvant treatment	Yes	No	Yes, for treatment of primary tumour	No	Yes	No	Yes
Tumour specific alteration	*EPHB1* SNV exon 7 >chr3: 135162098 A>G; *PES* SNV exon12 >chr22: 30579877 C>T	*KRAS* SNV (c.35G>A; VAF: 0.64), CDKN2A loss	*F13A1* SNV exon 4, >chr6: 6266605 C>T	*MTRR* SNV intron 13, >chr5: 7897041 G>T	*MYC* amp intron 13, >chr5: 7897041 G>T	*TP53* SNV (c.775G>T; VAF: 0.74)	*TP53* SNV (c.406C>T; VAF: 0.45)
Confirmed in 3D culture (analysis method)	No (Sanger sequencing)	Yes (Cancer Hot Spot Panel)	No (Sanger sequencing)	No (Sangerse quencing)	Yes (MYC IHC staining)	Yes (P53 IHC staining) but stopped growing	No (Cancer Hot Spot Panel)
Targetable alteration	BRCAness signature	*CDKN2A* loss	None	BRCAness signature	*MYC* amp	4q12 amp (*KIT, PDGFRA, KDR*)	None
Target specific drug	PARPi	Palbociclib	NA	PARPi	JQ1 or 10058-F4	Regorafenib	NA

Osteosarcoma MCTS production from 2D culture

Multicellular tumour spheroids (MCTS) were produced from conventionally cultured (2D) primary L6565 cells (OS MCTS). The cells were suspended in αMEM (#LO BE12-169F, Lonza, Basel, Switzerland) supplemented with 10% foetal bovine serum (FBS) and 100U/ml penicillin and 100µg/mL streptomycin (Life Technologies Limited) and 1% NEAAs (#11140050, Gibco, Waltham, USA). Additional supplementation with 50 µg/ml ascorbate 2-phosphate and 100nM dexamethasone was performed directly before culture. The medium contained 0.24% (w/v) methyl cellulose in order to improve reproducibility of spheroids. The cells were then seeded onto 1% (w/v) agarose coated (ultra-low attachment) plates at a density of 20,000 cells/well. They were cultured for 7 days in order to aggregate into a large mass and were subsequently used for therapeutic testing.

Osteosarcoma 3D primary line production (hydrogels and microsarcs)

After tissue digestion the cell suspension was strained using a 70µm cell strainer (#431751, Corning, New York, USA). If blood was present in the pellet, cells were additionally washed with 2mL PBS and treated with 4mL RBC lysis buffer (#00-4333-57, Invitrogen, Waltham, USA) for 4 mins. To stop the lysis 30mL of PBS was added and the cells were washed in cell culture medium. The cells were suspended in a collagen scaffold (2.5mg/mL collagen, 1x DMEM, 8.29µM NaOH, 0,38% alginate (w/v)) and plated out either in 12-well (for propagation) or 96-well (for therapeutic compound testing) non-treated cell culture plates into 10/80µL gels respectively. The plates were incubated at 37°C for 25 mins and then left at room temperature for an additional 5 mins. In order to gelate the alginate component of the scaffold and further stiffen the gel, the samples were incubated in 0.2M $CaCL_2$ solution for 5 mins. The samples were subsequently washed twice with 0.15M NaCl solution, followed by two washes with medium and placed in culture medium containing αMEM (#LO BE12-169F, Lonza, Basel, Switzerland) supplemented with 10% foetal bovine serum (FBS) and 100U/ml penicillin and 100µg/mL streptomycin (Life Technologies Limited) and 1% NEAAs (#11140050, Gibco, Waltham, USA). Additionally, medium was supplemented with 50 µg/ml ascorbate 2-phosphate and 100nM dexamethasone (osteogenic growth factors). Cells were grown in a humidified incubator with 1% O_2 and 5% CO_2 and cultured until >80% gel confluency for either passage or treatment. Cells were regularly STR-profiled using the GenePrint 10 system kit (Promega, Madison, WI, USA) and showed the same STR profile as the original tumour. In addition, all cells used for treatment were regularly tested for mycoplasma.

To passage the osteosarcoma hydrogels, cultures were first collected and washed once with PBS. In order to digest the scaffold 0.25mg/mL LiberaseTL (#5401020001, Roche, Basel, Switzerland) solution (in PBS) was added (4,375µL/µL scaffold). The scaffolds were incubated at 37°C for digestion and checked and vortexed after the first 10mins then subsequently 5min intervals until the gel was dissolved and the cells were released into a single cell solution. The digestion was quenched using medium and washed with medium. On a bi-passage basis the cells were strained further to remove debris using autoclaved 50µm cell strainers (#04-0042-2317, Sysmex, Kobe, Japan). The cells were then resuspended in new scaffold at a ratio of 1:2

for further culture or frozen for cryostorage. All osteosarcoma lines produced could be repropagated from frozen cryostock.

For further therapeutic testing, osteosarcoma microsarcs were additionally produced from the cell lines propagated in hydrogel culture. The method used to produce microsarcs was identical to the MCTS protocol described above, but a higher seeding density (50,000 cells/well) was used. Although the aggregation method of MCTS and microsarcs was the same, the cells were propagated in different environments previous to aggregation (2D/3D culture) since the beginning of *in vitro* culture.

Next generation sequencing data analysis

For whole exome sequencing, DNA was isolated from matched pairs of primary tumour and normal frozen tissue of seven patients using the Wizard Genomic DNA purification kit (Promega, Madison, WI, USA) according to the manufacturer's instructions. DNA samples were checked for degradation by gel electrophoresis. Whole exome sequencing with a minimum coverage of 100x was performed by GenomeScan BV (Leiden, the Netherlands) using the Illumina Novaseq6000 platform and the Agilent SureSelect Human All Exon V7 kit. The WES data were processed using the BioWDL somatic variant calling pipeline developed at LUMC (https://github.com/biowdl/germline-DNA/blob/v3.0.0/somatic.wdl). The quality control was first performed by FastQC (v0.11.9). Then the adapters were further clipped using Cutadapt (v2.8). The clean reads were aligned to the human reference genome GRCh38 using BWA-MEM (v0.7.17-r1188). According to the GATK best practice, duplicated mapped reads were marked using Picard (v2.20.5) and the base quality recalibration was performed using GATK4 (v 4.1.2.0) to generate the analysis-ready reads in the BAM format. Strelka (version 2.9.7) and Mutect2 (version 4.1.2.0) were used to detect small somatic variants from the matched tumour-normal samples. Only the variants meeting the criteria as determined by Strelka and Mutect2 were included in the downstream analysis. These variants were then normalized and decomposed using vt program (v2015.11.10) and subsequently annotated using VEP (v98) with SIFT and Polyphen-2 options enabled. VEP plugins and custom annotation files were also used to include annotations of CADD scores, dbNSFP3.5 (phastCons100way vertebrate & phyloP100way vertebrate), population allele frequency information (e.g., gnomAD version 3 and GoNL). Copy number variants (CNVs) were identified following GATK somatic CNV discovery best practice workflow (v4.1.4.0). Pre-selected targetable genes (**Supplementary Table 1**) were used to prioritize both small variants and CNV. Genes were labeled "targetable" when it occurred in more than one of the following targetable cancer gene panels: FoundationOne and FoundationOne Heme, MSK-IMPACT (12), Mi-oncoseq (13), and UCSF 500 Cancer Gene Panel.

For the customized Cancer Hotspot deep sequencing panel sequencing, DNA was isolated from osteosarcoma hydrogels of L6727 P5 and L6565 P15 using the Wizard Genomic DNA purification kit (Promega) according to the manufacturer's instructions. Libraries were generated using Life Technology's Ion AmpliSeq Cancer Hotspot Panel v6. Data analysis was

performed as described previously (14, 15). To confirm presence of non-driver tumour-specific variants in the 3D cultures, PCR and Sanger sequencing for the genes *EPHB1, PES, F13A1, USP43* and *MTRR* was performed.
The tumour mutational burden (TMB) was calculated per sample by dividing the number of protein-coding somatic mutations by the total size of the exome (30 Mb was used which is a commonly agreed standard). Using the fit_to_signatures_strict (cutoff = 0.010) from MutationalPatterns R-package (v3.0.1), mutational signature profiles per sample were generated based on SigProfiler exome SBS reference signatures (https://www.synapse.org/#!Synapse:syn12026190).

Immunohistochemistry
Whole slide sections of paraffin embedded tumour tissue or 4 µm paraffin embedded osteosarcoma hydrogels, osteosarcoma microsarcs or osteosarcoma MCTS were made and stained for haematoxylin and eosin or used for immunohistochemical staining after deparaffinization and rehydration. Tumour tissue sections were stained for SATB2 (clone CL0276, Sigma-Aldrich, Saint Louis, MO, USA). In addition, L6621 was stained for MYC (clone Y69, Abcam, Cambridge, UK) and L6647 was stained for p53 (clone DO-7, Dako, Agilent Technologies, CA, USA). Osteosarcoma hydrogels, osteosarcoma microsarcs, and osteosarcoma MCTS were stained for SATB2. Additional stainings were performed for L6565 hydrogels or MCTS: cleaved caspase 3 (Cell Signaling Technology, Leiden, The Netherlands), Ki67 (clone D2H10, Cell Signaling Technology), p16 (clone E6H4, CINTEC, Roche, Basel, Switzerland), Rb (clone G3245, BD Pharmingen, San Diego, CA, USA) and MYC. For SATB2, Ki67 and cleaved caspase 3 staining, antigen retrieval was performed by a 10 minute incubation in 10 mM citrate buffer (pH 6) followed by cooling down for two hours. For MYC, p53, p16 and Rb staining, antigen retrieval was performed using Tris-EDTA (pH 9). Sections were incubated with primary antibody (Ki67, 1:1600; MYC, 1:80; p53, 1:1; cleaved caspase 3, 1:800; Rb, 1:2000, SATB2, 1:10, p16, 1:1) overnight at 4 °C. The next day, sections were incubated with BrightVision one step detection system poly-HRP anti-mouse/rabbit (Immunologic, WellMed BV, Duiven, The Netherlands) for 30 minutes. Sections were washed with PBS and DAB+ Chromogen (Dako) was added to each slide for 10 minutes. Slides were counterstained with haematoxylin, dehydrated and mounted.

Drug treatment of osteosarcoma hydrogels and microsarcs
For drug treatment in osteosarcoma hydrogels, once near confluence, L6565 and L6621 was treated with palbociclib (20 or 45 µM, dissolved in PBS; Selleckchemicals, Houston, TX, USA), JQ1 (1 or 10 µM; Selleckchemicals), 10058-F4 (10 or 50 µM; Selleckchemicals) or solvent controls (PBS and DMSO) for 72 hours. Dosage for drug treatment was selected based on results from previously published studies (16-18) in which a similar concentration range was used. For drug treatment in osteosarcoma microsarcs, L6565 was seeded at 50,000 cells per well in a 96-well plate. One week after the generation of osteosarcoma microsarcs , cells were treated with palbociclib (20 or45 µM) or PBS for 72 hours.

Drug screening in L6565

For a focused drug screen in L6565 cultures, compounds were selected based on recent literature (19). These included an IGF pathway inhibitor (linisitinib) (20, 21), a tyrosine kinase inhibitor (regorafenib) (22), and an mTOR inhibitor (rapamycin) (23). In addition, standard chemotherapeutic agents used in sarcomas, i.e. doxorubicin and cisplatin were included, while palbociclib was used as positive control.

For drug screens in 2D cultured cells, L6565 cells were seeded at 4000 cells per well of a 96-well plate. For monotherapy treatment, the next day cells were treated for 72 hours with doxorubicin or cisplatin (both in-house hospital pharmacy of Leiden University Medical Center), palbociclib, rapamycin, linsitinib, or regorafenib (all Selleckchemicals) in concentrations ranging from 0.001 to 100000 nM. For combination treatments, cells were seeded in medium containing cisplatin or doxorubicin for 24 hours. The next day, cisplatin or doxorubicin was removed, and palbociclib was added for 72 hours. Pre-treatment of cisplatin and doxorubicin was based on a previously published study indicating simultaneous addition of chemotherapy with palbociclib will result in interference between the drugs (24). The combination treatment of rapamycin and palbociclib was performed by simultaneous addition of each drug 24 hours after seeding for 72 hours, which is based on the experimental set-up of a previously published study in which rapamycin and palbociclib were added simultaneously (25).

For drug screens in osteosarcoma MCTS and hydrogels, L6565 was treated with cisplatin, doxorubicin, rapamycin and palbociclib for 72 hours.

Cell viability and nuclei count assays

After drug treatment, cell viability was determined by Presto Blue Cell Viability reagent after 90 minutes (for osteosarcoma hydrogels, microsarcs or MCTS) or 60 minutes (for 2D cultured cells) incubation, after which fluorescence was measured at 550/600 nm using a microplate reader (Infinite M Plex, Tecan Group Ltd., Zürich, Switzerland) . Osteosarcoma hydrogels were formalin fixed and paraffin embedded after read-out.

2D cultured cells were fixed in formalin and Hoechst (Invitrogen Life Technologies) was added to each well after read-out. Nuclei were counted using Cellomics HCS viewer Software V9. Cell viability and nuclei count reads were determined relative to PBS or DMSO control after correcting for background reads and reads prior to the start of treatment (day 0), as described in (26)

Statistical analysis

For statistical comparisons between groups, a Kruskal-Wallis test was performed using Dunn's correction for multiple testing. All statistical analyses were performed using GraphPad Prism v.8. Comparisons were considered statistically significant using a significance level of $p \leq 0.05$.

Results

Long-term genetically stable 3D osteosarcoma hydrogel cultures can be established from human osteosarcoma resection material

Osteosarcoma hydrogel lines were established from osteosarcoma resection material of seven individual patients **(Fig 1A)**. The selection consisted of a variety of osteosarcoma specimens, including pre-treated tumours and different osteosarcoma subtypes **(Table 1)**. All seven osteosarcoma hydrogel lines were cultured in collagen-based scaffolds over the course of 44-120 days to at least passage 7. This demonstrates long-term propagation of such lines fully in 3D cell culture, allowing their expansion and use for therapeutic testing and mechanistic studies whilst preserving their *in vivo* behaviour **(Fig 1B)**. However, during the COVID-19 pandemic, lab work was suspended and all cultures were frozen down, which may have affected the recovery and propagation time of cultures. Osteosarcoma hydrogels showed the lowest cell density as compared to osteosarcoma microsarcs or MCTS (**Fig 1C**). Morphology of the cells was reminiscent of the original tumour, for example, cells within osteosarcoma hydrogels of L6565 showed a spindle-shaped morphology, similar to the original tumour (**Fig 1C**). However, none of the patient-derived lines displayed evidence of osteoid deposition, and SATB2 immunohistochemistry was negative in the osteosarcoma hydrogels, microsarcs, and MCTS (**Supplementary Fig S1**). The selected patient lines (L6565 and L6621) used for therapeutic screening proliferated up to passage 30, allowing for multiple testing of therapeutic strategies.

Whole-exome sequencing of primary osteosarcoma reveals targetable alterations

For all seven patient-derived osteosarcoma hydrogels whole exome sequencing was performed on the DNA from the corresponding original tumour tissue as well as on DNA from non-neoplastic tissue from the same patient to evaluate the presence of targetable molecular alterations for each patient and to identify specific alterations that can be used to confirm tumorigenicity of each osteosarcoma hydrogel.

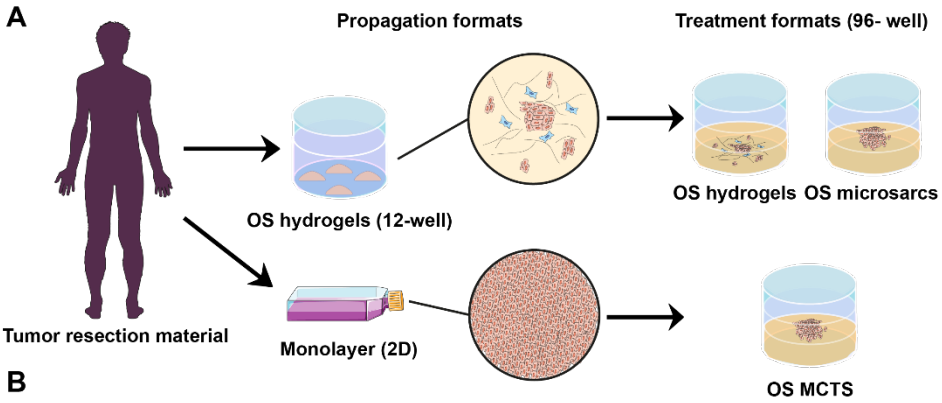
A
Propagation formats
Treatment formats (96- well)
OS hydrogels (12-well)
OS hydrogels
OS microsarcs
Tumor resection material
Monolayer (2D)
OS MCTS

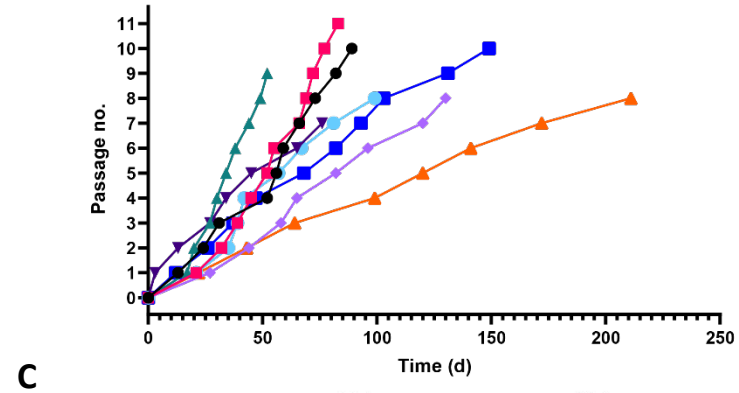
B
Passage no.
Time (d)
L6565
L6558
L6581
L6620
L6621
L6647
L6727
L6748

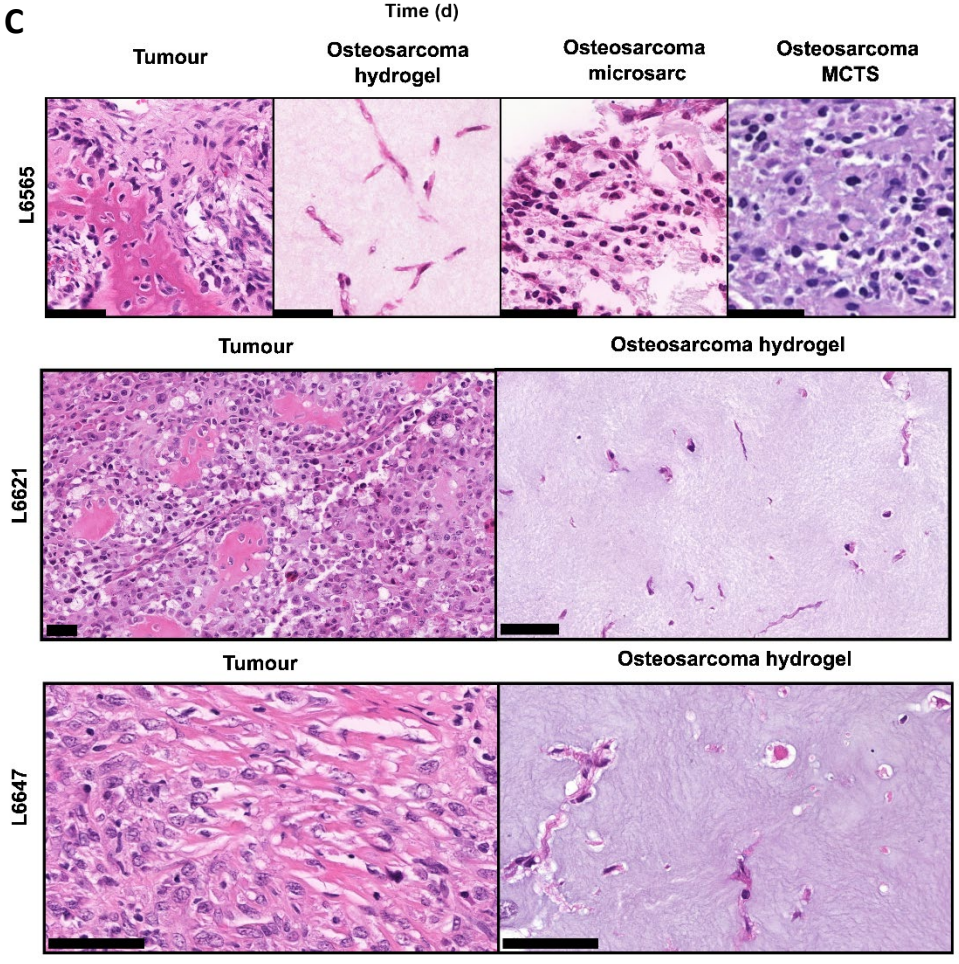
C
Tumour
Osteosarcoma hydrogel
Osteosarcoma microsarc
Osteosarcoma MCTS
L6565
Tumour
Osteosarcoma hydrogel
L6621
Tumour
Osteosarcoma hydrogel
L6647

Figure 1. Growth rate and histology of seven established primary 3D osteosarcoma cultures. (**A**) Osteosarcoma patient resection material was digested to single-cell suspensions, which were then propagated in a collagen-based scaffold with optimized osteosarcoma medium (OS hydrogels) or cultured in monolayer (2D). For treatment of osteosarcoma hydrogels, the culture format was switched to 96-well plate hydrogels or to microsarc format. For treatment of cultures derived from monolayer, cells were seeded as multi-cellular tumour spheroids (MCTS). (**B**) Seven osteosarcoma lines were established and cultured for at least seven passages without signs of a growth plateau. (**C**) H&E staining of the original tumours and the corresponding patient-derived osteosarcoma hydrogels, microsarcs or MCTS. Scalebar represents 50 µm.

Detection of targetable alterations

WES data analysis revealed that the total number of single nucleotide variants of each tumour varied among patients (**Fig 2A**). The tumour mutational burden in all osteosarcoma patients was low to intermediate, with an average of 9.0 mutations per megabase (**Fig 2B**) (27). The copy number profiles of most of the osteosarcoma samples demonstrated a highly complex genome with many copy number alterations, although the level of complexity varied. In contrast, L6565 only showed a small number of copy number changes (L6565 and L6621 shown in **Fig 2C**, rest of samples in **Supplementary Figure S2**). Mutational signature analysis revealed that two COSMIC mutational signatures were dominant (signature SBS5 and SBS31, **Supplementary Figure S3**), although these were not associated with a specific etiology. In L6558 and L6620 the mutational signature SBS3 was identified, albeit at a low level, which is associated with a BRCAness signature, and may suggest sensitivity to PARP inhibitors (28). Both tumours did not show alterations in homologous recombination deficiency related genes (15).

All seven osteosarcoma tumour samples were analysed for the presence of targetable alterations (**Table 1**). To identify which genetic alterations are targetable for each patient, genetic alterations including single nucleotide variants and copy number alterations, were filtered using a pre-defined list of targetable genes (**Supplementary Table 1).** L6565 was revealed to have a *KRAS* mutation (c.35G>A; VAF: 0.64) and homozygous loss of *CDKN2A*, the latter is targetable by CDK4/CDK6 inhibitors such as palbociclib. L6621 showed a *MYC* amplification, which can be targeted by MYC inhibitors such as JQ1 and 10058-F4. L6647 carried an amplification in the region 4q12, which contains the genes *KIT*, *PDGFRA* and *KDR* which can be targeted by receptor tyrosine kinase inhibitors such as regorafenib. For two tumours, L6581 and L6727, no targetable alterations were identified. An overview of identified targetable alterations is shown in **Table 1**.

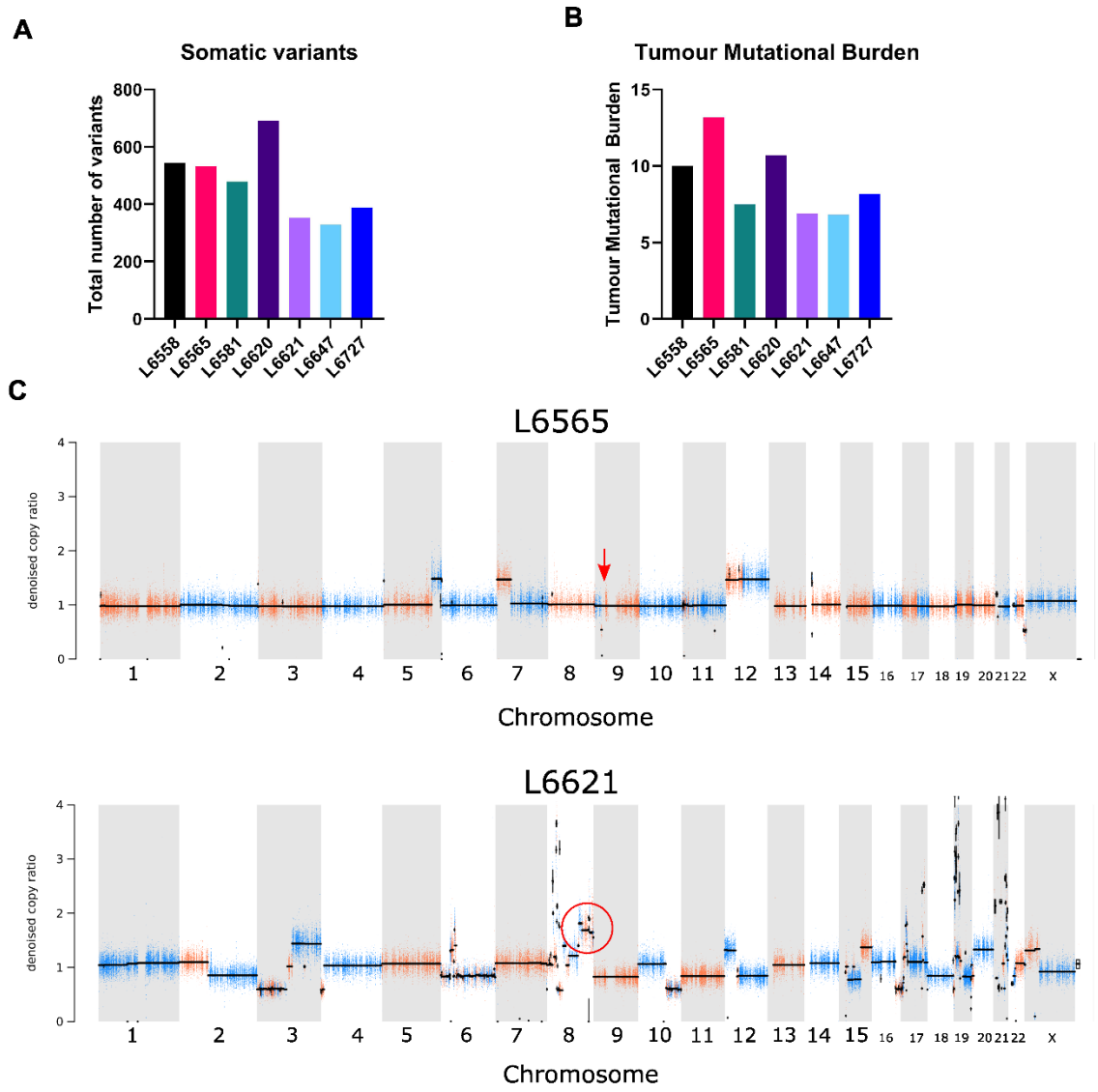

Figure 2. Whole exome sequencing analysis of osteosarcoma tumour samples. (**A**) Total number of somatic single nucleotide variants per tumour. Bars represent the number of overlapping variants identified by different variant callers (Strelka, Mutect2). (**B**) Tumour mutational burden per patient. Values are expressed as mutations per megabase. (**C**) Copy number profiles of L6565 and L6621. For L6565 the copy number loss of *CDKN2A* is indicated with a red arrow. For L6621 the MYC amplification is indicated with a red circle.

Molecular confirmation of the presence of tumour cells in the 3D cultures

The presence of tumour specific alterations was investigated in the osteosarcoma hydrogels to confirm the presence of tumour cells instead of normal fibroblasts in the 3D cultures. Using a a customized Cancer Hotspot deep sequencing panel, it was confirmed that L6565 osteosarcoma hydrogels contained the same driver mutations as the original tumour, including the identical *KRAS* mutation and homozygous loss of *CDKN2A* (**Supplementary Figure S4**). Moreover, L6565 osteosarcoma hydrogels indeed showed loss of p16 protein expression (**Figure 3**). Because for L6727, L6558, L6620, and L6581 no driver mutations were available other somatic variants were used to compare the primary tumour with the 3D cultures. Single nucleotide variants were selected on the basis of coverage (>100) and variant allele frequency (>0.3) and include a *TP53* point mutation (c.406C>T, VAF: 0.45), a *EPHB1*

point mutation, a *MTRR* point mutation, and a *F13A1* point mutation respectively. Unfortunately, these mutations were not found in the 3D cultured cells. This may imply that tumour cells were overgrown by normal fibroblasts in 3D culture. For L6621, the positive immunohistochemical staining for MYC suggested that the *MYC* amplification as identified by WES in the L6621 primary tumour tissue, was also present in the L6621 3D cultured cells (**Fig 3**. Likewise, L6647 3D cultured cells showed p53 overexpression suggestive of the presence of the *TP53* mutation (c.775G>T; VAF: 0.47) that was found using WES in the L6647 primary tumour tissue (**Figure 3**). Thus, in total three out of seven 3D osteosarcoma hydrogel cultures consisted of tumour cells and could therefore be used to test targeted therapies (**Table 1**). Unfortunately, the patient derived osteosarcoma hydrogel line L6647 did not grow sufficiently for further testing, which left two patient derived osteosarcoma hydrogel lines (L6565 and L6621) for drug testing.

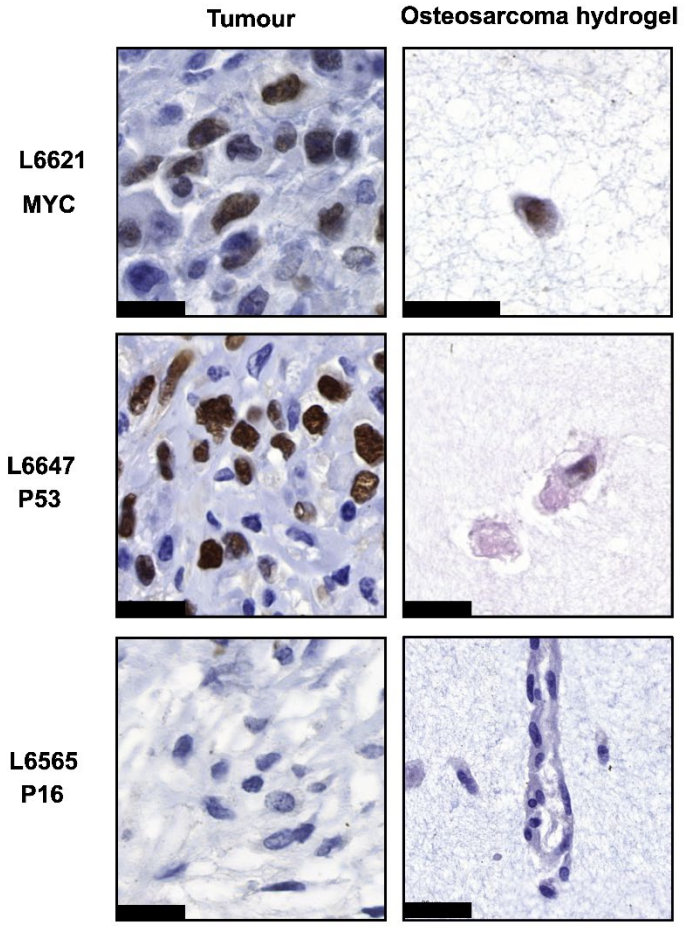

Figure 3. Osteosarcoma hydrogels carry the same alteration as the original tumour. Loss of immunohistochemical expression of P16, or overexpression of MYC and P53 were confirmed in the osteosarcoma hydrogels derived from L6565, L6621 and L6647 respectively. Scalebar represents 20 µm.

Targeted treatment of patient-derived 3D osteosarcoma cell cultures

L6621, which displayed a *MYC* amplification, was treated with BET bromodomain inhibitor JQ1, which was shown to downregulate MYC transcription (29), as well as a specific MYC inhibitor, 10058-F4 (30). Osteosarcoma hydrogels of L6621 that were treated for 72 hours with 1 or 10 µM JQ1 did not show a reduction in cell viability after treatment, whereas treatment of 10 µM or 50 µM 10058-F4 reduced cell viability to 70% ($P = 0.0046$) and 40% ($P < 0.001$) respectively (**Fig 4A**). However, the presence or absence of a MYC amplification did not predict response, since osteosarcoma hydrogels without *MYC* amplification (L6565) also showed a reduction in cell viability ($P < 0.001$)(**Fig 4B, 4C**).For L6565 the deletion of *CDKN2A* could indicate sensitivity to CDK4/CDK6 inhibition, provided Rb is functional. Rb status was determined for L6565 with immunohistochemistry and showed no loss of Rb in the osteosarcoma cells in hydrogel (**Figure 4C**). Thus, osteosarcoma hydrogels of L6565 were treated with CDK4/CDK6 inhibitor palbociclib for 72 hours which reduced cell viability ($P < 0.001$)(**Fig 4B**). However, no difference in morphology, apoptosis or proliferation between untreated and palbociclib treated osteosarcoma hydrogels was observed by Ki67 or cleaved caspase 3 staining (**Fig 4D, Supplementary Figure S5**). Since only few cells are visible per section in osteosarcoma hydrogels, L6565 was also cultured as microsarcs resulting in a similar reduction in cell viability as compared to osteosarcoma hydrogels ($P = 0.0146$) (**Fig 4E**). However, the presence or absence of *CDKN2A* did not predict the effect of palbociclib on cell viability in L6565, as L6621 osteosarcoma hydrogels (without loss of *CDKN2A*) also showed reduced cell viability upon palbociclib treatment ($P < 0.001$)(**Figure 4A**). The dosage of palbociclib used in this study was relatively high as compared to previous studies for the treatment of HER-2 negative breast cancer and breast cancer cell lines *in vitro* (31). Thus, to determine whether the dosage of palbociclib could be reduced further, different drug combinations with other promising novel osteosarcoma therapeutics were tested in 2D cultures of L6565. However, no combination therapy was able to reduce the dose of palbociclib (**Supplementary Figure S6**).

Osteosarcoma hydrogels are suitable to test novel treatment options

We further explored whether the generated osteosarcoma hydrogels could be used to test potential novel treatment options for osteosarcoma. L6565 2D cultured cells (**Fig 5A**) were used for prescreening of drugs and showed that cisplatin, doxorubicin, rapamycin (mTOR inhibitor) and palbociclib were able to induce a dose dependent response after 72 hours, whereas linsitinib (IGF pathway inhibitor) and regorafenib (broad receptor tyrosine kinase inhibitor) showed the highest IC_{50} values (2166 and 3013 nM, respectively) and induced more toxic responses at high doses. Therefore cisplatin, doxorubicin, and rapamycin were selected to validate further using multi-cellular tumour spheroids (MCTS) of L6565 cells. The same cells cultured as MCTS were less sensitive compared to 2D cultured cells (**Fig 5B**). Finally, the L6565 osteosarcoma hydrogels were less sensitive to drugs as compared to L6565 osteosarcoma MCTS or cells in monolayer (**Fig 5C**).

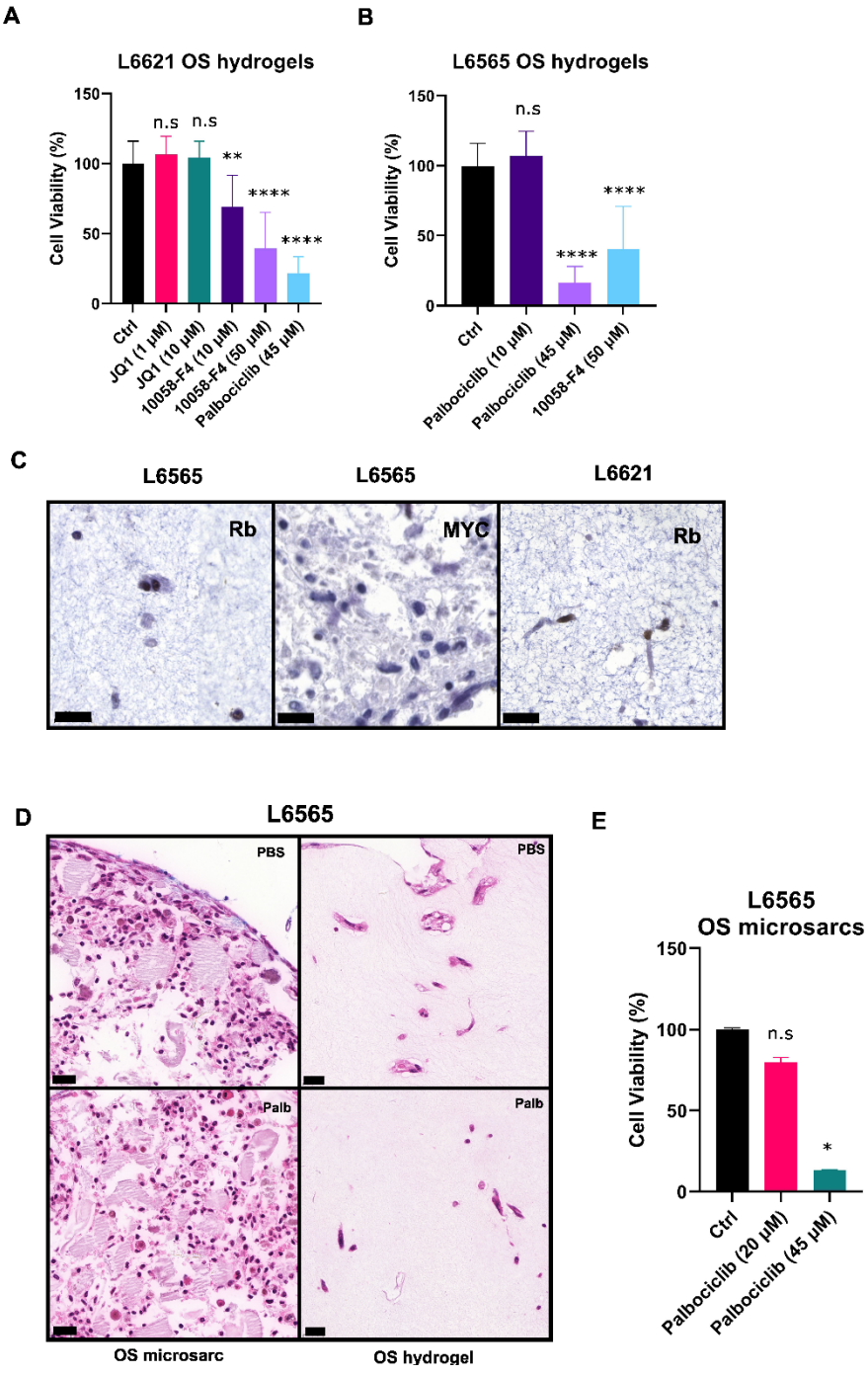

Figure 4. Targeted treatment for L6621 and L6565. (**A**) L6621 osteosarcoma hydrogels, with a MYC amplification, were treated with MYC inhibitors JQ1 and 10058-F4, or palbociclib for 72 hours, after which cell viability was determined. Bars represent the average of seven experiments performed In triplicate, with the standard deviation. Drug treated cells were compared to non-treated controls. ** = P ≤ 0.01; **** = P ≤ 0.001; n.s = not statistically significant. (**B**) L6565 osteosarcoma hydrogels with a loss of *CDKN2A* were treated with palbociclib or 10058-F4 for 72 hours, after which cell viability was determined. Bars represent the average of seven experiments performed in triplicate, with the standard deviation. Drug treated cells were compared to non-treated controls. **** = P ≤ 0.001; n.s = not statistically significant. (**C**) L6565 osteosarcoma hydrogels or microsarcs were stained for Rb and MYC respectively. L6621 osteosarcoma hydrogels were stained for Rb. Scalebar represents 20 µm. (**D**) L6565 osteosarcoma hydrogels and microsarcs did not show difference in morphology between treated (45 µM) and untreated conditions. Scalebar represent 20 µm (**E**) Osteosarcoma microsarcs were treated with palbociclib for 72 hours, after which cell viability was determined. Bars represent the average of one experiment performed in triplicate, with the standard deviation. Drug treated cells were compared to non-treated controls **** = P ≤ 0.05; n.s = not statistically significant

A

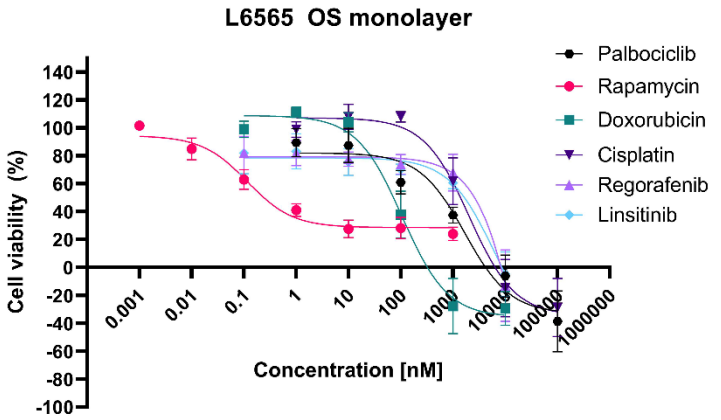

Drug	IC50 (nM)
Palbociclib	611
Rapamycin	0.19
Doxorubicin	71
Cisplatin	1473
Regorafenib	3013
Linsitinib	2166

B

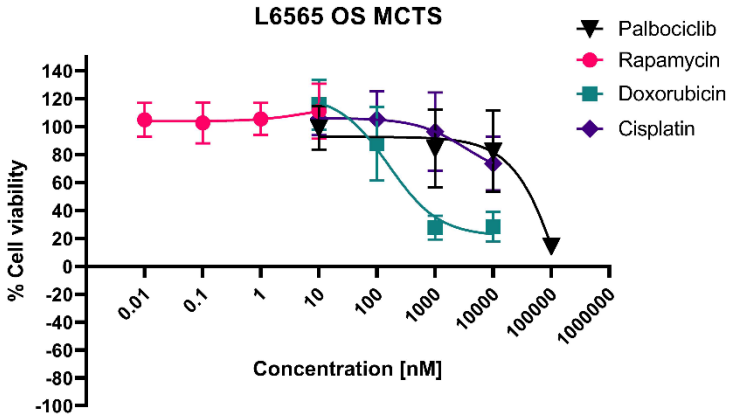

Drug	IC50
Palbociclib	45 µM
Rapamycin	N.A.
Doxorubicin	410 nM
Cisplatin	N.A.

C

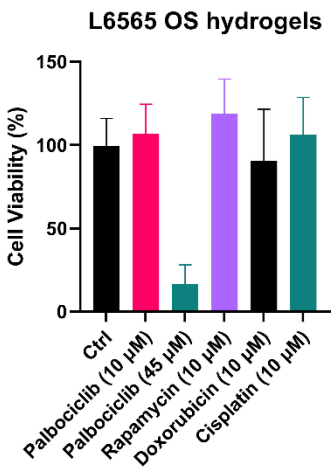

Figure 5. Literature-informed focused drug treatment for L6565. (**A**) 2D cultured cells were treated with each drug for 72 hours, after which cell viability and IC50 values were determined. Graph represents the average of three experiments performed In triplicate, with the standard deviation. (**B**) L6565 MCTS were treated with each drug for 72 hours, after which cell viability and IC50 values were determined. For drugs rapamycin and cisplatin no IC50 value could be determined (N.A.). Graph represents the average of three experiments performed in triplicate, with the standard deviation. (**C**) Osteosarcoma hydrogels of L6565 were treated with each drug for 72 hours. Bars represents the average of seven experiments performed in triplicate, with the standard deviation.

Discussion

Osteosarcoma is currently treated by a combination of (neo)adjuvant chemotherapy and surgery, which has not improved patients' survival over the last decades. Thus, novel therapies are urgently needed for osteosarcoma patients as survival rates remain disappointingly below 60%. To translate pre-clinical findings to the clinic, potential novel therapies should be tested in suitable, representative *in vitro* models. For this purpose, we have successfully established osteosarcoma hydrogels, long-term 3D cultures of primary tumours, derived straight from osteosarcoma patient resection material.

Of the established osteosarcoma hydrogels, 100% of the cultures were propagated until at least seven passages. Not all tested osteosarcoma hydrogels were observed to harbour the same genetic alterations as the original tumour, indicating that these osteosarcoma hydrogels did not contain tumour cells and were probably overgrown by fibroblasts, or that key alterations were lost at higher passages. Nevertheless, three out of seven (43%) osteosarcoma hydrogels tested contained tumour cells with identical genetic alterations as compared to the original tumour, irrespective of tumour status (primary/recurrence/metastasis) or treatment. Long-term (<6 months) growth of lung metastatic osteosarcoma was demonstrated previously by He and colleagues, however these methods did not succeed in establishing long-term non-metastatic osteosarcoma cultures (11). Osteosarcoma hydrogel production methods used in the current study are tailored to mimic the osteosarcoma microenvironment (collagen hydrogels and osteogenic growth factors), single-cell seeded and utilize less additional supplements compared to culture methods frequently used for organoid culture of epithelial cancers. Supplementation in a sarcoma context leads to a more representative and cost-effective culture of osteosarcoma patient samples and allows study of primary tumours as well as metastases. Additionally, the level of antibiotics used for culture of microsarcs should be as low as possible in future experiments, as they may have an effect on response to therapy (32).

Of all osteosarcoma cultures, L6565 was most successful, both in 2D as well as in 3D, although this osteosarcoma is slightly unusual due to the absence of the typical complex genome with a plethora of copy number changes. In fact, the patient presented with a pathological fracture of the left humerus and a lesion was seen in the left clavicle. Biopsies of the clavicle as well as the humerus revealed similar morphology displaying a low-grade undifferentiated spindle cell sarcoma without deposition of osteoid, and MDM2 amplification as determined by FISH was lacking. First, the 6 cm lesion in the clavicle was resected, showing a heterogeneous morphology, including an intermediate grade area with deposition of osteoid, resulting in the diagnosis of osteosarcoma. Resection of the humerus was performed, revealing a 20 cm tumour with similar morphology but also including areas of conventional high-grade osteosarcoma in addition to high grade spindle cell areas without deposition of osteoid. No fusions were detected using Archer fusionplex sarcoma analysis in routine diagnostics.

It was shown that L6565 carried a homozygous loss of *CDKN2A,* with intact Rb, thereby suggesting vulnerability to CDK4/CDK6 inhibitors. L6565 osteosarcoma hydrogels were indeed sensitive to CDK4/CDK6 inhibitor palbociclib, and showed no sensitivity towards drugs that did not inhibit the p16 pathway, including linsitinib, regorafenib and rapamycin. This result is in line with previous studies that a subset of osteosarcomas are vulnerable to palbociclib (16, 29, 33, 34). However, the dosage used in the current study was relatively high as compared to the dosage currently administered to patients with HER2 negative breast cancer (31). Combination with other drugs including rapamycin, doxorubicin or cisplatin could not increase sensitivity to palbociclib and therefore the dose could not be lowered. Nevertheless, our previous study and other studies using osteosarcoma cells have used a dosage in a similar (high) concentration range as the current study and showed promising results (33, 35). Moreover, there are currently two clinical trials ongoing that test CDK4/CDK6 inhibitors in osteosarcoma patients with a known alteration in the CDK4/CDK6 pathway (36, 37).

The primary tumour and patient-derived osteosarcoma hydrogel line L6621 had a *MYC* amplification, suggesting potential sensitivity to treatment with MYC inhibitors. *MYC* amplification occurs in 9% of the osteosarcoma patients (38) and correlates with worse overall survival (30). Moreover, MYC was shown to be a potential driver of osteosarcoma, since mouse bone marrow stromal cells with overexpression of MYC and loss of CDKN2A transformed towards osteosarcoma (39). In the present study, we have tested a bromodomain and extra terminal domain (BET) inhibitor, JQ1, which inhibits MYC activity indirectly by transcriptional repression of *MYC* (29). JQ1 was previously shown to inhibit growth of osteosarcoma cells (34, 40). In osteosarcoma hydrogels, L6621 did not display a reduced cell viability after JQ1 treatment. In contrast, a direct MYC inhibitor, 10058-F4, which was previously shown to decrease cell proliferation in osteosarcoma cells both in 2D and 3D culture models (30), reduced cell viability in L6621. The presence or absence of MYC amplification did not predict response to 10058-F4 in our small series, since also line L6565 – lacking *MYC* amplification - showed a decrease in cell viability after treatment. This suggests that treatment with 10058-F4 might be further explored as novel treatment strategy for osteosarcoma, irrespective of the MYC amplification status.

Drug responses were compared between osteosarcoma 2D culture, culture as MCTS, and a hydrogel culture of the L6565 line. The sensitivity to palbociclib in our study was independent of the 3D culture method, since both osteosarcoma hydrogels and osteosarcoma MCTS showed sensitivity. This indicates a successful inhibitor effect regardless of physiochemical environment and higher cellularity. Comparing all culture methods, as expected, 2D cultured cells were most sensitive to the tested therapeutics. The difference in sensitivity between 2D and 3D cultured cells is not surprising and can be explained by the increase in tight intercellular junctions which occur in 3D cultures and reduce drug penetration (41). However, the difference in sensitivity in 3D osteosarcoma hydrogels compared to 2D propagated cells transitioned to a 3D environment (MCTS) might be explained by additional changes occurring

upon continuous culturing on a 2D plastic surface (8, 9). Further investigation into benefits of 3D primary culture models that have never been in contact with a plastic surface, is required to determine increased representativity over 2D propagated 3D models.

The slow growth rate and continuous monitoring of culture conditions required for osteosarcoma hydrogels does not allow for patient-specific personalized treatment at this moment. Before these models can be used for personalized treatment, culture conditions would need optimization to allow short-term assessment of each patient-derived culture without 2D propagation. Nevertheless, the current study is a proof-of-principle that osteosarcoma hydrogels can be used for pre-clinical precision medicine. Currently, most often a drug discovery pipeline involves screening in 2D cultured cells, followed by *in vivo* testing, and finally clinical trials. Our results suggest that the inclusion of drug testing on 3D cultured cells prior to *in vivo* testing is feasible and may provide valuable information about drug response. In particular 3D primary cultures that have never been in contact with a 2D plastic surface, such as the ones used in this study, may be more representative of *in vivo* and should be studied further in order to determine optimal *in vitro* models for drug discovery pipeline integration.

References

1. WHO classification of tumours of soft tissue and bone, 5th edition. Lyon, France: WHO Classification of Tumours Editorial Board; 2020.
2. Smrke A, Anderson PM, Gulia A, Gennatas S, Huang PH, Jones RL. Future Directions in the Treatment of Osteosarcoma. Cells. 2021;10(1):172.
3. Sayles LC, Breese MR, Koehne AL, Leung SG, Lee AG, Liu H-Y, et al. Genome-Informed Targeted Therapy for Osteosarcoma. Cancer Discovery. 2019;9(1):46.
4. Bassi G, Panseri S, Dozio SM, Sandri M, Campodoni E, Dapporto M, et al. Scaffold-based 3D cellular models mimicking the heterogeneity of osteosarcoma stem cell niche. Scientific Reports. 2020;10(1):22294.
5. Monteiro MV, Gaspar VM, Ferreira LP, Mano JF. Hydrogel 3D in vitro tumor models for screening cell aggregation mediated drug response. Biomaterials Science. 2020;8(7):1855-64.
6. Kim J, Koo B-K, Knoblich JA. Human organoids: model systems for human biology and medicine. Nature Reviews Molecular Cell Biology. 2020;21(10):571-84.
7. Edmondson R, Broglie JJ, Adcock AF, Yang L. Three-dimensional cell culture systems and their applications in drug discovery and cell-based biosensors. Assay and drug development technologies. 2014;12(4):207-18.
8. Tibbitt MW, Anseth KS. Hydrogels as extracellular matrix mimics for 3D cell culture. Biotechnol Bioeng. 2009;103(4):655-63.
9. von der Mark K, Gauss V, von der Mark H, Müller P. Relationship between cell shape and type of collagen synthesised as chondrocytes lose their cartilage phenotype in culture. Nature. 1977;267(5611):531-2.
10. Mohseny AB, Machado I, Cai Y, Schaefer KL, Serra M, Hogendoorn PC, et al. Functional characterization of osteosarcoma cell lines provides representative models to study the human disease. Lab Invest. 2011;91(8):1195-205.
11. He A, Huang Y, Cheng W, Zhang D, He W, Bai Y, et al. Organoid culture system for patient-derived lung metastatic osteosarcoma. Medical Oncology. 2020;37(11):105.

12. Cheng DT, Mitchell TN, Zehir A, Shah RH, Benayed R, Syed A, et al. Memorial Sloan Kettering-Integrated Mutation Profiling of Actionable Cancer Targets (MSK-IMPACT): A Hybridization Capture-Based Next-Generation Sequencing Clinical Assay for Solid Tumor Molecular Oncology. J Mol Diagn. 2015;17(3):251-64.
13. Mody RJ, Wu YM, Lonigro RJ, Cao X, Roychowdhury S, Vats P, et al. Integrative Clinical Sequencing in the Management of Refractory or Relapsed Cancer in Youth. Jama. 2015;314(9):913-25.
14. Majoor BC, Boyce AM, Bovee JV, Smit VT, Collins MT, Cleton-Jansen AM, et al. Increased Risk of Breast Cancer at a Young Age in Women with Fibrous Dysplasia. J Bone Miner Res. 2018;33(1):84-90.
15. Cohen D, Hondelink LM, Solleveld-Westerink N, Uljee SM, Ruano D, Cleton-Jansen AM, et al. Optimizing Mutation and Fusion Detection in NSCLC by Sequential DNA and RNA Sequencing. J Thorac Oncol. 2020;15(6):1000-14.
16. Franceschini N, Gaeta R, Krimpenfort P, Briaire-de Bruijn I, Kruisselbrink AB, Szuhai K, et al. A murine mesenchymal stem cell model for initiating events in osteosarcomagenesis points to CDK4/CDK6 inhibition as a therapeutic target. Laboratory Investigation. 2021.
17. Lee DH, Qi J, Bradner JE, Said JW, Doan NB, Forscher C, et al. Synergistic effect of JQ1 and rapamycin for treatment of human osteosarcoma. Int J Cancer. 2015;136(9):2055-64.
18. Huang MJ, Cheng YC, Liu CR, Lin S, Liu HE. A small-molecule c-Myc inhibitor, 10058-F4, induces cell-cycle arrest, apoptosis, and myeloid differentiation of human acute myeloid leukemia. Exp Hematol. 2006;34(11):1480-9.
19. Fernandes I, Melo-Alvim C, Lopes-Brás R, Esperança-Martins M, Costa L. Osteosarcoma Pathogenesis Leads the Way to New Target Treatments. Int J Mol Sci. 2021;22(2).
20. Kuijjer M, Peterse EFP, Van den Akker BEWM, I.H. B-dB, Serra M, Meza-Zepeda LA, et al. IRIGF1R signaling as potential target for treatment of high-grade osteosarcoma. BMC Cancer. 2013;13(245).
21. Behjati S, Tarpey PS, Haase K, Ye H, Young MD, Alexandrov LB, et al. Recurrent mutation of IGF signalling genes and distinct patterns of genomic rearrangement in osteosarcoma. Nat Commun. 2017;8:15936.
22. Tian Z, Niu X, Yao W. Receptor Tyrosine Kinases in Osteosarcoma Treatment: Which Is the Key Target? Front Oncol. 2020;10:1642.
23. Perry JA, Kiezun A, Tonzi P, Van Allen EM, Carter SL, Baca SC, et al. Complementary genomic approaches highlight the PI3K/mTOR pathway as a common vulnerability in osteosarcoma. Proc Natl Acad Sci U S A. 2014;111(51):E5564-73.
24. Salvador-Barbero B, Álvarez-Fernández M, Zapatero-Solana E, El Bakkali A, Menéndez MDC, López-Casas PP, et al. CDK4/6 Inhibitors Impair Recovery from Cytotoxic Chemotherapy in Pancreatic Adenocarcinoma. Cancer Cell. 2020;37(3):340-53.e6.
25. Yamamoto T, Kanaya N, Somlo G, Chen S. Synergistic anti-cancer activity of CDK4/6 inhibitor palbociclib and dual mTOR kinase inhibitor MLN0128 in pRb-expressing ER-negative breast cancer. Breast Cancer Res Treat. 2019;174(3):615-25.
26. Hafner M, Niepel M, Chung M, Sorger PK. Growth rate inhibition metrics correct for confounders in measuring sensitivity to cancer drugs. Nature methods. 2016;13(6):`521-7.
27. Chalmers ZR, Connelly CF, Fabrizio D, Gay L, Ali SM, Ennis R, et al. Analysis of 100,000 human cancer genomes reveals the landscape of tumor mutational burden. Genome Med. 2017;9(1):34.
28. Póti Á, Gyergyák H, Németh E, Rusz O, Tóth S, Kovácsházi C, et al. Correlation of homologous recombination deficiency induced mutational signatures with sensitivity to PARP inhibitors and cytotoxic agents. Genome Biol. 2019;20(1):240.
29. Delmore JE, Issa GC, Lemieux ME, Rahl PB, Shi J, Jacobs HM, et al. BET bromodomain inhibition as a therapeutic strategy to target c-Myc. Cell. 2011;146(6):904-17.

30. Feng W, Dean DC, Hornicek FJ, Spentzos D, Hoffman RM, Shi H, et al. Myc is a prognostic biomarker and potential therapeutic target in osteosarcoma. Ther Adv Med Oncol. 2020;12:1758835920922055.
31. Cristofanilli M, Turner NC, Bondarenko I, Ro J, Im S-A, Masuda N, et al. Fulvestrant plus palbociclib versus fulvestrant plus placebo for treatment of hormone-receptor-positive, HER2-negative metastatic breast cancer that progressed on previous endocrine therapy (PALOMA-3): final analysis of the multicentre, double-blind, phase 3 randomised controlled trial. The Lancet Oncology. 2016;17(4):425-39.
32. Ryu AH, Eckalbar WL, Kreimer A, Yosef N, Ahituv N. Use antibiotics in cell culture with caution: genome-wide identification of antibiotic-induced changes in gene expression and regulation. Scientific Reports. 2017;7(1):7533.
33. Perez M, Galván SM, García MP, Marín JJ, Carnero A. Efficacy of CDK4 inhibition against sarcomas depends on their levels of CDK4 and p16ink4 mRNA. Oncotarget. 2015;6(30).
34. Sayles LC, Breese MR, Koehne AL, Leung SG, Lee AG, Liu HY, et al. Genome-Informed Targeted Therapy for Osteosarcoma. Cancer Discov. 2019;9(1):46-63.
35. Zhou Y, Shen JK, Yu Z, Hornicek FJ, Kan Q, Duan Z. Expression and therapeutic implications of cyclin-dependent kinase 4 (CDK4) in osteosarcoma. Biochim Biophys Acta Mol Basis Dis. 2018;1864(5 Pt A):1573-82.
36. Abemaciclib for Bone and Soft Tissue Sarcoma With Cyclin-Dependent Kinase (CDK) Pathway Alteration: Identifier NCT04040205; [Available from: https://clinicaltrials.gov/ct2/show/NCT04040205.
37. Trial of Palbociclib in Second Line of Advanced Sarcomas With CDK4 Overexpression: Identifier NCT03242382; [Available from: https://clinicaltrials.gov/ct2/show/study/NCT03242382.
38. Ueda T, Healey JH, Huvos AG, Ladanyi M. Amplification of the MYC Gene in Osteosarcoma Secondary to Paget's Disease of Bone. Sarcoma. 1997;1(3-4):131-4.
39. Shimizu T, Ishikawa T, Sugihara E, Kuninaka S, Miyamoto T, Mabuchi Y, et al. c-MYC overexpression with loss of Ink4a/Arf transforms bone marrow stromal cells into osteosarcoma accompanied by loss of adipogenesis. Oncogene. 2010;29(42):5687-99.
40. Baker EK, Taylor S, Gupte A, Sharp PP, Walia M, Walsh NC, et al. BET inhibitors induce apoptosis through a MYC independent mechanism and synergise with CDK inhibitors to kill osteosarcoma cells. Sci Rep. 2015;5:10120.
41. Gong X, Lin C, Cheng J, Su J, Zhao H, Liu T, et al. Generation of Multicellular Tumor Spheroids with Microwell-Based Agarose Scaffolds for Drug Testing. PLoS One. 2015;10(6):e0130348.

Supplementary Figures

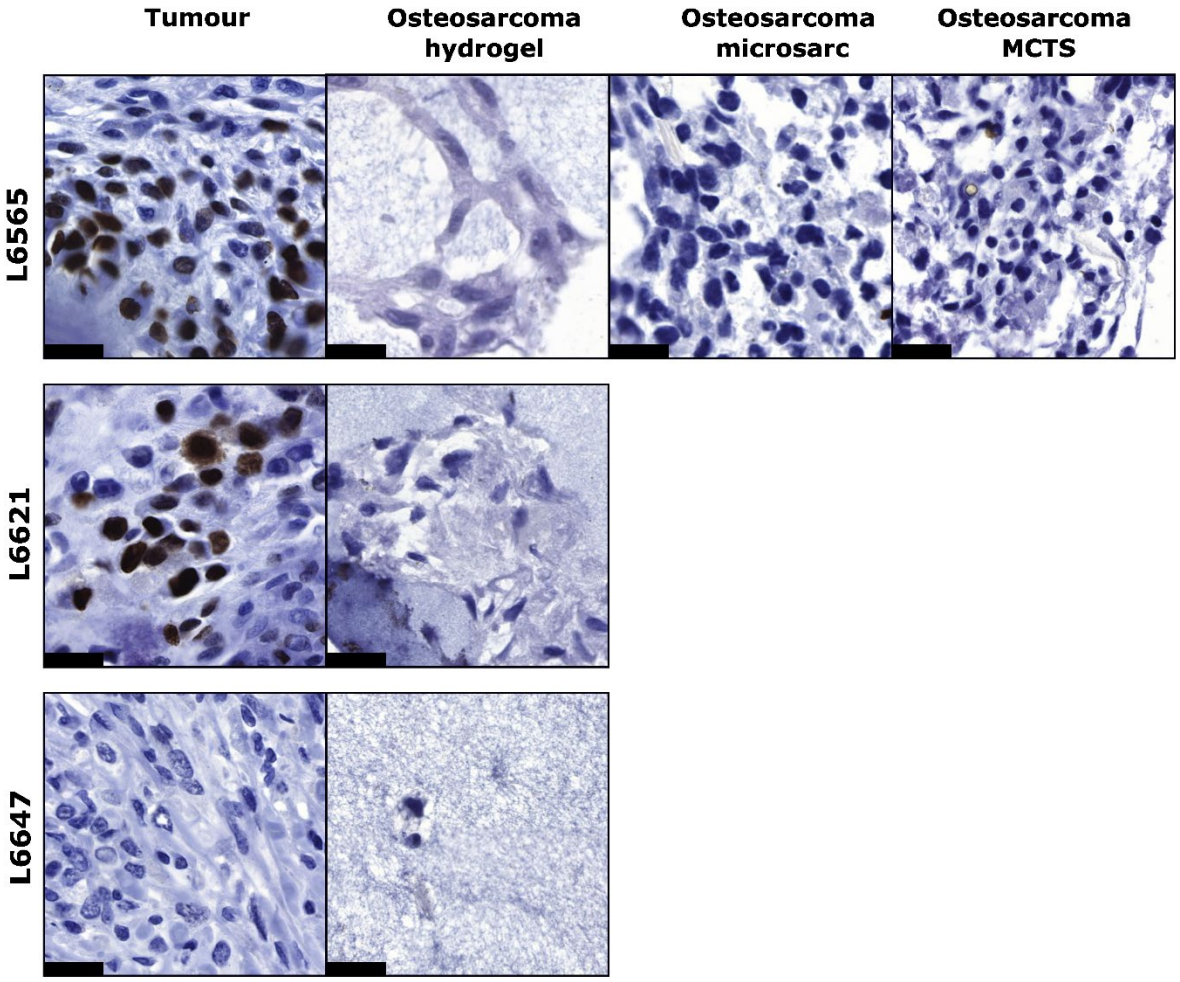

Figure S1. SATB2 staining of osteosarcomas L6565, L6621 and L6647 and the corresponding 3D cultures (hydrogel, microsarc or MCTS). Only these patient samples were stained for SATB2. Scalebar = 20 µm.

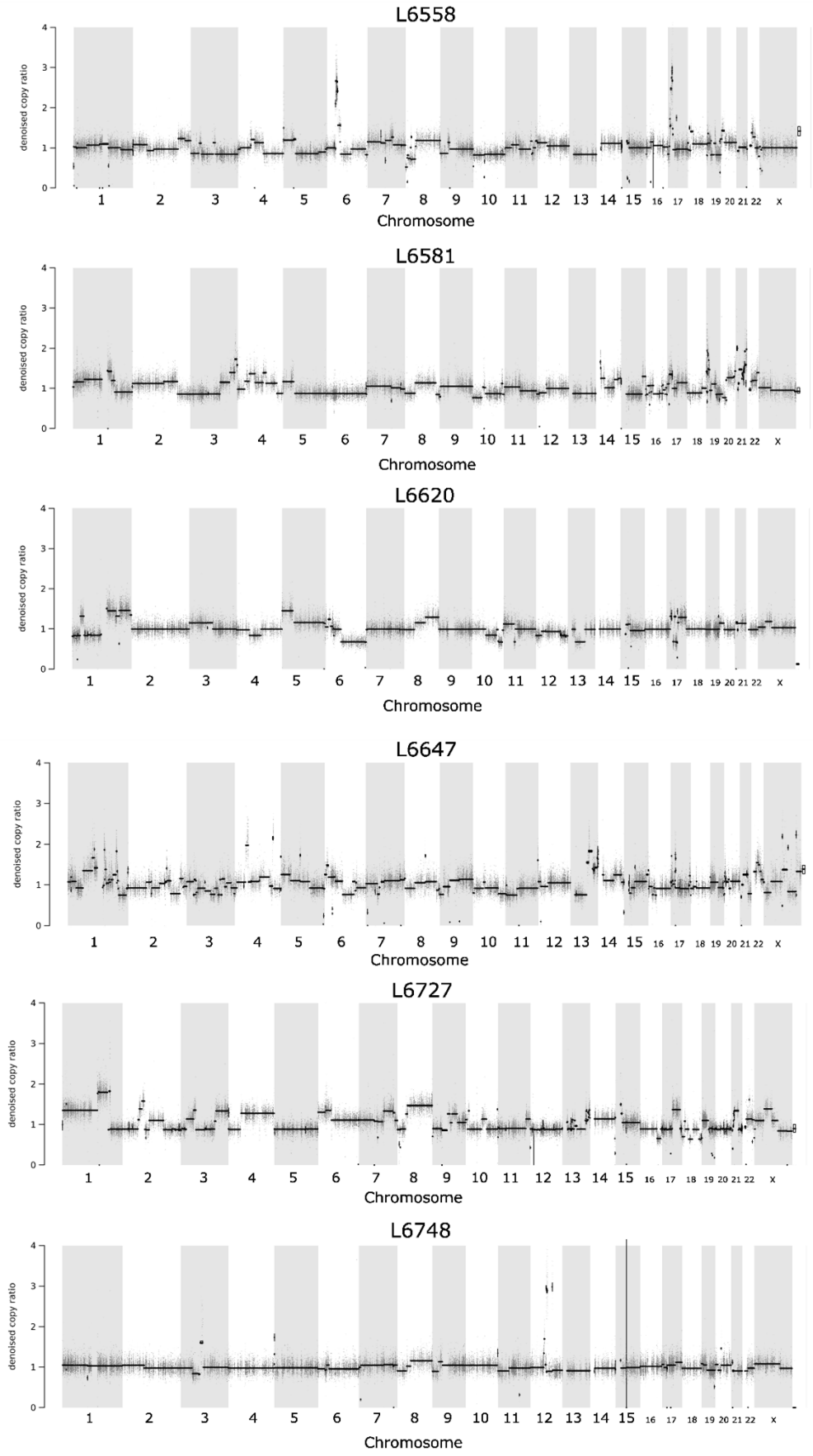

Figure S2. Copy number profiles of L6558, L6581, L6620, L6647, L6727 and L6748.

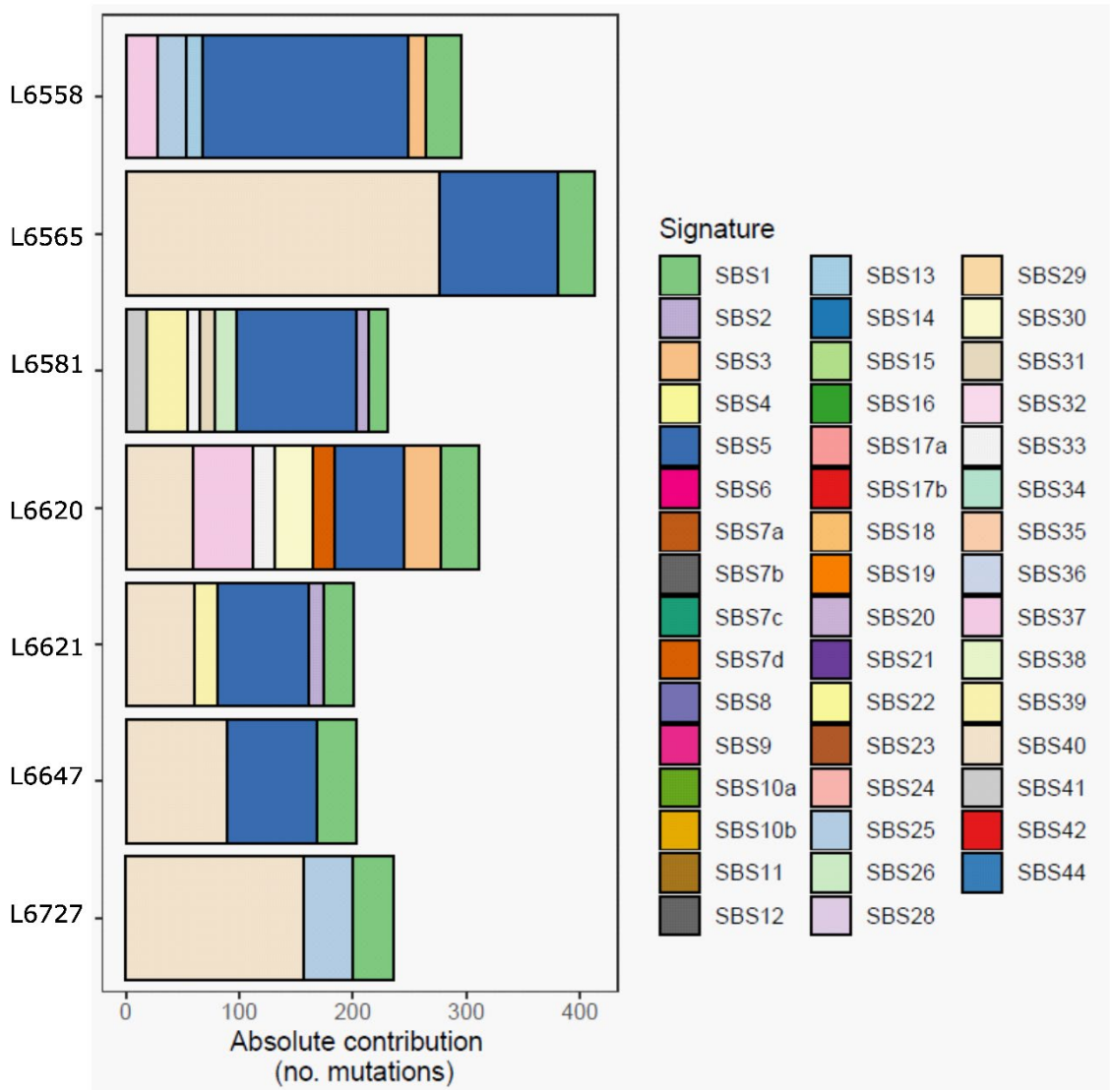

Figure S3. Mutational signatures for all osteosarcoma samples, based on SBS reference signatures.

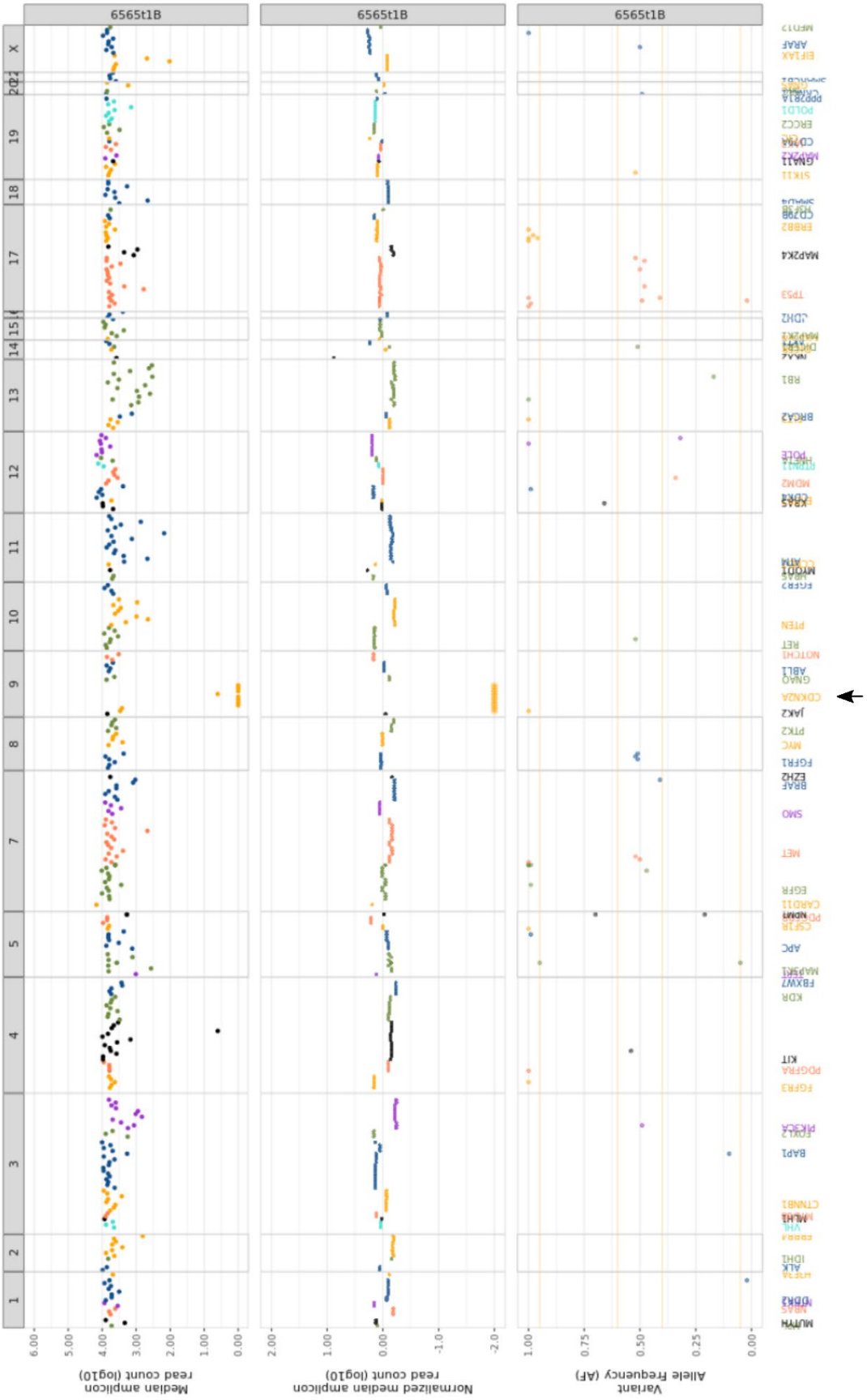

Figure S4. Copy number variation analysis based on Cancer hot spot panel sequencing of L6565. Upper panel: logarithmic scale, each dot represents the median read count per amplicon. Middle panel: normalized read counts. Lower panel: variant allele frequency. Arrow indicates the copy number loss of *CDKN2A*.

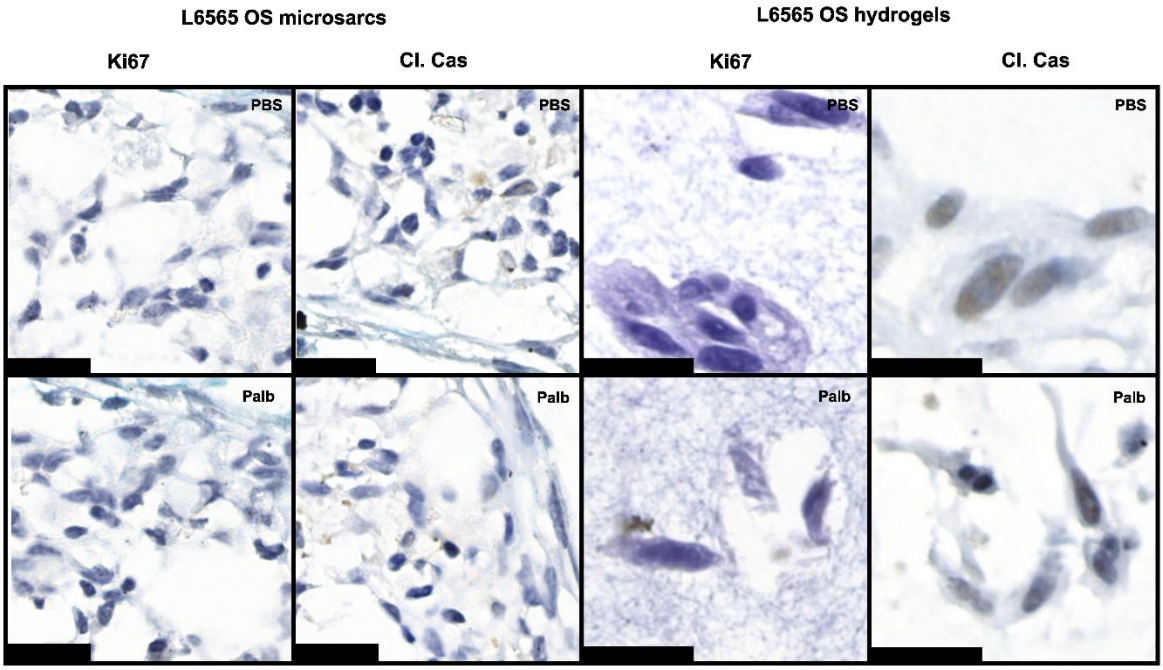

Figure S5. Ki67 and cleaved caspase 3 staining for L6565 osteosarcoma hydrogels and microsarcs. Scalebar = 20 µm

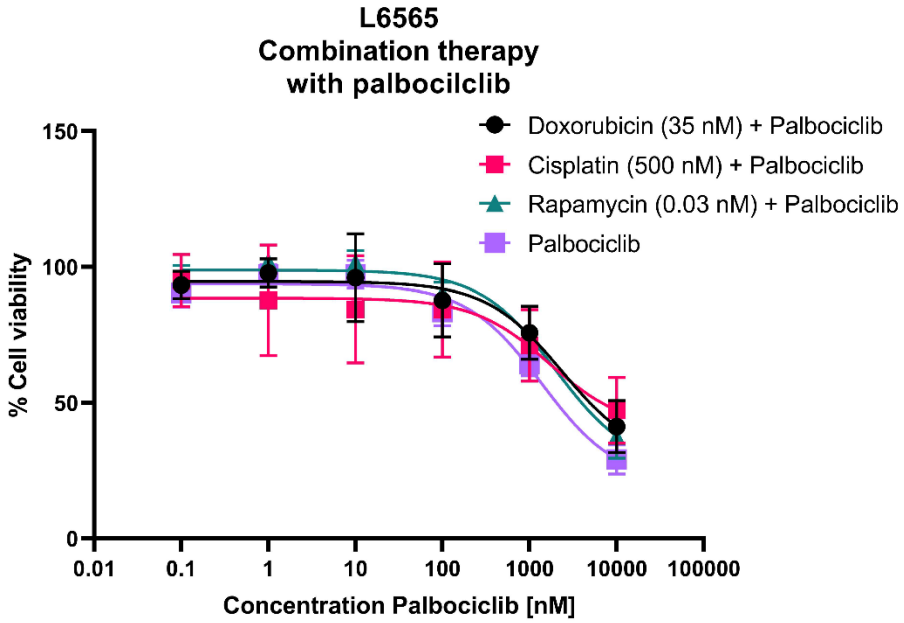

Figure S6. L6565 2D cultured cells were treated with different drugs combined with palbociclib. The x-axis depicts the concentration of palbociclib. Cells were pre-treated with doxorubicin (35 nM) and cisplatin (500 nM) for 24 hours, after which palbociclib was added for 72 hours in total. Rapamycin (0.03 nM) and palbociclib were administered simultaneously for 72 hours. Graph represents the average of three experiments performed In triplicate, with the standard deviation.

Chapter 8

Summary and concluding remarks

Summary

Bone-forming tumours are rare tumours characterized by bone deposition, and include osteoid osteoma, osteoblastoma and osteosarcoma (1). The molecular pathology differs greatly between osteosarcoma and osteoid osteoma/osteoblastoma. Osteoid osteoma and osteoblastoma are tumours with simple genomics and show translocations of the *FOS* gene in the majority of cases, whereas osteosarcoma is a tumour with complex genomics and not driven by a specific mutation or translocation. For osteoid osteoma and osteoblastoma the role of FOS in the pathogenesis is not completely understood. For osteosarcoma, the complex genomics hampers the identification of driver events and this is largely unknown. Thus, the main aim of this thesis was to study the pathogenesis of these bone-forming tumours. Furthermore, the aim was to investigate novel treatment options for osteosarcoma, since current treatment has not improved survival in the last decades. Good models are essential to study pathogenesis and therefore the first part of this thesis describes the development of *in vitro* models for functional analysis of molecular alterations in bone-forming tumours. In the second part of this thesis, in *vitro* models have been used to test novel therapeutic strategies for osteosarcoma.

Part 1: *in vitro* models for functional analysis of molecular alterations in bone-forming tumours

The *in vitro* models described in **chapter 3** and **chapter 4** of this thesis are cell-of-origin based models of bone-forming tumours, for which the mesenchymal stem cell was used as the cell-of-origin for functional analysis of molecular alterations. In part 2 we describe different *in vitro* models for drug testing. An overview of *in vitro* models most suitable for different research questions is presented in **Figure 1**.

Cell-of-origin based models for functional analysis of molecular alterations

In **chapter 3** we established a cell-of-origin based model for osteoid osteoma and osteoblastoma. These tumours are characterized by the deposition of immature woven bone (1). The underlying molecular alterations have recently been unraveled, and it was discovered that both osteoid osteoma and osteoblastoma show recurrent translocations in *FOS* leading to a truncation of the protein, and overexpression of truncated FOS due to loss of the C-terminal protein destabilizing motif (2, 3). Currently, cell models for osteoid osteoma and osteoblastoma are lacking. Thus, in this thesis a cell-based model for osteoid osteoma and osteoblastoma was generated, in which fetal mesenchymal stem cells have been transduced to overexpress a truncated form of FOS, lacking the last 90 amino acids of the C-terminal domain. These cells were characterized for their osteogenic differentiation potential and proliferation rate. It was demonstrated that mesenchymal stem cells overexpressing truncated FOS have slightly reduced osteogenic differentiation capacity, and a reduced proliferation rate. We have demonstrated that mesenchymal stem cells overexpressing

truncated FOS show similarities to osteoid osteoma and osteoblastoma, thus providing evidence that the presence of FOS translocations can be linked to the presence of immature woven bone in osteoid osteoma and osteoblastoma.

For osteosarcoma there is a plethora of cell-based models (4), and we have used a previously established model based on mesenchymal stem cells in **chapter 4**. Where previous studies have already demonstrated that murine mesenchymal stem cells undergo spontaneous transformation after long-term culture (5-7), we have now established that also canine mesenchymal stem cells may undergo spontaneous transformation, although less frequent compared to murine cells. Transformed murine and canine mesenchymal stem cells showed a myriad of genomic abnormalities, including aneuploidy, translocations, and copy number alterations, and are therefore genetically very similar to human osteosarcoma. More importantly, this thesis demonstrated that in our spontaneously transformed canine and murine mesenchymal stem cells model, *TP53* or *CDKN2A/CDKN2B* is lost, and this loss is a driving event in osteosarcomagenesis. Alterations in *TP53* and *CDKN2A/CDKN2B* are among the most common recurrent alterations in human osteosarcoma (8). These results support that our murine and canine mesenchymal stem cell model can be used as a model for osteosarcoma or other sarcomas with complex genomics. Furthermore, our model allows mapping the genetic events prior to transformation, which is particularly useful to study a tumour which is characterized by high genomic instability and for which no benign precursor is known.

Molecular alterations driving bone-forming tumours

The cell-of-origin based models that are described in this thesis, have been generated to better unravel the underlying mechanism of genetic alterations in bone-forming tumours. The aim of **chapter 3** was to study the role of FOS in osteoid osteoma and osteoblastoma. It is still not completely understood how translocations in *FOS* lead to the formation of osteoid osteoma or osteoblastoma. In **chapter 3**, we have demonstrated that mesenchymal stem cells overexpressing truncated FOS had slower proliferation rates compared to full length FOS expressing mesenchymal stem cells, and that overexpression of both truncated and full length FOS showed changes in osteogenic differentiation compared to non-manipulated wild-type mesenchymal stem cells. The reduced proliferation observed in fetal mesenchymal stem cells that overexpress truncated FOS compared to cells overexpressing full length FOS could explain the non-malignant nature of osteoid osteoma and osteoblastoma. Interestingly, in contrast to osteoid osteoma and osteoblastoma, osteosarcoma does not show frequent recurrent alterations of *FOS*, although overexpression of full length *FOS* can transform cells into osteosarcoma in c-fos transgenic mice (9-11). Indeed, our model shows that mesenchymal stem cells overexpressing full length FOS has the highest proliferation rate. Thus, the mesenchymal stem cell model expressing truncated or full length FOS can

recapitulate the phenotype observed in bone-forming tumours and suggests that the definitive phenotype is a careful balance between differentiation and proliferation.

The genetic alterations leading to the formation of osteosarcoma have been studied in **chapter 4** and **chapter 5** and here we demonstrated that both *TP53* and *CDKN2A*/*CDKN2B* are driving events in osteosarcoma, as loss of either gene results in spontaneous transformation *in vitro*. This observation is in line with literature, where loss of *TP53* or genes within the *RB*-pathway are most often affected (8, 12). Previous studies have also demonstrated that alterations in *TP53* or the *RB*-pathway are early events in osteosarcomagenesis (13, 14). Although alterations in *TP53* are common in different cancer types, mutations in *TP53* are often not an early event in tumorigenesis of epithelial tumours, but instead occur later in the process of tumorigenesis (15). Complicating the question what is driving osteosarcomagenesis is chromothripsis, the event in which one or a few chromosomes shatter in a random order or orientation. The percentage of osteosarcomas in which chromothripsis occurs varies between 30% and 90% (16, 17). The discrepancy may be attributed to the uncertain definition of chromothripsis (18). Chromothripsis and other catastrophic cellular events, such as chromoanagenesis or chromoplexy, are closely related and lead to genomic instability. Such catastrophic events could lead to the generation of alterations in genes such as *TP53* or *CDKN2A/CDKN2B* (17), which are genes that regulate genome maintenance pathways. Thus, it is not completely understood what the driving event is for osteosarcomagenesis, an event such as chromothripsis, or a direct alteration in *TP53* or *CDKN2A/CDKN2B,* and this warrants further investigation. Nevertheless, the transformed murine MSC model that was used in this thesis provides a tool to investigate which genetic alterations occur prior to an event such as chromothripsis.

In our model the transformed murine mesenchymal stem cells formed not only osteosarcoma but also undifferentiated pleomorphic sarcoma after subcutaneous injection in mice. Moreover, not all mesenchymal stem cells with loss of *TP53* or *CDKN2A*/*CDKN2B* were able to form colonies in soft agar, indicating only a specific combination of alterations lead to malignant transformation and osteosarcoma formation. However, it must be noted that osteosarcoma formation still occurred after injection of one transformed murine mesenchymal stem cell line, that did not show colonies in soft ager (B6_4). Thus, to answer the question which alterations lead to osteosarcoma formation, the ability to form *in vivo* tumors should be tested. The order of genetic alterations also determines which tumour (sub)type is formed (19). Furthermore, not only genetic alterations, but also epigenetic changes could play a role in determining the subtype of sarcoma (20). In this thesis, the MSC model was used to identify which mutations or copy number alterations occur prior to transformation, but further mapping of RNA expression profiles and protein networks would allow complete understanding of the transformation process (21). Thus, further research should be done to identify which combination of (epi)genetic changes, in what order these genetic alterations occur, and which stage of differentiation the cells are in, lead to the formation of different (osteo)sarcoma subtypes.

Part 2: Utilizing in vitro models to identify novel treatment options in osteosarcoma

For osteosarcoma the current treatment strategy of (neo)adjuvant chemotherapy in combination with surgery has not improved the outcome in the last decades (22). This underlines the importance of discovering novel therapeutic options, which can be tested pre-clinically using cell-based models. In part 2 of this thesis 2D and 3D cell culture models were used with the aim of pre-clinical testing of novel therapeutic options for osteosarcoma.

Novel therapeutic options for osteosarcoma patients

In **chapter 5** murine mesenchymal stem cells were used to identify that loss of *CDKN2A* and *CDKN2B* are early events in the transformation towards osteosarcoma, which implicates sensitivity towards CDK4/CDK6 inhibitor treatment (23). Indeed, we discovered that transformed murine mesenchymal stem cells and osteosarcoma cell lines with a loss of p16 are more sensitive to the CDK4/CDK6 inhibitor palbociclib compared to wild-type cells, provided Rb function is intact. In **chapter 7**, we have demonstrated that a primary tumour derived 3D culture, with confirmed loss of *CDKN2A,* was indeed sensitive to palbociclib. Therefore these results suggest that palbociclib can be considered as a novel therapeutic option for osteosarcoma patients. We have shown that there is indeed a subgroup of osteosarcoma patients (20-23%) that have overexpression of CDK4 or CDK6 or have loss of p16 with intact Rb, that could possibly benefit from palbociclib treatment. Previous studies have been published that demonstrate that CDK4/CDK6 inhibitors show promise as a novel treatment option (24, 25). However, the current study and others have used a relatively higher dose of palbociclib than is now considered for other cancer types, such as breast cancer (26). The currently ongoing clinical trials in which CDK4/CDK6 inhibitors are tested in osteosarcoma patients, should demonstrate whether these inhibitors are promising *in vivo* as well (27, 28).

Chapter 6 describes another potential treatment for osteosarcoma patients. It was demonstrated that osteosarcoma cells are sensitive to NAMPT inhibitor FK866, which targets the NAD salvage synthesis pathway. Osteosarcoma cells with low *NAPRT* RNA expression, or high *NAPRT* promotor methylation, were the most sensitive to FK866 treatment. Although the exact mechanism of the NAMPT inhibitor FK866 needs to be elucidated further, the current study demonstrates that targeting the NAD salvage pathway can be considered as a novel treatment option for osteosarcoma patients.

The results in **chapters 5** and **chapter 6** demonstrate there is unfortunately no 'one size fits all' treatment option for osteosarcoma patients, as only a subgroup of osteosarcoma patients has the potential to benefit from a treatment option such as FK866. In **chapter 7** we performed whole exome sequencing of osteosarcomas and established 3D primary cultures with proven genetic alterations that are identical to the original tumour to identify novel targeted treatment options. The genetic alterations could point towards novel targeted treatment options, such as MYC-inhibition. However, the response was not predicted by the

genetic biomarker and indicates that these novel treatment strategies can be further explored for osteosarcoma patients.

2D culture vs 3D culture

Throughout **chapters 5**, **6** and **7** different *In vitro* models for pre-clinical drug testing have been used: from 2D cell lines to 3D cultured multicellular tumour spheroids and primary tissue derived hydrogels. 3D models are aimed at mimicking the context of tumour cells *in vivo*. In **chapter 1** the different methods for 3D culture have been explained in detail. Since osteosarcoma cells produce their own extra-cellular matrix, we have not chosen the organoid model that is frequently used for epithelial cancers, but instead used the liquid overlay method as a scaffold-free 3D model and collagen/alginate hydrogels as a scaffold-based 3D model. Throughout this thesis we have generated scaffold-free multi-cellular tumour spheroids and established for the first time a long-term 3D culture of patient-derived tumours, cultured in collagen/alginate hydrogels. In **chapter 7** we compared these different 3D culture methods and conventional 2D culture methods.
We showed that drug response differs greatly among the different methods, where 3D cultures are less sensitive compared to 2D cultures. Moreover, 2D cells cultured in a 3D environment were also less sensitive compared to 3D cultured cells that have never grown on a plastic surface and are cultured as hydrogels. Thus, it is important to carefully consider which model is the most representative for the *in vivo* situation. In chapter 7, the difference in sensitivity among the different methods was evident. However, to determine which method is the most representative of the *in vivo* situation can only be determined when a drug is tested in animal models and in clinical studies. In general, the consensus is that 3D cultures are more representative compared to 2D cultures (29). However, 2D cultures are still useful for initial screening of potential novel therapeutic options. This is in particular important for high-throughput screening. The reproducibility, material cost and labor intensiveness are important factors to consider in 3D cultures, as these remain challenging (30). Especially patient-derived primary tumour hydrogels are labor-intensive and costly. Nevertheless, 3D cultures can be a valuable addition to the pre-clinical drug testing pipeline and minimize the need of *in vivo* models.

Biomarker identification for targeted treatment

The novel therapeutic strategies that have been tested in the studies presented in this thesis were targeted approaches, which is in contrast to the “one size fits all” strategy of chemotherapy. Therefore it is important to carefully consider the target prior to drug testing. We have discovered potential novel biomarkers to identify patients for which novel therapeutics might be promising. In **chapter 5** we identified that osteosarcoma cells with loss of p16, provided Rb is functional, are most sensitive to treatment with CDK4/CDK6 inhibitor palbociclib. Moreover, the patient subgroup with loss of p16 or overexpression of CDK6 showed worse overall survival and therefore novel therapeutic strategies could be valuable

to improve outcome. In **chapter 6** we have shown that osteosarcoma cells with low *NAPRT* RNA expression are particularly sensitive to NAMPT inhibitor treatment, FK866. Furthermore, *NAPRT* RNA expression positively correlated with promotor methylation, indicating that patients with low *NAPRT* RNA expression/high methylation of *NAPRT* could be selected for treatment. However, a clinical study is needed to investigate whether treatment of this group of patients with NAMPT inhibitor would also improve overall survival.
Once a novel biomarker has been discovered, it is important to consider how to identify the biomarker in patients. In **chapter 5** the p16, Rb, CDK4 and CDK6 status have been evaluated by immunohistochemical staining. Immunohistochemical expression of p16 and Rb has been shown to predict the genomic status (31, 32). Moreover, this method is easy to implement into daily clinical practice. This is in contrast with next-generation sequencing techniques, which we have used in **chapter 7** to identify targetable genomic alterations in osteosarcoma patients. Next-generation sequencing is costly and more time consuming compared to immunohistochemistry. However, more potential targets can be evaluated in each patient and deep sequencing is currently part of clinical practice in many institutes. Independent of the chosen detection method, the studies presented in this thesis demonstrate that valuable information from either immunohistochemistry or next-generation sequencing about potential targets can point to novel therapeutic options in osteosarcoma patients.

Concluding remarks

This thesis describes the generation of cell-of-origin based models, using mesenchymal stem cells, to further elucidate the underlying mechanism of molecular alterations of the bone-forming tumours osteoid osteoma, osteoblastoma and osteosarcoma. Furthermore, we describe the identification of novel treatment options for osteosarcoma using 2D and 3D *in vitro* models.

We have shown that the translocation of *FOS*, which is recurrent in osteoid osteoma and osteoblastoma, reduces osteogenic differentiation and proliferation rate of mesenchymal stem cells, thus providing a possible explanation of the phenotype observed in osteoid osteoma and osteoblastoma. For osteosarcoma, we have demonstrated that *TP53* and *CDKN2A/CDKN2B* are early events in osteosarcomagenesis. The loss of *CDKN2A/CDKN2B* can be exploited with CDK4/CDK6 inhibitor palbociclib, providing a potential novel treatment option for osteosarcoma patients. Another novel treatment option for osteosarcoma is targeting the NAD salvage pathway using NAMPT inhibitor FK866.

The investigation of the underlying mechanism of molecular alterations and the pre-clinical testing of novel treatment options described in this thesis, were performed using a variety of *in vitro* models. Not all models are suitable for every application. A suggestion for the different applications of each type of *in vitro* model described in this thesis is shown in **Figure 1**. Cell-of-origin based models are ideal for functional analysis of molecular alterations, whereas tumour cell lines cultured in 2D or in 3D are more suitable for pre-clinical drug testing.

Whether to choose 2D or 3D models should also be carefully considered. It was demonstrated that sensitivity to drugs differs greatly between 2D or 3D culture models, with 3D models the least sensitive, but perhaps the most representative of the *in vivo* situation. However, 2D models are more convenient for high-throughput screening given the ease of culture. In conclusion, in future research one should carefully consider which *in vitro* model is the most suitable given the research question.

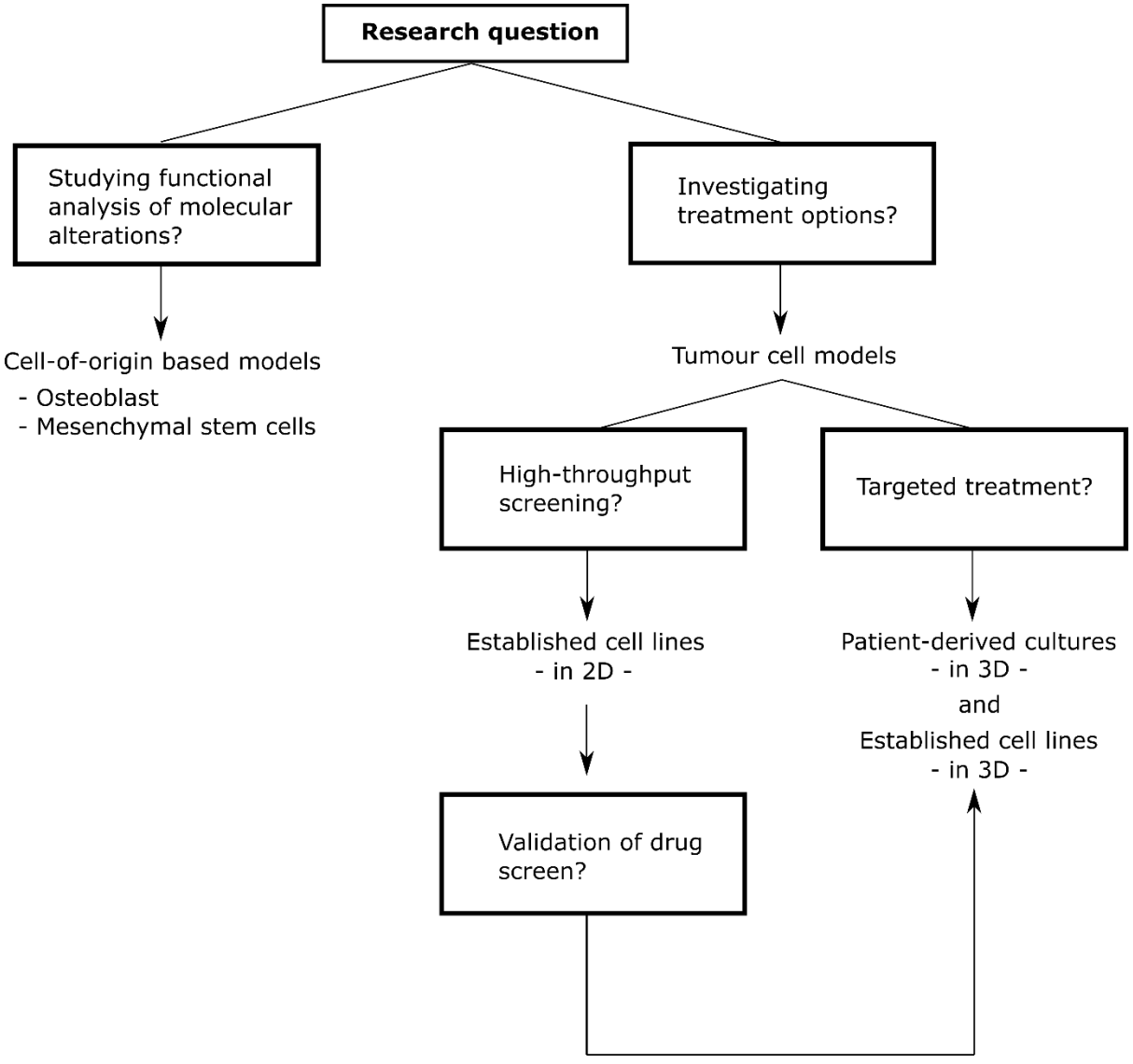

Figure 1. Flowchart of which in vitro model is most suitable for which research question.

References

1. WHO classification of tumours of soft tissue and bone, 5th edition. Lyon, France: WHO Classification of Tumours Editorial Board; 2020.
2. Fittall MW, Mifsud W, Pillay N, Ye H, Strobl AC, Verfaillie A, et al. Recurrent rearrangements of FOS and FOSB define osteoblastoma. Nat Commun. 2018;9(1):2150.
3. Lam SW, Cleven AHG, Kroon HM, Briaire-de Bruijn IH, Szuhai K, Bovee J. Utility of FOS as diagnostic marker for osteoid osteoma and osteoblastoma. Virchows Arch. 2020;476(3):455-63.
4. Mohseny AB, Hogendoorn PC, Cleton-Jansen AM. Osteosarcoma models: from cell lines to zebrafish. Sarcoma. 2012;2012:417271.
5. Tolar J, Nauta AJ, Osborn MJ, Panoskaltsis Mortari A, McElmurry RT, Bell S, et al. Sarcoma Derived from Cultured Mesenchymal Stem Cells. Stem Cells. 2007;25(2):371-9.
6. Mohseny AB, Szuhai K, Romeo S, Buddingh EP, Briaire-de Bruijn I, de Jong D, et al. Osteosarcoma originates from mesenchymal stem cells in consequence of aneuploidization and genomic loss of Cdkn2. J Pathol. 2009;219(3):294-305.
7. Zhou YF, Bosch-Marce M, Okuyama H, Krishnamachary B, Kimura H, Zhang L, et al. Spontaneous transformation of cultured mouse bone marrow-derived stromal cells. Cancer Res. 2006;66(22):10849-54.
8. Chen X, Bahrami A, Pappo A, Easton J, Dalton J, Hedlund E, et al. Recurrent somatic structural variations contribute to tumorigenesis in pediatric osteosarcoma. Cell Rep. 2014;7(1):104-12.
9. Grigoriadis AE, Schellander K, Wang Z, Wagner EF. Osteoblasts are target cells for transformation in c-fos transgenic mice. The journal of Cell Biology. 1993;122(3):685-701.
10. Wang ZQ, Lian J, Schellander K, Wagner EF, Grigoriadis AE. c-fos-induced Osteosarcoma Formation in Transgenic Mice: Cooperativity with c-jun and the role of endogenous c-fos. Cancer Research. 1995;55:6244-51.
11. Franchi A, Calzolari A, Zampi G. Immunohistochemical detection of c-fos and c-jun expression in osseous and cartilaginous tumours of the skeleton. Virchows Arch. 1998;432:515-9.
12. Kovac M, Blattmann C, Ribi S, Smida J, Mueller NS, Engert F, et al. Exome sequencing of osteosarcoma reveals mutation signatures reminiscent of BRCA deficiency. Nat Commun. 2015;6:8940.
13. Kovac M, Ameline B, Ribi S, Kovacova M, Cross W, Barenboim M, et al. The early evolutionary landscape of osteosarcoma provides clues for targeted treatment strategies. J Pathol. 2021.
14. Wang D, Niu X, Wang Z, Song CL, Huang Z, Chen KN, et al. Multiregion Sequencing Reveals the Genetic Heterogeneity and Evolutionary History of Osteosarcoma and Matched Pulmonary Metastases. Cancer Res. 2019;79(1):7-20.
15. Levine AJ. p53: 800 million years of evolution and 40 years of discovery. Nat Rev Cancer. 2020;20(8):471-80.
16. Stephens PJ, Greenman CD, Fu B, Yang F, Bignell GR, Mudie LJ, et al. Massive genomic rearrangement acquired in a single catastrophic event during cancer development. Cell. 2011;144(1):27-40.
17. Behjati S, Tarpey PS, Haase K, Ye H, Young MD, Alexandrov LB, et al. Recurrent mutation of IGF signalling genes and distinct patterns of genomic rearrangement in osteosarcoma. Nat Commun. 2017;8:15936.
18. Pellestor F, Gaillard JB, Schneider A, Puechberty J, Gatinois V. Chromoanagenesis, the mechanisms of a genomic chaos. Semin Cell Dev Biol. 2021.
19. Levine AJ, Jenkins NA, Copeland NG. The Roles of Initiating Truncal Mutations in Human Cancers: The Order of Mutations and Tumor Cell Type Matters. Cancer Cell. 2019;35(1):10-5.
20. Nacev BA, Jones KB, Intlekofer AM, Yu JSE, Allis CD, Tap WD, et al. The epigenomics of sarcoma. Nat Rev Cancer. 2020;20(10):608-23.

21. Zheng F, Kelly MR, Ramms DJ, Heintschel ML, Tao K, Tutuncuoglu B, et al. Interpretation of cancer mutations using a multiscale map of protein systems. Science (New York, NY). 2021;374(6563):eabf3067.
22. Smeland S, Bielack SS, Whelan J, Bernstein M, Hogendoorn P, Krailo MD, et al. Survival and prognosis with osteosarcoma: outcomes in more than 2000 patients in the EURAMOS-1 (European and American Osteosarcoma Study) cohort. Eur J Cancer. 2019;109:36-50.
23. Fry DW, Harvey PJ, Keller PR, Elliott WL, Meade M, Trachet E, et al. Specific inhibition of cyclin-dependent kinase 4/6 by PD 0332991 and associated antitumor activity in human tumor xenografts. Mol Cancer Ther. 2004;3(11):1427-38.
24. Perez M, Galván SM, García MP, Marín JJ, Carnero A. Efficacy of CDK4 inhibition against sarcomas depends on their levels of CDK4 and p16ink4 mRNA. Oncotarget. 2015;6(30).
25. Delmore JE, Issa GC, Lemieux ME, Rahl PB, Shi J, Jacobs HM, et al. BET bromodomain inhibition as a therapeutic strategy to target c-Myc. Cell. 2011;146(6):904-17.
26. Cristofanilli M, Turner NC, Bondarenko I, Ro J, Im S-A, Masuda N, et al. Fulvestrant plus palbociclib versus fulvestrant plus placebo for treatment of hormone-receptor-positive, HER2-negative metastatic breast cancer that progressed on previous endocrine therapy (PALOMA-3): final analysis of the multicentre, double-blind, phase 3 randomised controlled trial. The Lancet Oncology. 2016;17(4):425-39.
27. Trial of Palbociclib in Second Line of Advanced Sarcomas With CDK4 Overexpression: Identifier NCT03242382; [Available from: https://clinicaltrials.gov/ct2/show/study/NCT03242382.
28. Abemaciclib for Bone and Soft Tissue Sarcoma With Cyclin-Dependent Kinase (CDK) Pathway Alteration: Identifier NCT04040205; [Available from: https://clinicaltrials.gov/ct2/show/NCT04040205.
29. Edmondson R, Broglie JJ, Adcock AF, Yang L. Three-dimensional cell culture systems and their applications in drug discovery and cell-based biosensors. Assay and drug development technologies. 2014;12(4):207-18.
30. Langhans SA. Three-Dimensional in Vitro Cell Culture Models in Drug Discovery and Drug Repositioning. Frontiers in pharmacology. 2018;9:6.
31. Nielsen GP, Burns KL, Rosenberg AE, Louis DN. CDKN2A gene deletions and loss of p16 expression occur in osteosarcomas that lack RB alterations. The American journal of pathology. 1998;153(1):159-63.
32. Mohseny AB, Tieken C, van der Velden PA, Szuhai K, de Andrea C, Hogendoorn PC, et al. Small deletions but not methylation underlie CDKN2A/p16 loss of expression in conventional osteosarcoma. Genes Chromosomes Cancer. 2010;49(12):1095-103.

Chapter 9

Nederlandse samenvatting

Curriculum Vitae

List of publications

Nawoord

Nederlandse samenvatting

Botvormende tumoren zijn zeldzame tumoren die gekenmerkt worden door botafzetting. Hieronder vallen osteoïd osteoom, osteoblastoom en osteosarcoom. De moleculaire pathologie verschilt sterk tussen deze tumoren. Osteoïd osteoom en osteoblastoom zijn tumoren met een simpel genetisch profiel en vertonen vaak translocaties van het FOS-gen, terwijl osteosarcoom een tumor is met een complex genetisch profiel en niet wordt gekenmerkt door een specifieke mutatie of translocatie. De rol van FOS in de pathogenese van osteoïd osteoom en osteoblastoom is niet volledig bekend. Voor osteosarcoom belemmert het complexe genetische profiel de identificatie van driver genen.

Dit proefschrift beschrijft onderzoek met als doel de pathogenese van botvormende tumoren te bestuderen en om nieuwe behandelingsopties voor osteosarcoom te ontdekken. Goede modellen zijn essentieel om de pathogenese te bestuderen en daarom beschrijft het eerste deel van dit proefschrift de ontwikkeling van *in vitro* modellen voor de functionele analyse van moleculaire veranderingen in botvormende tumoren. In het tweede deel van dit proefschrift worden *in vitro* modellen gebruikt om nieuwe therapieën voor osteosarcoom te testen.

Deel 1: *in vitro* modellen voor de functionele analyse van moleculaire veranderingen in botvormende tumoren

In **hoofdstuk 3** is er een *in vitro* model ontwikkeld voor osteoid osteoom en osteoblastoom. Deze tumoren hebben vaak translocaties in het FOS-gen, dat leidt tot een verkorte versie van het FOS eiwit. Voor het *in vitro* model voor osteoid osteoom en osteoblastoom zijn foetale mesenchymale stamcellen getransduceerd en deze cellen brengen de verkorte versie van het FOS eiwit tot over-expressie. Dit hoofdstuk heeft aangetoond dat mesenchymale stamcellen die de verkorte versie van FOS tot expressie brengen een licht verminderd osteogeen differentiatievermogen hebben, en een verminderde proliferatiesnelheid. Hiermee vertonen deze cellen gelijkenissen met osteoid osteoom en osteoblastoom.

In **hoofdstuk 4** is er een *in vitro* model ontwikkeld voor osteosarcoom. Hiervoor zijn mesenchymale stamcellen van muizen en honden gebruikt. Eerdere studies hebben aangetoond dat mesenchymale stamcellen van muizen spontane transformatie ondergaan na langdurige kweek, maar in dit hoofdstuk is er voor het eerst vastgesteld dat ook mesenchymale stamcellen van honden spontane transformatie kunnen ondergaan. Getransformeerde mesenchymale stamcellen van muizen en honden vertonen een groot aantal structurele genetische afwijkingen, waaronder aneuploïdie en translocaties, en zijn daarom qua moleculaire genetica zeer goed vergelijkbaar met humaan osteosarcoom. Daarnaast heeft dit proefschrift ook aangetoond dat spontaan getransformeerde mesenchymale stamcellen van muizen en honden vaak de genen *TP53* of *CDKN2A/CDKN2B* verliezen. Deze genen zijn in humaan osteosarcoom ook het meest frequent aangedaan. Deze

resultaten laten zien dat dit *in vitro* model gebruikt kan worden als model voor osteosarcoom en andere sarcomen met een complex genetisch profiel.

Deel 2: Gebruik van *in vitro* modellen om nieuwe behandelingsmogelijkheden voor osteosarcoom te identificeren

In de laatste decennia is de behandelingsstrategie voor osteosarcoom nauwelijks verbeterd en dit onderstreept het belang van het ontdekken van nieuwe therapieën. In deel 2 van dit proefschrift werden 2D en 3D celkweekmodellen gebruikt voor het preklinisch testen van nieuwe therapieën voor osteosarcoom.

In **hoofdstuk 5** werden mesenchymale stamcellen van muizen gebruikt om aan te tonen dat verlies van de genen *CDKN2A* en *CDKN2B* vroege gebeurtenissen zijn in de transformatie naar osteosarcoom. Het verlies van *CDKN2A* en *CDKN2B* impliceert dat cellen gevoelig zijn voor behandeling met CDK4/CDK6 remmer palbociclib, en osteosarcoom cellijnen met een verlies van p16 waren inderdaad gevoeliger voor palbociclib vergeleken met wild-type cellen. Dit is ook aangetoond in hoofdstuk 7, waarin een 3D kweek van een osteosarcoom – met verlies van *CDKN2A* - gevoelig was voor palbociclib. Deze resultaten suggereren dat palbociclib mogelijk een nieuwe therapeutische optie voor osteosarcoompatiënten is. Andere preklinische studies hebben aangetoond dat CDK4/CDK6 remmers veelbelovend zijn als nieuwe behandelingsoptie. De klinische trials waarin CDK4/CDK6 remmers worden getest in osteosarcoompatiënten moeten uitwijzen of deze remmers ook *in vivo* veelbelovend zijn.

Hoofdstuk 6 beschrijft een andere potentiële therapie voor osteosarcoompatiënten. Hierin werd aangetoond dat osteosarcoom cellen gevoelig zijn voor de NAMPT remmer FK866. Osteosarcoom cellen met lage NAPRT RNA expressie, of hoge NAPRT promotor methylering, waren het meest gevoelig voor FK866. Hoewel het exacte mechanisme van de NAMPT remmer FK866 nog verder moet worden opgehelderd, suggereren deze resultaten dat FK866 mogelijk een nieuwe behandelingsoptie voor osteosarcoompatiënten is.

Hoofdstuk 5 en hoofdstuk 6 laten zien dat er helaas geen 'one size fits all' behandeling is voor osteosarcoompatiënten, aangezien slechts een subgroep van osteosarcoom patiënten baat heeft bij een behandeling zoals FK866. In hoofdstuk 7 is er dan ook *whole exome sequencing* uitgevoerd op osteosarcomen om specifieke genetische veranderingen per patiënt in kaart te brengen. De tumoren zijn in 3D gekweekt om vervolgens per patiënt een specifieke behandeling uit te testen. Echter werd de respons op een behandeling niet voorspeld door de genetische verandering en dit geeft aan dat er meer onderzoek nodig is naar nieuwe specifieke behandelingsstrategieën voor osteosarcoompatiënten.

2D kweken vs 3D kweken

In de hoofdstukken 5, 6 en 7 zijn verschillende *in vitro* modellen voor het preklinisch testen van geneesmiddelen gebruikt: van 2D cellijnen tot 3D gekweekte tumorcellen. In hoofdstuk 7

zijn deze verschillende 3D kweekmethoden vergeleken met conventionele 2D kweekmethoden.

Er is aangetoond dat de gevoeligheid van de kweken sterk verschilt, waarbij 3D kweken minder gevoelig zijn vergeleken met 2D kweken. Bovendien waren 2D cellen gekweekt in een 3D omgeving ook minder gevoelig vergeleken met 3D gekweekte cellen die nooit op een plastic oppervlak hebben gegroeid. Het is dus belangrijk om zorgvuldig af te wegen welk model het meest representatief is voor de *in vivo* situatie. Dit zal uiteindelijk moeten worden aangetoond in diermodellen en in klinische studies. Over het algemeen is men het erover eens dat 3D kweken wel representatiever zijn in vergelijking met 2D kweken, met name in sarcomen vanwege de meestal uitgebreide extra cellulaire matrix die alleen door tumorcellen wordt geproduceerd als deze in 3D groeien. 2D kweken zijn echter nog steeds nuttig voor een eerste screening van potentiële nieuwe behandelingen. Dit is met name van belang voor grootschalige *high-throughput screening*. De reproduceerbaarheid, materiaalkosten en arbeidsintensiviteit zijn belangrijke factoren waarmee rekening moet worden gehouden bij 3D kweken, aangezien 3D kweken nog steeds uitdagend blijken. Vooral 3D kweken direct afkomstig uit primaire tumoren zijn erg arbeidsintensief en kostbaar. Desalniettemin kunnen 3D kweken een waardevolle aanvulling vormen voor het preklinisch testen van geneesmiddelen en zo het gebruik van dierproeven tot een minimum beperken.

Concluderende opmerkingen

Dit proefschrift beschrijft het genereren van *in vitro* modellen op basis van mesenchymale stamcellen om het onderliggende moleculaire mechanisme van de botvormende tumoren osteoid osteoma, osteoblastoma en osteosarcoom verder op te helderen. Daarnaast wordt ook de identificatie van nieuwe behandelingsmogelijkheden voor osteosarcoom met behulp van 2D en 3D *in vitro* modellen in dit proefschrift beschreven.

Dit proefschrift heeft aangetoond dat de translocatie van FOS – veel voorkomend in osteoïd osteoom en osteoblastoom - de osteogene differentiatie en proliferatiesnelheid van mesenchymale stamcellen vermindert, en zo een mogelijke verklaring biedt voor het fenotype dat wordt waargenomen in osteoïd osteoom en osteoblastoma. Daarnaast is aangetoond dat veranderingen in de genen *TP53* en *CDKN2A/CDKN2B* al vroeg kunnen optreden tijdens het ontstaan van osteosarcoom. Deze ontdekking kan leiden tot nieuwe therapieën voor patiënten met osteosarcoom: zo kunnen patiënten met verlies van *CDKN2A/CDKN2B* behandeld worden met palbociclib.

Het onderzoek naar het moleculaire mechanisme en het preklinisch testen van nieuwe behandelingsopties in botvormende tumoren werd uitgevoerd met behulp van een verscheidenheid aan *in vitro* modellen. Niet alle modellen zijn geschikt voor elke toepassing. Cellijnen zijn ideaal voor functionele analyse van moleculaire veranderingen, terwijl gekweekt tumormateriaal meer geschikt is voor het preklinisch testen van geneesmiddelen. Ook moet zorgvuldig worden overwogen of voor 2D - dan wel voor 3D-modellen moet worden gekozen.

De gevoeligheid voor geneesmiddelen verschilt sterk tussen 2D- en 3D-kweekmodellen, waarbij 3D-modellen het minst gevoelig zijn, maar misschien wel het meest representatief voor de *in vivo* situatie. 2D-modellen zijn echter meer geschikt voor grotere drug screens gezien het gebruiksgemak. De onderzoeksvraag zal dus leidend zijn voor welk *in vitro* model gekozen kan worden.

Curriculum Vitae

Natasja Franceschini was born on 3 February 1993 in The Hague, the Netherlands. She attended high school at Stanislascollege in Delft, where she graduated in 2011. After obtaining her diploma, she studied Medicine at Leiden University, but quickly realized this study was not a good match with her. Afterwards, she decided to study Biomedical Sciences at the Vrije Universiteit in Amsterdam instead. She continued her studies in the biomedical sciences with a Masters in Molecular Medicine at the Erasmus University in Rotterdam and obtained her degree in 2017. During the Molecular Medicine track, she had the opportunity to join two research labs in the Erasmus Medical Center for an internship. Her first master internship focused on senescence in mesenchymal stem cells, in the research group of Prof. Dr. Gerjo van Osch. Her second internship focused on bone metastasis, in the research group of Dr. Marjolein van Driel. Combining both topics has led her to conduct her PhD research on modeling bone-forming tumours at the Pathology department in the Leiden University Medical Center, in the bone and soft tissue tumour group led by Prof. Dr. Judith Bovée. Natasja is currently working as a Program Manager at Lygature, where she is responsible for the management of public-private partnerships.

List of publications

Johannes Lehmann, Roberto Narcisi, **Natasja Franceschini**, Danai Chatzivasileiou, Cindy G. Boer, Wendy J. L. M. Koevoet, Diana Putavet, Dubravka Drabek, Rien van Haperen, Peter L. J. de Keizer, Gerjo J. V. M. van Osch, Derk ten Berge. WNT/beta-catenin signalling interrupts a senescence-induction cascade in human mesenchymal stem cells that restricts their expansion. Cell Mol Life Sci 2022. doi: 10.1007/s00018-021-04035-x

Natasja Franceschini, Raffaele Gaeta, Paul Krimpenfort, Inge Briaire-de Bruijn, Alwine B. Kruisselbrink, Karoly Szuhai, Ieva Palubeckaitė, Anne-Marie Cleton-Jansen, Judith V.M.G. Bovée. A murine mesenchymal stem cell model for initiating events in osteosarcomagenesis points to CDK4/CDK6 inhibition as a therapeutic target. Lab Invest 2021. doi: 10.1038/s41374-021-00709-z

Natasja Franceschini, Jan Oosting, Maud Tamsma, Bertine Niessen, Inge Briaire-de Bruijn, Brendy van den Akker, Alwine B. Kruisselbrink, Ieva Palubeckaite, Judith V.M.G. Bovée, Anne-Marie Cleton-Jansen. Targeting the NAD salvage synthesis pathway as a novel therapeutic strategy for osteosarcomas with low NAPRT expression. Int J Mol Sci 2021. doi: 10.3390/ijms22126273

Natasja Franceschini, Bas Verbruggen, Marianna A. Tryfonidou, Alwine B. Kruisselbrink, Hans Baelde, Karin E. de Visser, Anne-Marie Cleton-Jansen, Judith V.M.G. Bovée. Transformed canine and murine mesenchymal stem cells as a model for sarcoma with complex genomics. Cancers 2021. doi: 10.3390/cancers13051126

Natasja Franceschini, Suk Wai Lam, Anne-Marie Cleton-Jansen and Judith V.M.G. Bovée. What's new in bone forming tumours of the skeleton? Virchows Arch 2020. doi: 10.1007/s00428-019-02683-w

Nawoord

Ik wil graag iedereen bedanken die geholpen heeft met het tot stand komen van dit proefschrift.

Allereerst wil ik Judith Bovée en Anne-Marie Cleton-Jansen bedanken dat ik mijn promotieonderzoek heb mogen uitvoeren en voor alle hulp die het uiteindelijk tot een mooi geheel hebben gemaakt.

Inge, Pauline, Brendy, Alwine en Hans: bedankt voor alle hulp in het lab en in het bijzonder voor het afronden van alle experimenten nadat ik het lab al had verlaten. Karoly, thank you for all your support and for always being able to come up with new ideas for experiments.

All PhD students and postdocs in P1-39 and P1-40, thank you for making my time at Pathology much more enjoyable. In particular Sheena, thank you for your never-ending voice messages, the endlessly wrapped birthday gift that made me crazy, all your Netflix show recommendations, and the surprise chocolates when I needed them the most. To summarize: you were always there for me and I hope I can return the favour when you are finishing your PhD.

Tenslotte wil ik ook mijn familie en vrienden bedanken voor alle steun de afgelopen jaren, en één persoon in het bijzonder: lieve Luke, dank je wel voor alle support, de mooie reizen die we gemaakt hebben, en jouw grapjes en liedjes die me stiekem toch wel op weten te vrolijken. Ik ben je erg dankbaar voor alle mooie momenten die we al samen hebben beleefd en hoop dat er nog velen komen.